

Doctoral Thesis for the Hungarian Academy of Sciences

Karri Lamsa, Ph.D.

# **Regulation of cortical activity through inhibitory interneuron plasticity**

*Department of Physiology, Anatomy and Neuroscience,  
University of Szeged*

*and*

*The Hungarian Academy of Sciences Neuroscience  
Program*

## Table of Contents

<b>1. Summary of the scientific work</b> .....	3
<b>2. Introduction</b> .....	3
<b>3. Methods</b> .....	
3.1. <i>Experiments on rodent acute brain slices</i> .....	4
3.2. <i>Experiments in vivo rat</i> .....	7
3.3. <i>Human brain slices</i> .....	8
3.4. <i>Anatomical analyses and identification of neuron types</i> .....	10
<b>4. Results and discussion</b> .....	
4.1. <i>GABAergic interneurons exhibit various forms of synaptic plasticity and some are specific to interneuron type</i> .....	11
4.2. <i>Identified interneuron types show the learning-related long-term plasticity in vivo</i> .....	17
4.3. <i>Human cortical microcircuits show evolutionarily conserved interneuron plasticity with specific features</i> .....	19
4.4. <i>Interneuron long-term plasticity produces permanent changes in local network activity both in the rodent and in the human</i> .....	22
<b>5. Conclusions</b> .....	24
<b>6. References</b> .....	24
<b>7. Other scientific activities</b> .....	
7.1. <i>Original research articles forming the base of application</i> .....	29
7.2. <i>Most important talks at scientific conferences</i> .....	29
7.3. <i>Supervised Ph.D. students</i> .....	30
7.4. <i>Lectures given in doctoral programs</i> .....	30
7.5. <i>Training of postdoctoral fellows</i> .....	30
7.6. <i>Organization of domestic and international symposia</i> .....	30
7.7. <i>Memberships in editorial or review boards</i> .....	31
7.8. <i>Memberships in scientific committees</i> .....	31
7.9. <i>Scientific awards</i> .....	31
7.10 <i>Personal research grants and fellowships</i> .....	31
7.11 <i>Grant reviewing activities</i> .....	31
7.12 <i>Public outreach</i> .....	32
<b>8. Summary of the most significant results</b> .....	32
<b>9. Original research articles</b> .....	33

## 1. Summary of the scientific work

In this thesis, I will summarize recent developments in the field of “synaptic long-term plasticity in the cortical GABAergic interneurons” and discuss our research team's contribution to the topic. Indeed, we among other laboratories have demonstrated during the past decade that 1) excitatory glutamatergic synapses targeting the GABAergic interneurons in the hippocampus and the neocortex exhibit various different forms of activity-induced learning-related long-term plasticity (Lamsa et al. 2005; Lamsa et al. 2007a; Lamsa et al. 2007b). Importantly, we have demonstrated that the plasticity forms are often specific to interneuron type; anatomically specialized GABAergic interneurons exhibit distinct long-term plasticity mechanisms and require specific neuronal activity patterns for the plasticity induction (Oren et al. 2009; Nissen et al. 2010). 2) We have shown that the interneuron plasticity reported in acute brain slice preparations also occurs in the intact brain *in vivo*, and that the plasticity regulation *in vivo* brain is complex (Lau et al. 2017). 3) We have proven that common interneuron types exhibiting synaptic long-term plasticity in a rodent brain show plasticity in the human neocortex although with specific features. 4) Both in the rodent and in the human cortex, the interneuron plasticity strongly modifies the local neuronal network activities permanently changing signal transmission through polysynaptic circuits (Lamsa et al. 2005; Szegedi et al. 2016; Szegedi et al. 2017). In addition, our results indicate that interneuron plasticity is required to maintain high temporal precision of principal cells' signal processing in the cortex in the face of learning (Kullmann and Lamsa 2007; Kullmann and Lamsa 2011b).

## 2. Introduction

Salient and contextual information in the brain is encoded in firing of neurons as neuronal ensembles, and GABAergic ( $\gamma$ -aminobutyric acid -releasing) inhibitory interneurons play a pivotal role in this process. The activated neuronal ensembles (often referred to as engrams) are thought to represent means carrying relevant stored pieces of information, and they are promptly re-organized by learning (Tonegawa et al., 2015; Poo et al., 2016; Buzsaki and Llinas, 2017). The re-organisation of engrams is at least partly manifested by long-term synaptic plasticity between the excitatory glutamatergic pyramidal neurons (Lisman, 2017). However, it has been poorly understood whether and how long-term plasticity in GABAergic inhibitory

interneurons contributes to this process (McBain et al., 1999; Kullmann and Lamsa, 2011b). It is well established that glutamatergic excitatory neurons exhibit synaptic and non-synaptic long-term plasticity forms. In contrast, the GABAergic inhibitory neurons were initially considered rigid and unchangeable with a hypothesis that their function may not exhibit learning-associated permanent changes (McBain and Maccaferri, 1997; McBain et al., 1999; Ross and Soltesz, 2001). Yet, a past decade in the research of neocortical and hippocampal microcircuits has revealed sophisticated plasticity forms in synapses to the GABAergic inhibitory neurons (Kullmann and Lamsa, 2011a). Several research groups including ours have independently demonstrated that the GABAergic neurons undergo a wide range of synaptic and non-synaptic activity-induced plasticity processes (Laezza et al., 1999; Alle et al., 2001; Perez et al., 2001; Lamsa et al., 2005; Pelkey et al., 2005; Lamsa et al., 2007b; Lu et al., 2007; Galvan et al., 2010; Sambandan et al., 2010; Peterfi et al., 2012; Griguoli et al., 2013; Le Roux et al., 2013; Camire and Topolnik, 2014; Zarnadze et al., 2016; Nicholson and Kullmann, 2017). A remarkable feature in their plasticity is – in terms of its induction and expression – that it often (although not always) differs from that known to exist in the excitatory principal neurons (Kullmann and Lamsa, 2007; Pelkey and McBain, 2008; Bartos et al., 2011; Galvan et al., 2011; Kullmann et al., 2012; Topolnik, 2012). This thesis will shortly review the topic and explain how our research team activity has participated to the exciting and timely scientific endeavor of the learning-related cortical GABAergic interneuron plasticity. In four main chapters, I will review current understanding of the synaptic long-term plasticity in the interneurons summarizing (1) its induction and the mechanisms explored *in vitro* slice preparation, and (2) present evidence for the plasticity *in vivo* brain. In following chapters (3 and 4), I will elaborate the topic from the rodents (which are the most commonly used experimental animals in cellular neuroscience research) to the human cortex. This research thesis focuses on the learning-associated plasticity specifically in the excitatory synaptic input to the GABAergic neurons.

### **3. Methods**

#### *3.1. Experiments on rodent acute brain slices*

Three- to four- week old male Sprague-Dawley rats were killed by cervical dislocation and decapitated. The brain was rapidly removed and placed in ice-cold (0 to +4°C) sucrose cutting

solution containing (mM): 75 sucrose, 87 NaCl, 2.5 KCl, 0.5 CaCl<sub>2</sub>, 7 MgCl<sub>2</sub>, 1.0 NaH<sub>2</sub>PO<sub>4</sub>, 25 NaHCO<sub>3</sub>, 25 glucose, pH 7.4, bubbled with 95 % O<sub>2</sub> / 5 % CO<sub>2</sub> (Lamsa et al. 2005; Lamsa et al. 2007b; Oren et al. 2009; Nissen et al. 2010; Szabo et al. 2012). Transverse hippocampal slices (350 μm thickness) were cut using a vibrating microtome (Leica VT 1000S, Leica Microsystems, Germany). Slices were kept submerged at 32°C in the sucrose solution for 20–25 min before being transferred to an interface chamber where they were maintained in Earle's Balanced salt solution (EBSS) (Gibco-Invitrogen) with 3 mM Mg<sup>2+</sup> and 1 mM Ca<sup>2+</sup> at room temperature (20–25°C) for at least 60 min before starting experiments. Hippocampal or somatosensory neocortex slices (Szegedi et al. 2016) were placed in a recording chamber (Luigs & Neumann, Germany) mounted on the stage of an upright microscope (Olympus BX51WI, Japan), where they were held under a nylon mesh grid and superfused at 3–8 ml min<sup>-1</sup> with artificial cerebrospinal fluid (ACSF) at 31 – 33°C. The ACSF contained (mM): NaCl (119), KCl (2.5), CaCl<sub>2</sub> (2.5), MgSO<sub>4</sub> (1.3), NaH<sub>2</sub>PO<sub>4</sub> (1.25), NaHCO<sub>3</sub> (26), glucose (11); final pH 7.4 (equilibrated with 95% O<sub>2</sub> / 5% CO<sub>2</sub>) (except in Szegedi et al. 2016 where 3 mM Ca<sup>2+</sup> with 1.5 mM Mg<sup>2+</sup> was used instead). A cut was made between the CA3 and CA1 subfields in the hippocampus to prevent the spread of bursting activity. Slices were visualized using a 20x immersion objective with 2–4x zoom and infra-red differential interference contrast (DIC) optics. In the study using mice the hippocampal slices were similarly processed and maintained and prepared from heterozygous αCaMKII T286A-mutants (backcrossed into a hybrid C57BL6 – 129/Sv genetic background and interbred to obtain homozygous and wild-type (WT) littermates) (Lamsa et al. 2007a). Genotyping was carried out by PCR analysis with DNA obtained from tail biopsies on postnatal day 21, the day of weaning (Lamsa et al. 2007a). Male mice homozygous for αCaMKII T286A and WT littermates were used in the experiments.

Somatic perforated-patch microelectrode recordings (Lamsa et al. 2005; Lamsa et al. 2007a; Lamsa et al. 2007b; Oren et al. 2009; Nissen et al. 2010; Szabo et al. 2012) were made from neurons in CA1 area. Electrodes were prepared from borosilicate glass capillaries (GC150F, 1.5 mm o.d., Harvard Apparatus, UK) pulled on a Sutter microelectrode puller (Novato, CA, USA). Pipette resistance was typically 8–18 MΩ for perforated patch, and 4–7 MΩ for whole cell recordings. A Multiclamp 700B amplifier was used for recording (Molecular Devices, CA, USA). Infra red DIC images of the cell at different magnification (20x, 40x and 80x) were obtained with a CCD camera (Till Photonics, Germany) during electrophysiological experiments. Gramicidin stock solution (100 mg ml<sup>-1</sup>, Sigma) was prepared in dimethyl sulfoxide daily. The

pipette filling solution containing gramicidin was prepared by diluting the stock solution 1:1000 in potassium gluconate pipette solution. The pipette solution contained (mM): potassium gluconate (145), NaCl (8), KOH-HEPES (20-25), EGTA (0.2), and QX-314 Br (1-5); pH 7.2, osmolarity 295 mOsm  $l^{-1}$ . The electrode tip was filled with gramicidin-free filtered potassium gluconate solution. The series resistance was continuously monitored throughout the experiment, and recordings were started when it was  $< 150 M\Omega$ . Bridge balance and pipette capacitance compensation were adjusted throughout the recordings. The presence of QX-314 in the filling solution allowed for detection of inadvertent patch rupture. Suprathreshold depolarizing current steps were injected intermittently to evoke action potentials. Failure to generate action potentials indicated membrane rupture in which case the experiment was aborted. Upon completion of perforated patch recordings, the pipette was slowly retracted under infra red DIC observation. Once the pipette detached from the cell it was rapidly withdrawn from the slice. Next, the same cell was approached with a new pipette and re-patched in whole-cell configuration. Infra red images obtained during the perforated patch recording and the whole-cell recordings were compared to verify that the same cell was re-patched.

The whole-cell filling solution contained (mM) CsCl (135), KOH-HEPES (10), BAPTA (10), NaCl (8), Mg-ATP (2), GTP (0.3), and QX-314 Br (5); pH 7.2, 290 mOsm (Lamsa et al. 2005; Lamsa et al. 2007a; Lamsa et al. 2007b; Oren et al. 2009; Nissen et al. 2010; Szabo et al. 2012). Spermine tetrahydrochloride (0.5 mM, Tocris) was included in some studies in the filling solution to maintain polyamine-mediated rectification of AMPA/kainate receptors during whole cell recording. In addition, neurobiotin (0.3-0.5%, Alomone labs) or biocytin (0.3-0.5%, Sigma-Aldrich) was included in the solution for *post hoc* anatomical analysis of cells. Pipette capacitance compensation was applied in the cell-attached configuration before membrane rupture. Series resistance was not compensated during voltage clamp recordings, but regularly monitored with small hyperpolarizing voltage steps ( $-5$  mV). Data were not corrected for junction potentials.

Monosynaptic excitatory postsynaptic potentials (EPSPs) or excitatory postsynaptic currents (EPSCs) were evoked by alternately stimulating in the CA1 area at 0.067 Hz via two concentric bipolar electrodes (o.d. 125  $\mu$ m, FHC, ME USA), connected to constant current isolated stimulators (DS3, Digitimer UK, 20–200  $\mu$ A, duration 50  $\mu$ s). The stimulators were controlled

by a custom data acquisition program (LabView, National Instruments) or by pClamp 10 software (Axon Instruments). Evoked EPSPs were recorded from the resting membrane potential or in some experiments during a brief (500 ms) hyperpolarizing step (5–10 mV) to avoid action potential generation. For LTP induction one of the pathways was stimulated at 100 Hz for 1 s, delivered twice with a 20 s interval. Simultaneously, the postsynaptic cell was voltage clamped (1200-2000 ms) at  $-70$  –  $-90$  mV or at 0 mV (somatic potential). Miniature EPSCs (mEPSCs) were recorded in 120 s sweeps, with the seal test monitored in between sweeps (Oren et al. 2009). The first recordings were made after 15 min after breaking through into the whole cell configuration to allow for stabilization of the cell input resistance

In all recordings data were low-pass filtered (4 - 5 kHz) and acquired at 10 - 20 kHz on a PC for offline analysis. Data was analysed using LabView, pClamp 10 or in Igor Pro (Wavemetrics, USA). The GABA receptor blockers picrotoxin (100  $\mu$ M) and CGP55845 (1  $\mu$ M) were added to the extracellular solution. Where indicated, the NMDA receptor antagonist DL-2-Amino-5-phosphonovaleric acid (DL-APV, 100  $\mu$ M) or glutamate receptor antagonists philanthotoxin-433 (PhTx, 10  $\mu$ M) was also included. All drugs were applied via superfusion (3-5 ml/min). Tetrodotoxin (TTX 1  $\mu$ M) was present during mEPSC recordings. Chemicals were purchased from Sigma and drugs were purchased from Tocris Cookson (Bristol, UK) or Ascent Scientific (Weston-super-Mare, UK).

### *3.2. Experiments in vivo rat*

Experiments were carried out on adult male (weight 280–350 g) Sprague–Dawley rats (Charles River, UK) according to the Animal Scientific Procedures Act, 1986 (UK) using a heating mattress ( $37.5 \pm 0.5$  °C) with an external abdominal temperature measurement probe with feedback to the heating pad. Anesthesia was induced with isoflurane (4 % v/v in O<sub>2</sub>) and maintained by a single intraperitoneal (i.p.) injection of urethane (1.25–1.3 mg/kg in 0.9 % saline, i.p.). Ketamine (30 mg/kg i.p.) and xylazine (3 mg/kg i.p.) were given at the start of the procedure and in supplementary small doses during recording to maintain anesthesia. Saline-based glucose solution (5 % v/v glucose) was injected subcutaneously (2 ml/2 h) to compensate for fluid loss during the experiment. A rostrocaudal incision was performed to expose the skull, and surgical windows were made above the right and left dorsal hippocampal CA1 areas with a dental drill. A wall of dental cement was built to protect the

openings and saline was applied regularly to the exposed brain surface. For accurate measurement of penetration depth, saline solution was drained before inserting electrodes into the brain. The windows were covered with warm paraffin wax once the electrodes were lowered into the brain.

Microelectrodes were pulled from borosilicate glass capillaries (GC120F-10, Harvard Apparatus, UK) and were filled with 1.5–3 % (w/v) neurobiotin (Vector Laboratories, UK) in 0.5 M NaCl. The recording electrodes were lowered into the brain at 20  $\mu\text{m/s}$ , and into the hippocampus at 5  $\mu\text{m/s}$  using a micro drive holder (EXFO-8200 IMMS, Canada) and a computer-controlled 0.5  $\mu\text{m}$ -stepping interface. Stereotaxic co-ordinates for the recording electrodes were: 3.0 mm posterior to Bregma ( $\pm 0.3$  mm), 3.6 mm from midline ( $\pm 0.5$  mm), and depth 2.2 mm ( $\pm 0.3$  mm). The electrode resistance was 15–21 M $\Omega$ . Following extracellular recording, the electrode was moved into juxtacellular position and the recorded cells were modulated by applying a series of +10 to +50 nA square pulses of 200 ms duration in 30 s episodes for 2–3 minutes continuously (Lau et al. 2017). We verified that the action potential properties (extracellular spike kinetics) of the modulated cell corresponded to the action potential properties recorded during plasticity experiment. This labeling procedure was followed by a period from 1 to 5 hours (Lau et al. 2017), which allowed for the diffusion of neurobiotin inside the modulated cells. Signal was amplified 1000 $\times$  (10 $\times$ , head-stage amplifier, Axon Instruments, USA; 100 $\times$ , NL-106, Digitimer<sup>TM</sup>, UK) and band-pass filtered between 0.3 and 300 Hz for local field potentials (LFP) and between 300 Hz and 5 kHz for detection of single spikes. The LFP and single neuron activity were acquired at 1 and 19.841 kHz, respectively using Spike2 (version 7.0; Cambridge Electronic Design, UK). Concentric bipolar stimulating electrodes (125  $\mu\text{m}$  tip diameter, FHC Inc., USA) were stereotaxically placed in the left hippocampal CA1 area 3.0–3.2 mm posterior and 3.0–4.0 mm lateral to Bregma and at 2.1–2.5 mm depth from the cortical surface (Lau et al. 2017). Single-shock stimulation (100  $\mu\text{s}$ , 150–600  $\mu\text{A}$ ) was delivered every 5 s using current isolator stimulator (DS3; Digitimer, UK) to elicit spikes. The train of theta-burst stimulation (TBS) for plasticity induction consisted of 20 bursts (at 200 ms intervals) of five stimuli at 100 Hz.

### 3.3. Human brain slices

All procedures were performed according to the Declaration of Helsinki with the approval of the University of Szeged Ethical Committee and Regional Human Investigation Review Board (ref. 75/2014). Human neocortical slices were derived from material that had to be removed to gain access to the surgical treatment of deep-brain tumors from the left and right frontal, temporal, and parietal regions with written informed consent of the patients prior to surgery. The patients were 10–85 y of age (mean  $\pm$  SD = 50  $\pm$  4 y), including 17 males and 14 females. The tissue obtained from underage patients was provided with agreement from a parent or guardian. The resected samples were cut from the frontal and temporal lobes of left or right hemisphere. Anesthesia was induced with intravenous midazolam and fentanyl (0.03 mg/kg, 1–2  $\mu$ g/kg, respectively). A bolus dose of propofol (1–2 mg/kg) was administered intravenously. The patients received 0.5 mg/kg rocuronium to facilitate endotracheal intubation. After 2 min, the trachea was intubated and the patient was ventilated with O<sub>2</sub>/N<sub>2</sub>O mixture (a ratio of 1:2). Anesthesia was maintained with sevoflurane at monitored anesthesia care volume of 1.2–1.5. After surgical removal, the resected tissue blocks were immediately immersed in ice-cold standard solution containing (in mM): 130 NaCl, 3.5 KCl, 1 NaH<sub>2</sub>PO<sub>4</sub>, 24 NaHCO<sub>3</sub>, 1 CaCl<sub>2</sub>, 3 MgSO<sub>4</sub>, 10 D(+)-glucose, and saturated with 95% O<sub>2</sub> and 5% CO<sub>2</sub>. Slices were cut perpendicular to cortical layers at a thickness of 350  $\mu$ m with a microtome (Microm HM 650 V) and were incubated at room temperature (20–24°C) for 1 h in the same solution. The solution used during electrophysiology experiments was identical to the slicing solution, except it contained 3 mM CaCl<sub>2</sub> and 1.5 mM MgSO<sub>4</sub>. Recordings were performed in a submerged chamber (perfused 8 ml/min) at approximately 36–37°C. Cells were patched using water-immersion 20 $\times$  objective with additional zoom (up to 4 $\times$ ) and infrared differential interference contrast video microscopy. Micropipettes (5–8 M $\Omega$ ) were filled with intracellular solution for whole-cell patch-clamp recording (in mM): 126 K-gluconate, 8 KCl, 4 ATP-Mg, 0.3 Na<sub>2</sub>-GTP, 10 HEPES, 10 phosphocreatine (pH 7.20; 300 mOsm) with 0.3% (w/v) biocytin. Current and voltage clamp recordings were performed with Mutliclamp 2B amplifier (Axon Instruments), low-pass filtered at 6 kHz (Bessel filter). Series resistance (R<sub>s</sub>) and pipette capacitance were compensated in current clamp mode and pipette capacitance in voltage clamp mode. R<sub>s</sub> was monitored and recorded continuously during the experiments. The recording in voltage clamp mode was discarded if the R<sub>s</sub> was higher than 25  $\Omega$ M or changed more than 20%. Extracellular stimulation was applied with a concentric bipolar electrode (125  $\mu$ m tip diameter, FHC Inc., US) positioned on L2–3. Paired pulse stimuli (50  $\mu$ s, with 50 ms interval, intensity range from 20 to 300  $\mu$ A) were delivered every 15 s with

current isolator stimulator (Model DS3, Digitimer, UK). Compound EPSCs were confirmed by observing less than 100 pA increases in the evoked EPSC amplitude when gradually increasing stimulation intensity.

#### *3.4. Anatomical analyses and identification of neuron types*

Neurons were filled with neurobiotin (Vector Labs, UK) or biocytin (Sigma, UK) during whole cell recordings (at least 30 min). Slices were fixed overnight at 4°C in a solution containing 4 % paraformaldehyde, 0.05 % glutaraldehyde and 0.2 % picric acid in 0.1 M sodium phosphate buffer (PB). The next day, slices were washed thoroughly in 0.1 M phosphate-buffer and stored in PB plus 0.05 % sodium azide (BDH, UK) at 4°C. For re-sectioning, slices were embedded and fixed in 20 % gelatin and re-sectioned at 60-70 µm thickness using a vibrating microtome (Leica VT1000S, Leica Microsystems, Germany). The sections were washed once in 0.1 M PB, and several times in 50 mM Tris-buffered saline (TBS, Sigma, UK) with 0.3% Triton X-100, and then incubated for at least 5 hrs with Alexa Fluor 488-labeled streptavidin (Invitrogen, UK, diluted 1:1000) in TBS with 0.3 % Triton X-100. Human brain slices were permeabilized using a freeze and thaw procedure. Sections were mounted in Vectashield (Vector Laboratories, Burlingame, CA) under coverslips, and examined with a fluorescent microscope. Images were captured using a CCD camera (C4747-95; Hamamatsu Photonics, Hamamatsu, Japan) with an appropriate filter set and analyzed using the Openlab 4.0.4 image analysis software package (Improvision, Coventry, UK).

Images were constructed from Z-stacks using ImageJ 1.42 software (NIH, USA) and inverted to show the cell on white background; NeuronJ program was used for neurite tracing at a preset line thickness and quantification. Epifluorescent images were taken with the Zeiss AxioImager.Z1 microscope (Zeiss HE38 filter, 40x or 63x oil-immersion objective) using AxioVision software, and digital micrographs were constructed from Z-stacks with ImageJ software. Micrographs were not manipulated selectively, only brightness and contrast of the whole stacked image was adjusted. Interneuron types were identified as described in the original publications (Lamsa et al. 2007b; Oren et al. 2009; Nissen et al. 2010; Szabo et al. 2012; Szegedi et al. 2016; Lau et al. 2017; Szegedi et al. 2017). For immunofluorescence experiments, sections were processed as described in the original publications.

Some sections for cell structure illustrations (cells in Oren et al., 2009; Szegedi et al. 2016; Lau et al. 2017) were further incubated in a solution of conjugated avidin-biotin horseradish peroxidase (HRP; 1 : 300; Vector Labs) in Tris-buffered saline (TBS, pH = 7.4) at 4 °C overnight. Sections were post-fixed with 1 % OsO<sub>4</sub> in 0.1M PB. After several washes in distilled water, sections were stained in 1 % uranyl acetate, dehydrated in ascending series of ethanol. Sections were infiltrated with epoxy resin (Durcupan) overnight and embedded on glass slices. Three-dimensional light microscopic reconstructions from sections were carried out using Neurolucida system with 100 x objective (Olympus BX51, Olympus UPlanFI, Hungary). Images were collapsed in z-axis for illustration.

Sections from some axo-axonic cells were prepared for electron microscopic analysis (Nissen et al. 2010). After fixation and re-sectioning of slices (as above), selected sections were washed in 0.1M PB and then stored in 0.05% sodium azide with 0.1M PB. Following cryoprotection with sucrose and freeze-thaw to enhance penetration of reagents, the cells were revealed with HRP reaction (ABC *Elite* kit, Vector Laboratories; 0.05% DAB, Sigma, UK; 0.01% H<sub>2</sub>O<sub>2</sub>). The sections were treated with 1% OsO<sub>4</sub> (in PB; TAAB Laboratory Equipment Ltd, UK) and 1% aqueous uranyl acetate, dehydrated and embedded in epoxy resin (Durcupan, Fluka, UK).

## **4. Results and discussion**

### *4.1. GABAergic interneurons exhibit many forms of synaptic plasticity and some are specific to interneuron types*

Retrospectively, we can conclude that a large source of disagreement on whether the excitatory synapses onto interneurons undergo long-term plasticity stemmed from the experimental paradigms chosen to elicit plasticity, and from the diversity of GABAergic interneuron types. When initially testing a hypothesis on synaptic long-term potentiation (LTP) and –depression (LTD) in interneurons, it was assumed that the GABAergic neurons would undergo plasticity similar to that is seen in the principal pyramidal cells (for discussion, see McBain and Maccaferri (1997). However, later studies have revealed that many GABAergic interneuron subpopulations (but not all, see for instance Lamsa et al., 2005; Lamsa

et al., 2007a; Le Roux et al., 2013) fail to show the classic NMDA (N-methyl-D-aspartate) glutamate receptor-mediated synaptic LTP and LTD occurring in the pyramidal neurons (Kullmann and Lamsa, 2007). Instead, most GABAergic interneurons exhibit the LTP or the LTD with different induction mechanisms that require activation of metabotropic glutamate receptors (mGluRs), calcium-permeable  $\alpha$ -amino-3-hydroxy-5-methyl-4-isoxazolepropionic acid -glutamate receptors (CP-AMPA) or voltage-gated calcium channels (Galvan et al., 2011; Kullmann and Lamsa, 2011b; Pelkey et al., 2017). The LTP and LTD reported in interneurons in different brain regions in a rodent are summarized in **Figure 1**.

Another important reason explaining why no consensus existed for a long time with the interneuron plasticity results (see McBain and Maccaferri, 1997; Kullmann and Lamsa, 2011b) is the diversity of cortical GABAergic interneuron types (Ascoli et al., 2008; Klausberger and Somogyi, 2008). Cortical GABAergic neurons are currently classified into at least five different major subclasses whose specific features already emerge during early ontogenic development (for a review, see Pelkey et al., 2017). Thus, the pioneering studies examining synaptic plasticity in the GABAergic cortical neurons expected the interneurons to behave in this regard as a relatively homogenous group, akin to what had been observed with the principal neurons (Buzsaki and Eidelberg, 1982; Maccaferri and McBain, 1996; McMahan and Kauer, 1997; Cowan et al., 1998; Mahanty and Sah, 1998). Yet, later it was demonstrated that distinct interneuron subpopulations as well as different afferent pathways to an individual interneuron can strongly differ in their plasticity features (Lei and McBain, 2004; Lamsa et al., 2005; Nissen et al., 2010; Sambandan et al., 2010; Le Roux et al., 2013; Galvan et al., 2015; Zarnadze et al., 2016). Consequently, various early attempts to address the question whether the synaptic long-term potentiation exists in the GABAergic cells produced variable and inconclusive results (for a review see McBain and Maccaferri 1997). As more recent studies have shown, it is crucial that the cortical interneurons are tested for the hypothesis as distinct subgroups rather than as an entity (Lei and McBain, 2004; Kullmann and Lamsa, 2011b; Le Roux et al., 2013).

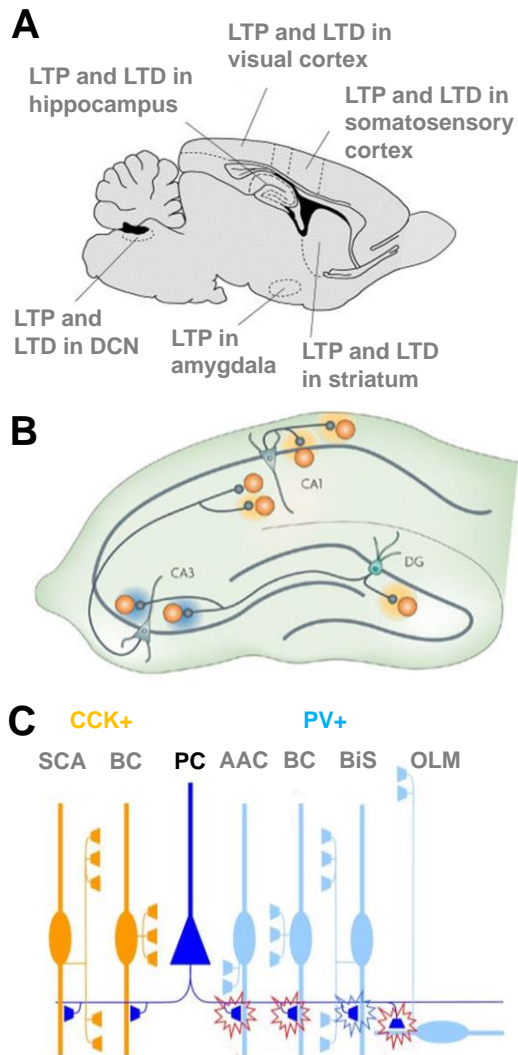


**Figure 1.** Synaptic long-term potentiation (LTP) and -depression (LTD) in the excitatory glutamatergic connections to GABAergic interneurons in different brain areas and postsynaptic interneuron types.

A) Schematic shows LTP and LTD as has been reported in different brain areas in a rodent. The original research articles describing the plasticity forms are enlisted in (Kullmann and Lamsa, 2011b). DCN states for a dorsal cochlear nucleus. B) LTP and LTD in unidentified GABAergic interneurons in the hippocampal CA1 and CA3 areas and the dentate gyrus (DG). Schematic depicts a transversal hippocampal slice with four excitatory synaptic pathways. Blue shading in a synapse indicates LTD, and yellow shows LTP.

C) NMDA receptor-independent LTP and LTD (or their absence) in the identified CA1 area interneuron types. Blue framing of a synapse indicates LTD, red means LTP. SCA, Schaffer collateral associated cell. BC, basket cell. PC, pyramidal neuron. AAC, axo-axonic cell. BiS, bistratified cell. OLM, oriens-lacunosum moleculare cell. CCK+, expressing cholecystinin. PV+, expressing parvalbumin. Modified images are based on: A, Kullmann and Lamsa (2011b); B, Kullmann and Lamsa (2007); C, Lamsa et al. (2010).

Work from many laboratories, including seminal work of prof. Peter Somogyi in the University of Oxford (UK), has demonstrated that hippocampal GABAergic interneurons represent various specialized cell types (Somogyi and Klausberger, 2005). Consequently, in the hippocampal CA1 area (field 1 in hippocampal area named as *Cornu Ammonis*) alone there are roughly twenty different GABAergic interneuron types (Klausberger and Somogyi, 2008). The hippocampus with its clearly identified GABAergic cell types allowed us to test a hypothesis whether synaptic long-term plasticity in interneurons was actually cell-type specific. Our results at least partly explained the previously inconsistent outcome of the interneuron plasticity experiments.

In 2005, we published a research article with prof. Dimitri Kullmann (University College London, UK) demonstrating that the hippocampus shows a clear spatial pattern for one

specific type of LTP (NMDAR-dependent) among the CA1 area interneurons (Lamsa et al., 2005).

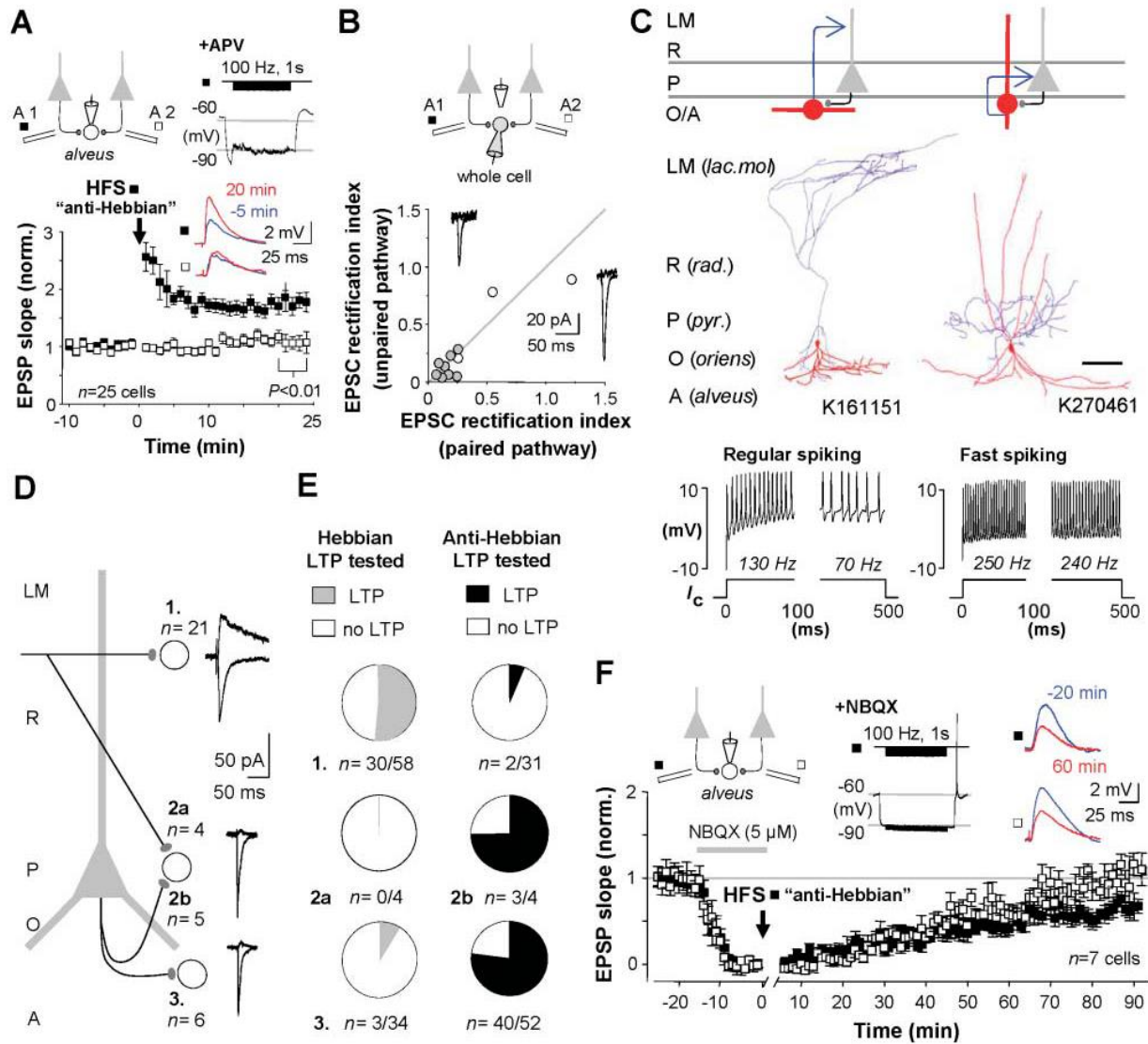


**Figure 2.** Hippocampal fast-spiking interneurons in the CA1 area exhibit a specific type of synaptic LTP that requires calcium-permeable AMPA receptors (CP-AMPA) and a different induction pattern than the LTP in pyramidal cells. A) Application of high-frequency stimulation to a synaptic pathway (black symbols) when a postsynaptic interneuron is hyperpolarized elicits the NMDAR-independent LTP, which is pathway specific (open symbols show control pathway). B) The glutamatergic synapses in the interneurons have CP-AMPA receptors indicated by EPSC inward rectification (rectification index below 1). C) Two visualized and identified cells showing the LTP; OLM cell and a fast-spiking basket cell. Scale 200 μm D) CP-AMPA receptors and the NMDAR-independent LTP are common in interneurons located in strata pyramidale (P) and oriens (O), and rare in GABAergic cells in strata radiatum (R) and locum-moleculare (LM). E) The NMDAR-dependent and the independent LTP occur in distinct CA1 area interneuron subpopulations. Note that not all tested interneurons show either type of LTP. F) The NMDAR-independent "anti-Hebbian" LTP requires CP-AMPA receptors. Transient blockade of AMPA receptors (by NBQX, horizontal bar) during the high-frequency stimulation prevents LTP in interneurons. Image adapted from Lamsa et al. (2007b).

We discovered that when using an associative pre- and postsynaptic discharge pairing protocol (identical to what is commonly used for LTP induction in pyramidal cells), less than half of the tested postsynaptic GABAergic cells showed LTP, while a majority failed to show plasticity. We reported these findings in two separate articles published in *Nature Neuroscience* (Lamsa et al., 2005) and *The Journal of Physiology* (Lamsa et al., 2007a), the former describing the phenomenon in interneurons and the latter uncovering its induction mechanism downstream to the NMDAR activation (which we found is different from that existing in pyramidal cells, since in the interneurons a beta isoform of Ca<sup>2+</sup>/calmodulin-dependent protein kinase II -enzyme is required for LTP, whereas in the CA1 pyramidal cells alpha isoform is necessary for the long-term potentiation).

The bimodal expression pattern of the NMDAR-mediated LTP among the CA1 area interneurons encouraged us to approach an anatomy specialist, prof. Somogyi, and suggest a collaboration project to test whether the plasticity in hippocampal interneurons is associated with anatomically specialized interneuron types. We set a simple hypothesis: testing two common LTP induction protocols, we investigated whether there is a correlation between the plasticity result and an identified postsynaptic interneurons type? This required rigorous *post hoc* anatomical and immunohistochemical analyses of the electrophysiologically investigated postsynaptic neurons. We first focused on the hippocampal O-LM interneuron type (named as *Oriens-Lacunosum Moleculare* interneuron because its axon characteristically occupies these layers) (McBain et al., 1994) in the CA1 area to test this idea. The O-LM cell was a good candidate to study this question, because there was already evidence in the literature showing that LTP often occurs in interneurons with soma in *stratum oriens* layer of the CA1 area (Perez et al., 2001). The O-LM interneuron somata locate in *stratum oriens*. Indeed, we were able to demonstrate that the O-LM cells consistently show LTP, which in addition was mechanistically different from the LTP in pyramidal cells. We published these findings in two research articles first showing the novel type of LTP occurring in many CA1 area interneurons (but not in pyramidal cells) and then demonstrating that it requires the activation of postsynaptic calcium-permeable AMPA receptors and group I metabotropic glutamate receptors (Lamsa et al., 2007b).

In addition, we demonstrated in the articles that the synapses to interneurons with this type of LTP do not show the conventional "pyramidal cell-like LTP" that requires the glutamatergic



postsynaptic cell was first recorded using a perforated patch -method to minimize dilution of the intracellular contents. It was crucial for stable long-lasting recordings that allowed testing subsequent plasticity protocols in the same neuron. For anatomical identification of postsynaptic cell type, the recorded neurons were re-patched with a conventional whole-cell micropipette, and the cells were filled with a marker molecule (neurobiotin or biocytin) for their *post hoc* visualization. The results played a key role in our review article published the same year in *Nature Reviews Neuroscience* (Kullmann and Lamsa, 2007).

This project generated two further research articles both released in *The Journal of Neuroscience* and published with Prof. Somogyi while I was in Oxford. We showed that the CP-AMPA-dependent LTP occurs not only in O-LM cells but in addition in other neurons expressing parvalbumin (PV) (note: some O-LM cells also exhibit this marker although weakly, see Ferraguti et al., 2004), more specifically basket cells and in axo-axonic cells, and in interneurons with no PV but with neuronal nitric acid synthase (nNOS) (Nissen et al., 2010; Szabo et al., 2012). On the contrary, this plasticity was absent in the CA1 area interneurons expressing cholecystinin (CCK) but not PV (Nissen et al., 2010). Key results of these findings are illustrated in **Figure 3**. In addition, we demonstrated that the O-LM cells and the nNOS-expressing ivy cells both exhibit CP-AMPA receptors and the CP-AMPA-dependent LTP because they lack the glutamate AMPA receptor subunit 2 (GluA2) (Szabo et al., 2012). Interestingly, later studies have revealed that interneuron types with CP-AMPA receptors are mostly derived from the same developmental brain area during early ontogenesis (Akgul and McBain, 2016). Hence, we speculate that the specific type of plasticity is already programmed in the interneurons during early ontogenesis.

#### *4.2. Identified interneuron types show the learning-related long-term plasticity in vivo*

Although *in vitro* slice preparation studies enabled the detailed investigation of interneuron plasticity mechanisms in many identified cell types – because the method easily allows long and stable recording from identified cells – it still remained open whether the same cell types would similarly show plasticity in the intact brain of a living animal. Interestingly, some publications already existed showing indirect evidence for the activity-induced long-term potentiation and -depression in interneurons of the hippocampal CA1 area (Buzsaki and Eidelberg, 1982; Dupret et al., 2013). In these articles, which utilized extracellular recording of

spiking activity of unidentified CA1 area interneurons, it was demonstrated that spike coupling of the presynaptic pyramidal cells (or their fibers) and the interneurons in a rat hippocampus was permanently strengthened or weakened by either a common LTP-induction paradigm (applying repetitive extracellular electrical stimulation, see Buzsaki and Eidelberg, 1982) or following spatial learning tasks (Dupret et al., 2013). However, neither of these studies did or was able to identify the postsynaptic interneuron types for methodological reasons.

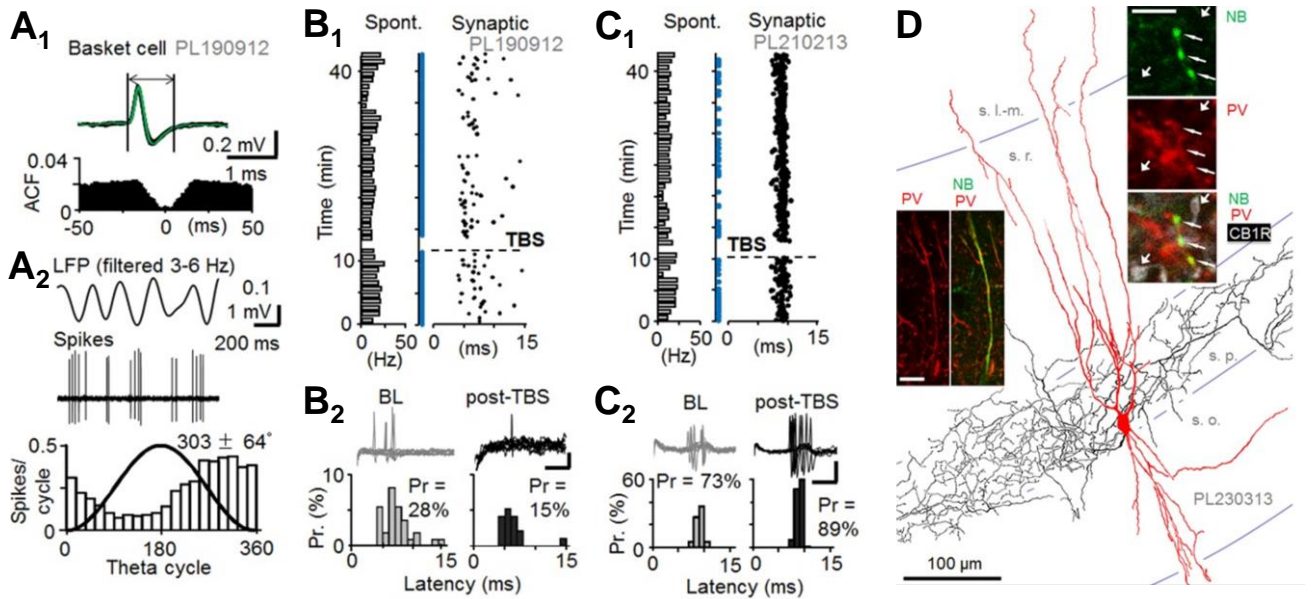


**Figure 4.** Fast-spiking PV+ basket cells (BCs) show long-term plasticity in a rat hippocampus *in vivo*. A) PV+ BCs in urethane-anaesthetized rats show characteristic spontaneous firing at low frequency (Klausberger et al., 2003). A1) Extracellularly recorded BC spikes in the CA1 area exhibit fast kinetics. Spontaneous firing shows no autocorrelative pattern. A2) The spontaneous firing occurs at low frequency and it is characteristically phase-locked to descending phase of the local field potential (LFP) theta oscillation cycle (Klausberger et al. 2003). B-C) High-frequency stimulation (HFS) induces either LTD- or LTP-like change in the single pulse stimulation-evoked spiking probability of the PV+ BCs. B1) A BC fires (“synaptic”) with a 5-10 ms delay to the contralateral site hippocampal CA1 stimulation, and the HFS induces a long-term decrease in the evoked spike probability. Note that spontaneous firing activity (shown left with bars) remains unaltered. B2) Individual traces and histograms summarize the reduced single shock-evoked basket cell firing probability after the HFS. Data shown in baseline and 30 min following the HFS. Scale 0.2 mV, 5 ms. C1-C2) Similar experiment from another PV+ BC showing long-term potentiation of the evoked spike probability. D) One recorded BC (with LTP) illustrated with immunoreactions. NB, neurobiotin. PV, parvalbumin. CB1R, cannabinoid receptor type 1. Image adapted from Lau et al. (2017).

Hence, we next investigated the long-term plasticity of synaptic excitatory drive of anatomically identified CA1 area interneurons *in vivo*. To optimize long-term stability of the recordings, the rats were anaesthetized during experiments (by combination of urethane, xylazine and ketamine). Rather than using a multichannel electrode (Dupret et al., 2013), we studied the interneuron spiking probability with an extracellularly juxtapositioned glass micropipette in response to microelectrode stimulation of afferent glutamatergic projection

fibers. The juxtacellular glass microelectrode recording method allowed us to label the studied cells with neurobiotin for *post hoc* anatomical analyses and identify interneuron type (Lau et al., 2017). We focused the study on the postsynaptic fast-spiking PV+ basket cells and the non fast-spiking nNOS+ (immunopositive for neuronal nitric oxide synthase) ivy cells, which we and others had previously shown in the *in vitro* slice preparation to exhibit robust LTP by the high-frequency stimulation (Alle et al., 2001; Nissen et al., 2010; Szabo et al., 2012; Campanac et al., 2013; Le Roux et al., 2013).

Similar to the results by Dupret et al. (2013) as well as Buzsaki and Eidelberg (1982), we found that the fast-spiking CA1 interneurons can generate either LTP or LTD following high-frequency glutamatergic fiber activity. Interestingly, when identifying the interneuron types we found that both the PV+ basket cells as well as the ivy cells could generate either LTP or LTD in these conditions. Because the results differed from what we had previously observed in slice preparations (*in vitro* the LTP was consistently generated in both of these CA1 interneuron types), we hypothesized that the direction of plasticity *in vivo* might be regulated by the underlying brain state in the anaesthetized animal defined by the local field potential oscillation pattern at the time when the plasticity was induced (see Kullmann and Lamsa, 2007). However, we found that neither did the occurrence of predominant theta (4-8 Hz) oscillation or slow wave (1 Hz) activity manage to explain whether the LTP or the LTD was generated in these interneurons (Lau et al., 2017).

Hence, we suggested that the complex plasticity results *in vivo* could possibly emerge from variable underlying modulatory effects of monoaminergic, cholinergic or endocannabinoid system in the experiments. Indeed, such modulations have been reported with pharmacological agents in slice preparations (Peterfi et al., 2012; Griguoli et al., 2013), and in intact brain such effects could be generated endogenously. Our results *in vivo* rat hippocampus were first reported in *Brain Structure and Function* (Lau et al., 2017) and the key findings are illustrated in **Figure 4**.

#### *4.3. Human cortical microcircuits show evolutionarily conserved interneuron plasticity with specific features*

We asked whether the interneuron plasticity reported in the rodent occurs similarly in the human brain, or if there are specific plasticity features in the human cortex not present in a rat or mice? The question is highly relevant, since recent studies have demonstrated that the human neocortical microcircuits are not identical to rodents but show various specializations in the intrinsic neuronal and synaptic functions (Molnar et al., 2008; Blazquez-Llorca et al., 2010; Defelipe, 2011; Testa-Silva et al., 2014; Eyal et al., 2016; Molnar et al., 2016; Sousa et al., 2017). Many of these adaptations are either enhancing the temporal signal processing or the spatial propagation of neuronal activity in the human neocortex. There is an emerging idea that some of these features may have evolved during the human evolution to enhance the brain computational power (DeFelipe et al., 2002; Lourenco and Bacci, 2017; Sousa et al., 2017). However, it had remained unknown whether the plasticity of GABAergic inhibitory circuits also showed specific functional features in the human cortex.

We investigated the question in acute slices prepared from neocortical tissue samples resected in a deep brain oncology or aneurism surgery in order to have the access to subcortical pathological target (Molnar et al., 2008; Szegedi et al., 2017). Such samples represent the closest to healthy control tissue, since the patients are typically operated with a short delay from the first symptoms and they lack systematic and persistent pre-medication (unlike the epilepsy patients) (Lourenco and Bacci, 2017). Importantly, the resected neocortical tissue samples in the operations locate far from the pathological target. For clarity, we have systematically reported in our studies the operated patient age, gender and their primary clinical diagnosis leading to the operation (Szegedi et al., 2016; Szegedi et al., 2017).

Whole-cell recordings from the layer 2-3 PV+ basket cells revealed a robust LTD in their glutamatergic afferents by the high-frequency bursting of the fibers. The LTD was similarly generated by extracellular stimulation in a rat and in the human (Szegedi et al. 2016). In both cases, the LTD showed presynaptic expression site and it was blocked by antagonist of the group I metabotropic glutamate receptors. The results are well in line with previous reports in rodents (Yazaki-Sugiyama et al., 2009) showing that metabotropic receptors mediate the LTD in the fast-spiking cortical interneurons (Lu et al., 2007; Peterfi et al., 2012).

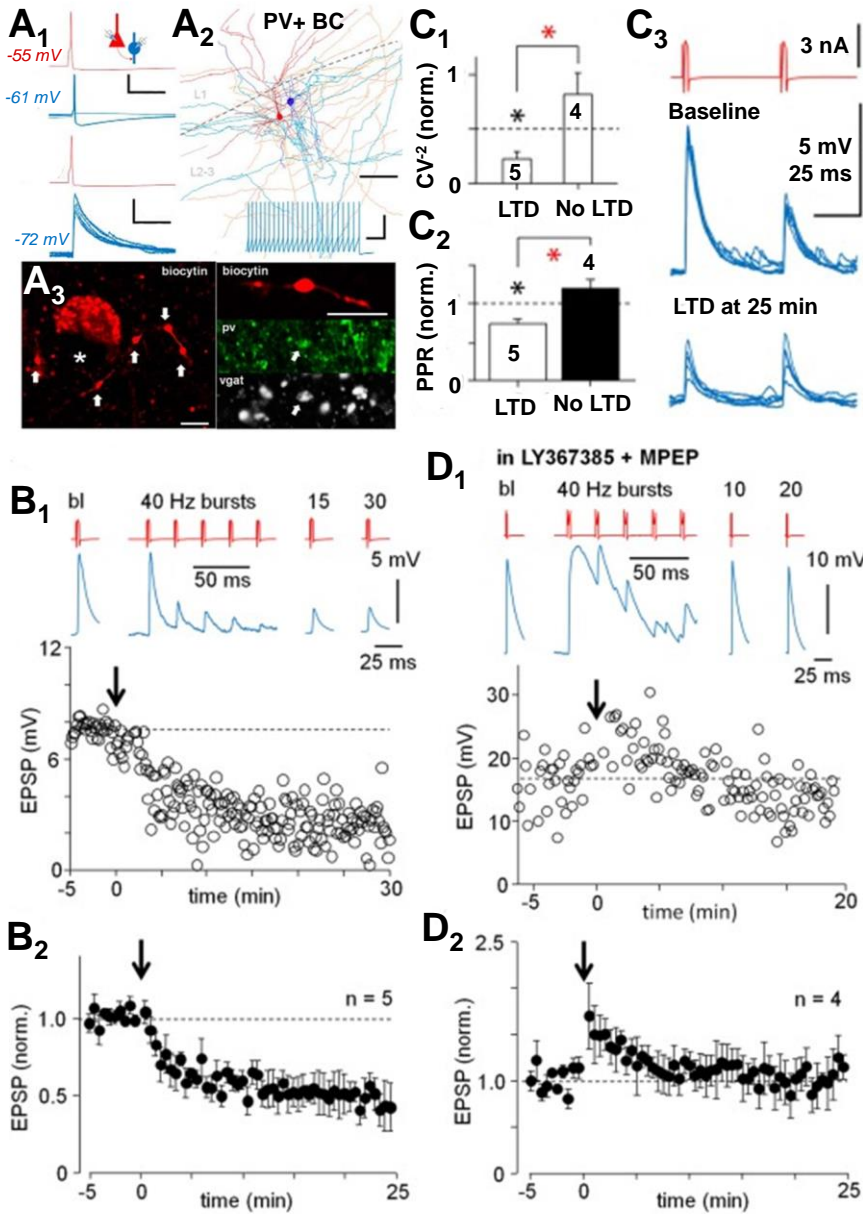


**Figure 5.** Fast-spiking PV+ basket cells (BCs) show synaptic long-term plasticity in human neocortex with specific features. Unlike rodents, the human neocortex contains very strong glutamatergic synapses that connect the layer 2-3 pyramidal cells (PCs) specifically to GABAergic interneurons (Molnar et al., 2008). These VLE connections (Very Large EPSPs) are based on synapses with multivesicular transmitter release (Molnar et al., 2016) and the EPSPs evoked in the BCs are often suprathreshold (Szegedi et al., 2017). **A<sub>1</sub>**) Visualized PC (red) to PV+ BC (blue; scale 40 mV, 20 ms) connection with a suprathreshold VLE (top). Bottom: post-synaptic hyperpolarization reveals the VLE. Blue trace scale 4 mV, 20 ms. **A<sub>2</sub>**) Illustration of the cell pair (PC red, BC blue). Scale 100  $\mu$ m. Inset shows the BC high-frequency firing pattern (scale 60 mV, 100 ms). **A<sub>3</sub>**) The BC axon (used to identify the cell) in the layer 2-3. Left: The boutons (arrow) are arranged around a nearby cell soma (asterisk). Confocal micrographs show the boutons are immunopositive for vgat and PV. Right: Scale bar 5  $\mu$ m. **B**) PC firing with high-frequency bursts (5 pulses at 40 Hz, 40 repeats) induces LTD in VLEs synapses. **B<sub>1</sub>**) A sample experiment. **B<sub>2</sub>**) Mean and s.e.m. of 5 experiments. **C**) LTD has presynaptic expression site indicated by the EPSP amplitude coefficient of variation (**C<sub>1</sub>**) and paired-pulse ratio (**C<sub>2</sub>**) in LTD. **C<sub>3</sub>**) Paired-pulse EPSPs in baseline and in LTD. **D**) LTD is blocked by antagonist of group I mGluRs. **D<sub>1</sub>**) A sample experiment. **D<sub>2</sub>**) Mean and s.e.m. of 4 experiments. Images adapted from Szegedi et al. (2016) and (2017).

Yet, about 15 % of pyramidal cell to fast-spiking interneuron connections in the human neocortex layer 2-3 exhibit very large monosynaptic glutamatergic EPSPs (VLEs, average amplitude 13 mV) elicited by single pyramidal cell spike (Molnar et al., 2008; Komlosi et al., 2012; Szegedi et al., 2016; Szegedi et al., 2017). The VLEs are often suprathreshold hence representing a microcircuit feature not occurring in a rat and being possibly specific to the human neocortex (Molnar et al., 2016). Importantly, we found that the strong synaptic VLE-connections are able to trigger the mGluR-dependent LTD independently; a high frequency bursting activity of just single pyramidal cell triggers the LTD, which in a rat required simultaneous co-activation of multiple glutamatergic fibers. The LTD in the single cell connections in the human is shown in detail in **Figure 5**. In our research article published in

*PLoS Biology*, we speculated that the VLE synapses – with their multivesicular glutamate release (Molnar et al., 2016) – may be sufficient to activate perisynaptic mGluRs critical for the LTD in postsynaptic PV+ cells. In the rat neocortex the mGluR activation requires spill-over glutamate released from several simultaneously active adjacent synapses (Rusakov et al., 1999).

Altogether, we found that similar plasticity – in terms of its induction by the high-frequency afferent fiber bursting and the pharmacological sensitivity – is induced in a rat and in the human neocortex glutamatergic synapses to PV+ basket cells. However, the strong VLE connections between two individual neurons in the human can trigger the plasticity independently. The results suggest an evolutionarily conserved mechanism for the interneuron plasticity in the mammalian neocortex, but reveal microcircuit level specializations between the species in the learning-related interneuron plasticity.

#### *4.4. Interneuron long-term plasticity produces permanent changes in local network activity both in the rodent and in the human*

Since GABAergic interneurons play a pivotal role in organizing the space and the time of cortical ensemble activity (see Introduction), we finally investigated whether the interneuron plasticity was sufficient to alter the activity in neuronal networks. First, we investigated this in the rodent hippocampus inducing the long-term plasticity in the CA1 area circuitry so that LTP was either restricted to postsynaptic pyramidal cells, or that it in parallel also occurred in the GABAergic interneurons.

The results summarized in **Figure 6** show that LTP in both the pyramidal cells and in the disynaptic GABAergic inhibition (i.e. LTP in interneurons) is required to preserve the high temporal fidelity of the CA1 pyramidal cells' input-output transformation (meaning the temporal accuracy how synaptic inputs from the CA3 area are integrated in the CA1 cells to generate their action potential firing) following CA3 area high-frequency bursting (Lamsa et al., 2005). In other words, we demonstrated that LTP in GABAergic interneurons is needed to preserve fast co-incidence detection in the excitatory signal transmission from the CA3 to CA1 area in the face of learning and LTP in pyramidal neurons. The results stress the importance of GABAergic interneuron long-term plasticity during hippocampal learning processes.

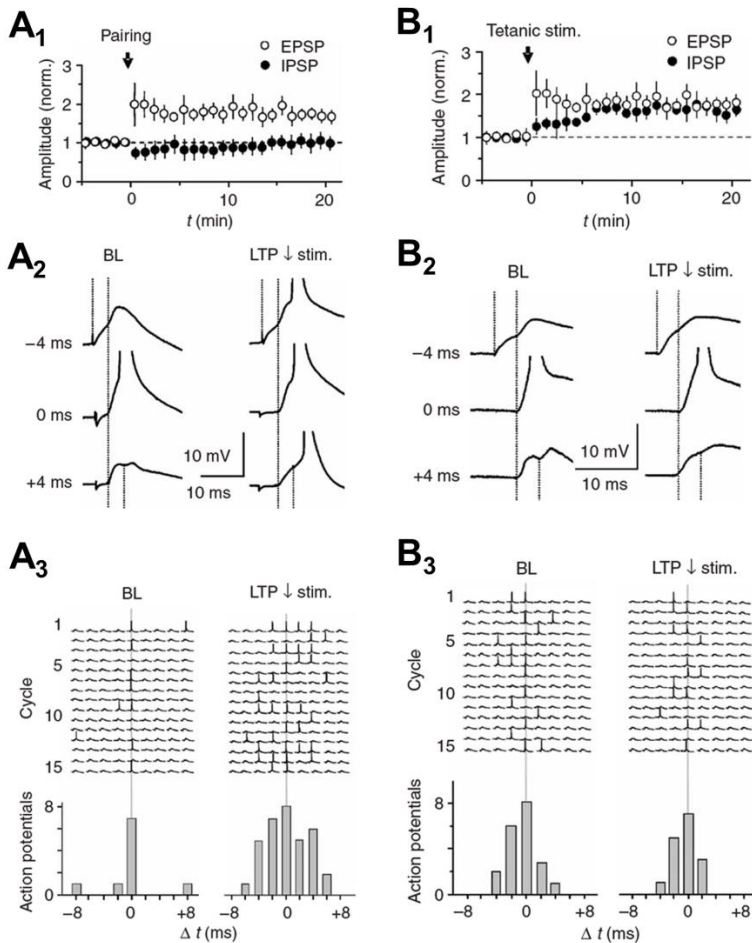


**Figure 6.** Synaptic plasticity in hippocampal interneurons permanently modifies input integration in the CA1 area pyramidal cells (PCs). A) LTP restricted between PC synapses compromises temporal fidelity of the input-output operation in the CA1 circuit. A1) LTP in single-shock (extracellular stimulation) -evoked monosynaptic EPSP, but not in disynaptic IPSP in a CA1 pyramidal cell. The LTP was induced by low-frequency (1 Hz) stimulation of the pathway paired with postsynaptic depolarization (timing indicated by “pairing”). A2) Temporal summation of two such pathways. In baseline, the PC generates action potential only when the two input pathways are active precisely at the same time (lag 0 ms). Following the LTP, the spike generation occurs in a wider time window. A3) Consecutive cycles pairing the two pathways with different lags (from -8 ms to +8 ms) in baseline and following the LTP. Histograms summarize widening of the time window for spike generation after the LTP. B) Parallel LTP in monosynaptic EPSP and disynaptic IPSP preserves narrow time window for spike generation in the CA1 pyramidal cells. B1) High-frequency extracellular stimulation (“tetanic stim.”) results in LTP of both the EPSP and the disynaptic IPSP. B2) Sample traces showing temporal integration of two input pathways with EPSP and disynaptic IPSP. Both in the baseline and LTP, the spike generation only occurs when the two input pathways are activated with zero lag. A3) Fifteen consecutive cycles in baseline and in the LTP in one experiment showing the input integration in a CA1 PC with different lag in their activation (from -8 ms to +8 ms). Adapted from Lamsa et al. (2005).

Correspondingly, in the human neocortex the layer 2-3 single pyramidal cell spike -evoked network activity (called complex events or the ensembles) allowed us to test if the plasticity in pyramidal cell-to-interneuron synapses was able to modify the evoked network activity. Indeed, we found that in parallel with the mGluR-dependent LTD in the fast-spiking PV+ basket cells, there was a change in the complex event pattern evoked; the PV+ basket cells, which are characteristically activated at the earliest phase of the complex events (Szegedi et al., 2017), were silenced in the evoked ensembles by the mGluR-dependent LTD (Szegedi et al., 2016). These results show that also in human neocortex the long-term plasticity in PV+ interneurons leaves a permanent imprint in the network activity pattern evoked in the local circuitry.

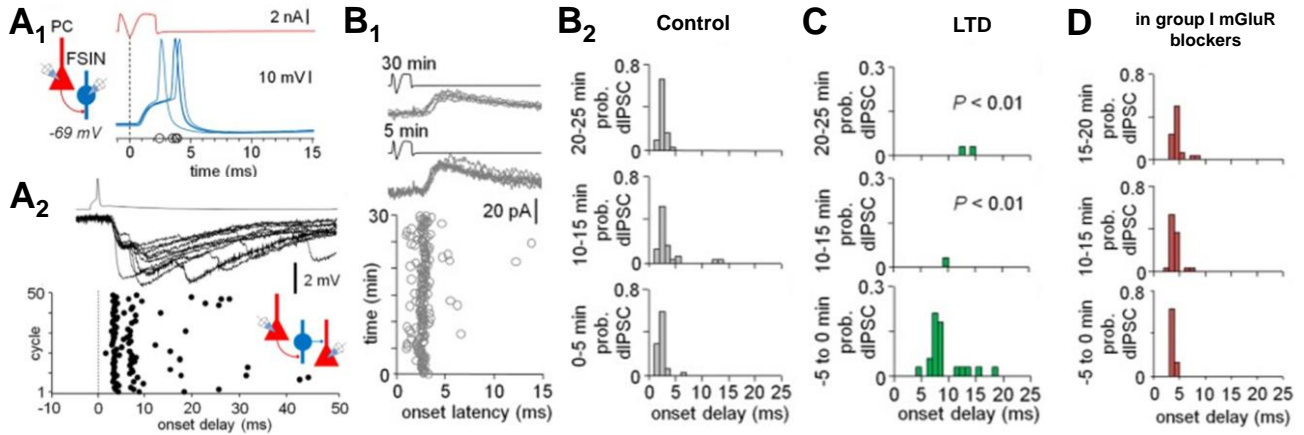


**Figure 7.** Long-term plasticity in interneurons alters the neuronal ensemble activation in the human neocortex. A1) Single spike in layer 2-3 pyramidal cell (PC) elicits a large amplitude EPSP (VLE) in fast-spiking interneuron (FSIN). A2) In parallel a PC spike triggers a complex event with di- and polysynaptic IPSPs in a nearby pyramidal cell. Plot shows 50 consecutive complex events triggered by the PC. Note that first wave of IPSPs is similarly time-locked to PC spike as the basket cell firing in A1. B1) The first wave of inhibition in complex events plotted for 30 consecutive events (recorded in voltage clamp). B2) Histogram plotting the first IPSCs in control conditions in the 30 cycles. C) Same high-frequency PC bursting pattern that elicits the LTD in VLE synapses onto basket cells, causes a permanent suppression of the first wave of the complex event. Note that the time-locked early IPSC (bottom) disappears after the PC bursting (middle and upper histograms). D) The suppression of the early complex event activity is blocked by group I mGluR antagonist, similar to the LTD in PC to BC synapses shown in Figure 5. Images adapted from Szegedi et al. (2016) and (2017).

## 5. Conclusions

Various laboratories during the past decade have shown that learning-related and activity-induced long term plasticity occurs not only in the cortical pyramidal cells but in addition in the GABAergic inhibitory interneurons. Our laboratory has contributed to this endeavor showing that glutamatergic excitatory fibers undergo long-term plasticity in specialized anatomically identified cortical interneuron types in a rodent as well as in the human. We have demonstrated that same cell types that exhibit the plasticity *in vitro* slice preparations, do also show LTP and LTD *in vivo* rodent brain. Importantly, in these interneurons the cellular mechanisms and the induction pattern of LTP often differ from that known in pyramidal cells. The interneuron-specific plasticity mechanisms may reflect their different physiological firing pattern in learning processes, such as in the hippocampus during spatial learning tasks (Klausberger and Somogyi, 2008).

## 6. References

Akgul G, McBain CJ (2016) Diverse roles for ionotropic glutamate receptors on inhibitory interneurons in developing and adult brain. *The Journal of Physiology* 594:5471-5490.

- Alle H, Jonas P, Geiger JR (2001) PTP and LTP at a hippocampal mossy fiber-interneuron synapse. *Proceedings of the National Academy of Sciences of the United States of America* 98:14708-14713.
- Ascoli GA et al. (2008) Petilla terminology: nomenclature of features of GABAergic interneurons of the cerebral cortex. *Nature Reviews Neuroscience* 9:557-568.
- Bartos M, Alle H, Vida I (2011) Role of microcircuit structure and input integration in hippocampal interneuron recruitment and plasticity. *Neuropharmacology* 60:730-739.
- Blazquez-Llorca L, Garcia-Marin V, DeFelipe J (2010) GABAergic complex basket formations in the human neocortex. *The Journal of Comparative Neurology* 518:4917-4937.
- Buzsaki G, Eidelberg E (1982) Direct afferent excitation and long-term potentiation of hippocampal interneurons. *Journal of Neurophysiology* 48:597-607.
- Buzsaki G, Llinas R (2017) Space and time in the brain. *Science* 358:482-485.
- Camire O, Topolnik L (2014) Dendritic calcium nonlinearities switch the direction of synaptic plasticity in fast-spiking interneurons. *The Journal of Neuroscience* 34:3864-3877.
- Campanac E, Gasselín C, Baude A, Rama S, Ankri N, Debanne D (2013) Enhanced intrinsic excitability in basket cells maintains excitatory-inhibitory balance in hippocampal circuits. *Neuron* 77:712-722.
- Cowan AI, Stricker C, Reece LJ, Redman SJ (1998) Long-term plasticity at excitatory synapses on aspiny interneurons in area CA1 lacks synaptic specificity. *Journal of Neurophysiology* 79:13-20.
- Defelipe J (2011) The evolution of the brain, the human nature of cortical circuits, and intellectual creativity. *Frontiers in Neuroanatomy* 5:29.
- DeFelipe J, Alonso-Nanclares L, Arellano JI (2002) Microstructure of the neocortex: comparative aspects. *Journal of Neurocytology* 31:299-316.
- Dupret D, O'Neill J, Csicsvari J (2013) Dynamic reconfiguration of hippocampal interneuron circuits during spatial learning. *Neuron* 78:166-180.
- Eyal G, Verhoog MB, Testa-Silva G, Deitcher Y, Lodder JC, Benavides-Piccione R, Morales J, DeFelipe J, de Kock CP, Mansvelder HD, Segev I (2016) Unique membrane properties and enhanced signal processing in human neocortical neurons. *eLife* 5.
- Ferraguti F, Cobden P, Pollard M, Cope D, Shigemoto R, Watanabe M, Somogyi P (2004) Immunolocalization of metabotropic glutamate receptor 1alpha (mGluR1alpha) in distinct classes of interneuron in the CA1 region of the rat hippocampus. *Hippocampus* 14:193-215.
- Galvan EJ, Cosgrove KE, Barrionuevo G (2011) Multiple forms of long-term synaptic plasticity at hippocampal mossy fiber synapses on interneurons. *Neuropharmacology* 60:740-747.
- Galvan EJ, Perez-Rosello T, Gomez-Lira G, Lara E, Gutierrez R, Barrionuevo G (2015) Synapse-specific compartmentalization of signaling cascades for LTP induction in CA3 interneurons. *Neuroscience* 290:332-345.
- Galvan EJ, Cosgrove KE, Mauna JC, Card JP, Thiels E, Meriney SD, Barrionuevo G (2010) Critical involvement of postsynaptic protein kinase activation in long-term potentiation at hippocampal mossy fiber synapses on CA3 interneurons. *The Journal of Neuroscience* 30:2844-2855.
- Griguoli M, Cellot G, Cherubini E (2013) In hippocampal oriens interneurons anti-Hebbian long-term potentiation requires cholinergic signaling via alpha7 nicotinic acetylcholine receptors. *The Journal of Neuroscience* 33:1044-1049.
- Klausberger T, Somogyi P (2008) Neuronal diversity and temporal dynamics: the unity of hippocampal circuit operations. *Science* 321:53-57.

- Klausberger T, Magill PJ, Marton LF, Roberts JD, Cobden PM, Buzsaki G, Somogyi P (2003) Brain-state- and cell-type-specific firing of hippocampal interneurons in vivo. *Nature* 421:844-848.
- Komlosi G, Molnar G, Rozsa M, Olah S, Barzo P, Tamas G (2012) Fluoxetine (prozac) and serotonin act on excitatory synaptic transmission to suppress single layer 2/3 pyramidal neuron-triggered cell assemblies in the human prefrontal cortex. *The Journal of Neuroscience* 32:16369-16378.
- Kullmann DM, Lamsa KP (2007) Long-term synaptic plasticity in hippocampal interneurons. *Nature Reviews Neuroscience* 8:687-699.
- Kullmann DM, Lamsa KP (2011a) Interneurons go plastic. *Neuropharmacology* 60:711.
- Kullmann DM, Lamsa KP (2011b) LTP and LTD in cortical GABAergic interneurons: emerging rules and roles. *Neuropharmacology* 60:712-719.
- Kullmann DM, Moreau AW, Bakiri Y, Nicholson E (2012) Plasticity of inhibition. *Neuron* 75:951-962.
- Laezza F, Doherty JJ, Dingledine R (1999) Long-term depression in hippocampal interneurons: joint requirement for pre- and postsynaptic events. *Science* 285:1411-1414.
- Lamsa K, Heeroma JH, Kullmann DM (2005) Hebbian LTP in feed-forward inhibitory interneurons and the temporal fidelity of input discrimination. *Nature Neuroscience* 8:916-924.
- Lamsa K, Irvine EE, Giese KP, Kullmann DM (2007a) NMDA receptor-dependent long-term potentiation in mouse hippocampal interneurons shows a unique dependence on Ca(2+)/calmodulin-dependent kinases. *The Journal of Physiology* 584:885-894.
- Lamsa KP, Kullmann DM, Woodin MA (2010) Spike-timing dependent plasticity in inhibitory circuits. *Frontiers in Synaptic Neuroscience* 2:8.
- Lamsa KP, Heeroma JH, Somogyi P, Rusakov DA, Kullmann DM (2007b) Anti-Hebbian long-term potentiation in the hippocampal feedback inhibitory circuit. *Science* 315:1262-1266.
- Lau PY, Katona L, Saghy P, Newton K, Somogyi P, Lamsa KP (2017) Long-term plasticity in identified hippocampal GABAergic interneurons in the CA1 area in vivo. *Brain Structure & Function* 222:1809-1827.
- Le Roux N, Cabezas C, Bohm UL, Poncer JC (2013) Input-specific learning rules at excitatory synapses onto hippocampal parvalbumin-expressing interneurons. *The Journal of Physiology* 591:1809-1822.
- Lei S, McBain CJ (2004) Two Loci of expression for long-term depression at hippocampal mossy fiber-interneuron synapses. *The Journal of Neuroscience* 24:2112-2121.
- Lisman J (2017) Criteria for identifying the molecular basis of the engram (CaMKII, PKMzeta). *Molecular Brain* 10:55.
- Lourenco J, Bacci A (2017) Human-Specific Cortical Synaptic Connections and Their Plasticity: Is That What Makes Us Human? *PLoS Biology* 15:e2001378.
- Lu JT, Li CY, Zhao JP, Poo MM, Zhang XH (2007) Spike-timing-dependent plasticity of neocortical excitatory synapses on inhibitory interneurons depends on target cell type. *The Journal of Neuroscience* 27:9711-9720.
- Maccaferri G, McBain CJ (1996) Long-term potentiation in distinct subtypes of hippocampal nonpyramidal neurons. *The Journal of Neuroscience* 16:5334-5343.
- Mahanty NK, Sah P (1998) Calcium-permeable AMPA receptors mediate long-term potentiation in interneurons in the amygdala. *Nature* 394:683-687.
- McBain CJ, Maccaferri G (1997) Synaptic plasticity in hippocampal interneurons? A commentary. *Canadian Journal of Physiology and Pharmacology* 75:488-494.

- McBain CJ, DiChiara TJ, Kauer JA (1994) Activation of metabotropic glutamate receptors differentially affects two classes of hippocampal interneurons and potentiates excitatory synaptic transmission. *The Journal of Neuroscience* 14:4433-4445.
- McBain CJ, Freund TF, Mody I (1999) Glutamatergic synapses onto hippocampal interneurons: precision timing without lasting plasticity. *Trends in Neurosciences* 22:228-235.
- McMahon LL, Kauer JA (1997) Hippocampal interneurons express a novel form of synaptic plasticity. *Neuron* 18:295-305.
- Molnar G, Rozsa M, Baka J, Holderith N, Barzo P, Nusser Z, Tamas G (2016) Human pyramidal to interneuron synapses are mediated by multi-vesicular release and multiple docked vesicles. *eLife* 5.
- Molnar G, Olah S, Komlosi G, Fule M, Szabadics J, Varga C, Barzo P, Tamas G (2008) Complex events initiated by individual spikes in the human cerebral cortex. *PLoS Biology* 6:e222.
- Nicholson E, Kullmann DM (2017) T-type calcium channels contribute to NMDA receptor independent synaptic plasticity in hippocampal regular-spiking oriens-alveus interneurons. *The Journal of Physiology* 595:3449-3458.
- Nissen W, Szabo A, Somogyi J, Somogyi P, Lamsa KP (2010) Cell type-specific long-term plasticity at glutamatergic synapses onto hippocampal interneurons expressing either parvalbumin or CB1 cannabinoid receptor. *The Journal of Neuroscience* 30:1337-1347.
- Oren I, Nissen W, Kullmann DM, Somogyi P, Lamsa KP (2009) Role of ionotropic glutamate receptors in long-term potentiation in rat hippocampal CA1 oriens-lacunosum moleculare interneurons. *The Journal of Neuroscience* 29:939-950.
- Pelkey KA, McBain CJ (2008) Target-cell-dependent plasticity within the mossy fibre-CA3 circuit reveals compartmentalized regulation of presynaptic function at divergent release sites. *The Journal of Physiology* 586:1495-1502.
- Pelkey KA, Lavezzari G, Racca C, Roche KW, McBain CJ (2005) mGluR7 is a metaplastic switch controlling bidirectional plasticity of feedforward inhibition. *Neuron* 46:89-102.
- Pelkey KA, Chittajallu R, Craig MT, Tricoire L, Wester JC, McBain CJ (2017) Hippocampal GABAergic Inhibitory Interneurons. *Physiological Reviews* 97:1619-1747.
- Perez Y, Morin F, Lacaille JC (2001) A hebbian form of long-term potentiation dependent on mGluR1a in hippocampal inhibitory interneurons. *Proceedings of the National Academy of Sciences of the United States of America* 98:9401-9406.
- Peterfi Z, Urban GM, Papp OI, Nemeth B, Monyer H, Szabo G, Erdelyi F, Mackie K, Freund TF, Hajos N, Katona I (2012) Endocannabinoid-mediated long-term depression of afferent excitatory synapses in hippocampal pyramidal cells and GABAergic interneurons. *The Journal of Neuroscience* 32:14448-14463.
- Poo MM, Pignatelli M, Ryan TJ, Tonegawa S, Bonhoeffer T, Martin KC, Rudenko A, Tsai LH, Tsien RW, Fishell G, Mullins C, Goncalves JT, Shtrahman M, Johnston ST, Gage FH, Dan Y, Long J, Buzsaki G, Stevens C (2016) What is memory? The present state of the engram. *BMC Biology* 14:40.
- Ross ST, Soltesz I (2001) Long-term plasticity in interneurons of the dentate gyrus. *Proceedings of the National Academy of Sciences of the United States of America* 98:8874-8879.
- Rusakov DA, Kullmann DM, Stewart MG (1999) Hippocampal synapses: do they talk to their neighbours? *Trends in Neurosciences* 22:382-388.
- Sambandan S, Sauer JF, Vida I, Bartos M (2010) Associative plasticity at excitatory synapses facilitates recruitment of fast-spiking interneurons in the dentate gyrus. *The Journal of Neuroscience* 30:11826-11837.
- Somogyi P, Klausberger T (2005) Defined types of cortical interneurone structure space and spike timing in the hippocampus. *The Journal of Physiology* 562:9-26.

- Sousa AMM, Meyer KA, Santpere G, Gulden FO, Sestan N (2017) Evolution of the Human Nervous System Function, Structure, and Development. *Cell* 170:226-247.
- Szabo A, Somogyi J, Cauli B, Lambolez B, Somogyi P, Lamsa KP (2012) Calcium-permeable AMPA receptors provide a common mechanism for LTP in glutamatergic synapses of distinct hippocampal interneuron types. *The Journal of Neuroscience* 32:6511-6516.
- Szegedi V, Paizs M, Csakvari E, Molnar G, Barzo P, Tamas G, Lamsa K (2016) Plasticity in Single Axon Glutamatergic Connection to GABAergic Interneurons Regulates Complex Events in the Human Neocortex. *PLoS Biology* 14:e2000237.
- Szegedi V, Molnar G, Paizs M, Csakvari E, Barzo P, Tamas G, Lamsa K (2017) High-Precision Fast-Spiking Basket Cell Discharges during Complex Events in the Human Neocortex. *eNeuro* 4.
- Testa-Silva G, Verhoog MB, Linaro D, de Kock CP, Baayen JC, Meredith RM, De Zeeuw CI, Giugliano M, Mansvelder HD (2014) High bandwidth synaptic communication and frequency tracking in human neocortex. *PLoS Biology* 12:e1002007.
- Tonegawa S, Pignatelli M, Roy DS, Ryan TJ (2015) Memory engram storage and retrieval. *Current Opinion in Neurobiology* 35:101-109.
- Topolnik L (2012) Dendritic calcium mechanisms and long-term potentiation in cortical inhibitory interneurons. *The European Journal of Neuroscience* 35:496-506.
- Yazaki-Sugiyama Y, Kang S, Cateau H, Fukai T, Hensch TK (2009) Bidirectional plasticity in fast-spiking GABA circuits by visual experience. *Nature* 462:218-221.
- Zarnadze S, Bauerle P, Santos-Torres J, Bohm C, Schmitz D, Geiger JR, Dugladze T, Gloveli T (2016) Cell-specific synaptic plasticity induced by network oscillations. *eLife* 5.

## 7. Other scientific activities

### 7.1. Original research articles forming the base of application

i. Hebbian LTP in feed-forward inhibitory interneurons and the temporal fidelity of input discrimination

**Lamsa K**, Heeroma JH, Kullmann DM.  
*Nat Neurosci.* 2005. (7):916-24

ii. Anti-Hebbian long-term potentiation in the hippocampal feedback inhibitory circuit

**Lamsa K**, Heeroma JH, Somogyi P, Rusakov DA, Kullmann DM.  
*Science.* 2007. 315(5816):1262-6

iii. Cell type-specific long-term plasticity at glutamatergic synapses onto hippocampal interneurons expressing either parvalbumin or CB1 cannabinoid receptor.

Nissen W, Szabo A, Somogyi J, Somogyi P, **Lamsa K**.  
*The Journal of Neuroscience.* 2010. 30:1337-1347

iv. Long-term plasticity in identified hippocampal GABAergic interneurons in the CA1 area in vivo

Lau PY, Katona L, Saghy P, Newton K, Somogyi P, **Lamsa K**  
*Brain Struct Funct.* 2017. 222(4):1809-1827

v. Plasticity in Single Axon Glutamatergic Connection to GABAergic Interneurons Regulates Complex Events in the Human Neocortex

Szegedi V, Paizs M, Csakvari E, Molnar G, Barzo P, Tamas G, **Lamsa K**.  
*PLoS Biol.* 2016. 9;14(11):e2000237

### 7.2. Most important talks at scientific meetings

- 06/2018 EMBO workshop "Cortical Interneurons in Health and Disease", 17-20 June 2018, Mallorca, Spain
- 04/2018 Symposium "Neuroplasticity: from synapses to circuits", 15-16 April 2018, Marseille, France
- 09/2017 Symposium "Human-specific cortical microcircuit function and structure" in FENS Regional Meeting (20-23 September, 2017) in Pecs, Hungary
- 06/2016 Symposium "Heterogeneity and convergence: synaptic and network pathophysiology in brain disorders", 13 June, Hungarian Academy of Sciences, KOKI, Budapest, Hungary
- 12/2015 Symposium "Brain and Mind" in Helsinki, 15 Dec, 2015, Finland
- 03/2014 The Oxford Neuroscience Symposium, 26th March, 2014, Oxford, UK
- 09/2013 Symposium "Inhibitory Interactions In Brain Plasticity" in Cracow, 5-7 Sept, 2013, Poland
- 07/2013 Symposium Neurosciences at the European Biophysics Congress, EBSA2013, 13-17 July, 2013 Lisbon, Portugal
- 06/2013 Symposium in Spring Hippocampal Research Conference, 9-14 June, 2013 Taormina, Sicily
- 03/2013 Symposium "Synaptic plasticity in GABAergic cells" in 92nd Annual Meeting of the German Physiological Society, Heidelberg March 2-5, 2013, Germany

- 11/2012 Janelia Conference, 'Neuron Types in the Hippocampal Formation: Structure, Activity, and Molecular Genetics', November 11 - 14, 2012, USA
- 10/2011 BCCN-lecture in Bernstein Center for Computational Neuroscience, Berlin, Germany
- 6/2009 Symposium "Cortical interneurons in health and disease", Costa d'En Blanes, Mallorca, Spain
- 10/2009 B.R.A.I.N platform lecture, University of Toronto, Canada
- 12/2006 Inhibition symposium in Cold Spring Harbour, USA

### *7.3. Supervised PhD students*

- D.Phil. supervisor to Ms Wiebke Nissen (2008-2012 in Oxford University, UK). Currently Research Scientist in Boehringer Ingelheim Ltd, Germany
- D.Phil. supervisor to Mr Joram van Rheede (2010-2013 in Oxford University, UK). Currently Postdoctoral fellow in Nuffield Department of Clinical Neurosciences, Oxford University, UK
- D.Phil. supervisor to Ms Petrina Lau (2010-2015 in Oxford University, UK). Currently Postdoctoral Fellow in MRC Harwell, Mammalian Genetics Unit, Oxfordshire, UK
- D.Phil. supervisor to Mr Dimitrios Kotzadimitriou (2012-2017 in Oxford University, UK). Currently Postdoctoral Fellow in ION/UCL, London, UK

### *7.4. Lectures given in doctoral programs*

- Finland: Visiting teacher in "Neuronal Signaling and Plasticity lecture series" in University of Helsinki Neuroscience Center (2004-)
- UK Plymouth Microelectrode Workshop (2006-2015) organized by the Physiological Society UK (one lecture and one week supervisor of daily practicals).
- UK Oxford University (2008-2014):
  - 2 lectures per year; "Inhibition in the CNS" and "Experimental epilepsy"
  - 2 lectures in per year; "Introduction to the CNS" and "Neurotransmission in the CNS"
  - 1 lecture per year in Oxford Medical School; "Mechanisms of synaptic inhibition in the brain"
  - 8 days per year giving practicals (4 hours each) in Oxford Medical faculty, second year student course for clinical students: "Effects of drugs on neuromuscular transmission"

### *7.5. Training of postdoctoral fellows*

- Dr Andras Szabo (Oxford University, UK), 2009-2011
- Dr Wiebke Nissen (Oxford University, UK), 2012-2013
- Dr Petrina Yau-Pok Lau (Oxford University, UK), 2015
- Dr Eszter Csakvari (Szeged University, Hungary), 2016-2017
- Dr Viktor Szegedi (Szeged University, Hungary), 2015-till present
- Dr Melinda Paizs (Szeged University, Hungary), 2015-till present

### *7.6. Organization of domestic and international symposia*

- MRC Anatomical Neuropharmacology Science Day (29 May, 2013) in Oxford University, UK
- Organizer of symposium: "Human-specific cortical microcircuit function and structure", FENS Regional Meeting (20-23 September, 2017) in Pecs, Hungary

### *7.7. Memberships in editorial or review boards*

- Guest Editor in Neuropharmacology special issue “Synaptic Plasticity and Interneurons”, Autumn 2010.
- Associate Editor in Frontiers in Synaptic Neuroscience, March 2012-
- Reviewing Editor in Frontiers in Molecular Neuroscience, Apr 2015-
- Guest Editor in Frontiers in Neural circuits special issue “Calcium-permeable AMPAR-mediated plasticity”, Autumn 2017-Spring 2018.

### *7.8. Memberships in scientific committees*

- France: Member of external scientific evaluation committee for AERES (Evaluation Agency for Research and Higher education) for research groups in Institut du Fer a Moulin, Paris France (Feb, 2013).
- UK: Member of interview and advisory committee for Wellcome Trust/NIH Four Year PhD Programme (Feb, 2013).
- Finland: University of Helsinki, assessing applications for Docentship (adjunct professor) (Jan 2015).
- Hungary: Member of the review panel of the Hungarian Scientific Research Fund (OTKA) in the field of Neurosciences (2015-2018).
- Hungary: Member of the internal evaluation committee of the Hungarian Scientific Research Fund (OTKA) in Neurosciences (2016-2018).
- Pakistan: Evaluating Faculty Professorship Promotions for NUST (2016, 2017).

### *7.9. Scientific awards*

- Best physiological thesis of the year awarded by the Finnish Physiological Society, Finland (2000).

### *7.10. Personal research grants and fellowships*

- The Academy of Finland personal grant for research work abroad 01/02-12/03 (EUR 51.000)
- Wellcome Trust Travelling Research Fellowship 10/02-09/04 (£103,645)
- Wellcome Trust Research Career Development Fellowship 09/07-08/12 (£904,112)
- John Fell OUP Funds (University of Oxford) Research Development Grant 04/10-04/12 (£35,500)
- The Physiological Society, International Junior Research Grant for Mr Tamas Bellak (host Dr Lamsa) 09/10 (£5,000)
- Medical Research Council (Senior Scientist funding) 09/12-03/15 (£215,739)
- The Hungarian Academy of Sciences (MTA) 01/01/15-31/12/2017 (199,958,000 HUF).
- The Hungarian Academy of Sciences (MTA) 01/01/18-31/12/2021 (120,000,000 HUF)

### *7.11. Grant reviewing activities*

- UK
  - BBSRC, grant application peer reviews (2013-)
  - Wellcome Trust, grant application peer reviews (2007-); Fellowship application peer reviews (2009, 2011);
  - Medical Research Council, grant application peer reviews (2007-).

- Canada
  - Foundation for Innovation competition (Dec, 2011),
  - University of Toronto grant application reviews (2012).
- EU
  - ERC Advanced grant call application reviews (2017).
- France
  - The National Research Agency (ANR) (2012, 2016, 2017).
  - Young Researchers Program (2013).
- Hungary
  - the Hungarian Scientific Research Fund in Neurosciences (2015-2018).
  - research grants evaluation for IDEGT (2016).
- Netherlands
  - The Netherlands Organisation for Scientific Research (NWO) (2016).
- Republic of South Africa
  - National Research Foundation, Scholarships & Fellowships Programme (2012).

### *7.12. Public outreach*

- Expert commentaries in Tiede –scientific magazine (Sanoma Magazines, Finland)
- Interview in an article in Yliopistolainen- newspaper on Finnish brain drain in science (Issue Nov, 2008).
- Presentation (1 min 30 sec) in local TV news on research of human brain tissue in the University of Szeged, Hungary, 8th Jan 2016
- Interview in TV science documentary (10 min) on human brain evolution. Local television channel, Hungary, 11th Jan 2016
- Interview in a county newspaper “Délmagyarország” on the human tissue research in our laboratory 18th Jan 2016
- Public lecture “What makes us human?” 30 Mar 2017, Budapest embassy of Finland

## **8. Summary of the most significant results**

Our results have shown that learning-related synaptic plasticity takes place in the cortical inhibitory interneurons in a cell type-specific manner (Kullmann and Lamsa 2007, 2011a, 2011b). Distinct GABAergic cell subclasses, defined by their protein expression profile and the anatomy structure, prefer different neuronal activity patterns to generate the plasticity and they show different molecular mechanisms in the plasticity process (Lamsa et al. 2005, 2007; Nissen et al. 2010). We have demonstrated this in a rodent and more recently also in the human cortex (Lau et al. 2017, Szegedi et al. 2016). In addition, we have shown that the interneuron plasticity is sufficient to permanently alter the signal transduction in local neuronal networks both in the rodent and in the human cortex. Our results suggest that synaptic long-term plasticity in the GABAergic inhibitory neurons takes place during normal learning processes in the cortex (Lamsa et al. 2005, Szegedi et al. 2016).

## **9. Original research articles**

**I**

# Hebbian LTP in feed-forward inhibitory interneurons and the temporal fidelity of input discrimination

Karri Lamsa, Joost H Heeroma & Dimitri M Kullmann

Cortical information processing requires a delicate balance of excitatory and inhibitory signaling. How is this balance preserved during hippocampal memory encoding, which involves NMDA receptor-dependent long term potentiation (LTP)? This form of LTP occurs at synapses between pyramidal neurons but has not been detected in feed-forward inhibitory interneurons. We show that paired pre- and postsynaptic activity evokes pathway-specific LTP in half of rat stratum radiatum interneurons if cytoplasmic integrity is preserved. LTP occurs in aspiny feed-forward interneurons and propagates to pyramidal neurons as an enhancement of disinaptic inhibition. We also show that when LTP is restricted to synapses on pyramidal neurons, the temporal fidelity of synaptic integration and action potential generation in pyramidal cells is compromised. However, when LTP also occurs at synapses on feed-forward interneurons, temporal fidelity is preserved. We propose that Hebbian LTP at synapses driving disinaptic inhibition is necessary to maintain information processing without degradation during memory encoding.

NMDA receptor-dependent LTP underlies several forms of memory formation and has been extensively documented in hippocampal pyramidal neurons, where its cardinal features include pathway specificity and dependence on the conjunction of pre- and postsynaptic activity. These phenomena are generally thought to reflect compartmentalization by dendritic spines<sup>1,2</sup> and coincidence detection by NMDA receptors (NMDARs)<sup>3</sup>, respectively. Although LTP in pyramidal neurons is often evoked by presynaptic tetanization, it can also be elicited by low-frequency pairing of presynaptic action potentials with postsynaptic depolarization<sup>4,5</sup>, approximating the requirements postulated by Hebb to allow memory storage<sup>6,7</sup>.

In contrast to the abundant evidence for Hebbian (pathway-specific, pairing-evoked) LTP in pyramidal neurons, there is very little evidence that this occurs in inhibitory interneurons. Indeed, although LTP of glutamatergic transmission has been reported in some interneurons, this requires tetanic or theta-burst stimulation of presynaptic afferents<sup>8–11</sup> or metabotropic glutamate receptor activation<sup>12</sup> for induction. It has also been reported to spread to other synapses<sup>13,14</sup>. Low-frequency pairing of presynaptic stimulation with interneuron depolarization has actually been reported to evoke no long-lasting changes in glutamatergic transmission<sup>15–17</sup> (although see ref. 18).

Absence of Hebbian pathway-specific LTP in interneurons is paradoxical: because input discrimination depends on a balance of excitation and inhibition (for example, see refs. 19,20), selective potentiation of excitatory transmission to pyramidal neurons, without corresponding potentiation of inhibitory transmission, might compromise its precision. Thus, we are faced with the prediction that learning comes at the price of degradation in the fidelity of signal processing.

Attempts to induce LTP in interneurons have generally relied on sharp microelectrode or whole-cell patch-clamp recording, both of

which potentially compromise neuronal integrity. Indeed, prolonged whole-cell recording jeopardizes the ability to induce LTP in pyramidal neurons<sup>21</sup>. We speculated that interneurons might be especially vulnerable to this artifact, and we therefore performed perforated-patch recordings<sup>22</sup> from rat hippocampal interneurons, with the goal of minimizing disruption of the neuronal biochemistry. This revealed robust Hebbian LTP in approximately half of stratum radiatum interneurons, which were aspiny, implying that dendritic spines are not necessary either for LTP<sup>1,2</sup> or for pathway specificity<sup>13</sup>. We further show that LTP in feed-forward interneurons is associative and propagates to pyramidal neurons. Finally, we examine the effect of LTP on a simple form of information processing. When LTP is restricted to pyramidal neurons, the temporal fidelity of synaptic integration and action potential generation in the principal cells is indeed degraded. When, however, LTP is induced both in pyramidal neurons and in interneurons, temporal fidelity is, in contrast, preserved. We argue that LTP at glutamatergic synapses driving feed-forward inhibition resolves the paradox outlined above: in keeping with intuition, memory encoding need not occur at the expense of the fidelity of information processing.

## RESULTS

### Pairing-evoked LTP in stratum radiatum interneurons

We elicited EPSPs in visualized CA1 stratum radiatum interneurons in rat hippocampal slices by alternately stimulating two electrodes in different locations in stratum radiatum (**Fig. 1a**). After a baseline period we paired low-frequency stimulation of one pathway with postsynaptic firing. This was achieved by switching to voltage-clamp mode and delivering 50-ms depolarizing commands, nominally to 0 mV, to coincide with each presynaptic stimulus. Because of the high,

Institute of Neurology, University College London, Queen Square, London WC1N 3BG, UK. Correspondence should be addressed to D.M.K. (d.kullmann@ion.ucl.ac.uk).

Published online 5 June 2005; doi:10.1038/nn1486

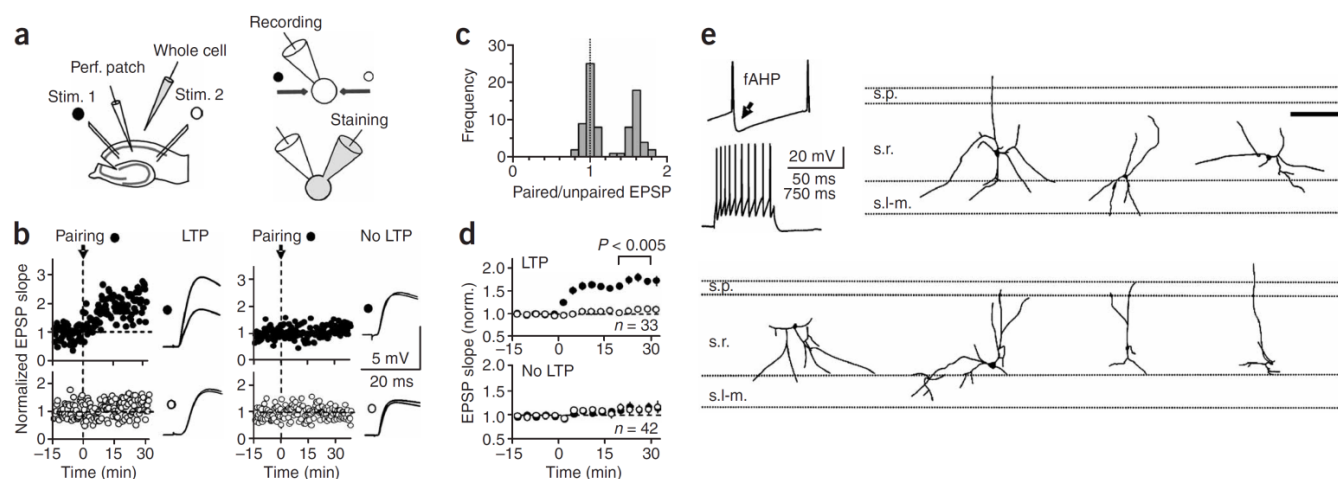


**Figure 1** Hebbian LTP in CA1 stratum radiatum interneurons. **(a)** Schematic showing the design of the experiment. A whole-cell recording was obtained via a second pipette at the end of some experiments to load interneurons with biocytin. **(b)** EPSP slopes, normalized by baseline values, plotted against time before and after pairing in two interneurons, one of which demonstrated LTP (left). Filled circles represent paired pathways, and open circles represent control pathways. Insets: superimposed averages of 15 consecutive EPSPs before and after pairing. **(c)** Frequency histogram showing the ratio of the normalized EPSP slope in the paired and unpaired pathways, taken 20 min after pairing. **(d)** Time course of the average normalized EPSP slope in the paired and unpaired pathways ( $\pm$  s.e.m.) in the two populations of interneurons showing either LTP or no LTP. **(e)** Somatodendritic morphology of interneurons showing LTP, projected on the borders between strata pyramidale (s.p.), radiatum (s.r.) and lacunosum-moleculare (s.l-m.). Scale bar: 300  $\mu$ m. Inset: representative train of action potentials evoked by current injection, showing a fast after-hyperpolarization (fAHP) typical of the interneurons.

uncompensated series resistance, this caused the interneuron to fire 'escape' action currents during the pairing (**Supplementary Fig. 1**). In 16/30 interneurons, pairing for 1 min at 2 Hz led to persistent potentiation of the EPSP initial slope, restricted to the paired pathway (**Fig. 1b**). In the remaining cells, there was no long-term (> 15 min) change in either pathway. LTP could also be induced by depolarizing the postsynaptic neuron continuously while one pathway was stimulated at low frequency. This allowed the stimuli to evoke escape currents, which occurred with a latency of 3–7 ms (**Supplementary Fig. 1**), satisfying Hebb's rule<sup>6</sup>. This protocol yielded pathway-specific LTP in 17/45 interneurons. We measured the ratio of normalized EPSP slopes between the two pathways. Results obtained from all experiments showed a bimodal distribution (**Fig. 1c**). LTP (defined as > 25% pathway-specific potentiation) was stable for at least 30 min (**Fig. 1d**).

We avoided 'giant' glutamatergic cells, which occur at low frequency close to stratum pyramidale<sup>15,23,24</sup>, by targeting small stratum radiatum interneurons close to stratum lacunosum-moleculare. All interneurons showed a prominent fast after-hyperpolarization (**Fig. 1e** inset) that does not occur in giant cells<sup>23,24</sup>.

When interneurons showing LTP were filled with biocytin through a second pipette in whole-cell mode (**Supplementary Fig. 2**) and subsequently imaged they had a bi- or multipolar morphology with dendrites frequently extending into strata oriens and/or lacunosum moleculare (**Fig. 1e**). They had few or no dendritic spines, in contrast to pyramidal neurons. They did not differ from neurons that showed no LTP with respect to the position of the soma, passive membrane properties or maximal spiking frequency (**Supplementary Fig. 3**).

### LTP in stratum radiatum interneurons is Hebbian

In six neurons where pairing led to an increase in EPSP slope in the first pathway, we subsequently paired the second pathway. In all cases this led to potentiation of the second pathway (**Fig. 2a**). LTP was not accompanied by any detectable change in paired-pulse ratio (**Fig. 2b**). In five other cells showing LTP of the first pathway, we washed in the NMDAR antagonist AP5 (D,L-2-amino-5-phospho-

nopentanoic acid; 100  $\mu$ M) before pairing the second pathway. This uniformly prevented LTP of the second pathway without reversing established LTP in the first pathway (**Fig. 2c**). Thus, LTP in interneurons shares several properties with LTP in pyramidal neurons: it depends on NMDARs, is pathway-specific and is not associated with robust changes in short-term plasticity. Notably, these results argue against an obligatory role for spines either for LTP induction or for pathway specificity.

### Whole-cell recording prevents LTP and causes NMDAR run-down

Why has pairing-evoked NMDAR-dependent LTP in stratum radiatum interneurons not been reported previously? In agreement with previous reports<sup>15,16</sup>, LTP could not be evoked when recording in whole-cell mode, in contrast to pyramidal cells that were recorded with the same pipette solution, recording duration ( $\leq 7$  min baseline) and access resistance (data not shown). In interneurons where pairing was ineffective, the whole-cell pipette was withdrawn to allow the membrane to re-seal, and we subsequently obtained a perforated-patch recording. In five out of eight cells, when pairing was repeated (> 30 min after terminating the whole-cell recording), LTP was evoked (**Fig. 2d**). Thus, impairment of LTP with whole-cell recording is reversible.

When recorded in whole-cell mode, pharmacologically isolated NMDAR-mediated EPSPs attenuated rapidly, in contrast to AMPA/kainate receptor-mediated EPSPs (**Fig. 2e**). Run-down of NMDAR-mediated signaling provides a potential explanation for the failure to elicit LTP in whole-cell mode. If so, the finding that impairment of LTP induction can be reversed (**Fig. 2d**) implies that NMDAR-mediated EPSPs should recover if whole-cell recording is interrupted. To determine if run-down could be reversed, we monitored an NMDAR-mediated EPSP through a perforated-patch electrode and obtained a G $\Omega$  seal with a second pipette applied to the same interneuron. Break-in via the second pipette (held in 0 current mode) was followed by a progressive decline in EPSP amplitude measured via the perforated patch (**Fig. 2f**). When the second pipette was withdrawn, the EPSP recovered ( $n = 3$ ). NMDAR-mediated responses in inter-

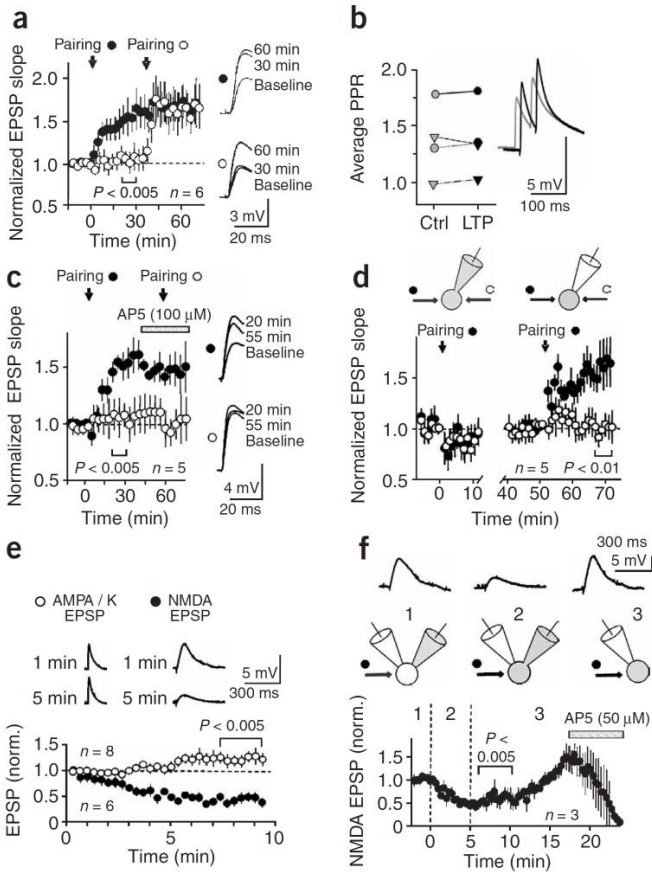


**Figure 2** Induction of LTP requires activation of NMDARs and cellular integrity. (a) In six out of six interneurons where pairing one pathway (filled circles) evoked LTP, subsequent pairing of the second pathway > 30 min later (open circles) also evoked LTP (traces at right: averages of 15 trials from one cell at the times indicated). (b) LTP was not accompanied by detectable change in the paired-pulse ratio (PPR;  $n = 4$ ). Traces: averages of 45 EPSPs recorded in one experiment before (gray) and 15–30 min after (black) pairing. (c) Blockade of NMDARs (by AP5) prevented LTP induction in the second pathway, without reversing LTP in the first. (d) In eight out of eight cells, pairing one pathway (filled circles) did not induce LTP when recording in whole-cell mode (< 7 min). In five of these cells LTP was evoked when pairing was repeated subsequently in perforated-patch mode. (e) Pharmacologically isolated NMDA (filled circles) or AMPA/kainate (open circles) receptor-mediated EPSPs (normalized by the first four responses), plotted against time from break-in (stimulation started > 15 min before break-in). NMDAR-mediated EPSPs show a rapid and selective run-down. (f) Reversible depression of NMDAR-mediated EPSPs by whole-cell recording. Top: experimental design, with EPSP traces measured through the perforated-patch pipette in a representative experiment. The second pipette was initially in the cell-attached configuration (1). Break-in (confirmed by epifluorescence imaging) was followed by EPSP run-down (2), which recovered after withdrawal of the pipette and membrane re-sealing (3). AP5 was applied at the end of the experiment.

neurons are thus unusually labile, possibly explaining previous failure to observe LTP.

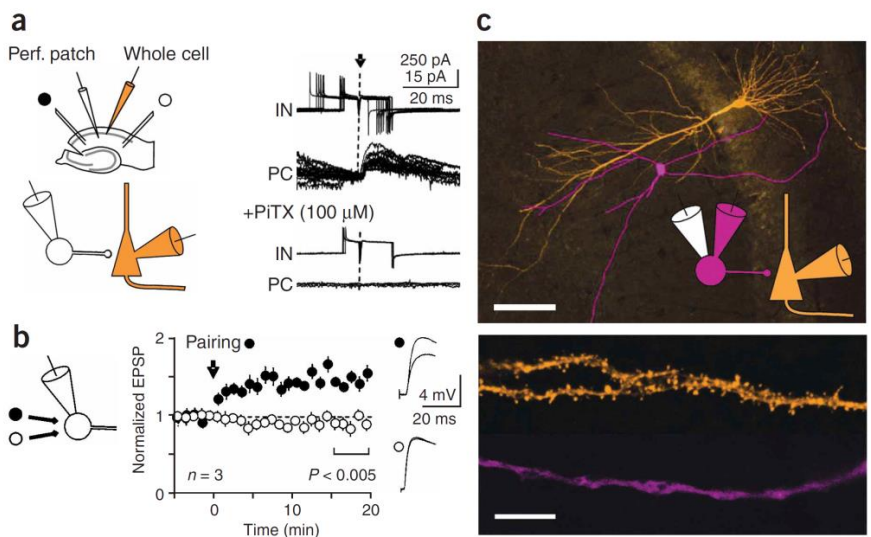
**LTP in feed-forward interneurons**

Interneurons in stratum radiatum are heterogeneous<sup>25,26</sup>. Rather than performing an exhaustive neurochemical and anatomical characterization, we asked if LTP could be elicited in feed-forward interneurons (defined as cells that are excited by Schaffer collaterals and that inhibit

CA1 pyramidal neurons). We evoked action potentials in interneurons via a perforated-patch pipette and searched among pyramidal neurons until a monosynaptic inhibitory postsynaptic current (IPSC) was obtained (GABA<sub>A</sub> receptor blockers were omitted). The success rate for obtaining a monosynaptic IPSC was approximately 1:30 (Fig. 3a). We then blocked GABA receptors and evoked EPSPs in the interneuron by stimulating either of two Schaffer collateral pathways. Low-frequency pairing of one pathway with postsynaptic depolarization led to pathway-specific LTP in three out of five identified feed-forward interneurons (Fig. 3b). Both the feed-forward interneuron and the synaptically coupled pyramidal neuron were visualized post-hoc (Fig. 3c). We conclude that at least some of the stratum radiatum interneurons that demonstrate LTP are indeed feed-forward interneurons.

Although LTP is confined to the paired pathway, the experiments above do not address whether it spreads to other interneurons innervated by the same axons<sup>27</sup>. We therefore recorded from two interneurons simultaneously (Fig. 4a) and paired high-frequency stimulation of one of two afferent pathways (100 Hz, 1 s, delivered

**Figure 3** Hebbian plasticity occurs in feed-forward interneurons. (a) A synaptically coupled interneuron–pyramidal cell pair. Superimposed traces are taken from the presynaptic interneuron (IN, aligned to an escape action current evoked by a depolarizing voltage clamp command), and from the postsynaptic pyramidal neuron (PC), before (top) and after (bottom) blockade of GABA<sub>A</sub> with picrotoxin (PiTX). Current scalings apply to IN and PC, respectively. (b) Pairing-induced pathway-specific LTP in three interneurons confirmed to project monosynaptically to a pyramidal neuron. Filled circles: paired pathways; open circles: control pathways. Traces obtained from one cell: baseline, and 20 min after pairing. (c) Feed-forward interneuron (purple) showing LTP and postsynaptic pyramidal neuron (orange). Insets: dendritic segments. Scale bar: 300 μm (low magnification), 80 μm (high magnification).



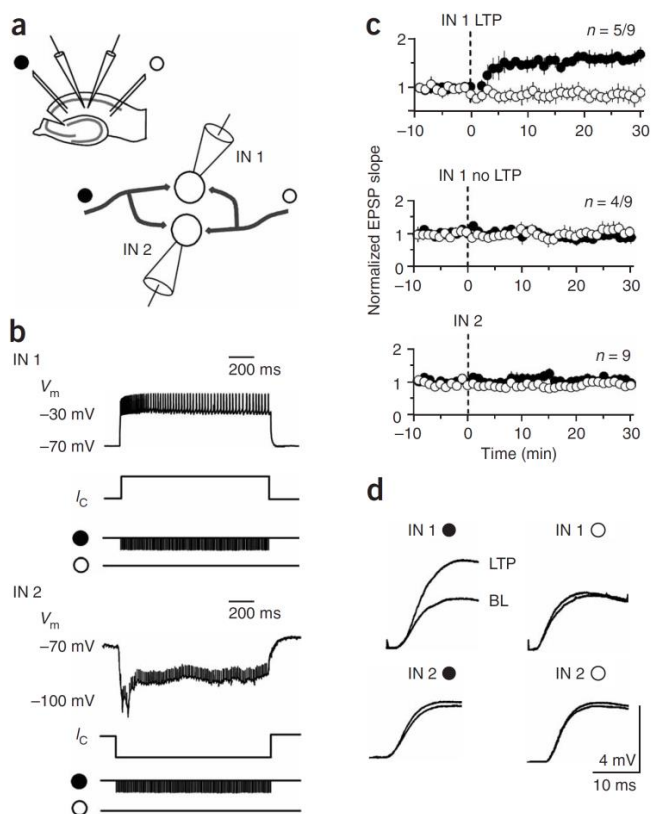


**Figure 4** LTP does not spread to other interneurons. (a) Schematic showing the experimental arrangement. Two stratum radiatum interneurons were recorded with perforated-patch pipettes. (b) Traces obtained simultaneously from two interneurons during tetanic stimulation of one pathway (filled circles). Depolarizing current was injected into one interneuron (IN 1), whereas the other was hyperpolarized (IN 2). (c) The depolarized interneuron demonstrated either LTP (top) or no change in transmission in either pathway (middle). Neither LTP nor LTD was observed in the hyperpolarized interneuron (bottom). (d) Sample traces obtained before and after the induction protocol in one experiment.

solution containing the  $\text{Ca}^{2+}$  chelator BAPTA (10 mM). Stratum radiatum stimuli evoked IPSCs, which were confirmed as disynaptic because they were abolished by the AMPA/kainate blocker NBQX (25  $\mu\text{M}$ ) at the end of every experiment (Fig. 5a). After recording the IPSCs in the two pathways during a baseline period, we delivered brief high-frequency stimulus bursts via a third electrode in stratum radiatum to depolarize the interneurons, synchronous with single stimuli delivered to one of the test pathways. The other test pathway was stimulated out of phase. This 'conjunctive pairing' led to LTP of the in-phase pathway (Fig. 5b,c). This IPSC potentiation was superimposed on a transient depression in both pathways and a small persistent decrease in the out-of-phase pathway (Fig. 5c), possibly reflecting endocannabinoid-mediated decrease of GABA release resulting from intense stimulation via the third electrode<sup>28</sup>. Nevertheless, LTP of the in-phase pathway was highly significant when the two pathways were compared ( $P = 0.001$ , paired  $t$ -test; Fig. 5d shows the ratio of IPSCs in the in-phase and out-of-phase pathways as a cumulative frequency plot). Thus, LTP in feed-forward interneurons propagates to principal cells as a persistent enhancement of disynaptic inhibition. Importantly, this result also shows that synaptic activation of interneurons can substitute for direct depolarization, underlining the physiological relevance of the phenomenon.

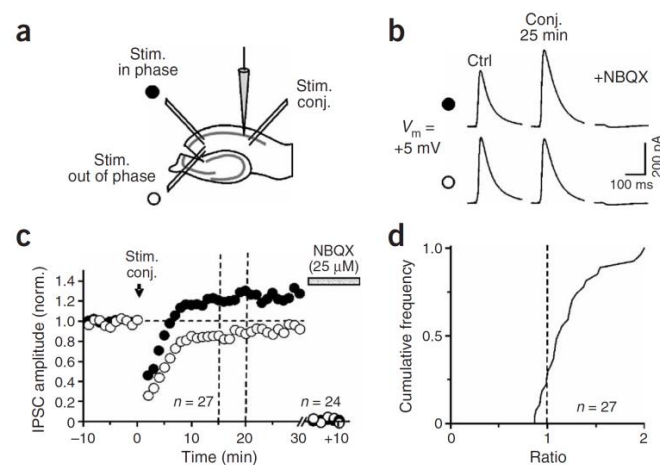
#### LTP potentially compromises temporal fidelity of integration

It has recently been shown<sup>19</sup> that precise signal processing depends on monosynaptic excitation and disynaptic inhibition: when two afferent inputs are stimulated asynchronously, there is a very narrow integration window for action potential generation in pyramidal cells that is shorter than the underlying synaptic conductances. This phenomenon provides an opportunity to test the hypothesis that LTP in feed-forward interneurons is required to preserve temporal fidelity of information processing during memory encoding.

twice, 20-s interval) with depolarizing current injection (200–350 pA) in one interneuron. The other interneuron was simultaneously hyperpolarized (–150 to –200 pA) to prevent it from spiking (Fig. 4b). This led to robust LTP in the paired (depolarized) interneuron in five of nine experiments and no change in transmission in the other four experiments (Fig. 4c,d). LTP did not spread to the other interneuron. We did not observe either homosynaptic or heterosynaptic long-term depression (LTD; Supplementary Fig. 1).

We then asked if LTP in interneurons propagates to pyramidal neurons as an increase of disynaptic inhibition. We adapted an experimental design used to demonstrate pairing-evoked LTP in principal cells<sup>4</sup>. Pyramidal cells were held in whole-cell voltage clamp close to the reversal potential for glutamate receptors with a pipette

**Figure 5** Hebbian LTP can be elicited by synaptic depolarization and propagates to pyramidal neurons. (a) 'Conjunctive pairing': disynaptic IPSCs were recorded in a pyramidal cell voltage-clamped in whole-cell mode close to the reversal potential for ionotropic glutamate receptors but positive to the reversal potential for  $\text{GABA}_A$  receptors. One pathway (filled circles) was stimulated at 1 Hz (2 min) synchronously with brief tetani delivered via a third stimulus electrode designed to depolarize interneurons ('Stim. conj.'). The other pathway (open circles) was stimulated out of phase to ensure that it received the same number of stimuli. (b) Traces obtained from one experiment showing averages of 45 trials before and after pairing and after blocking AMPA/kainate receptors (NBQX) to confirm the disynaptic nature of the IPSCs. (c) Time course of LTP of IPSCs and effect of blocking AMPA/kainate receptors. LTP was superimposed on a transient depression in both pathways. The points show the means of 27 experiments (error bars omitted).  $P = 0.001$ , paired  $t$ -test (time interval used for statistics indicated by dotted lines). (d) Cumulative frequency plot showing the ratio of normalized disynaptic IPSCs between the two test pathways (in-phase and out-of-phase) during the time interval used for statistics.



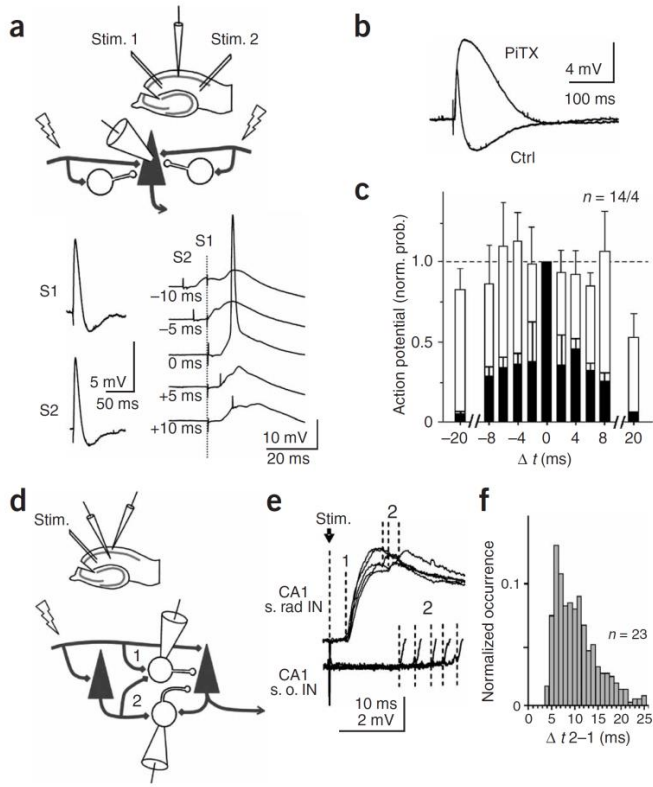


**Figure 6** Measurement of the time window for action potential generation in the face of asynchronous afferent stimulation. **(a)** EPSP-IPSP sequences evoked in a pyramidal neuron by two stimuli delivered separately, and individual trials showing the effect of varying the inter-stimulus interval (top to bottom:  $-10$  to  $+10$  ms, 5-ms steps). **(b)** Picrotoxin (PITX) blocked the late IPSP (averaged traces from one cell). **(c)** Average normalized probability of evoking an action potential with different intervals in 14 cells recorded without picrotoxin (black bars) and in four cells recorded with picrotoxin (white bars). Stimuli were adjusted to evoke similar-sized EPSPs in both pathways and to obtain an action potential upon synchronous stimulation in  $\sim 50\%$  of trials. The spike probability in each cell was normalized by the probability at 0 interval. Blocking GABAergic transmission degraded the temporal fidelity of action potential integration. **(d)** Schematic showing how feed-forward and feedback inhibition converge on a pyramidal neuron (cell at extreme right). Recruitment of local pyramidal cells imposes an additional delay for feedback inhibition. **(e)** Estimation of latency from disynaptic feed-forward to trisynaptic feedback inhibition. The traces show the latency difference for early monosynaptic EPSPs in stratum radiatum (s. rad.) interneurons (1) and for later disynaptic EPSPs, which occurred with a variable delay both in the same interneuron and in simultaneously recorded stratum oriens (s. o.) interneurons (2). **(f)** Frequency histogram for the latency difference (2–1). The modal additional delay for trisynaptic over disynaptic inhibition was  $\sim 7$  ms.

We measured the integration window for spike generation in pyramidal cells with perforated-patch recordings, because this also allowed the EPSP-IPSP sequences to be monitored before and after LTP induction in a relatively noninvasive manner (**Fig. 6a,b**). Stimuli delivered via either of two electrodes in stratum radiatum were adjusted to evoke a spike in 40–50% of trials when delivered synchronously but were sub-threshold when delivered alone. The spike success rate fell steeply when the stimuli were delivered asynchronously, with an inter-stimulus interval as short as 2 ms (**Fig. 6c**). This reflects the brief delay between monosynaptic excitation and disynaptic feed-forward inhibition<sup>19</sup>. We confirmed that blocking disynaptic inhibition with picrotoxin (**Fig. 6b**) caused the relationship between spike probability and inter-stimulus interval to flatten (**Fig. 6c**)<sup>19</sup>.

Before determining how LTP affects temporal fidelity, we asked whether trisynaptic inhibition (resulting from firing of CA1 pyramidal neurons and recruitment of feedback interneurons) also contributes to the narrow integration window. In separate control experiments, we recorded pharmacologically isolated EPSPs in stratum radiatum interneurons or, simultaneously in stratum radiatum and stratum oriens interneurons, evoked by strong stimuli designed to recruit CA1 pyramidal neurons (**Fig. 6d**). Stratum radiatum interneurons showed a biphasic EPSP, with the second component occurring  $>5$  ms after the first. The onset latency of the first EPSP detected in stratum oriens interneurons was also consistently  $>5$  ms after the onset of the first EPSP in stratum radiatum interneurons (**Fig. 6e**). **Figure 6f** shows a frequency histogram for the latency difference between the first component (in stratum radiatum cells) and the second component (in either stratum radiatum or stratum oriens cells), corresponding to mono- and disynaptic excitation. The modal latency difference ( $\sim 7$  ms; see also ref. 15) represents the additional synaptic delay and integration time in the pyramidal neurons that contribute to feedback inhibition. This latency difference was greater

than the width of the coincidence detection window in pyramidal neurons (**Fig. 6c**). We thus conclude that trisynaptic inhibition does not contribute to coincidence detection in pyramidal neurons within a  $\pm 6$ -ms time window.

Having measured the integration window for spike generation in a pyramidal neuron, we asked whether LTP affects its width. First, we deliberately restricted LTP experimentally to glutamatergic synapses on the same pyramidal neuron where the integration window was measured. Because perforated-patch recordings were used, low-frequency pairing-evoked LTP could be elicited even after a long baseline period. After waiting for LTP to reach a plateau ( $>15$  min; **Fig. 7a**), the stimulus intensities in both pathways were decreased to return the EPSP amplitude to baseline (and further adjusted if necessary to return the spike probability for synchronous stimulation to baseline). This was accompanied by a reduction in the IPSP amplitude (**Fig. 7b**).

We then repeated the measurement of the integration window for spike generation. When the stimuli were delivered asynchronously, the action potential probability was higher than the baseline before LTP induction (**Fig. 7c,d**). The probability of spiking (normalized by the probability at 0 interval; **Fig. 7d,e**), plotted as a one-sided function of the interval, was shallower than before LTP induction (**Fig. 7f**). Thus, if LTP occurs only at synapses on pyramidal cells, it is accompanied by a widening of the time window for action potential generation. This implies that if memory encoding is exclusively mediated by an enhancement of monosynaptic excitation (as expected if interneurons were unable to exhibit Hebbian LTP<sup>17</sup>), it is accompanied by a degradation of the fidelity of temporal input discrimination. In control experiments, we verified that when the experiment was carried out in the continued presence of picrotoxin to block disynaptic inhibition, the relationship between inter-stimulus interval and normalized action potential probability remained flat before and after pairing-evoked LTP and stimulus adjustment (**Supplementary Fig. 4**).

#### LTP in feed-forward interneurons rescues temporal fidelity

LTP in feed-forward interneurons provides a potential mechanism to rescue temporal fidelity of signal processing during memory encoding. In a separate series of experiments, we again

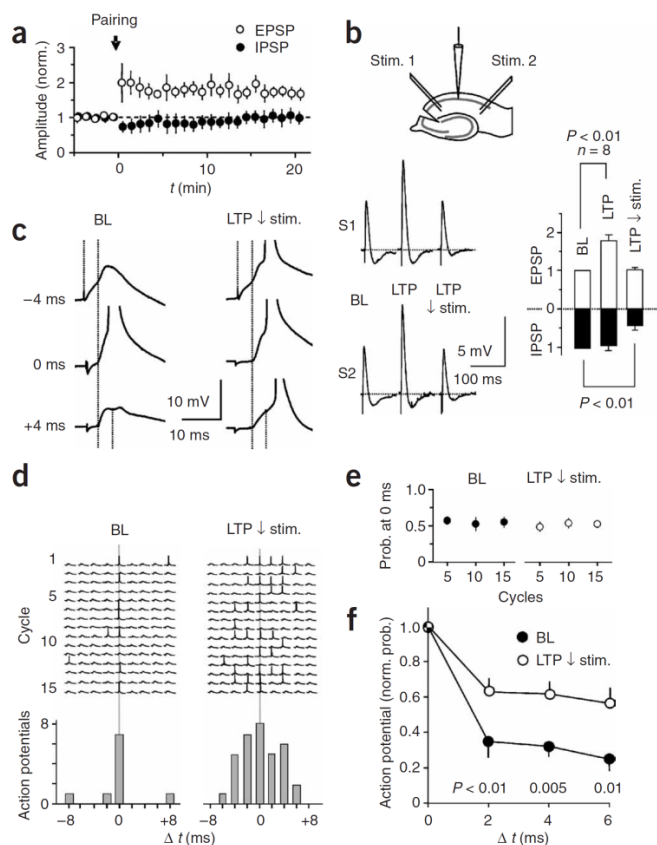


**Figure 7** LTP in pyramidal cells compromises the fidelity of coincidence detection in pyramidal cells. **(a)** Time course of pairing-evoked LTP of EPSPs recorded in pyramidal neurons ( $n = 8$  pathways in four cells). The later IPSP amplitude underwent no change. **(b)** Traces obtained from one experiment showing EPSP-IPSP sequences obtained by stimulating either of two pathways (S1 and S2) during a baseline period after pairing-induced LTP and after reducing the stimulus intensity to return the spike probability for synchronous stimulation at 0 interval to baseline ('LTP ↓ stim'). The histogram shows the normalized amplitudes of the EPSP and IPSP. **(c)** Traces obtained from one experiment showing individual trials obtained by stimulating both pathways with different inter-stimulus intervals before (BL) and after pairing-evoked LTP was elicited in both pathways, followed by stimulus reduction ('LTP ↓ stim'). **(d)** Top: individual traces, obtained from 15 repetitions of a cycle of nine intervals, from one experiment. Bottom: frequency histogram showing the spike occurrence for different intervals between stimuli (in ms). The spike rate for asynchronous stimulation was elevated after LTP. **(e)** The action potential probability for synchronous stimulation was stable both before and after LTP and stimulus reduction ( $n = 4$ ). **(f)** Action potentials occurred with a decreasing probability with increasing interval between the two stimuli. The spike probability interval slope (plotted as a one-sided graph) was shallower after LTP (open circles) than during the baseline period (BL, filled circles), implying impaired temporal precision of coincidence detection.

measured the integration window for spike generation before and after LTP, with one modification: instead of inducing LTP only at Schaffer collateral synapses on pyramidal neurons (**Fig. 7**), we induced LTP more extensively in the network by tetanizing both afferent pathways (100 Hz, 1 s, delivered twice, 20-s interval, **Fig. 8a**). By analogy with the experiments in **Figure 4** and **Figure 5**, tetanization should evoke LTP at least at some Schaffer collateral synapses on feed-forward interneurons. Indeed, we observed an increase of both the monosynaptic EPSP and the IPSP (histogram in **Fig. 8b**). (Note, however, that although trisynaptic inhibition has

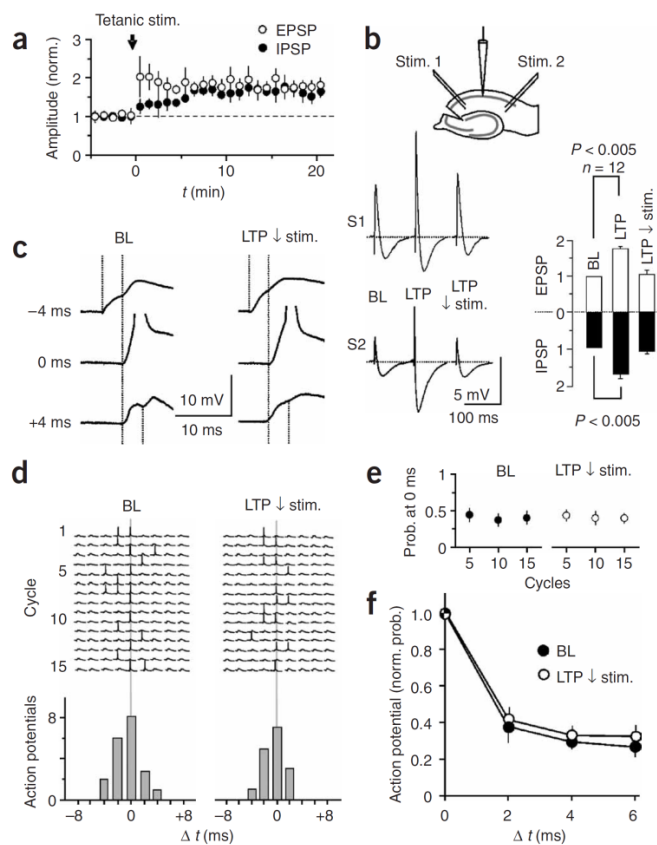


**Figure 8** Tetanic stimulation-evoked LTP, designed to potentiate not only synapses on pyramidal neurons but also on feed-forward interneurons, preserves the fidelity of coincidence detection. **(a)** Tetanic stimulation was accompanied by an increase in amplitude of the later IPSP, although this lagged behind LTP of the EPSP ( $n = 12$  pathways in six cells). **(b)** EPSP-IPSP sequences in one experiment, before and after tetanic LTP, and after reducing stimulus intensity to return the spike probability for synchronous stimulation to baseline. The histogram shows the relative changes in the EPSP and later IPSP. **(c)** Traces obtained from one experiment showing the effect of stimulating both pathways with different intervals before (BL) and after ('LTP ↓ stim') LTP and stimulus reduction. **(d)** Top: traces obtained from one experiment, showing no change in the time window for stochastic action potential generation before and after LTP and stimulus reduction. Bottom: frequency histogram showing no broadening of the relationship between spike occurrence and interval. **(e)** The spike probability for synchronous stimulation was stable both before and after LTP and stimulus reduction ( $n = 6$  cells). **(f)** Spike probability interval plot showing no change in slope after LTP (filled circles: baseline; open circles: after tetanic LTP).

no role in maintaining a narrow integration window for spike generation at small intervals (**Fig. 6d-f**), it potentially contaminates the late IPSP recorded in pyramidal neurons<sup>15</sup>. Therefore, it is not possible to use its amplitude as a direct estimate of LTP in feed-forward interneurons.)

In contrast to pairing-induced LTP, the action potential probability interval relationship was unchanged relative to baseline, in spite of a similar magnitude of LTP before stimulus adjustment (**Fig. 8c-f**). When spike integration in pyramidal cells was used to measure the temporal fidelity of information processing, Hebbian plasticity had no deleterious effect. LTP at glutamatergic synapses on interneurons can explain the difference between the effects of pairing-induced and tetanic LTP on the integration window for spike generation. Hebbian plasticity in interneurons may therefore allow the

temporal fidelity of coincidence detection to be preserved during memory encoding.

## DISCUSSION

The present study yields two surprising conclusions. First, about half of stratum radiatum interneurons demonstrate Hebbian LTP. Second, pathway-specific LTP does not require dendritic spines. LTP occurs in feed-forward interneurons, identified as such by their inhibition of pyramidal neurons monosynaptically, and LTP in interneurons propagates to pyramidal cells as a persistent enhancement of disynaptic feed-forward inhibition. LTP in interneurons can also be elicited by synaptic depolarization. Finally, we draw attention to an important paradox: if memory encoding mediated by Hebbian LTP enhances only monosynaptic excitation but not disynaptic inhibition of principal cells, this will degrade the fidelity of information processing. However, the occurrence of LTP also in feed-forward interneurons resolves this paradox. In keeping with this, the temporal fidelity of synaptic integration and action potential generation in pyramidal neurons is degraded if LTP is restricted to monosynaptic excitation but is preserved if LTP is also allowed to occur in feed-forward interneurons.

Stratum radiatum interneurons studied here fall into two categories: in cells that show LTP in one pathway, subsequent pairing of the other pathway also invariably results in LTP. Other cells are resistant to the different induction protocols tested here. We have not characterized interneurons neurochemically, so it remains to be determined whether the presence or absence of a particular membrane receptor, Ca<sup>2+</sup>-binding protein or other marker correlates with the ability to elicit LTP. Although NR1 subunits seem to be absent in some interneurons<sup>29</sup>, we found that NMDAR-mediated synaptic responses could be elicited in all stratum radiatum interneurons tested (data not shown), so absence of NMDARs is unlikely to be the explanation.

Pathway-specific LTP in aspiny interneurons argues against an obligatory role for spines in compartmentalizing changes in synaptic strength<sup>1,2,13</sup>. There is a precedent for this in the finding that pairing can result in the appearance of AMPA receptor-mediated EPSCs in nascent pyramidal neurons before the formation of spines<sup>30</sup>. A possible subcellular substrate is localized Ca<sup>2+</sup> elevation, which has been reported to be restricted to micron-scale segments of aspiny interneuron dendrites<sup>31</sup>. This might allow some spread of LTP among closely spaced synapses, which cannot be excluded by the present study. NMDARs contribute to the Ca<sup>2+</sup> influx underlying dendritic transients detected in interneurons<sup>32</sup> and that these interact with back-propagating action potentials<sup>33</sup>. Notably, we found that LTP could be triggered by allowing the presynaptic stimuli to evoke action potentials, a naturalistic Hebbian situation that is likely to pertain *in vivo*. This might differ from a previous study in which LTP was not evoked in a few interneurons despite the use of perforated-patch recordings<sup>15</sup>.

Although spines may not be essential for pathway-specific LTP, their absence might contribute to the labile nature of NMDAR-mediated signaling in aspiny interneurons, as demonstrated by whole-cell recording. We tentatively suggest that when the cytoplasm is dialyzed, they are relatively less well protected than NMDARs at spiny synapses in pyramidal cells, explaining the profound run-down of NMDAR-mediated EPSPs and inability to elicit LTP. In this study, neither NMDAR run-down nor failure to elicit LTP with whole-cell recording are irreversible: after removing the whole-cell pipette, we observed a recovery both of NMDAR-mediated EPSPs and of the ability to evoke LTP in a similar proportion of interneurons as when perforated-patch recording was used *ab initio*. This recovery can be explained by postulating that a cytoplasmic constituent required for

NMDAR function is replenished by an endogenous mechanism. We are currently investigating several candidates.

Robust LTP of feed-forward inhibition is apparently at odds with the observation that tetanic stimulation-induced LTP, studied with field potential electrodes, is accompanied by an increase in the ratio of population action potential amplitude to EPSP slope<sup>34</sup>. This 'E-S' potentiation has been attributed to relatively selective LTP of excitatory signaling in pyramidal neurons<sup>35</sup> and/or to simultaneous depression of inhibition, either because LTD is induced in interneurons<sup>16,36</sup> or because GABAergic transmission to pyramidal neurons is downregulated through a calcineurin-dependent mechanism<sup>33</sup>. However, in the present study, tetanic LTP was associated with a similar increase of EPSPs and IPSPs in pyramidal neurons when these were recorded via perforated patches (Fig. 8a,b), arguing instead that the mechanisms underlying E-S potentiation are not directly related to GABAergic transmission. Consistent with this, several studies have shown that E-S potentiation accompanies LTP when the experiments are performed during the continual presence of GABA<sub>A</sub> receptor blockers<sup>37–40</sup> (although see refs. 41,42).

The temporal fidelity of input integration and firing in pyramidal neurons is a simple measure of information processing in the hippocampus. The finding that pairing-induced LTP was accompanied by a broadening of the temporal integration window is in keeping with the principle that the balance of monosynaptic excitation and disynaptic inhibition is essential for temporal fidelity. Selectively potentiating monosynaptic excitation is analogous to a relative weakening of disynaptic inhibition, which also causes a widening of the integration window (Fig. 6c)<sup>19</sup>. By showing that tetanic stimulation allows LTP to be evoked without widening the integration window, we argue that Hebbian plasticity in interneurons preserves temporal fidelity of information processing. What other explanations are available for the different results of pairing-induced and tetanic LTP? We verified that trisynaptic inhibition is unlikely to affect spike generation at short inter-stimulus intervals (Fig. 6d–f), thus reducing the circuitry necessary to explain the narrow window on the basis of monosynaptic excitation and disynaptic inhibition. Changes in the intrinsic properties of pyramidal neurons are also unlikely to explain the difference, because they underwent similar voltage excursions in both cases. Plasticity of glutamatergic synapses on interneurons thus seems to be the only candidate mechanism that distinguishes the two cases. This is only a preliminary insight into the interaction between Hebbian plasticity and information processing, providing fertile ground for further research.

## METHODS

**Hippocampal Slice preparation.** Three- to four-week-old male Sprague-Dawley rats were killed according to the Animals (Scientific Procedures) Act 1986. Hippocampal slices (300- to 350- $\mu$ m-thick) were visualized with infrared differential interference contrast and epifluorescence imaging. A cut was made between CA1 and CA3 to prevent propagation of recurrent excitation in Schaffer collaterals. The perfusion medium contained (in mM): NaCl (119), KCl (2.5), MgCl<sub>2</sub> (1.3), CaCl<sub>2</sub> (2.5), NaHCO<sub>3</sub> (25), NaH<sub>2</sub>PO<sub>4</sub> (1), glucose (11), equilibrated with 95% O<sub>2</sub>/5% CO<sub>2</sub> (pH 7.4, 31–32 °C). For measurement of NMDAR-mediated responses, Mg<sup>2+</sup> was omitted and AMPA/kainate and metabotropic glutamate receptors were blocked with NBQX (25  $\mu$ M) and LY341495 (1 mM). For measurement of AMPA receptor-mediated EPSPs, NMDARs were blocked with AP5 (100  $\mu$ M). The GABA receptor blockers picrotoxin (PiTX, 100  $\mu$ M) and CGP52432 (5  $\mu$ M) were added to the solution for all except the experiments with paired recordings (Fig. 3), conjunctive pairing (Fig. 5) and temporal discrimination (Figs. 6–8).

**Electrophysiological recordings.** Perforated-patch recordings were made with 12–18 M $\Omega$  pipettes containing gramicidin (100  $\mu$ g/ml) in a solution containing (in mM): K-gluconate (145), NaCl (8), KOH-HEPES (20 – 25), EGTA (0.2),



and QX-314 Br (5; pH 7.2, 295 mOsm). The electrode tip was filled with gramicidin-free solution. Series resistance was continuously monitored throughout the experiment, and depolarizing currents were intermittently injected to evoke action potentials to verify patch integrity. In some experiments, AlexaFluor 488 was also included and the neuron was imaged with epifluorescence to monitor dye penetration. Recordings in bridge balance mode were started when the series resistance was <150 M $\Omega$ .

Whole-cell recordings from CA1 pyramidal cells were made with a solution containing Cs-gluconate (117.5), CsCl (17.5), KOH-HEPES (10), BAPTA (10), NaCl (8), Mg-ATP (2), GTP (0.3), and QX-314 Br (5; pH 7.2, 290 mOsm). The pipette solution used in the whole-cell interneuron recordings contained K-gluconate (145), NaCl (8), Mg-ATP (2), GTP (0.3), KOH-HEPES (20–25), EGTA (0.2), and Alexa 488 (20–50  $\mu$ M) (pH 7.2, 295 mOsm). Biocytin (0.4%) was included in some experiments. Series resistance (<20 M $\Omega$ ) was monitored throughout the experiment using a  $-5$  or  $-10$  mV step command. Cells showing unstable series resistance or holding current were rejected.

Stimuli (50  $\mu$ s, 50–500  $\mu$ A) were delivered via bipolar stainless steel electrodes in stratum radiatum, with a 15- to 20-s inter-trial interval. For low-frequency pairing the cells were voltage clamped nominally at 0 mV (because of the high uncompensated series resistance, the estimated  $V_m$  was between  $-30$  and  $-20$  mV). The test pathway was stimulated at 2 Hz for 60 s. For conjunctive pairing, pyramidal cells were recorded in whole-cell voltage clamp mode nominally at  $+10$  to  $+15$  mV (estimated at  $-5$  to  $0$  mV after compensating for the liquid junction potential and series resistance). Two stimulus electrodes were positioned in CA1 stratum radiatum distant (>1 mm) from the recording site. A third electrode was set close to the pyramidal neuron (<250  $\mu$ m) to deliver brief tetani (5–10 pulses at 200 Hz) simultaneously with the paired pathway at 1 Hz for two minutes. The control pathway was stimulated out of phase (with a 500-ms delay after the train). The stimulus intensity for the third electrode was chosen to evoke a maximal single-shock IPSC.

Cells were recorded with a Multiclamp 700 amplifier (Axon Instruments). Evoked EPSPs were recorded from a resting membrane potential ( $-70.7 \pm 4.9$  mV, liquid junction potential corrected), low-pass filtered (5 Hz) and acquired at 20 kHz on PC for offline analysis (LabView, National Instruments). In some experiments EPSPs were recorded during a brief (500-ms) hyperpolarizing step (5–10 mV) to avoid action potential generation. The initial slope (<10 ms from onset) of the EPSPs was analyzed to restrict attention to monosynaptic excitatory inputs in LTP experiments. To study pharmacologically isolated NMDA or AMPA/kainate receptor-mediated EPSPs, the amplitude of the monosynaptic response was analyzed. Data are shown as mean  $\pm$  s.e.m., normalized by baseline values, and analyzed with Student's paired *t*-test.

**Anatomical experiments.** For morphology studies, a whole-cell recording was obtained from the same cell with a pipette containing the perforated-patch pipette solution, without gramicidin but with the inclusion of Mg-ATP (2 mM), GTP (0.3 mM), and 0.4% biocytin or biocytin conjugated to the fluorescent dye Alexa Fluor 488. Slices were fixed overnight in 4% paraformaldehyde at 4  $^{\circ}$ C. After permeabilization in 0.1% Triton X-100, slices were incubated in 0.1% streptavidin–Alexa 488 conjugate, mounted in DABCO anti-fading medium and imaged with a Zeiss LSM 510 meta-confocal microscope.

**Drugs and reagents.** Chemicals were purchased from Sigma. Receptor antagonists were purchased from Tocris Cookson. Streptavidin–Alexa 488 and biocytin–Alexa 488 were obtained from Molecular Probes.

*Note: Supplementary information is available on the Nature Neuroscience website.*

#### ACKNOWLEDGMENTS

We thank D.A. Rusakov, R.A. Silver, M.C. Walker and R.W. Tsien for comments. Supported by the Wellcome Trust, the Academy of Finland and the UK Medical Research Council.

#### AUTHOR CONTRIBUTIONS

K.L. performed electrophysiological experiments; J.H.H. performed anatomical experiments and K.L., J.H.H. and D.M.K. designed the study and wrote the manuscript.

#### COMPETING INTERESTS STATEMENT

The authors declare that they have no competing financial interests.

Received 22 April; accepted 18 May 2005

Published online at <http://www.nature.com/natureneuroscience/>

- Harris, K.M. & Kater, S.B. Dendritic spines: cellular specializations imparting both stability and flexibility to synaptic function. *Annu. Rev. Neurosci.* **17**, 341–371 (1994).
- Yuste, R., Majewska, A. & Holthoff, K. From form to function: calcium compartmentalization in dendritic spines. *Nat. Neurosci.* **3**, 653–659 (2000).
- Bliss, T.V. & Collingridge, G.L. A synaptic model of memory: long-term potentiation in the hippocampus. *Nature* **361**, 31–39 (1993).
- Wigstrom, H. & Gustafsson, B. Postsynaptic control of hippocampal long-term potentiation. *J. Physiol. (Paris)* **81**, 228–236 (1986).
- Kauer, J.A., Malenka, R.C. & Nicoll, R.A. A persistent postsynaptic modification mediates long-term potentiation in the hippocampus. *Neuron* **1**, 911–917 (1988).
- Hebb, D.O. *The Organization of Behavior* (Wiley, New York, 1949).
- Bi, G. & Poo, M. Synaptic modification by correlated activity: Hebb's postulate revisited. *Annu. Rev. Neurosci.* **24**, 139–166 (2001).
- Ouardouz, M. & Lacaille, J.C. Mechanisms of selective long-term potentiation of excitatory synapses in stratum oriens/alveus interneurons of rat hippocampal slices. *J. Neurophysiol.* **73**, 810–819 (1995).
- Mahanty, N.K. & Sah, P. Calcium-permeable AMPA receptors mediate long-term potentiation in interneurons in the amygdala. *Nature* **394**, 683–687 (1998).
- Alle, H., Jonas, P. & Geiger, J.R. PTP and LTP at a hippocampal mossy fiber-interneuron synapse. *Proc. Natl. Acad. Sci. USA* **98**, 14708–14713 (2001).
- Laezza, F. & Dingledine, R. Voltage-controlled plasticity at GluR2-deficient synapses onto hippocampal interneurons. *J. Neurophysiol.* **92**, 3575–3581 (2004).
- Perez, Y., Morin, F. & Lacaille, J.C. A Hebbian form of long-term potentiation dependent on mGluR1a in hippocampal inhibitory interneurons. *Proc. Natl. Acad. Sci. USA* **98**, 9401–9406 (2001).
- Cowan, A.I., Stricker, C., Reece, L.J. & Redman, S.J. Long-term plasticity at excitatory synapses on aspiny interneurons in area CA1 lacks synaptic specificity. *J. Neurophysiol.* **79**, 13–20 (1998).
- Bauer, E.P. & LeDoux, J.E. Heterosynaptic long-term potentiation of inhibitory interneurons in the lateral amygdala. *J. Neurosci.* **24**, 9507–9512 (2004).
- Maccaferri, G. & McBain, C.J. Long-term potentiation in distinct subtypes of hippocampal nonpyramidal neurons. *J. Neurosci.* **16**, 5334–5343 (1996).
- McMahon, L.L. & Kauer, J.A. Hippocampal interneurons express a novel form of synaptic plasticity. *Neuron* **18**, 295–305 (1997).
- McBain, C.J., Freund, T.F. & Mody, I. Glutamatergic synapses onto hippocampal interneurons: precision timing without lasting plasticity. *Trends Neurosci.* **22**, 228–235 (1999).
- Wang, J.H. & Kelly, P. Calcium-calmodulin signalling pathway up-regulates glutamatergic synaptic function in non-pyramidal, fast spiking rat hippocampal CA1 neurons. *J. Physiol. (Lond.)* **533**, 407–422 (2001).
- Pouille, F. & Scanziani, M. Enforcement of temporal fidelity in pyramidal cells by somatic feed-forward inhibition. *Science* **293**, 1159–1163 (2001).
- Marino, J. *et al.* Invariant computations in local cortical networks with balanced excitation and inhibition. *Nat. Neurosci.* **8**, 194–201 (2005).
- Kato, K., Clifford, D.B. & Zorumski, C.F. Long-term potentiation during whole-cell recording in rat hippocampal slices. *Neuroscience* **53**, 39–47 (1993).
- Horn, R. & Marty, A. Muscarinic activation of ionic currents measured by a new whole-cell recording method. *J. Gen. Physiol.* **92**, 145–159 (1988).
- Gulyas, A.I., Toth, K., McBain, C.J. & Freund, T.F. Stratum radiatum giant cells: a type of principal cell in the rat hippocampus. *Eur. J. Neurosci.* **10**, 3813–3822 (1998).
- Christie, B.R., Franks, K.M., Seamans, J.K., Saga, K. & Sejnowski, T.J. Synaptic plasticity in morphologically identified CA1 stratum radiatum interneurons and giant projection cells. *Hippocampus* **10**, 673–683 (2000).
- Gulyas, A.I., Hajos, N. & Freund, T.F. Interneurons containing calretinin are specialized to control other interneurons in the rat hippocampus. *J. Neurosci.* **16**, 3397–3411 (1996).
- Parra, P., Gulyas, A.I. & Miles, R. How many subtypes of inhibitory cells in the hippocampus? *Neuron* **20**, 983–993 (1998).
- Schuman, E.M. & Madison, D.V. Locally distributed synaptic potentiation in the hippocampus. *Science* **263**, 532–536 (1994).
- Chevalyere, V. & Castillo, P.E. Heterosynaptic LTD of hippocampal GABAergic synapses: a novel role of endocannabinoids in regulating excitability. *Neuron* **38**, 461–472 (2003).
- Nyiri, G., Stephenson, F.A., Freund, T.F. & Somogyi, P. Large variability in synaptic N-methyl-D-aspartate receptor density on interneurons and a comparison with pyramidal-cell spines in the rat hippocampus. *Neuroscience* **119**, 347–363 (2003).
- Durand, G.M., Kovalchuk, Y. & Konnerth, A. Long-term potentiation and functional synapse induction in developing hippocampus. *Nature* **381**, 71–75 (1996).
- Goldberg, J.H., Tamas, G., Aronov, D. & Yuste, R. Calcium microdomains in aspiny dendrites. *Neuron* **40**, 807–821 (2003).
- Goldberg, J.H., Yuste, R. & Tamas, G. Ca<sup>2+</sup> imaging of mouse neocortical interneurone dendrites: contribution of Ca<sup>2+</sup>-permeable AMPA and NMDA receptors to subthreshold Ca<sup>2+</sup>-dynamics. *J. Physiol. (Lond.)* **551**, 67–78 (2003).
- Kaiser, K.M., Lubke, J., Zilberter, Y. & Sakmann, B. Postsynaptic calcium influx at single synaptic contacts between pyramidal neurons and bitufted interneurons in layer 2/3 of



- rat neocortex is enhanced by backpropagating action potentials. *J. Neurosci.* **24**, 1319–1329 (2004).
34. Andersen, P., Sundberg, S.H., Sveen, O., Swann, J.W. & Wigstrom, H. Possible mechanisms for long-lasting potentiation of synaptic transmission in hippocampal slices from guinea-pigs. *J. Physiol. (Lond.)* **302**, 463–482 (1980).
35. Abraham, W.C., Gustafsson, B. & Wigstrom, H. Long-term potentiation involves enhanced synaptic excitation relative to synaptic inhibition in guinea-pig hippocampus. *J. Physiol. (Lond.)* **394**, 367–380 (1987).
36. Lu, Y.M., Mansuy, I.M., Kandel, E.R. & Roder, J. Calcineurin-mediated LTD of GABAergic inhibition underlies the increased excitability of CA1 neurons associated with LTP. *Neuron* **26**, 197–205 (2000).
37. Asztely, F. & Gustafsson, B. Dissociation between long-term potentiation and associated changes in field EPSP waveform in the hippocampal CA1 region: an in vitro study in guinea pig brain slices. *Hippocampus* **4**, 148–156 (1994).
38. Jester, J.M., Campbell, L.W. & Sejnowski, T.J. Associative EPSP–spike potentiation induced by pairing orthodromic and antidromic stimulation in rat hippocampal slices. *J. Physiol. (Lond.)* **484**, 689–705 (1995).
39. Sourdet, V., Russier, M., Daoudal, G., Ankri, N. & Debanne, D. Long-term enhancement of neuronal excitability and temporal fidelity mediated by metabotropic glutamate receptor subtype 5. *J. Neurosci.* **23**, 10238–10248 (2003).
40. Wang, Z., Xu, N.L., Wu, C.P., Duan, S. & Poo, M.M. Bidirectional changes in spatial dendritic integration accompanying long-term synaptic modifications. *Neuron* **37**, 463–472 (2003).
41. Chavez-Noriega, L.E., Halliwell, J.V. & Bliss, T.V. A decrease in firing threshold observed after induction of the EPSP–spike (E-S) component of long-term potentiation in rat hippocampal slices. *Exp. Brain Res.* **79**, 633–641 (1990).
42. Marder, C.P. & Buonomano, D.V. Timing and balance of inhibition enhance the effect of long-term potentiation on cell firing. *J. Neurosci.* **24**, 8873–8884 (2004).

**II**

The effects of our amendments on both the POA/SOA split and the total OA burden are shown in Fig. 4. The traditional model predicts substantial contributions from POA, whereas the revised model predicts that ambient OA is dominated by SOA during the summer. Such a shift is consistent with recent field measurements indicating dominant contributions from SOA (8–10) while remaining consistent with POA estimates based on low-volatility tracers. In terms of the overall OA budget, the revised model decreases predicted OA in urban areas by as much as 50% and increases it in many rural areas by 15 to 30% (Fig. 4C), reducing the large urban-to-regional gradients predicted by the traditional model and resulting in considerably better agreement with measured urban-to-regional OA ratios (Fig. 4D).

This work has several implications for our understanding of OA. The semivolatile character of primary emissions requires that instead of measuring fixed POA EFs, we must measure the volatility distribution of the emissions. Models and inventories must account for these distributions and their evolution with photochemical age. Regulations and control technologies may also need to be revised to control SVOC and IVOC emissions because of their importance as SOA precursors. The results also imply that, except for people living close to sources, the majority of the population (even in urban areas) is exposed mostly to SOA. Ultimately, a rela-

tively local urban emissions problem is transformed into a regional source of oxidized and presumably hydrophilic OA. The health consequences and climate effects of this oxidized material are almost certainly dramatically different from those of primary emissions.

#### References and Notes

1. M. Kanakidou *et al.*, *Atmos. Chem. Phys.* **5**, 1053 (2005).
2. J. J. Schauer, W. F. Rogge, L. M. Hildemann, M. A. Mazurek, G. R. Cass, *Atmos. Environ.* **30**, 3837 (1996).
3. M. Zheng, G. R. Cass, J. J. Schauer, E. S. Edgerton, *Environ. Sci. Technol.* **36**, 2361 (2002).
4. B. J. Turpin, J. J. Huntzicker, *Atmos. Environ.* **29**, 3527 (1995).
5. J. C. Cabada *et al.*, *Aerosol Sci. Technol.* **38**, 140 (2004).
6. S. Vutukur, R. J. Griffin, D. Dabdub, *J. Geophys. Res.* **111**, D10512 (2006).
7. B. K. Pun *et al.*, *Environ. Sci. Technol.* **37**, 3647 (2003).
8. Q. Zhang, D. R. Worsnop, M. R. Canagaratna, J. L. Jimenez, *Atmos. Chem. Phys.* **5**, 3289 (2005).
9. R. Volkamer *et al.*, *Geophys. Res. Lett.* **33**, L17811 (2006).
10. J. A. de Gouw *et al.*, *J. Geophys. Res.* **110**, D16305 (2005).
11. D. Johnson *et al.*, *Atmos. Chem. Phys.* **6**, 403 (2006).
12. C. L. Heald *et al.*, *Geophys. Res. Lett.* **32**, L18809 (2005).
13. J. J. Schauer, M. J. Kleeman, G. R. Cass, B. R. T. Simoneit, *Environ. Sci. Technol.* **36**, 1169 (2002).
14. J. J. Schauer, M. J. Kleeman, G. R. Cass, B. R. T. Simoneit, *Environ. Sci. Technol.* **33**, 1578 (1999).
15. J. J. Schauer, M. J. Kleeman, G. R. Cass, B. R. T. Simoneit, *Environ. Sci. Technol.* **35**, 1716 (2001).
16. L. M. Hildemann, G. R. Cass, G. R. Markowski, *Aerosol Sci. Technol.* **10**, 193 (1989).

17. M. K. Shrivastava, E. M. Lipsky, C. O. Stanier, A. L. Robinson, *Environ. Sci. Technol.* **40**, 2671 (2006).
18. N. M. Donahue, A. L. Robinson, C. O. Stanier, S. N. Pandis, *Environ. Sci. Technol.* **40**, 2635 (2006).
19. Materials and methods are available as supporting material on Science Online.
20. J. R. Odum *et al.*, *Environ. Sci. Technol.* **30**, 2580 (1996).
21. E. M. Lipsky, A. L. Robinson, *Environ. Sci. Technol.* **40**, 155 (2006).
22. Y. B. Lim, P. J. Ziemann, *Environ. Sci. Technol.* **39**, 9229 (2005).
23. B. Y. Koo, A. S. Ansari, S. N. Pandis, *Atmos. Environ.* **37**, 4757 (2003).
24. D. E. Heard, M. J. Pilling, *Chem. Rev.* **103**, 5163 (2003).
25. R. Atkinson, J. Arey, *Chem. Rev.* **103**, 4605 (2003).
26. W. J. Bloss *et al.*, *Faraday Discuss. Chem. Soc.* **130**, 425 (2005).
27. M. Y. Chung, C. Maris, U. Krischke, R. Meller, S. E. Paulson, *Atmos. Environ.* **37** (suppl. 2), S159 (2003).
28. R. Bahreini *et al.*, *Environ. Sci. Technol.* **39**, 5674 (2005).
29. This research has been funded by the U.S. Environmental Protection Agency (EPA) through grants RD-83108101 and R832162. It has not been subjected to the agency's required peer and policy review and therefore does not necessarily reflect the views of the agency; no official endorsement should be inferred. The Proton Transfer Reaction-Mass Spectrometer and AMS were acquired with support from NSF (grant ATM-0420842).

#### Supporting Online Material

www.sciencemag.org/cgi/content/full/315/5816/1259/DC1

Materials and Methods

Table S1

References

26 July 2006; accepted 17 January 2007

10.1126/science.1133061

## Anti-Hebbian Long-Term Potentiation in the Hippocampal Feedback Inhibitory Circuit

Karri P. Lamsa,<sup>1</sup> Joost H. Heeroma,<sup>1</sup> Peter Somogyi,<sup>2</sup> Dmitri A. Rusakov,<sup>1</sup> Dimitri M. Kullmann<sup>1\*</sup>

Long-term potentiation (LTP), which approximates Hebb's postulate of associative learning, typically requires depolarization-dependent glutamate receptors of the NMDA (*N*-methyl-D-aspartate) subtype. However, in some neurons, LTP depends instead on calcium-permeable AMPA-type receptors. This is paradoxical because intracellular polyamines block such receptors during depolarization. We report that LTP at synapses on hippocampal interneurons mediating feedback inhibition is "anti-Hebbian": It is induced by presynaptic activity but prevented by postsynaptic depolarization. Anti-Hebbian LTP may occur in interneurons that are silent during periods of intense pyramidal cell firing, such as sharp waves, and lead to their altered activation during theta activity.

Associative *N*-methyl-D-aspartate receptor (NMDAR)-dependent LTP is induced by coincident activity in afferent pathways sufficient to depolarize postsynaptic neurons (1). However, the voltage dependence of Ca<sup>2+</sup>-permeable  $\alpha$ -amino-3-hydroxy-5-methyl-4-

isoxazolepropionic acid receptors (CP-AMPA) is opposite to that of NMDARs (2, 3). Because CP-AMPA receptors are blocked by cytoplasmic polyamines upon depolarization (4, 5), maximal Ca<sup>2+</sup> influx occurs when the membrane potential is relatively negative. LTP dependent on CP-AMPA receptors occurs in interneurons of the spinal cord and amygdala (6, 7), but its postsynaptic voltage dependence has not been explored. In hippocampal interneurons, CP-AMPA receptors have been implicated in long-term depression (8–10), and contribute to synaptic Ca<sup>2+</sup> transients, especially in the stratum

oriens/alveus (11). Many interneurons in the oriens/alveus also show NMDAR-independent LTP (12). We therefore looked for associative LTP in these cells, while recording with the gramicidin perforated patch technique to preserve intracellular polyamines (13).

Stimulation of pyramidal cell axon collaterals in the alveus evoked monosynaptic excitatory postsynaptic potentials (EPSPs) subthreshold for evoking action potentials. After recording a baseline, we paired high-frequency burst (HFB) stimulation (five pulses at 100 Hz, repeated 20 times) with stimulation of a second, supra-threshold, alveus pathway. "In-phase" associative pairing (phase difference  $\Delta\Phi = 0^\circ$ ) failed to elicit associative LTP in either pathway ( $n = 7$ ; Fig. 1, A and B). In a further set of experiments, we alternately stimulated two weak pathways, and then delivered HFBs to both pathways antiphase ( $\Delta\Phi = 180^\circ$ ). This evoked a persistent increase in EPSP initial slope in one or both pathways in all cells ( $n = 7$ ; Fig. 1, C and D). LTP was elicited even when HFB stimuli were delivered to only one weak pathway ( $n = 7$ ; Fig. 1, E and F). Thus, LTP at excitatory synapses on interneurons in the oriens/alveus is prevented by associative pairing, in direct contrast to NMDAR-dependent LTP (1).

Can direct manipulation of the postsynaptic membrane potential similarly gate LTP induction? We delivered HFBs to one pathway

<sup>1</sup>Institute of Neurology, University College London, Queen Square, London WC1N 3BG, UK. <sup>2</sup>Anatomical Neuropharmacology Unit, Medical Research Council, Oxford University, Mansfield Road, Oxford OX1 3HT, UK.

\*To whom correspondence should be addressed. E-mail: d.kullmann@ion.ucl.ac.uk

dc\_1581\_18

coinciding with the trough (somatic voltage:  $-90$  mV) of an imposed 4-Hz sinusoidal somatic membrane potential oscillation. HFBs were then delivered to the other pathway coinciding with the depolarizing phase. In 8 out of 11 cells, pairing with hyperpolarization, but not with depolarization, resulted in LTP (Fig. 2, A and B). One cell showed the opposite behavior, and the other two showed no effect of either pairing (fig. S1). Single alveus stimuli in phase with maximum hyperpolarization (100 times) also induced LTP ( $n = 10$ ; Fig. 2C), but pairing with depolarization was ineffective (Fig. 2D). Thus, even low-frequency stimulation can trigger LTP if interneurons are hyperpolarized.

Because the induction requirements for LTP in most interneurons in the oriens/alveus are diametrically opposite to Hebb's postulate (14, 15), we refer to it as "anti-Hebbian." We tested the same LTP induction protocols in interneurons in the stratum radiatum. Hebbian LTP could be elicited in about half of these cells, many of which mediate feedforward inhibition (16), whereas pairing either HFB or low-frequency stimuli with hyperpolarization was uniformly unsuccessful (figs. S1 and S2). Anti-Hebbian LTP is thus characteristic of excitatory synapses made by local pyramidal cells on interneurons in the oriens/alveus but not of

Schaffer collateral synapses on interneurons in the stratum radiatum.

Can differences in synaptic glutamate receptors explain whether Hebbian, anti-Hebbian, or no LTP is elicited? When interneurons in the oriens/alveus were recorded in whole-cell voltage clamp [with  $\gamma$ -aminobutyric acid (GABA) receptors blocked, and with spermine included in the pipette solution], synaptic AMPARs activated by alveus stimulation were generally strongly rectifying (Fig. 2E), consistent with expression of CP-AMPA receptors (11). Furthermore, only small NMDAR-mediated synaptic currents were detected at a positive holding potential, consistent with low synaptic expression of the NR1 subunit (17).

We tested interneurons in the oriens/alveus, recorded in perforated patch mode, with a further anti-Hebbian protocol. High-frequency stimulation of one alveus pathway (100 Hz, 100 pulses, delivered twice) paired with hyperpolarization, with NMDARs blocked, elicited LTP in 25 out of 31 cells (Figs. 3A and 4C). We repatched 11 of these cells in whole-cell voltage-clamp mode and found pronounced synaptic AMPAR rectification in every cell where anti-Hebbian LTP was evoked. The rectification index did not differ detectably between control and potentiated pathways (Fig. 3B), yielding no evidence for an LTP-related change

in the permeability of synaptic AMPARs to  $\text{Ca}^{2+}$  (18).

In contrast, repatched interneurons in the stratum radiatum generally showed nonrectifying AMPARs and a large NMDAR-mediated component of Schaffer collateral-evoked synaptic currents (fig. S2) (9). The anti-Hebbian LTP induction protocol was successful in only 2 out of 20 cells in the stratum radiatum. AMPARs at Schaffer collateral synapses on 11 cells (none of which showed anti-Hebbian LTP) were nonrectifying (fig. S3).

Anti-Hebbian LTP thus typically occurs at synapses on interneurons in the oriens/alveus equipped with rectifying CP-AMPA receptors. Are these a uniform subgroup? Seven interneurons were regular-spiking oriens-lacunosum moleculare (O-LM) cells (Fig. 3C, fig. S4), which mediate feedback inhibition of the apical dendrites of pyramidal neurons (19). Twelve other interneurons had horizontal dendrites and electrophysiological properties typical of O-LM cells, but axon visualization was incomplete (fig. S5). Anti-Hebbian LTP, however, also occurred in 17 out of 24 fast-spiking interneurons in the strata oriens or pyramidal, including one anatomically confirmed axo-axonic and two basket cells, which are innervated by CA1 pyramidal cells and target their perisomatic area. Seven other cells could not be classified.

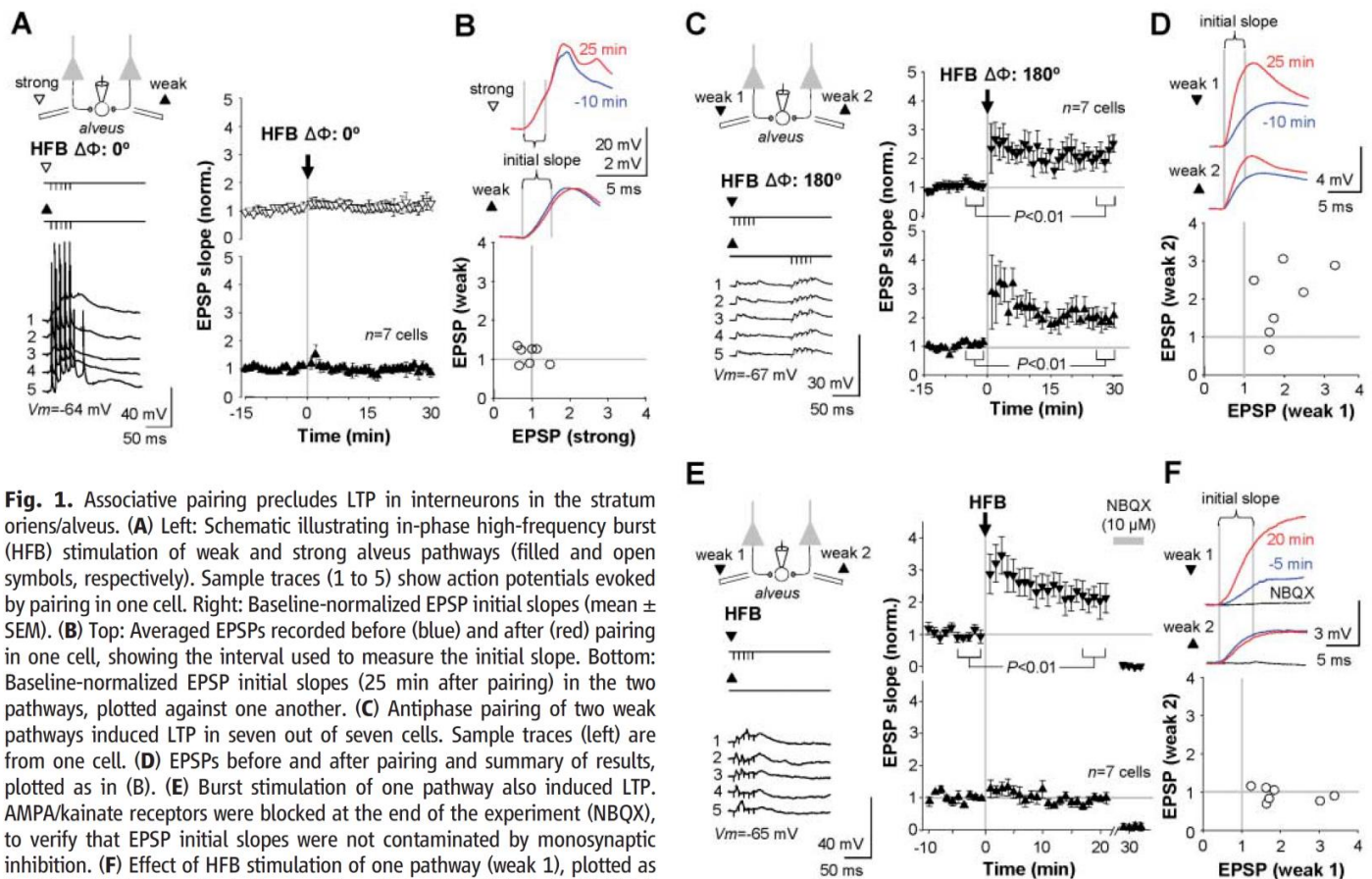


**Fig. 1.** Associative pairing precludes LTP in interneurons in the stratum oriens/alveus. **(A)** Left: Schematic illustrating in-phase high-frequency burst (HFB) stimulation of weak and strong alveus pathways (filled and open symbols, respectively). Sample traces (1 to 5) show action potentials evoked by pairing in one cell. Right: Baseline-normalized EPSP initial slopes (mean  $\pm$  SEM). **(B)** Top: Averaged EPSPs recorded before (blue) and after (red) pairing in one cell, showing the interval used to measure the initial slope. Bottom: Baseline-normalized EPSP initial slopes (25 min after pairing) in the two pathways induced LTP in seven out of seven cells. **(C)** Antiphase pairing of two weak pathways induced LTP in seven out of seven cells. Sample traces (left) are from one cell. **(D)** EPSPs before and after pairing and summary of results, plotted as in **(B)**. **(E)** Burst stimulation of one pathway also induced LTP. AMPA/kainate receptors were blocked at the end of the experiment (NBQX), to verify that EPSP initial slopes were not contaminated by monosynaptic inhibition. **(F)** Effect of HFB stimulation of one pathway (weak 1), plotted as for **(B)** and **(D)**. Traces (top) also show the effect of NBQX. Data in **(C)** (right) and **(E)** (right) are shown as the mean  $\pm$  SEM.  $V_m$ , membrane potential.

Anti-Hebbian LTP is, however, rare at Schaffer collateral synapses on interneurons in the stratum radiatum, which generally mediate feedforward inhibition and express nonrectifying receptors (Fig. 3, D and E). Synaptic responses evoked by stratum radiatum stimulation in fast-spiking interneurons in the stratum pyramidale, however, had strongly rectifying AMPARs and a small NMDA component, and the Hebbian LTP induction protocol was uniformly unsuccessful ( $n = 4$ ; fig. S6).

Does rectification of CP-AMPA receptors fully explain the anti-Hebbian nature of LTP in interneurons in the oriens/alveus? We first verified that AMPA/kainate receptors are necessary for induction, by pairing HFS with postsynaptic hyperpolarization while AMPA/kainate receptors were blocked with 2,3-dihydroxy-6-nitro-7-sulfamoylbenzof[*q*]quinoxaline (NBQX, 5  $\mu$ M): After wash-out of the antagonist, EPSPs in the tetanized and control pathways recovered to the same extent ( $n = 7$ ; Fig. 3F). We then explored systematically the voltage dependence of LTP. In five cells in the oriens/alveus where anti-Hebbian LTP was evoked in one alveus pathway, subsequent pairing of the other pathway with depolarization only evoked short-lived post-tetanic potentiation

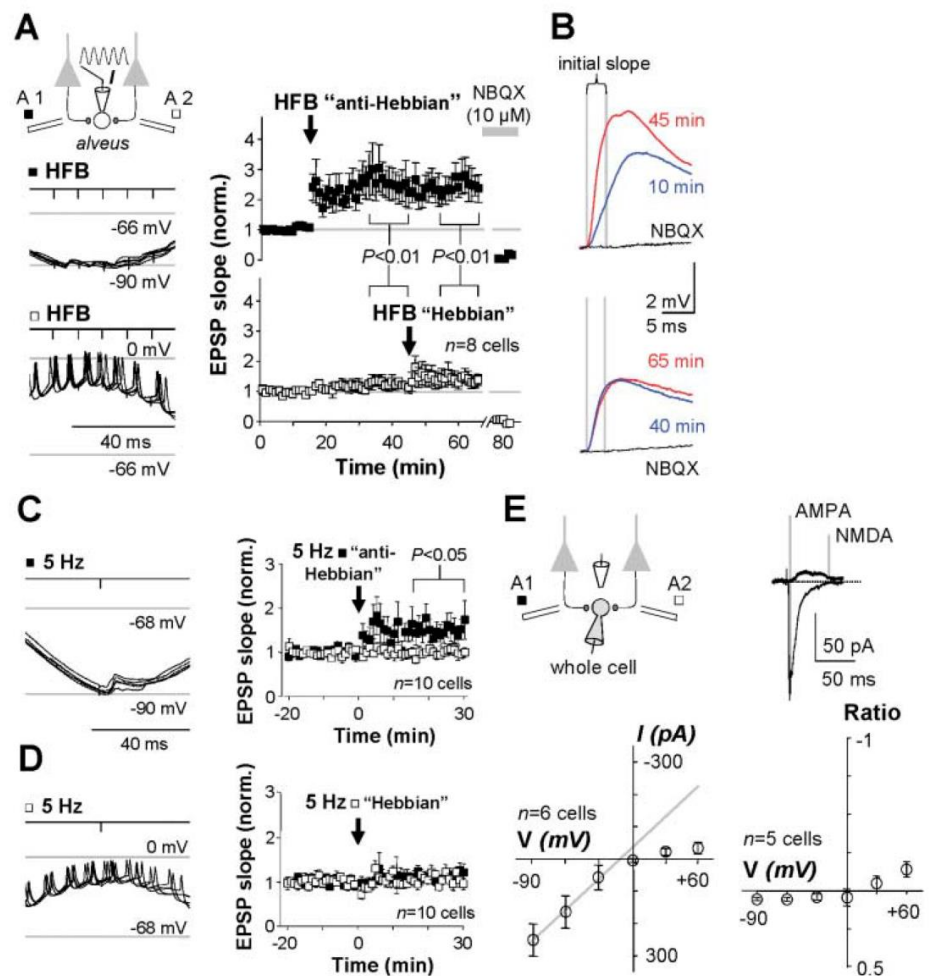
(Fig. 4A). In six other cells, pairing the second pathway with hyperpolarization elicited robust LTP in all cases (Fig. 4, B and C). We then adapted this experimental design to explore the effect of manipulating the rectification properties of CP-AMPA receptors. Having demonstrated anti-Hebbian LTP in one pathway, we repatched the interneuron in whole-cell mode either with or without spermine in the pipette solution. Following a short baseline recording ( $\leq 7$  min from patch rupture), we then paired HFS of the second pathway either with depolarization (+20 mV) or with hyperpolarization (-90 mV). When spermine was omitted, pairing with depolarization evoked LTP in five out of five cells (Fig. 4D), consistent with  $Ca^{2+}$  influx via CP-AMPA receptors rendered non-rectifying by removal of polyamines (4). In contrast, HFS paired with depolarization failed to elicit LTP in five cells that were repatched with a spermine-containing pipette (Fig. 4E). In five other interneurons repatched with a spermine-containing solution, pairing HFS of the second pathway with hyperpolarization to -90 mV evoked LTP (Fig. 4F).

Polyamine-mediated rectification of AMPARs (and/or kainate receptors) thus explains the voltage dependence of LTP induction in these

interneurons and reconciles our results with previous reports that a Hebbian protocol induces LTP in interneurons in the oriens/alveus when recorded with a polyamine-free whole-cell pipette solution (12). Also consistent with these reports, blockade of group I metabotropic glutamate receptors prevented LTP induction in interneurons with horizontal dendrites in the oriens/alveus (fig. S7). Finally, we looked for evidence that anti-Hebbian LTP is accompanied by an increase in glutamate-release probability (12), by applying extracellular polyamines, which also block CP-AMPA receptors in a use-dependent manner (20). After inducing anti-Hebbian LTP in one pathway, bath perfusion of *N*-(4-hydroxyphenylpropanoyl)-spermine (5 to 10  $\mu$ M) caused a progressive decrease in EPSP initial slope, which was significantly faster in the paired than in the control pathway ( $n = 7$ ; fig. S8). Given that anti-Hebbian LTP did not alter AMPAR rectification (Fig. 3B), this result is consistent with presynaptic expression.

Anti-Hebbian LTP may play distinct roles in neurons that show characteristic phase relationships in different network states (21, 22). During sharp-wave ripples, O-LM cells are typically silent, while many of their input pyramidal neu-

**Fig. 2.** Postsynaptic membrane potential gates anti-Hebbian LTP induction. **(A)** LTP was evoked by pairing presynaptic stimulation with the hyperpolarizing but not the depolarizing phase of an imposed sinusoidal membrane potential oscillation. Left: Schematic and sample membrane potential traces during pairing in one cell (five sweeps superimposed for each pairing protocol). Right: Baseline-normalized EPSP initial slopes in eight cells showing LTP after anti-Hebbian pairing of one pathway with hyperpolarization. Subsequent Hebbian pairing of the other pathway with depolarization was ineffective. AMPA/kainate receptors were blocked at the end of the experiment (NBQX). Data are shown as the mean  $\pm$  SEM. **(B)** Averaged EPSPs in one cell taken at the times indicated and after NBQX addition. Top: Anti-Hebbian pairing. Bottom: Hebbian pairing. **(C)** LTP was induced by pairing single stimuli at 5 Hz with hyperpolarization. Left: Sample traces during pairing. Right: Averages of all cells tested. Data are shown as the mean  $\pm$  SEM. **(D)** Pairing with depolarization failed to induce LTP. Left: Sample traces during pairing. Right: Averages of all cells tested. Data are shown as the mean  $\pm$  SEM. **(E)** Repatched interneurons recorded in whole-cell voltage-clamp mode show rectifying AMPARs and a negligible NMDAR-mediated component (GABA receptors blocked). Traces: Averaged EPSCs at +60 and -60 mV, showing the times at which the two components were measured. Bottom: current-voltage (*I*-*V*) relation of AMPAR-mediated EPSCs in six repatched interneurons (left). *I*-*V* relation for the NMDAR-mediated component, normalized by the AMPA EPSC at -60 mV (right).



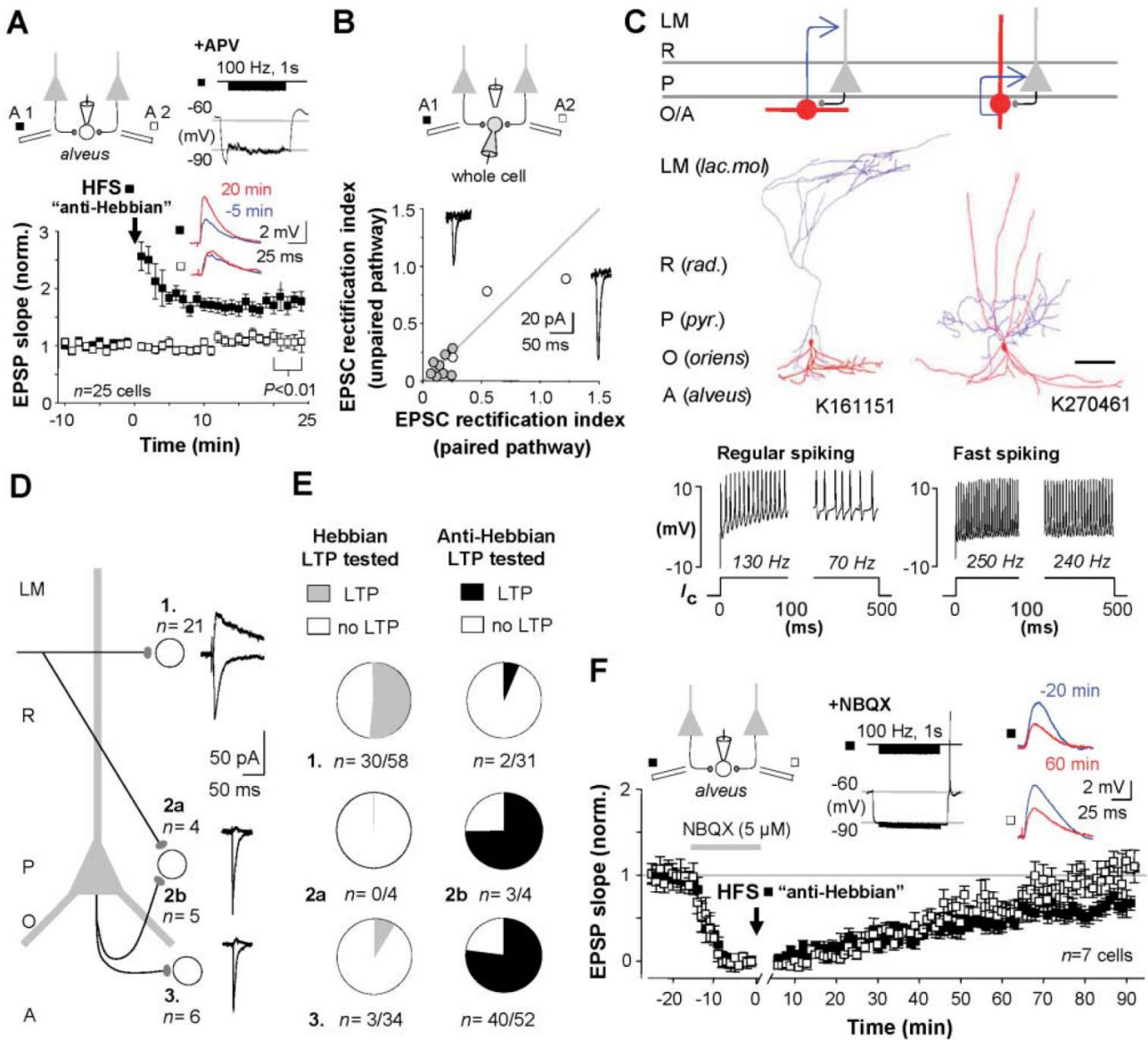


**Fig. 3.** Anti-Hebbian LTP occurs in interneurons with rectifying AMPARs in the feedback circuit. **(A)** High-frequency stimulation (HFS) paired with hyperpolarization evoked LTP in 25 out of 31 interneurons in the oriens/alveus [NMDARs blocked with 100  $\mu$ M D,L-2-amino-5-phosphonovaleate (APV)]. Insets: Averaged EPSPs before and after LTP induction, and membrane potential during pairing, in one interneuron. Data are shown as the mean  $\pm$  SEM. **(B)** Repatched interneurons recorded in whole-cell voltage-clamp mode revealed strongly rectifying synaptic AMPARs (rectification index  $<$  0.3). Gray and open symbols show cells that did and did not exhibit LTP, respectively. Insets: Averaged EPSCs at  $-60$  and  $+60$  mV in one cell that showed anti-Hebbian LTP. **(C)** O-LM cells were the commonest identified interneuron type exhibiting anti-Hebbian LTP (left: schematic, with dendritic and axonal arborizations for one cell shown in red and blue, respectively).

Three fast spiking perisomatic-projecting neurons were also identified, including a basket cell (right). Scale bar: 200  $\mu$ m. Firing patterns in response to current injection ( $I_c$ ) are shown below. **(D)** Typical layer- and pathway-specific properties of EPSCs in experiments where NMDARs were not blocked ( $n$ , number of repatched interneurons). Interneurons were recorded in the stratum radiatum (1), stratum pyramidale (2), and stratum oriens/alveus (3). **(E)** Success rates for eliciting Hebbian or anti-Hebbian LTP at synapses made by axons illustrated in (D). **(F)** Anti-Hebbian LTP requires activation of AMPA/kainate receptors. HFS stimulation of one pathway (filled symbols) was paired with hyperpolarization in NBQX (5  $\mu$ M) (inset). After wash-out, EPSPs in both pathways recovered at the same rate. Inset: Averaged EPSPs before pairing (blue) and after recovery (red) in the two pathways in one experiment. Data are shown as the mean  $\pm$  SEM.

rons fire at high frequency (21), possibly satisfying the induction conditions for anti-Hebbian LTP. Binding of pyramidal neurons to a spatial map may occur during periods of high-frequency firing (23), similar to sharp-wave ripples. In contrast, during theta activity, which is associated with exploratory behavior (24), O-LM cells fire

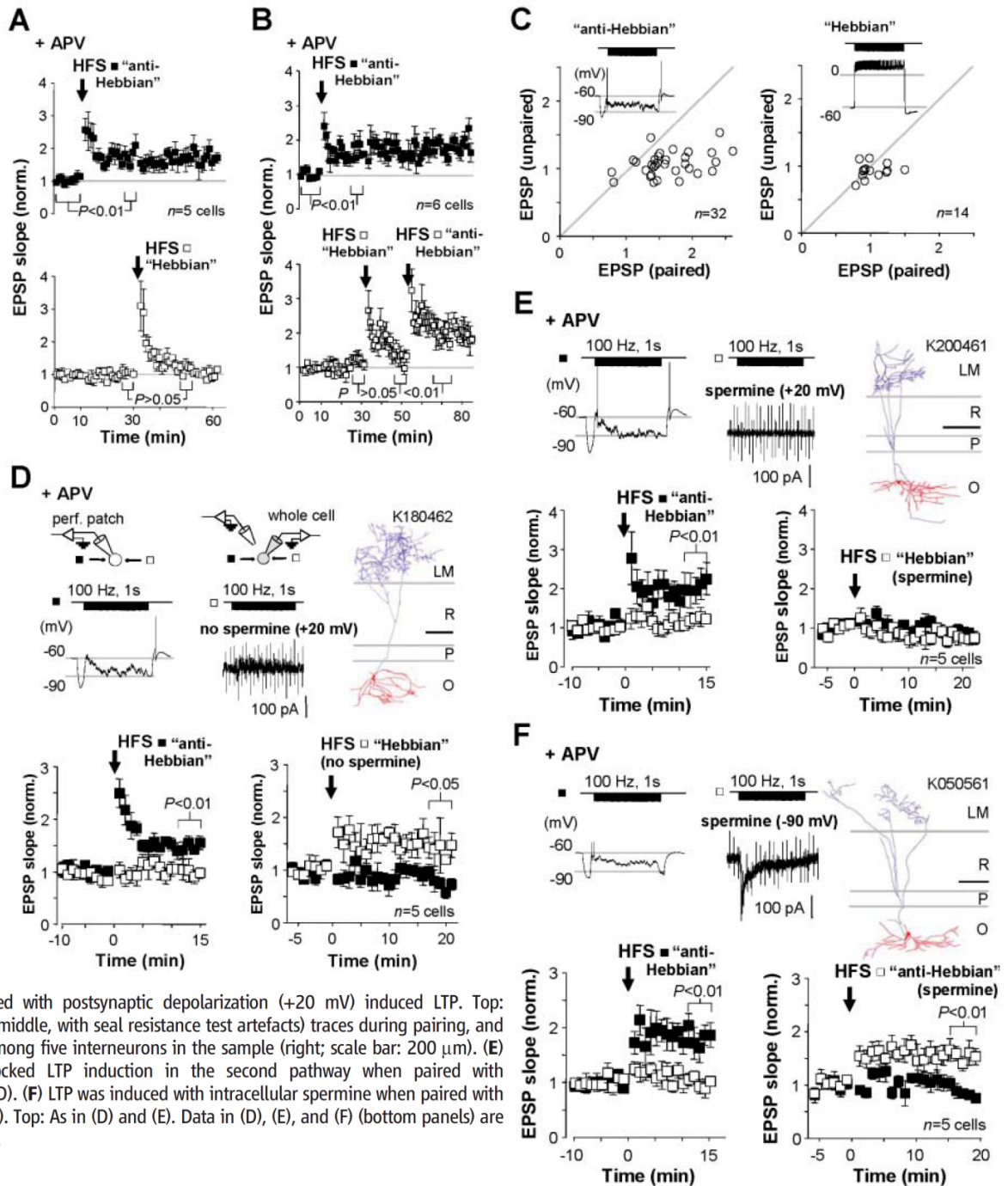
in phase with pyramidal cells (21) and may contribute to this oscillation through phase-locked dendritic inhibition (25). Anti-Hebbian LTP induced during ripples may therefore result in a long-term alteration of pyramidal cell excitation of O-LM cells, which persists during theta activity, and may therefore contribute to

spatial memory formation, the early stages of which have been shown to withstand NMDAR blockade (26).

**References and notes**

1. T. V. Bliss, G. L. Collingridge, *Nature* **361**, 31 (1993).
2. P. Jonas, C. Racca, B. Sakmann, P. H. Seeburg, H. Monyer, *Neuron* **12**, 1281 (1994).

**Fig. 4.** Intracellular polyamines determine the voltage dependence of anti-Hebbian LTP. **(A)** Postsynaptic depolarization prevents LTP induction. Data from cells recorded in perforated patch mode, showing LTP induced by pairing high-frequency stimulation (HFS) of one pathway with hyperpolarization (top, "anti-Hebbian"), and failure to induce LTP by pairing the other pathway with depolarization (bottom, "Hebbian"). NMDARs were blocked throughout. Data are the mean  $\pm$  SEM. **(B)** In six other cells, the second pathway was subsequently paired with hyperpolarization, yielding anti-Hebbian LTP in all cases. Data are the mean  $\pm$  SEM. **(C)** Baseline-normalized EPSP slopes plotted against one another 20 min after anti-Hebbian (left) and Hebbian (right) pairing. Insets: Sample membrane potential traces during pairing. **(D)** Anti-Hebbian LTP was first induced in one pathway (left, filled symbols). The interneuron was then repatched in whole-cell mode with a polyamine-free pipette solution. HFS delivered to the second pathway (right, open symbols) paired with postsynaptic depolarization (+20 mV) induced LTP. Top: Voltage (left) and current (middle, with seal resistance test artefacts) traces during pairing, and one O-LM cell identified among five interneurons in the sample (right; scale bar: 200  $\mu$ m). **(E)** Intracellular spermine blocked LTP induction in the second pathway when paired with depolarization. Top: As in (D). **(F)** LTP was induced with intracellular spermine when paired with hyperpolarization (-90 mV). Top: As in (D) and (E). Data in (D), (E), and (F) (bottom panels) are shown as the mean  $\pm$  SEM.



- M. S. Washburn, M. Numberger, S. Zhang, R. Dingledine, *J. Neurosci.* **17**, 9393 (1997).
- S. D. Donevan, M. A. Rogawski, *Proc. Natl. Acad. Sci. U.S.A.* **92**, 9298 (1995).
- D. Bowie, M. L. Mayer, *Neuron* **15**, 453 (1995).
- J. G. Gu, C. Albuquerque, C. J. Lee, A. B. MacDermott, *Nature* **381**, 793 (1996).
- N. K. Mahanty, P. Sah, *Nature* **394**, 683 (1998).
- F. Laezza, J. J. Doherty, R. Dingledine, *Science* **285**, 1411 (1999).
- S. Lei, C. J. McBain, *Neuron* **33**, 921 (2002).
- F. Laezza, R. Dingledine, *J. Neurophysiol.* **92**, 3575 (2004).
- L. Topolnik, P. Congar, J. C. Lacaillle, *J. Neurosci.* **25**, 990 (2005).
- Y. Perez, F. Morin, J. C. Lacaillle, *Proc. Natl. Acad. Sci. U.S.A.* **98**, 9401 (2001).
- Materials and methods are available as supporting material on Science Online.
- D. O. Hebb, *The Organization of Behavior* (Wiley, New York, 1949).
- G. Bi, M. Poo, *Annu. Rev. Neurosci.* **24**, 139 (2001).
- K. Lamsa, J. H. Heeroma, D. M. Kullmann, *Nat. Neurosci.* **8**, 916 (2005).
- G. Nyiri, F. A. Stephenson, T. F. Freund, P. Somogyi, *Neuroscience* **119**, 347 (2003).
- K. Plant *et al.*, *Nat. Neurosci.* **9**, 602 (2006).
- J. M. Blasco-Ibanez, T. F. Freund, *Eur. J. Neurosci.* **7**, 2170 (1995).
- Z. F. Mainen, Z. Jia, J. Roder, R. Malinow, *Nat. Neurosci.* **1**, 579 (1998).
- T. Klausberger *et al.*, *Nature* **421**, 844 (2003).
- T. Klausberger *et al.*, *Nat. Neurosci.* **7**, 41 (2004).
- G. Dragoi, K. D. Harris, G. Buzsaki, *Neuron* **39**, 843 (2003).
- G. Buzsaki, *Neuron* **33**, 325 (2002).
- M. J. Gillies *et al.*, *J. Physiol.* **543**, 779 (2002).
- C. Kentros *et al.*, *Science* **280**, 2121 (1998).
- Animal procedures followed the Animals (Scientific Procedures) Act 1986. Supported by the Wellcome Trust, the Academy of Finland, and the Medical Research Council. We are grateful to M. C. Walker and K. Volynski for comments, and to J. D. B. Roberts for help with histological processing.

**Supporting Online Material**  
www.sciencemag.org/cgi/content/full/315/5816/1262/DC1  
Materials and Methods  
Figs. S1 to S8  
References  
13 November 2006; accepted 1 February 2007  
10.1126/science.1137450

**III**

# Cell Type-Specific Long-Term Plasticity at Glutamatergic Synapses onto Hippocampal Interneurons Expressing either Parvalbumin or CB<sub>1</sub> Cannabinoid Receptor

Wiebke Nissen,<sup>1</sup> Andras Szabo,<sup>1</sup> Jozsef Somogyi,<sup>2</sup> Peter Somogyi,<sup>2</sup> and Karri P. Lamsa<sup>1</sup>

<sup>1</sup>Department of Pharmacology, Oxford University, Oxford OX1 3QT, United Kingdom, and <sup>2</sup>Medical Research Council Anatomical Neuropharmacology Unit, Oxford University, Oxford OX1 3TH, United Kingdom

Different GABAergic interneuron types have specific roles in hippocampal function, and anatomical as well as physiological features vary greatly between interneuron classes. Long-term plasticity of interneurons has mostly been studied in unidentified GABAergic cells and is known to be very heterogeneous. Here we tested whether cell type-specific plasticity properties in distinct GABAergic interneuron types might underlie this heterogeneity. We show that long-term potentiation (LTP) and depression (LTD), two common forms of synaptic plasticity, are expressed in a highly cell type-specific manner at glutamatergic synapses onto hippocampal GABAergic neurons. Both LTP and LTD are generated in interneurons expressing parvalbumin (PV+), whereas interneurons with similar axon distributions but expressing cannabinoid receptor-1 show no lasting plasticity in response to the same protocol. In addition, LTP or LTD occurs in PV+ interneurons with different efferent target domains. Perisomatic-targeting PV+ basket and axo-axonic interneurons express LTP, whereas glutamatergic synapses onto PV+ bistratified cells display LTD. Both LTP and LTD are pathway specific, independent of NMDA receptors, and occur at synapses with calcium-permeable (CP) AMPA receptors. Plasticity in interneurons with CP-AMPA receptors strongly modulates disynaptic GABAergic transmission onto CA1 pyramidal cells. We propose that long-term plasticity adjusts the synaptic strength between pyramidal cells and interneurons in a cell type-specific manner and, in the defined CA1 interneurons, shifts the spatial pattern of inhibitory weight from pyramidal cell dendrites to the perisomatic region.

## Introduction

Synapses between cortical excitatory principal cells show relatively stereotypical activity-induced plasticity and may express either long-term potentiation (LTP) or long-term depression (LTD) depending on glutamate NMDA receptors (NMDARs). Concomitant with LTP in hippocampal pyramidal cells, the strength of local inhibition is often altered (Kullmann and Lamsa, 2007; McBain, 2008; Pelletier and Lacaille, 2008). Parallel modulation of inhibition is likely to be required to balance changes in the network excitability caused by plasticity between principal cells (Kullmann and Lamsa, 2007), as well as to maintain fidelity, threshold, and gain of pyramidal cell responses to their excitatory inputs (Lamsa et al., 2005; Carvalho and Buonomano, 2009).

However, plasticity reported in GABAergic interneurons is highly heterogeneous and varies between hippocampal areas and layers (McMahon and Kauer, 1997; Cowan et al., 1998; Alle et al., 2001; Perez et al., 2001; Lei and McBain, 2004; Lamsa et al., 2005, 2007; Galván et al., 2008), possibly reflecting the high diversity of GABAergic cells in the hippocampus (Kullmann and Lamsa, 2007; McBain, 2008). Cell type-specific firing patterns of many interneurons *in vivo* suggest that distinct GABAergic cell types have highly specified roles in the hippocampal function (Klausberger et al., 2003, 2005). Excitatory glutamatergic synapses onto many hippocampal interneurons have calcium-permeable (CP) AMPA receptors (AMPA receptors), and these synapses often express NMDA receptor-independent LTP or LTD (Laezza et al., 1999; Perez et al., 2001; Laezza and Dingledine, 2004; Lei and McBain, 2004; Lamsa et al., 2007; Oren et al., 2009). Afferent stimulation of glutamatergic pathways, which elicits LTP in principal cells in the hippocampal CA1 or dentate gyrus, can induce parallel potentiation of GABAergic transmission (Buzsáki and Eidelberg, 1982; Kairiss et al., 1987; Lapointe et al., 2004; Lamsa et al., 2005). It has been suggested that this might result from LTP of excitatory glutamatergic synapses driving a subpopulation of local inhibitory interneurons (Kullmann and Lamsa, 2007; Pelletier and Lacaille, 2008). Equally, afferent stimulation of hippocampal mossy fibers can elicit either LTP or LTD in CA3 inhibitory cells in a layer-specific manner (Maccaferri et al., 1998; Lei and McBain, 2004; Galván et al., 2008; McBain, 2008), but each hippocampal layer may contain several types of interneurons, as defined by their

Received July 16, 2009; revised Oct. 12, 2009; accepted Nov. 22, 2009.

This work was supported by the Wellcome Trust, the United Kingdom Medical Research Council, and the German Academic Exchange Service (Deutscher Akademischer Austausch Dienst). We are grateful to Tamas Bellak, Wendy Tynan, Kristina Detzner, and David Roberts for expert technical assistance. We thank Drs. Colin Akerman, Marlene Bartos, Marco Capogna, Jozsef Csicsvari, Dimitri Kullmann, Peter Magill, and Trevor Sharp for comments on this manuscript. We thank the following scientists for their generous gifts of antibodies: K. G. Baimbridge (antibody to parvalbumin), A. Buchan (to somatostatin), T. Gorcs (to VIP), A. Varro (to pro-CCK), M. Watanabe (to CB<sub>1</sub> receptor, VGluT3), and S. El Mestikawy (to VGluT3). Antibodies 9303 and 55 raised against CCK and VIP, respectively, were provided by the Center for Ulcer Research/Digestive Diseases Research Center, Antibody/Radioimmunoassay Core (National Institutes of Health Grant DK41301).

Correspondence should be addressed to K. Lamsa, Department of Pharmacology, Oxford University, Mansfield Road, Oxford OX1 3QT, UK. E-mail: karri.lamsa@pharm.ox.ac.uk.

J. Somogyi's present address: JSW Life Sciences, Parkring 12, Grambach A-8074, Austria.

DOI:10.1523/JNEUROSCI.3481-09.2010

Copyright © 2010 the authors 0270-6474/10/301337-11\$15.00/0

neurochemical markers and the pyramidal cell membrane domains that their axons target. To understand the nature and functional significance of heterogeneous interneuron plasticity in the hippocampus, it is therefore important to identify the interneurons studied in terms of their axonal projections and molecular expression profiles.

Here we test how consistent long-term plasticity is across five common interneuron types innervating different domains of pyramidal cells in the hippocampal CA1 area. We hypothesized that plasticity properties might systematically vary between individual GABAergic interneuron types. In the CA1 area, interneurons immunopositive for parvalbumin (PV+) or cannabinoid receptor 1 (CB<sub>1</sub>R+) collectively target the whole postsynaptic surface of local pyramidal cells, but individual cell types preferentially innervate one or more specific membrane domains of their targets. We demonstrate that there are cell type-specific rules of plasticity that emphasize distinct roles of interneurons in hippocampal function.

## Materials and Methods

### Hippocampal slice preparation

Three- to 4-week-old male Sprague Dawley rats were killed according to the Animals (Scientific Procedures) Act 1986, and transverse hippocampal slices (350  $\mu$ m thickness) were prepared as described by Oren et al. (2009) (supplemental Methods, available at [www.jneurosci.org](http://www.jneurosci.org) as supplemental material). Hippocampal slices were placed in a recording chamber (Luigs & Neumann) mounted on the stage of an upright microscope (Olympus BX51WI), where they were held under a nylon mesh grid and superfused at 3–5 ml/min with artificial CSF at 31–33°C. Slices were visualized using a 20 $\times$  immersion objective with 2–4 $\times$  zoom and infrared differential interference contrast (DIC) optics. A cut was made between CA1 and CA3 to prevent propagation of recurrent excitation from the CA3. The perfusion medium contained the following (in mM): 119 NaCl, 2.5 KCl, 2.5 CaCl<sub>2</sub>, 1.3 MgSO<sub>4</sub>, 1.25 NaH<sub>2</sub>PO<sub>4</sub>, 25 NaHCO<sub>3</sub>, and 11 glucose, final pH 7.4 (equilibrated with 95% O<sub>2</sub>/5% CO<sub>2</sub>). Glutamate NMDARs were blocked with DL-APV (100  $\mu$ M) unless stated otherwise. The GABA receptor blockers picrotoxin (PitX) (100  $\mu$ M) and CGP55845 [(2S)-3-[(1S)-1-(3,4-dichlorophenyl)ethyl]amino-2-hydroxypropyl](phenylmethyl)phosphonic acid] (1  $\mu$ M) were added to the solution for all experiments except those for recording IPSCs (see Figs. 5, 6) (supplemental Figs. S3, S4, available at [www.jneurosci.org](http://www.jneurosci.org) as supplemental material). In experiments with cannabinoid receptor type 1 antagonist AM-251 [N-1-(2,4-dichlorophenyl)-5-(4-iodophenyl)-4-methyl-N-1-piperidinyl-1H-pyrazole-3-carboxamide] (5–10  $\mu$ M), slices were incubated with the drug for at least 1 h before recording, and the drug was present in the perfusion solution. Glutamate receptor antagonists philanthotoxin-433 (PhTx) (10  $\mu$ M) and NBQX (10  $\mu$ M) were applied via perfusion. Chemicals were purchased from Sigma-Aldrich and drugs from Tocris Bioscience or Ascent Scientific.

### Electrophysiological recordings

**Perforated patch.** For additional details, see supplemental Methods (available at [www.jneurosci.org](http://www.jneurosci.org) as supplemental material). Somatic perforated-patch recordings were made from neurons close to or inside CA1 stratum (str.) pyramidale using pipettes containing gramicidin (50–200  $\mu$ g/ml). Electrodes were made from borosilicate glass capillaries. Pipette resistance was 8–15 M $\Omega$ . Filling solution contained the following (in mM): 145 K-gluconate, 8 NaCl, 20–25 K-HEPES, 0.2 EGTA, and 5 QX-314 Br [N-(2,6-dimethylphenylcarbamoylmethyl)triethylammonium bromide], pH 7.2 (osmolarity, 295 mOsm/L). The electrode tip was filled with gramicidin-free solution. Recordings were started when series resistance was below 150 M $\Omega$ . Series resistance was continuously monitored but not recorded.

**Repatch.** After completion of perforated patch recordings, the pipette was slowly retracted under infrared DIC observation. Once the pipette detached from the cell, it was rapidly withdrawn from the slice. Next, the same cell was approached with a new pipette and repatched in whole-cell

configuration. Infrared images of the cell at different magnification were obtained with a CCD camera during perforated patch recording and compared in whole-cell recordings to verify that the same cell was repatched (supplemental Fig. 1, available at [www.jneurosci.org](http://www.jneurosci.org) as supplemental material) (Lamsa et al., 2005, 2007; Oren et al., 2009). Voltage-clamp recording of EPSCs was performed in repatched cells only if access resistance was <20 M $\Omega$ .

**Whole cell.** For additional details, see supplemental Methods (available at [www.jneurosci.org](http://www.jneurosci.org) as supplemental material). The whole-cell recordings were made with a solution containing the following (in mM): 145 CsCl, 20 HEPES, 0.2 Cs-EGTA, 8 NaCl, 2 Mg-ATP, 0.3 GTP, and 5 QX-314 Br, pH 7.2 (295 mOsm). In some experiments, 145 mM Cs-methanesulphonate was used instead of CsCl. Spermine tetrahydrochloride (0.5 mM; Tocris Bioscience) was included in the filling solution to maintain polyamine-mediated rectification of AMPA/kainate receptors during whole-cell recording. In addition, Neurobiotin (0.2–0.5%; Vector Laboratories) or biocytin (0.5%; Sigma-Aldrich) was included in the solution to enable *post hoc* anatomical analysis. Electrode input resistance for whole-cell recordings was 4–6 M $\Omega$ .

**Electrical stimulation.** For additional details, see supplemental Methods (available at [www.jneurosci.org](http://www.jneurosci.org) as supplemental material). Monosynaptic EPSPs or EPSCs were evoked by alternately stimulating (50–100  $\mu$ s) in the str. oriens/alveus in area CA1 with 15 s interevent interval via two concentric bipolar electrodes, connected to constant-current isolated stimulators. In some experiments, the stimulation electrode for control pathway was positioned in str. radiatum (supplemental Tables 1, 2, available at [www.jneurosci.org](http://www.jneurosci.org) as supplemental material). Evoked EPSPs were recorded from the resting membrane potential or in some experiments during a brief (500 ms) hyperpolarizing step (5–10 mV) to avoid action potential generation. In whole-cell recordings, EPSC current–voltage relationships were estimated over a postsynaptic membrane potential range from –90 to +60 mV using 1 s steps in voltage-clamp mode. The EPSC rectification index (RI) was obtained by dividing the amplitude of the EPSC recorded at +60 mV by that measured at –60 mV. A Multiclamp 700B amplifier was used for recording. In all recordings, data were low-pass filtered (4–5 kHz) and acquired at 10–20 kHz on a personal computer for offline analysis. Data were analyzed using LabView and pClamp 10. Disynaptic IPSCs were evoked by stimulation in str. oriens/alveus and voltage clamping the postsynaptic cell between 0 and +10 mV (Cs-methanesulphonate-containing filling solution was used). Maximum disynaptic IPSC was screened by increasing stimulation intensity voltage using fixed duration (100–150  $\mu$ s). Submaximal amplitude IPSCs were evoked by shortening the stimulation duration (up to 25  $\mu$ s).

**Statistics.** Data are shown as mean  $\pm$  SE. Data on postsynaptic potentials/currents were baseline normalized within each pathway and analyzed with Student's paired *t* test. Within each cell, the change in the initial slope (3–5 ms from onset) of the paired pathway was compared with that of the control pathway with an unpaired *t* test.

### Anatomical analysis

**Tissue processing.** For additional details, see supplemental Methods (available at [www.jneurosci.org](http://www.jneurosci.org) as supplemental material). Neurons were filled with Neurobiotin (Vector Laboratories) or biocytin (Sigma) during whole-cell recordings, fixed, and examined as described by Oren et al. (2009). For illustration, selected cells were digitally photographed from one or two 70- $\mu$ m-thick sections using structured illumination microscopy (AxioImager ApoTome, Carl Zeiss AxioImager.Z1) with a Carl Zeiss 38HE filter, 40 $\times$  oil-immersion objective and AxioVision Release 4.7.1 software. Images were constructed from Z-stacks using NIH ImageJ 1.42 software and inverted to show the cell on a white background; NeuronJ program was used for neurite tracing at a preset line thickness and quantification. Dendrites were manually selected from microscopic examination and are shown in a color different from the axon. Epifluorescent images were taken with the Carl Zeiss AxioImager.Z1 microscope (Carl Zeiss HE38 filter, 40 $\times$  or 63 $\times$  oil-immersion objective) using AxioVision software, and digital micrographs were constructed from Z-stacks with NIH ImageJ software. Micrographs were not

manipulated selectively; only brightness and contrast of the whole stacked image was adjusted.

**Immunohistochemistry.** For additional details, see supplemental Methods (available at [www.jneurosci.org](http://www.jneurosci.org) as supplemental material). Sections were blocked in normal horse serum (Vector Laboratories) for 1 h and incubated in mixtures of appropriate primary antibodies for 48 h at 4°C. A complete list of primary antibodies, their species, dilution, source, and specificity references is given in supplemental Table 3 (available at [www.jneurosci.org](http://www.jneurosci.org) as supplemental material). When fluorescence was not detectable in the relevant area of the section in which similar parts of other unfilled cells were immunopositive, cells were considered immunonegative. If a decision about immunoreactivity could not be clearly made because the cell appeared to be negative but the immunoreactivity in unrecorded cells of the slice was low or mostly absent, then the immunoreaction test does not inform about the presence or absence of the molecule in that specific cell. Furthermore, in cases of low immunoreactivity levels, when a conclusion could not be reached by several investigators, the test was considered inconclusive [indicated as reacted but not tested (“nt”) in supplemental Tables 1, 2, available at [www.jneurosci.org](http://www.jneurosci.org) as supplemental material].

**Electron microscopy.** Sections from two putative axo-axonic cells were prepared for electron microscopic analysis (supplemental Table 1, available at [www.jneurosci.org](http://www.jneurosci.org) as supplemental material). After fixation and resectioning of slices (as above), selected sections were washed in 0.1 M phosphate buffer (PB) and then stored in 0.05% sodium azide with 0.1 M PB. After cryoprotection with sucrose and freeze–thaw to enhance penetration of reagents, the cells were revealed with HRP reaction [ABC Elite kit (Vector Laboratories); 0.05% DAB (Sigma) and 0.01% H<sub>2</sub>O<sub>2</sub>]. The sections were treated with 1% OsO<sub>4</sub> (in phosphate buffer; TAAB Laboratory Equipment) and 1% aqueous uranyl acetate, dehydrated, and embedded in epoxy resin (Durcupan; Fluka). The axons were examined for the identity of postsynaptic targets without lead staining (Klausberger et al., 2003).

## Results

### Cell type-specific LTP in CA1 perisomatic-targeting interneurons

We studied long-term plasticity in glutamatergic afferents onto five different GABAergic interneuron types or groups in the hippocampal CA1 area, as defined by their axonal projections and molecular expression profiles (Klausberger and Somogyi, 2008). We patched putative interneurons inside or in the vicinity of str. pyramidale in the CA1 area of hippocampal slices. Perforated patch recording was used to minimize disruption of intracellular postsynaptic content of interneurons (Kullmann and Lamsa, 2007). Interneurons were then repatched with a new pipette in whole-cell mode, studied in voltage clamp, and filled with biocytin for *post hoc* anatomical identification (Lamsa et al., 2007; Oren et al., 2009). Cells were identified on the basis of axonal pattern and neurochemical marker expression. Briefly, cell types were as follows: axo-axonic cells innervating mainly or exclusively the axon initial segment of pyramidal cells; basket cells innervating somata and proximal dendrites as predicted from the concentration of their axon in str. pyramidale and expressing either PV or CB<sub>1</sub>R; and bistratified cells innervating mainly dendrites in str. radiatum and oriens and expressing PV, neuropeptide Y (NPY), and/or somatostatin (Halasy et al., 1996; Losonczy et al., 2002; Pawelzik et al., 2002; Klausberger et al., 2004; Baude et al., 2007). The fifth group of interneurons included several cell types in terms of synaptic targets, as predicted from the absence of axon concentration to str. pyramidale and, for brevity, will be called “non-basket cell CB<sub>1</sub>R-expressing cell type” because, in slice preparations, often insufficient axon is revealed for accurate identification (Klausberger and Somogyi, 2008). Cells classified as CB<sub>1</sub>R+ non-basket cells had their soma in either str. radiatum

( $n = 11$ ) or str. oriens ( $n = 3$ ). They presented radially or diagonally oriented dendrites in strata oriens and radiatum, sometimes with small dendritic tufts into str. lacunosum moleculare, and large axon arbors in strata oriens and/or radiatum, hardly ever crossing the border to str. lacunosum moleculare. The proportion of innervation to str. oriens or str. radiatum differed between individual cells (for examples, see Fig. 2*D,E*). Long axon collaterals traveling across strata oriens and radiatum were characteristic of most CB<sub>1</sub>R+ non-basket cells. Others were more reminiscent of bistratified cells with denser axon clusters above and below str. pyramidale, but the pyramidal layer itself always had sparse innervation in contrast to typical basket cells. Only cells that fit the criteria for one of the categories above were included in this study. Data for identification of all interneurons studied are presented in supplemental Tables 1 and 2 (available at [www.jneurosci.org](http://www.jneurosci.org) as supplemental material).

We elicited EPSPs by alternately stimulating two electrodes in different locations in str. oriens/alveus to activate pyramidal cell axons (see Materials and Methods). GABA receptors were blocked by PiTX (100  $\mu$ M) and CGP55845 (1  $\mu$ M), and glutamate NMDARs were blocked with DL-APV (100  $\mu$ M). After a baseline period of at least 10 min, high-frequency stimulation (HFS) (100 Hz for 1 s, delivered twice, 20 s interval) was delivered to one pathway, whereas the other pathway served as a control. Unlike the long-term plasticity in pyramidal cells, LTP and LTD in many hippocampal interneurons is NMDAR independent and involves CP-AMPA receptors (Laezza et al., 1999; Lamsa et al., 2007; Oren et al., 2009). Postsynaptic somatic potential was voltage clamped to  $-70$  mV (or more negative down to  $-90$  mV) during HFS to maximize conductance of CP-AMPA (Geiger et al., 1995) (supplemental Fig. 1, available at [www.jneurosci.org](http://www.jneurosci.org) as supplemental material). After the HFS, EPSPs were recorded for at least 20 min before cells were repatched (in three cells, LTP was followed up to 30 min). Analysis of EPSPs was focused on initial slope of EPSPs (3–5 ms from onset) to avoid contamination by polysynaptic EPSPs (Maccaferri and McBain, 1996; Lamsa et al., 2005). The high-frequency stimulation did not cause long-lasting changes in the resting membrane potential of the interneurons (supplemental Fig. 1, available at [www.jneurosci.org](http://www.jneurosci.org) as supplemental material) (Ross and Soltesz, 2001).

Visualization of the cells (see Materials and Methods) revealed that LTP was elicited in 7 of 14 interneurons whose axon targeted specifically the perisomatic domain of CA1 pyramidal cells. LTP was defined as potentiation of EPSP initial slope at least to 125% of baseline (tested with paired *t* test) and specific to the pathway (significant difference to control pathway, tested with unpaired *t* test). In cells with significant potentiation and pathway specificity, EPSP in the tetanized pathway increased to  $156 \pm 8\%$  ( $p < 0.005$ ,  $n = 7$ , 20 min after HFS), whereas EPSP in the control pathway did not change ( $102 \pm 6\%$ ) (Fig. 1*A–C*). Four of the interneurons with LTP were identified as axo-axonic cells, based on their axonal patterns showing radial bouton rows that follow axon initial segments of pyramidal cells (Somogyi et al., 1985). Two cells randomly selected were confirmed by electron microscopy to innervate axon initial segments, and two were confirmed as expressing PV (Klausberger et al., 2003). The three other cells showing LTP and targeting pyramidal cells perisomatically were identified as basket cells. Immunohistochemical testing showed that these basket cells were all positive for PV and negative for CB<sub>1</sub>R (Fig. 1*D,E*) (supplemental Table 1, available at [www.jneurosci.org](http://www.jneurosci.org) as supplemental material). One additional axo-axonic cell failed to show LTP. Average potentiation of EPSP in all eight PV+

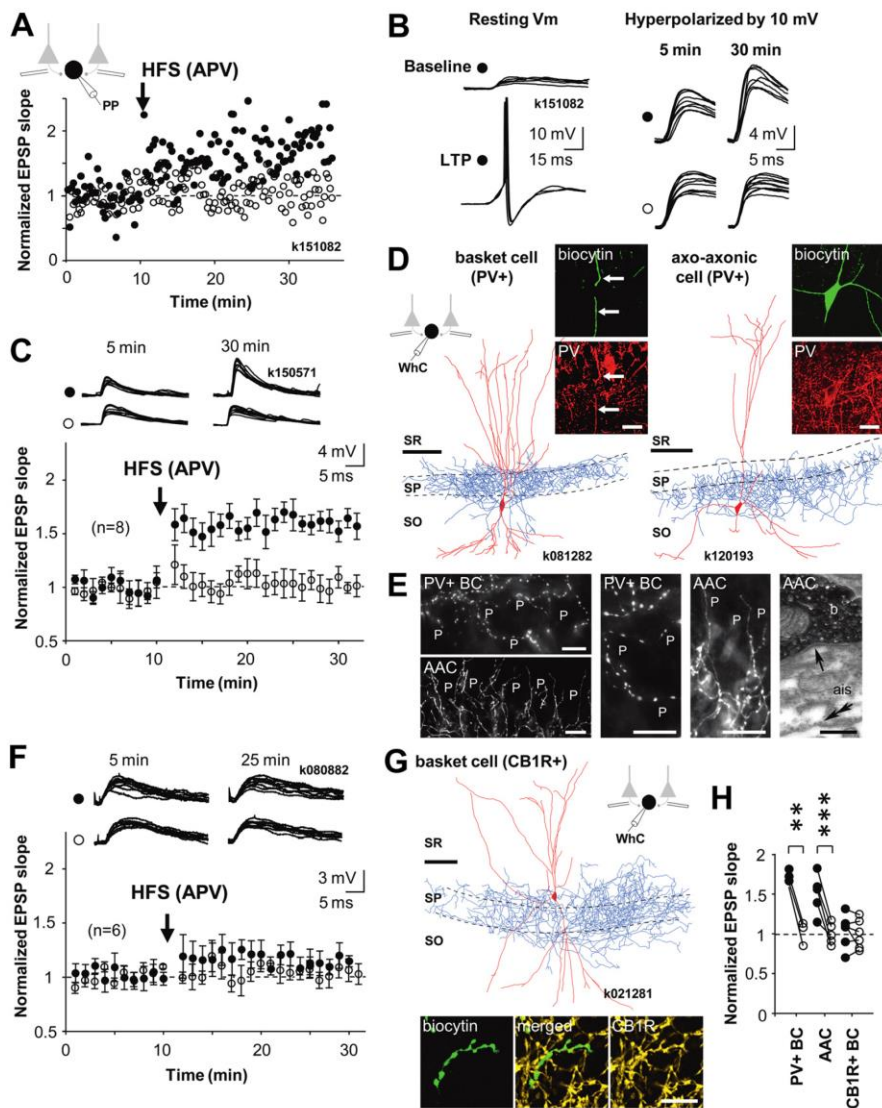


**Figure 1.** Cell type-specific LTP in interneurons innervating the perisomatic domain of pyramidal cells. **A–G**, LTP is generated in PV+ basket cells and axo-axonic cells but not in basket cells expressing CB<sub>1</sub>R. Recordings were made in perforated patch; cells were repatched in whole cell for *post hoc* identification using biocytin labeling. **A**, Pathway-specific LTP in a PV+ basket cell. Two glutamatergic afferent pathways were stimulated with electrodes in str. oriens/aleveus. After baseline period, HFS (100 Hz, 1 s, two times) was delivered to one pathway (filled symbols), whereas the other pathway served as control (open symbols). Schematic shows experimental design during perforated patch (PP) recording. Timing of HFS is indicated by an arrow. During HFS, the postsynaptic cell was voltage clamped to  $-70$  mV. Potentiation of EPSP lasted at least 25 min and was restricted to the stimulated pathway. **B**, Consecutive EPSPs in the basket cell in **A** during baseline and 20 min after the HFS. Left, EPSP at resting membrane potential (resting Vm) triggered action potentials after LTP. To avoid action potentials, EPSPs were recorded during a hyperpolarizing step ( $-10$  mV) throughout the experiment. Symbols indicate tetanized and control pathways as in **A**. **C**, EPSP slope mean  $\pm$  SE in eight identified perisomatic-targeting PV+ interneurons. Data include three PV+ basket cells and five axo-axonic cells, and symbols indicate tetanized and control pathway as in **A**. Top, Consecutive EPSPs in the two pathways during baseline and 20 min after the HFS. **D**, Digital visualization of PV+ basket cell k081282 (left; dendrites in red from two 70- $\mu$ m-thick sections, axon in blue, from one section) and axo-axonic cell k120193 (right, one section) recorded in whole cell (WhC). Images produced from confocal microscopic image stacks. Scale bar, 100  $\mu$ m. Insets, Immunofluorescence micrographs of the labeled cells demonstrating the expression of PV in the dendrites (indicated by arrow) and soma of the cells. Laser confocal microscope images; biocytin is in green and PV is in red. Scale bar, 20  $\mu$ m. SR, str. radiatum; SP, str. pyramidale; SO, str. oriens. **E**, Distinct axonal patterns of a basket cell and an axo-axonic cell within the pyramidal cell layer. Left, Epifluorescent micrographs of a PV+ basket cell (PV+ BC, k151082) showing undulating bouton laden axon collaterals, often running parallel with the pyramidal cell layer, among pyramidal cells (P), and an axo-axonic cell (AAC, k100871), showing their characteristic radial bouton bundles. The axo-axonic bouton rows follow axon initial segments of pyramidal cells (P) toward str. oriens. Scale bar, 20  $\mu$ m. Middle, Higher-magnification epifluorescent micrographs of the same PV+ basket cell (PV+ BC, middle left) and axo-axonic cell (AAC, middle right). Scale bar, 20  $\mu$ m. Right, Electron micrograph showing a synapse (arrow) received by an axon initial segment (ais) from a bouton (b) of axo-axonic cell k100871. The bouton is identified by the electron opaque HRP end product and the ais by the membrane undercoating (double arrow). Scale bar, 0.25  $\mu$ m. **F**, EPSPs in basket cells expressing CB<sub>1</sub>R do not show lasting plasticity. EPSP slope mean  $\pm$  SE in six basket cells tested for LTP and plotted as above. Top, EPSPs during baseline and 15 min after the HFS. **G**, Visualization of one CB<sub>1</sub>R+ basket cell by digital rendering of fluorescent images (two superimposed 70- $\mu$ m-thick sections). Scale

perisomatic-targeting interneurons is shown in Figure 1C. The remaining six perisomatic-targeting cells that did not show LTP were negative for parvalbumin and positive for CB<sub>1</sub>R (Fig. 1F,G) (supplemental Table 2, available at www.jneurosci.org as supplemental material). We conclude that perisomatic-targeting interneurons positive for either PV or CB<sub>1</sub>R show strict cell type-specific plasticity in the CA1 area. LTP was induced in seven of eight identified PV+ perisomatic-targeting interneurons but not in any of the identified CB<sub>1</sub>R+ basket cells (Fig. 1H).

**LTP or LTD occurs in interneurons with distinct axonal target domains**

In contrast to the perisomatic-targeting interneurons, dendrite-targeting PV+ or CB<sub>1</sub>R+ interneurons did not show LTP at all. Seven cells tested with HFS were identified as bistratified cells. This cell type is immunopositive for PV, somatostatin, and NPY, and their axons innervate mainly pyramidal cell dendrites in str. radiatum and oriens (Halasy et al., 1996; Pawelzik et al., 2002; Klausberger et al., 2004). Remarkably, in five of seven bistratified cells, HFS induced LTD (reduction of the EPSP initial slope to at least 75% of baseline), whereas two cells showed no significant change in EPSP slope (Fig. 2A,B). LTD ( $63 \pm 3\%$ ,  $p < 0.005$ ,  $n = 5$ ) in the bistratified cells was restricted to the stimulated pathway (control pathway,  $105 \pm 3\%$ ). The systematic difference in plasticity between perisomatic- and dendrite-targeting PV+ cells reported here is unlikely to be explained by different postsynaptic membrane potential or action potential firing in these cells during afferent stimulation, because these measures were similar in the cell types (supplemental Fig. 1, available at www.jneurosci.org as supplemental material). Five interneurons, also studied with HFS, with axons mainly in the dendritic layers, were immunopositive for CB<sub>1</sub>R and negative for PV (Ali, 2007) (supplemental Table 2, available at www.jneurosci.org as supplemental material). None of these CB<sub>1</sub>R+ non-basket cells

←  
 bar, 100  $\mu$ m. Bottom, Immunofluorescence micrographs of a biocytin-labeled (green) axon segment (CB<sub>1</sub>R, yellow, laser confocal image). Scale bar, 10  $\mu$ m. **H**, Comparison of baseline-normalized average EPSPs in all perisomatic-targeting cells 15–20 min after HFS relative to control pathways. Filled symbols indicate tetanized pathway, and open symbols show the control pathway. LTP is consistent in the PV+ interneuron types. Significance levels indicate a difference between pathways (\*\* $p < 0.01$ , \*\*\* $p < 0.005$ , unpaired  $t$  test).

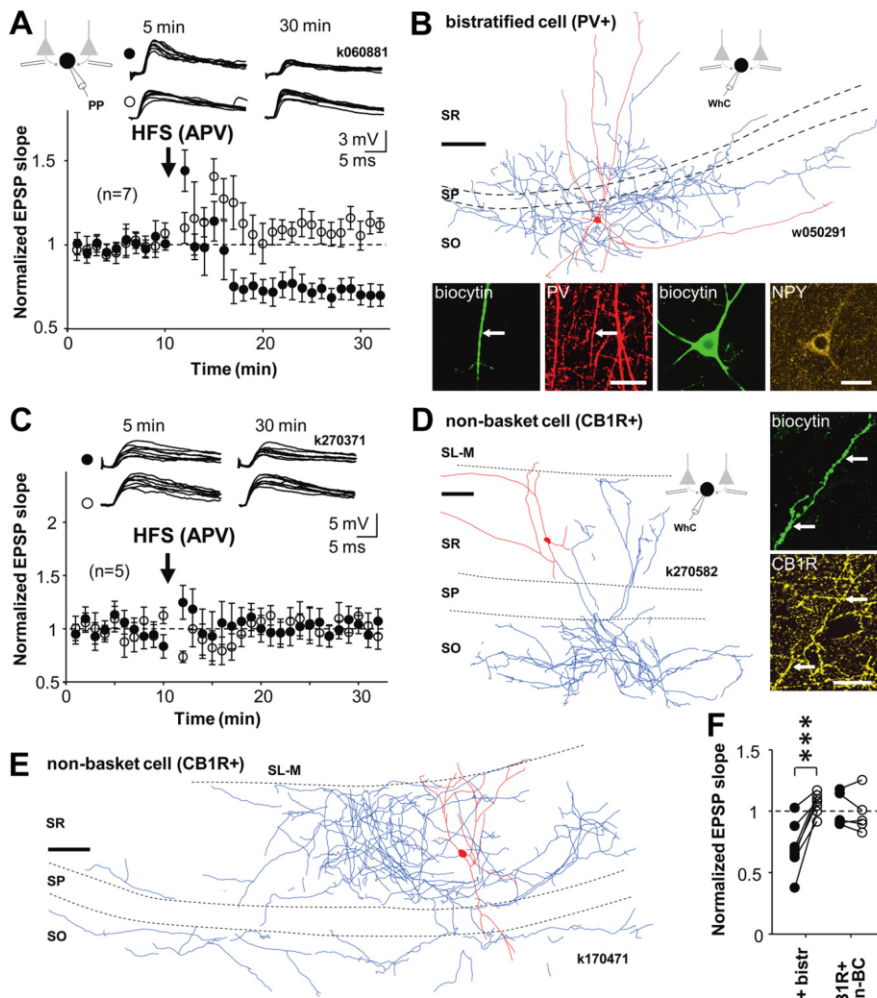


**Figure 2.** LTP is specific to perisomatic-targeting PV+ cell types. EPSPs in PV+ bistratified cells that target to the dendritic domain of CA1 pyramidal cells show LTD. EPSPs in interneurons that express CB<sub>1</sub>R and innervate pyramidal cell dendrites show no lasting plasticity. Perforated patch (PP) recordings. **A**, Mean  $\pm$  SE of EPSP slope in seven identified bistratified cells. HFS to one of the pathways (filled symbols) induced pathway-specific LTD. Open symbols show EPSP in the untetanized control pathway. Top, Consecutive EPSP traces during baseline and 20 min after the HFS in the two pathways. Schematic shows experimental design. **B**, Visualization of one bistratified cell by digital rendering of fluorescent images (dendrites in red and axon in blue, from one 70  $\mu$ m section) recorded in whole cell (WhC). Scale bar, 100  $\mu$ m. Fluorescence micrographs demonstrating immunopositivity for PV (red, laser confocal images) as tested in a dendrite (indicated by arrow) and for neuropeptide Y (yellow, structured illumination microscope images) in the soma. Biocytin is shown in green. Scale bar, 20  $\mu$ m. **C**, Mean  $\pm$  SE of EPSP slope from five cells identified as dendrite-targeting CA1 interneurons expressing CB<sub>1</sub>R. None of the cells showed significant lasting plasticity in the EPSP. Top, Consecutive EPSPs in the two pathways during baseline and 20 min after HFS. **D**, Visualization of a CB<sub>1</sub>R+ non-basket cell (k270582, reconstruction from two 70- $\mu$ m-thick sections), recorded in perforated and whole-cell mode. Axon ramifies in strata oriens and radiatum but not in pyramidal. It was verified that the main axon originated 55  $\mu$ m away from the soma at a point at which the dendrite turned by 90° degrees. Scale bar, 100  $\mu$ m. Fluorescence micrographs demonstrating immunopositivity for CB<sub>1</sub>R in an axon visualized with biocytin (green, indicated by arrow; structured illumination microscopic images). Scale bar, 20  $\mu$ m. **E**, Another example of a non-basket cell (k170471, dendrites in red, from three 70- $\mu$ m-thick sections, axon in blue, from two sections) recorded in whole-cell mode that was also confirmed to be positive for CB<sub>1</sub>R (data not shown) (but see supplemental Table 2, available at [www.jneurosci.org](http://www.jneurosci.org) as supplemental material). Note the rich axon arborization in strata radiatum and oriens but the clear absence of axon concentration in str. pyramidal. Scale bar, 100  $\mu$ m. **F**, Comparison of baseline-normalized EPSP slopes after HFS (20 min) in the two types of dendrite-targeting interneurons. Filled and open symbols indicate tetanized and control pathways, respectively (\*\*\* $p$  < 0.005, unpaired  $t$  test). SL-M, str. lacunosum moleculare; SR, str. radiatum; SP, str. pyramidal; SO, str. oriens.

showed a significant change in EPSP slope 15 min after the HFS, indicating an absence of LTP or LTD (Fig. 2C–E). Thus, LTD occurred specifically in dendrite-innervating PV+ bistratified cells under this induction protocol (Fig. 2F).

### CB<sub>1</sub>R+ interneuron types with intact NMDAR-mediated transmission do not show LTP or LTD

Although CB<sub>1</sub>R+ basket cells did not demonstrate NMDAR-independent LTP, we asked whether they might show NMDAR-dependent LTP similar to pyramidal cells and some GABAergic interneurons in other hippocampal circuits (Kullmann and Lamsa, 2007). We performed experiments in four *post hoc* identified CB<sub>1</sub>R+ basket cells in the absence of NMDAR blockers and depolarized the postsynaptic cell to 0 mV in current clamp during HFS. This was associated with intense firing of the postsynaptic cell ( $63.3 \pm 3.7$  action potentials evoked by a 100-pulse train,  $n = 8$  in 4 cells). This protocol, however, also failed to induce a lasting ( $\geq 15$  min) change in the EPSPs (Fig. 3A, B).

Next, we asked whether CB<sub>1</sub>R+ cells would show plasticity with a different stimulation protocol. In 10 additional identified CB<sub>1</sub>R+ cells, we used theta-burst stimulation (TBS) while the postsynaptic cell was in current clamp at resting membrane potential. After baseline, high-frequency stimulation trains (100 Hz, five pulses) were delivered to one pathway at theta frequency (5 Hz, four cycles), whereas the second pathway served as control. The protocol was applied five times with 20 s interval (100 stimulation pulses altogether) (Fig. 3C). The afferent stimulation induced depolarization above firing threshold in the cells ( $34.0 \pm 8.8$  postsynaptic action potentials by 100 stimulation pulses). Both pathways were followed at least 15 min after TBS. Four cells were identified as CB<sub>1</sub>R+ basket cells (Fig. 3D) and six cells as CB<sub>1</sub>R+ non-basket cells (Fig. 3E). Neither of these cell populations showed significant potentiation or depression (paired  $t$  test) or difference between the pathways 15 min after the TBS (unpaired  $t$  test). Averages of baseline-normalized EPSPs are shown in Figure 3F.

### Plasticity occurs in interneurons with CP-AMPA receptors

We next asked whether this cell type-specific plasticity we observed was correlated with the presence of CP-AMPA receptors in these cells (Lei and McBain, 2004; Isaac et al., 2007; Lamsa et al., 2007). We recorded EPSCs in whole-cell mode from the re-patched cells (when access resistance allowed voltage clamp; see Materials and Methods). In addition, we recorded from a separate set of interneurons in whole-

cell only and subsequently identified their cell type (supplemental Tables 1, 2, available at [www.jneurosci.org](http://www.jneurosci.org) as supplemental material). Stimulation from str. oriens/alveus in all PV+ cells, including both control and tetanized pathways in repatched cells,

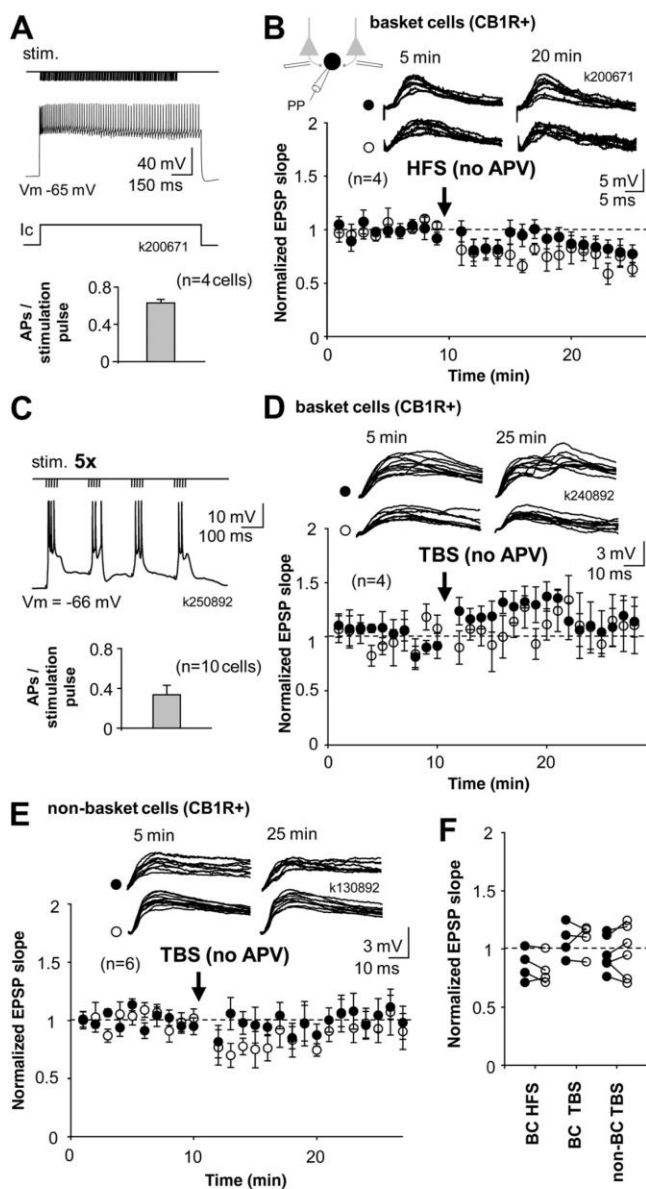


**Figure 3.** CB<sub>1</sub>R+ basket cells and non-basket cells with intact NMDAR-mediated transmission fail to show long-term plasticity. **A**, Schematic shows HFS protocol; tetanic stimulation (stim.) to one pathway is paired with depolarization of postsynaptic cell to 0 mV in current clamp (Ic). NMDARs are not blocked. Histogram shows that intense firing of postsynaptic action potentials (APs) was associated with presynaptic stimuli. **B**, Mean  $\pm$  SE of EPSP slope from four cells recorded in perforated patch and identified *post hoc* as CB<sub>1</sub>R+ basket cells. None of the cells showed significant lasting plasticity in the EPSP. Top, EPSPs in the two pathways during baseline and 10 min after HFS. **C**, Schematic shows TBS stimulation protocol; trains of stimuli (100 Hz, five pulses) are delivered to one pathway at 5 Hz, while postsynaptic cell is at resting membrane potential (action potentials truncated). Histogram shows number of postsynaptic action potentials elicited by presynaptic stimuli. **D**, Perforated patch recording from four CB<sub>1</sub>R+ basket cells showed EPSPs without lasting plasticity. EPSP slope in theta-burst pathway was not different from baseline or from control pathway 15 min after the TBS. Top, Consecutive EPSP traces from one experiment. **E**, Similar recordings show lack of long-term plasticity of EPSPs in CB<sub>1</sub>R+ non-basket cells ( $n = 6$ ). Cells were repatched and identified as above. Top, EPSPs from an individual experiment. **F**, Baseline-normalized average EPSPs in the three types of experiments shown above. Filled symbols indicate HFS- or TBS-treated pathway, and open symbols show the control pathway. Data are taken 10–15 min after the HFS or TBS.

elicited strongly inward rectifying EPSCs (Fig. 4A), indicating a high percentage of CP-AMPA receptors in these synapses under baseline conditions as well as after plasticity (Jonas et al., 1994; Geiger et al., 1995; Lei and McBain, 2004; Lamsa et al., 2007). The RI (see

Materials and Methods) of EPSCs was consistently low in PV+ cell types (Catania et al., 1998). RI in axo-axonic cells was  $0.09 \pm 0.02$  ( $n = 13$  stimulation pathways tested in 8 cells), in basket cells was  $0.12 \pm 0.03$  ( $n = 10$  in 6 cells), and in bistratified cells was  $0.11 \pm 0.02$  ( $n = 22$  in 12 cells). Although in most PV+ cells two stimulation pathways from str. oriens/alveus were tested, in some cells, the control pathway was stimulated in str. radiatum. EPSCs evoked from str. radiatum showed similar strong inward rectification (RI of  $0.07 \pm 0.05$ ,  $n = 6$  pathways). In contrast, RI in CB<sub>1</sub>R+ basket cells ( $n = 16$  in 14 cells) and non-basket cells ( $n = 14$  in 10 cells) was  $0.72 \pm 0.03$  ( $n = 30$ ), reminiscent of that recorded in pyramidal cells (supplemental Fig. 2, available at www.jneurosci.org as supplemental material). In only 5 of the 30 pathways recorded in CB<sub>1</sub>R+ cells was rectification prominent (RI  $< 0.5$ ) (Fig. 4B). In some recordings, another stimulation was delivered from str. radiatum, which evoked EPSCs with RI of  $0.67 \pm 0.07$  ( $n = 7$  pathways).

We next tested the effect of blocking CP-AMPA receptors on synaptic excitation of these interneuron types. EPSCs recorded in identified interneurons in whole-cell mode were evoked by stimulation in str. oriens/alveus, and they were strongly suppressed after wash-in of the CP-AMPA blocker PhTx ( $10 \mu\text{M}$ ) in all PV+ interneuron types (Fig. 4C,D). EPSC amplitude was reduced to  $44 \pm 6\%$  ( $p < 0.005$ , paired  $t$  test) by PhTx ( $n = 9$ , includes 3 axo-axonic, 3 basket cells, and 3 bistratified cells). In contrast, PhTx had a small effect on EPSCs in CB<sub>1</sub>R+ basket cells (in PhTx:  $86 \pm 9\%$ ,  $n = 11$  cells,  $p < 0.05$ ). As a reference, we confirmed that PhTx had no effect on synaptic excitation of identified CA1 pyramidal cells with a linear EPSC  $I$ - $V$  relation (supplemental Fig. 2, available at www.jneurosci.org as supplemental material). Thus, CP-AMPA blockade inhibits excitation of PV+ interneurons to a much stronger degree than of CB<sub>1</sub>R+ interneurons.

### Disynaptic GABAergic transmission in CA1 pyramidal cells is strongly suppressed by CP-AMPA blockers

Based on the strong effect of CP-AMPA blockade on the excitation of PV+ interneurons, we tested the effect of PhTx on disynaptic inhibition in CA1 pyramidal cells. We recorded from the soma in whole-cell mode and stimulated in str. oriens/alveus far ( $\geq 1$  mm) from the recording site and close to the subiculum. GABA<sub>B</sub> and glutamate NMDA receptors were blocked with CGP55845 ( $1 \mu\text{M}$ ) and DL-APV ( $100 \mu\text{M}$ ), respectively. Cells were voltage clamped to the reversal of glutamatergic EPSCs (0 to +10 mV). We first measured maximum disynaptic IPSC (the disynaptic nature was verified at the end by applying NBQX at  $10 \mu\text{M}$ ) for stimulation pathways. Next, stimuli with reducing intensities were applied to dissect the contribution of interneurons with CP-AMPA receptors at various stimulation strengths (see Materials and Methods). IPSCs were recorded in control conditions and after wash-in of PhTx ( $10 \mu\text{M}$ ). PhTx significantly reduced the amplitude of disynaptic IPSCs at each stimulation strength, but the inhibitory effect of PhTx was most pronounced in low-amplitude IPSCs (Fig. 5A). When  $\sim 30\%$  of the maximum IPSC was used, PhTx suppressed the disynaptic IPSC to  $26 \pm 3\%$  of control ( $n = 5$  slices,  $p < 0.005$ ) (Fig. 5B), indicating a strong contribution of interneurons with CP-AMPA receptors to the IPSC (Jonas et al., 2004). In comparison, when the 100% IPSC was tested, PhTx reduced the disynaptic IPSC to  $74 \pm 4\%$  ( $p < 0.01$ ). We confirmed that PhTx had no direct effect on GABAergic IPSCs (supplemental Fig. 3, available at www.jneurosci.org as supplemental material).

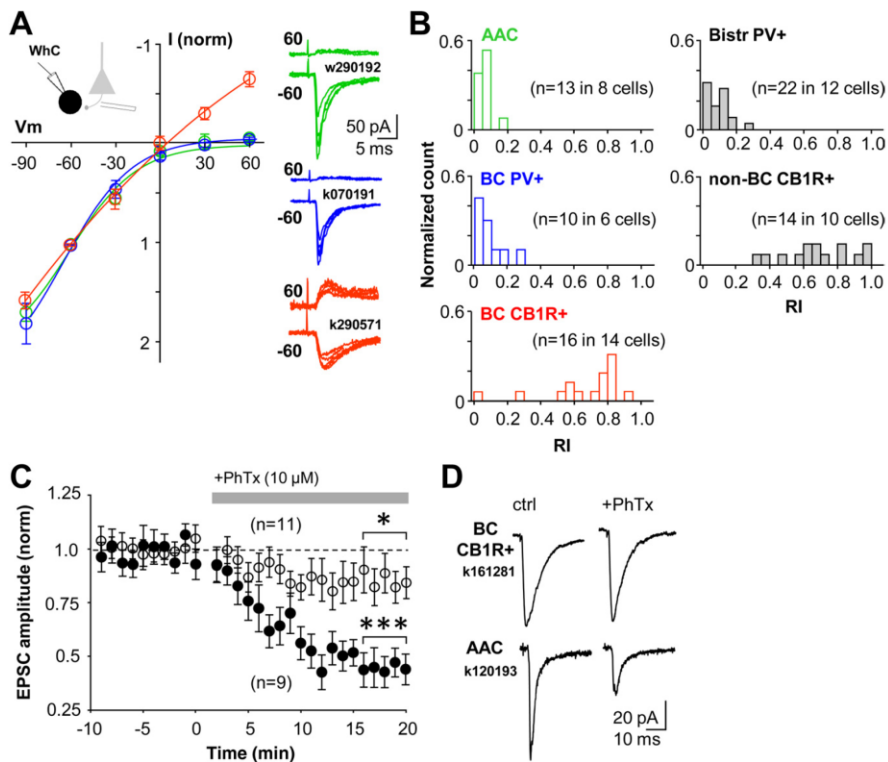


**Figure 4.** PV+ interneurons are excited via CP-AMPA and CB<sub>1</sub>R-expressing interneurons via calcium-impermeable AMPARs in the CA1 area. **A**, *I*–*V* relations of AMPAR-mediated EPSCs are interneuron type specific. PV+ basket cells and axo-axonic cells have highly inward rectifying EPSCs, which is a hallmark of CP-AMPA. In contrast, EPSCs in CB<sub>1</sub>R+ basket cells show more linear current–voltage relation. EPSCs were evoked by stimulation in str. oriens/alveus. Mean  $\pm$  SE of normalized *I*–*V* relationship in the three perisomatic-targeting cell types illustrated in colors (green for axo-axonic, blue for PV+ basket cells, and red for CB<sub>1</sub>R+ basket cells). Right, EPSCs at +60 and –60 mV in three different cells (color coding indicates cell type as above). WhC, Whole-cell mode. **B**, Histograms showing EPSC RIs in the five different interneuron types. RIs in PV+ interneuron types (AAC, PV+ BC, Bistr PV+) are on average 0.11, whereas in CB<sub>1</sub>R-expressing interneurons (BC CB<sub>1</sub>R+ and non-BC CB<sub>1</sub>R+) RIs are on average 0.75. Color coding of perisomatic-targeting interneuron types is as in **A**. **C**, CP-AMPA blocker PhTx blocks excitatory input to PV+ interneuron types (filled symbols) but has a small effect on EPSCs in CB<sub>1</sub>R+ cells ( $n = 11$ ,  $p > 0.05$ ; open symbols). Data show mean  $\pm$  SE, and a horizontal bar indicates timing of PhTx wash-in. PV+ cells include three basket, three axo-axonic, and three bistratified cells. CB<sub>1</sub>R+ cells are basket cells. Significance level indicates difference from baseline (\*\*\* $p < 0.005$ , paired *t* test). **D**, Averaged EPSCs in one CB<sub>1</sub>R-expressing basket cell and in an axo-axonic cell during baseline and after wash-in of PhTx (20 min).

### Long-term potentiation of disynaptic GABAergic transmission involves interneurons with CP-AMPA

Finally, we asked whether plasticity in the inputs to interneurons with CP-AMPA could change disynaptic inhibition projected onto CA1 pyramidal cells. Given that LTP or LTD in interneurons with CP-AMPA is induced without strong postsynaptic depolarization and that repetitive afferent stimulation induces robust plasticity in synapses recruiting these cells, we hypothesized that the same afferent stimulation might be able to potentiate or depress disynaptic GABAergic transmission. We recorded IPSCs in whole-cell mode from CA1 pyramidal cell soma clamped to the reversal of glutamatergic EPSCs as above and stimulated at two different locations in str. oriens/alveus. One electrode was positioned as above close to subiculum and another electrode close to the CA2 area. GABA<sub>B</sub> and glutamate NMDARs were blocked. Given that endocannabinoid receptor activation can mediate depression in certain GABAergic synapses onto pyramidal cells (Földy et al., 2007; Heifets et al., 2008) and because this depression may also be induced by high-frequency electrical stimulation (Chevalyere and Castillo, 2003; Lamsa et al., 2005), CB<sub>1</sub>Rs were blocked with AM-251 (5–10  $\mu$ M). Stimulation intensity was set to  $\sim$ 30% of the maximum disynaptic IPSC amplitude in the pathways as above to maximize relative

contribution of CP-AMPA-containing interneurons in disynaptic IPSC (supplemental Fig. 4, available at [www.jneurosci.org](http://www.jneurosci.org) as supplemental material). After a baseline, the disynaptic pathway from the subicular site was stimulated with HFS, whereas the untetanized pathway was used as control (Fig. 6A). Significant LTP (potentiation of averaged IPSC amplitude to at least 125% of baseline) was generated in five of eight slices, although potentiation varied in amplitude. Baseline-normalized average of IPSC amplitudes in all eight slices showed potentiation in the tetanized pathway to  $139 \pm 8\%$  ( $p < 0.005$ , 25 min after the HFS), whereas the average of the control pathway did not change ( $89 \pm 7\%$ ) (Fig. 6B). Pathway specificity of LTP was tested with unpaired *t* test ( $p < 0.005$ ) (Fig. 6C). Again, the disynaptic nature of IPSCs was verified by blockade of the IPSC with NBQX (10  $\mu$ M) at the end of each experiment.

We repeated the same experiment in the presence of PhTx (10  $\mu$ M) to block excitation of interneurons with CP-AMPA. IPSC intensity was set up similarly to  $\sim$ 30% in the pathways (supplemental Fig. 4, available at [www.jneurosci.org](http://www.jneurosci.org) as supplemental material), and HFS was delivered to the disynaptic pathway from the subicular site (Fig. 6D). Interestingly, HFS did not elicit lasting potentiation in any of the eight slices studied (Fig. 6E). Twenty minutes after the tetanus, IPSC amplitudes were  $82 \pm 5\%$  in the tetanized pathway and  $88 \pm 7\%$  in the untetanized control pathways (Fig. 6F). Although this moderate suppression of IPSC was significant ( $p < 0.05$ ) compared with baseline, it was not pathway specific. We confirmed that HFS does not change the amplitude of monosynaptic GABAergic IPSCs by reproducing the experiment above but in the continuous presence of NBQX (10  $\mu$ M) and stimulating closer to the recording site in str. oriens (Fig. 6G). Together, the results demonstrate that LTP of disynaptic GABAergic transmission recorded in CA1 pyramidal cell somata involves interneurons with CP-AMPA.

### Discussion

Here we have shown that excitatory connections to hippocampal interneurons express long-term plasticity in a cell type-dependent manner (Kullmann and Lamsa, 2007; Klausberger and Somogyi, 2008). Lasting plasticity in the GABAergic interneurons correlates with the expression of certain neurochemical markers and the axonal target domain of the interneurons. These results highlight the importance of carefully identifying interneurons in long-term plasticity studies. The two forms of plasticity are likely to modulate the synaptic strength from pyramidal cells to local GABAergic interneurons. Localization of LTP and LTD at separate and defined GABAergic microcircuits emphasizes the specified roles of distinct interneuron types in hippocampal function (Santhakumar and Soltesz, 2004; Freund and Katona, 2007; Klausberger and Somogyi, 2008).

Our results demonstrate that activity-induced plasticity takes place at excitatory synapses onto hippocampal PV+ interneurons, whereas afferents onto CB<sub>1</sub>R+ cells do not show plasticity. Although PV+ and CB<sub>1</sub>R+ interneurons provide parallel sources for perisomatic and dendritic innervation of pyramidal cells, PV+ neurons presumably play a major role in the synchronization of neuronal groups that process, transfer, and store information during network oscillations (Buzsáki and Draguhn, 2004; Bartos et al., 2007; Fuchs et al., 2007; Mann and Paulsen, 2007; Tukker et al., 2007; Klausberger and Somogyi, 2008; Cardin et al., 2009; Sohal et al., 2009). CB<sub>1</sub>R+ interneurons may be less critical for synchronizing pyramidal cells, and they may modulate ensemble activities as a function of subcortical inputs (Freund and Katona, 2007). Activity-induced synaptic plasticity and modulatory fine-tuning plasticity appear to be located in separate and complementary GABAergic microcircuits provided by PV+ and CB<sub>1</sub>R+ cells, respectively (Freund and Katona, 2007). However, we cannot fully exclude a possibility that synapses onto CB<sub>1</sub>R+ cells could undergo long-term plasticity under certain conditions. For example, permissive signal from an extrahippocampal locus might be needed to allow plasticity in these cells (Isaac et al., 2009; Varga et al., 2009). In addition, afferent pathways emerging from a distinct population of glutamatergic hippocampal cells may behave differently. This, however, would not change the fact that, in general, the plasticity rules are very different in PV+ and CB<sub>1</sub>R+ cells.

PV+ cells show plasticity that is specific to the efferent target domain, such that perisomatic-targeting GABAergic circuits are potentiated and dendritic-targeting neurons are depressed. LTP increases the excitatory drive onto perisomatic-targeting inhibitory interneurons in a synapse-specific manner. The potentiated excitatory afferent synapse at the GABAergic cell has an increased contribution to its firing and consequently to the synchronization of its target cell assembly during network oscillation. In addition, depressed recruitment of dendritic-targeting bistratified cells would promote temporal integration of excitatory input to pyramidal cells from the CA3 area (Cossart et al., 2001). This in turn might increase the ability of CA1 cells to resonate with CA3 pyramidal cells and could lower the threshold for LTP in CA3–CA1 synapses (Gustafsson et al., 1987), supporting rearrangement of temporal relationships within affected CA1 populations (Dragoi et al., 2003). However, because the inputs to different PV+ cell types likely arrive at distinct phases of oscillations *in vivo* (Klausberger and Somogyi, 2008), each interneuron type would possibly experience optimal plasticity-inducing conditions at different times (Kullmann and Lamsa, 2007).

Information processing requires the interactions within or between cell assemblies to be flexible, but the inputs to PV+ cells have long been considered poorly modifiable. Synchronized cell assembly formation during oscillations is dynamic and applies to particular representations and contexts. It is therefore expected

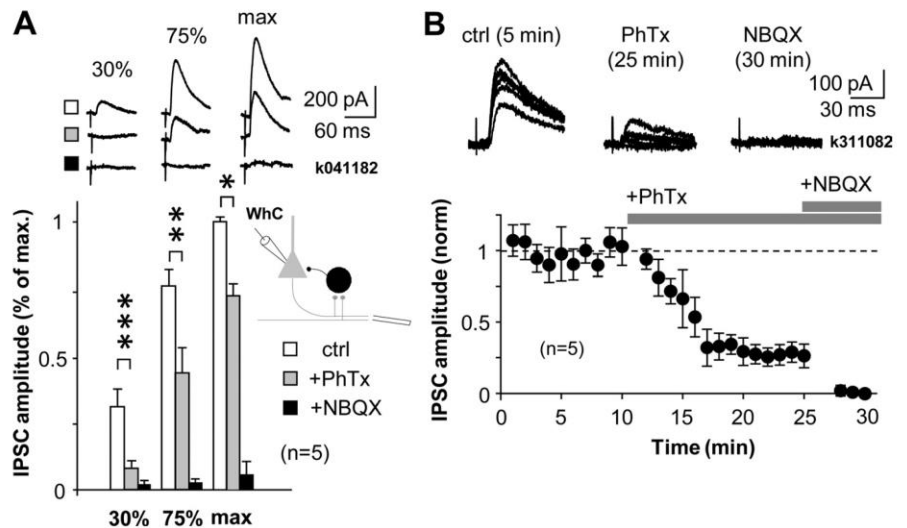


**Figure 5.** Disynaptic GABAergic transmission in the CA1 involves activation of interneurons with CP-AMPA receptors. CP-AMPA receptor blocker PhTx (10  $\mu$ M) strongly inhibits disynaptic IPSCs recorded in the pyramidal cell soma. The effect of PhTx was studied at three different IPSC amplitudes relative to the maximum (maximum, 75%, and 30% amplitudes) and was most pronounced at lower amplitudes of disynaptic IPSCs, indicating strong contribution of interneurons with CP-AMPA receptors. **A**, Top, IPSC averages in one experiment. Symbols indicate ctrl, +PhTx, and +NBQX as below. Bottom, Histogram shows IPSC amplitudes at three different stimulus intensities relative to the maximum disynaptic IPSC. IPSCs were evoked by extracellular stimulation in oriens/aleveus close to subiculum. Schematic shows experimental design. Open bars show IPSCs (mean  $\pm$  SE) in control, and gray bars show IPSCs after wash-in of PhTx (15 min) ( $*p < 0.05$ ,  $**p < 0.01$ ,  $***p < 0.005$ , paired *t* test). Disynaptic origin of IPSCs was confirmed at the end by NBQX application (10  $\mu$ M, filled bars). Whc, Whole-cell mode. **B**, Temporal properties of blocking disynaptic IPSCs by PhTx when 30% of maximum IPSC was used throughout experiment. Horizontal bars indicate timing of drug application as indicated. Top, Consecutive IPSCs in one experiment during baseline and after exposure to the drugs.

that the synaptic strengths between pyramidal cells and interneurons also change in behaviorally relevant timescales (Csicsvari et al., 1998). The cell type-specific plasticity that we demonstrate here and, in particular, the contrasting effect of the same induction pattern leading to LTP or LTD in perisomatic- or dendrite-targeting PV+ cells, respectively, is a good candidate mechanism for maintaining the necessary flexibility in connection strengths during the formation or dissolution of cell assemblies.

What might be potential cellular mechanisms for LTP and LTD in PV+ cells? Plasticity was independent of NMDARs and occurred at synapses with CP-AMPA receptors. Long-term plasticity in many interneurons depends on CP-AMPA receptors (Mahanty and Sah, 1998; Laezza et al., 1999; Kullmann and Lamsa, 2007; Lamsa et al., 2007; Oren et al., 2009). Both LTP and LTD in PV+ interneuron types were induced at membrane potentials below somatic firing threshold, consistent with previous reports on CP-AMPA-mediated LTP and LTD (Laezza et al., 1999; Lamsa et al., 2007) and AMPAR subunit expression patterns in interneurons (Jonas et al., 1994; Geiger et al., 1995; Catania et al., 1998). In line with this, potentiation of disynaptic GABAergic transmission recorded in pyramidal cells required interneurons with CP-AMPA receptors, although this does not necessarily indicate an inductive role for these receptors in the LTP (Asrar et al., 2009). However, CP-AMPA receptors would provide temporally and spatially highly restricted calcium influx in aspiny postsynaptic interneuron dendrites (Goldberg and Yuste, 2005). Contributions of CP-AMPA receptors and other mechanisms including metabotropic glutamate receptors and voltage-gated calcium channels to LTP and LTD (Laezza et al., 1999; Alle et al., 2001; Perez et al., 2001; Lei and McBain, 2004; Lamsa et al., 2007; Galván et al., 2008; Sarihi et al., 2008) remain to be dissected in PV+ interneurons. Properties may vary between distinct afferent pathways to the same cell (Tóth and McBain, 1998). Most glutamatergic inputs to

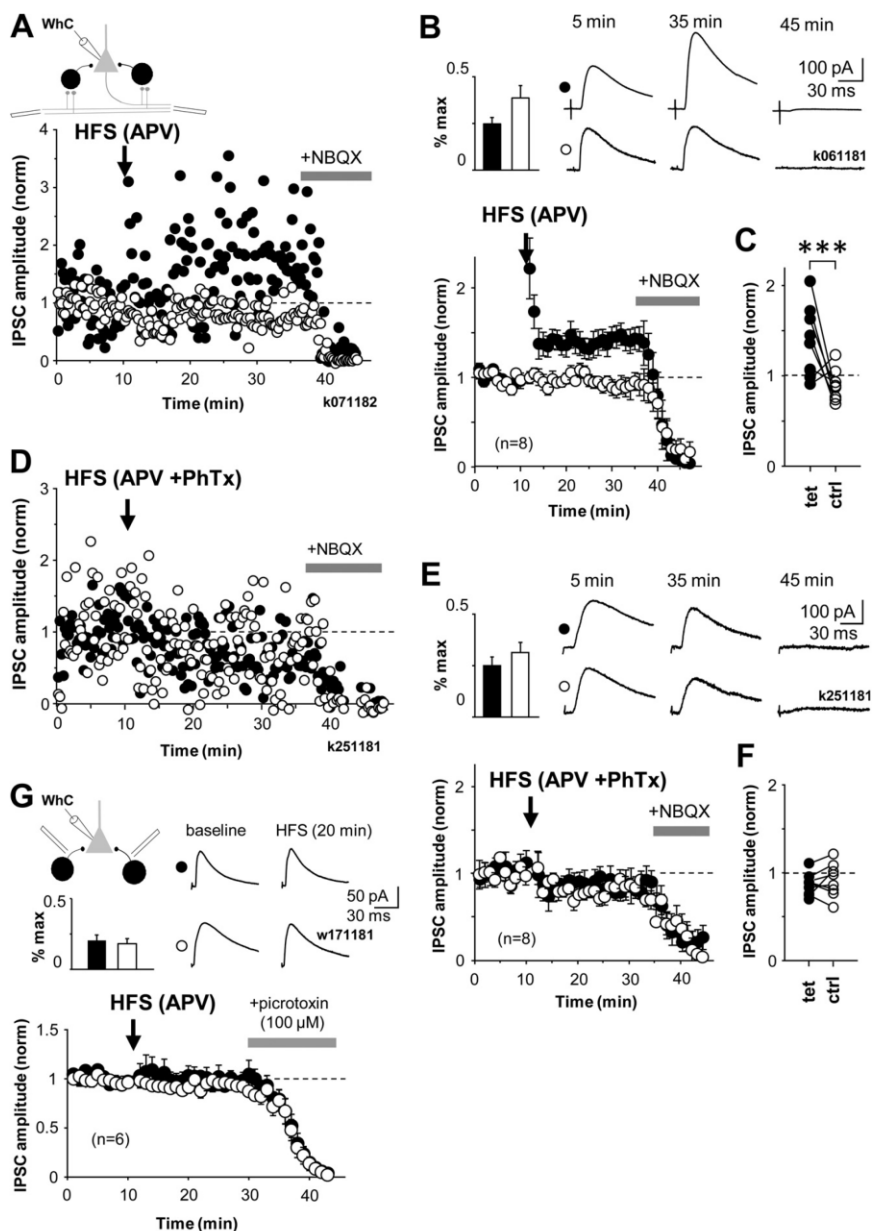


**Figure 6.** LTP of disynaptic GABAergic transmission in str. oriens is NMDAR independent, pathway specific, and requires interneurons with CP-AMPA receptors. **A**, HFS induces long-term potentiation in disynaptic IPSCs recorded in CA1 pyramidal cell somata. Two disynaptic pathways were stimulated with electrodes positioned in str. oriens/alveus. Schematic shows experimental design. IPSC amplitude was adjusted to  $\sim 30\%$  of maximum. After a baseline, HFS was given to one of the two pathways (filled symbols), the other pathway was not tetanized and was used as a control (open symbols). LTP was observed for 25 min. Full blockade of IPSCs at the end by NBQX (wash-in indicated by horizontal bar) confirmed the disynaptic nature of the IPSCs. Data are from one cell, in the presence of DL-APV ( $100 \mu\text{M}$ ) and CGP55845 ( $1 \mu\text{M}$ ). In addition, cannabinoid receptors were blocked with AM-251 ( $10 \mu\text{M}$ ). Whc, Whole-cell mode. **B**, Similar recordings as in **A**, averaged from eight cells showing mean  $\pm$  SE of disynaptic IPSC amplitude. Top left, Bar histogram shows disynaptic IPSC strength relative to maximum in the pathways during baseline (mean  $\pm$  SE). Top right, Averaged IPSCs at different time points in one cell as indicated. **C**, Comparison of averages of baseline-normalized IPSC amplitudes in all experiments 20 min after the HFS. Filled and open symbols indicate tetanized and control pathways as above ( $***p < 0.005$ , unpaired *t* test). **D**, LTP of disynaptic GABAergic transmission fails in the presence of the CP-AMPA blocker PhTx. Similar experiment as in **A** but in the presence of PhTx ( $10 \mu\text{M}$ ). **E**, Disynaptic IPSC mean  $\pm$  SE eight experiments in the presence of PhTx as in **D**. Insets as in **B**. **F**, Averages of baseline-normalized IPSCs in all experiments 20 min after the HFS. **G**, HFS does not change monosynaptic GABAergic IPSC. Monosynaptic IPSCs measured in CA1 pyramidal cell soma elicited by stimulation from str. oriens. IPSC amplitudes were adjusted on average below  $30\%$  of maximum (inset bar histogram). HFS was applied to one pathway (filled symbols) after a baseline period. Control pathway is shown by open symbols. HFS failed to induce lasting changes in the monosynaptic IPSC. Plot shows mean  $\pm$  SE of baseline-normalized IPSC amplitude in six cells. IPSCs were blocked by picrotoxin at the end. GABA<sub>B</sub>, ionotropic glutamate, and CB<sub>1</sub>Rs were blocked with CGP55845 ( $1 \mu\text{M}$ ), NBQX ( $10 \mu\text{M}$ ), DL-APV ( $100 \mu\text{M}$ ), and AM-251 ( $10 \mu\text{M}$ ). Averaged IPSCs are shown from one experiment during baseline and after HFS (20 min).

the three PV+ cell types reported here probably originate from CA1 and CA3 pyramidal cells, but the relative weight of these inputs is not known (Gulyás et al., 1999).

Synapses with CP-AMPA receptors provide the major pathway for long-term potentiation of disynaptic inhibition in the CA1 str. oriens/alveus, although potentiation level varied considerably between slices. This might be attributable to several factors. First, parallel depression of IPSCs in the dendritic domain of pyramidal cells might partially mask potentiation of IPSCs generated by perisomatic-targeting cells, although it is unclear whether LTD in bistratified cells results in reduced GABAergic transmission to pyramidal cell dendrites. However, because bistratified cells selectively target pyramidal cell dendrites, IPSCs from these interneuron types are much smaller at the level of the soma than IPSCs evoked by PV+ basket cells and axo-axonic cells (Maccaferri et al., 2000). In addition, number of bistratified cells is only one-quarter of all PV+ cells in the CA1 stratum pyramidale (Baude et al., 2007). This might explain why in most experiments IPSC potentiation was seen and why net depression of IPSC was not systematically observed. Second, stimulation of excitatory fibers in some cases may not have recruited PV+ perisomatic-targeting cells or the excitatory input failed to induce plasticity in these cells. If plasticity in PV+ cells follows the anti-Hebbian rule, strong depolarization during afferent stimulation would compromise or prevent LTP in some cells (Kullmann and Lamsa, 2007; Lamsa et al., 2007). Although LTP in oriens-lacunosum moleculare interneurons (Perez et al., 2001; Lamsa et al., 2007), which also express PV at low level (Klausberger et al., 2003), may contribute to the potentiation of disynaptic IPSC, their selective innervation of pyramidal cell distal dendritic domains elicits strongly attenuated IPSCs at the level of pyramidal cell soma (Maccaferri et al., 2000).

In conclusion, our findings reveal remarkable cell type-specific plasticity rules in the highly diverse hippocampal GABAergic interneuron population. We suggest that cell type-dependent plasticity in interneurons may not be restricted to the hippocampal CA1 area. Similar rules might occur in other brain areas with region- and afferent-specific variability. Because the interneuron types studied in this work are found in most cortical areas, their plasticity may also have widespread contributions to cortical networks outside

the hippocampus (Buzsáki and Draguhn, 2004; Santhakumar and Soltesz, 2004; Yazaki-Sugiyama et al., 2009).

## References

- Ali AB (2007) Presynaptic inhibition of GABA<sub>A</sub> receptor-mediated unitary IPSPs by cannabinoid receptors at synapses between CCK-positive interneurons in rat hippocampus. *J Neurophysiol* 98:861–869.
- Alle H, Jonas P, Geiger JR (2001) PTP and LTP at a hippocampal mossy fiber-interneuron synapse. *Proc Natl Acad Sci U S A* 98:14708–14713.
- Asrar S, Zhou Z, Ren W, Jia Z (2009) Ca permeable AMPA receptor induced long-term potentiation requires PI3/MAP kinases but not Ca/CaM-dependent kinase II. *PLoS ONE* 4:e4339.
- Bartos M, Vida I, Jonas P (2007) Synaptic mechanisms of synchronized gamma oscillations in inhibitory interneuron networks. *Nat Rev Neurosci* 8:45–56.
- Baude A, Bleasdale C, Dalezios Y, Somogyi P, Klausberger T (2007) Immunoreactivity for the GABA<sub>A</sub> receptor alpha1 subunit, somatostatin and Connexin36 distinguishes axoaxonic, basket, and bistratified interneurons of the rat hippocampus. *Cereb Cortex* 17:2094–2107.
- Buzsáki G, Draguhn A (2004) Neuronal oscillations in cortical networks. *Science* 304:1926–1929.
- Buzsáki G, Eidelberg E (1982) Direct afferent excitation and long-term potentiation of hippocampal interneurons. *J Neurophysiol* 48:597–607.
- Cardin JA, Carlen M, Meletis K, Knoblich U, Zhang F, Deisseroth K, Tsai LH, Moore CI (2009) Driving fast-spiking cells induces gamma rhythm and controls sensory responses. *Nature* 459:663–667.
- Carvalho TP, Buonomano DV (2009) Differential effects of excitatory and inhibitory plasticity on synaptically driven neuronal input-output functions. *Neuron* 61:774–785.
- Catania MV, Bellomo M, Giuffrida R, Giuffrida R, Stella AM, Albanese V (1998) AMPA receptor subunits are differentially expressed in parvalbumin- and calretinin-positive neurons of the rat hippocampus. *Eur J Neurosci* 10:3479–3490.
- Chevalyere V, Castillo PE (2003) Heterosynaptic LTD of hippocampal GABAergic synapses: a novel role of endocannabinoids in regulating excitability. *Neuron* 38:461–472.
- Cossart R, Dinocourt C, Hirsch JC, Merchán-Pérez A, De Felipe J, Ben-Ari Y, Esclapez M, Bernard C (2001) Dendritic but not somatic GABAergic inhibition is decreased in experimental epilepsy. *Nat Neurosci* 4:52–62.
- Cowan AI, Stricker C, Reece LJ, Redman SJ (1998) Long-term plasticity at excitatory synapses on aspiny interneurons in area CA1 lacks synaptic specificity. *J Neurophysiol* 79:13–20.
- Csicsvari J, Hirase H, Czurko A, Buzsáki G (1998) Reliability and state dependence of pyramidal cell-interneuron synapses in the hippocampus: an ensemble approach in the behaving rat. *Neuron* 21:179–189.
- Dragoi G, Harris KD, Buzsáki G (2003) Place representation within hippocampal networks is modified by long-term potentiation. *Neuron* 39:843–853.
- Földy C, Lee SY, Szabadics J, Neu A, Soltesz I (2007) Cell type-specific gating of perisomatic inhibition by cholecystokinin. *Nat Neurosci* 10:1128–1130.
- Freund TF, Katona I (2007) Perisomatic inhibition. *Neuron* 56:33–42.
- Fuchs EC, Zivkovic AR, Cunningham MO, Middleton S, Lebeau FE, Bannerman DM, Rozov A, Whittington MA, Traub RD, Rawlins JN, Monyer H (2007) Recruitment of parvalbumin-positive interneurons determines hippocampal function and associated behavior. *Neuron* 53:591–604.
- Galván EJ, Calixto E, Barrionuevo G (2008) Bidirectional Hebbian plasticity at hippocampal mossy fiber synapses on CA3 interneurons. *J Neurosci* 28:14042–14055.
- Geiger JR, Melcher T, Koh DS, Sakmann B, Seeburg PH, Jonas P, Monyer H (1995) Relative abundance of subunit mRNAs determines gating and Ca<sup>2+</sup> permeability of AMPA receptors in principal neurons and interneurons in rat CNS. *Neuron* 15:193–204.
- Goldberg JH, Yuste R (2005) Space matters: local and global dendritic Ca<sup>2+</sup> compartmentalization in cortical interneurons. *Trends Neurosci* 28:158–167.
- Gulyás AI, Megias M, Emri Z, Freund TF (1999) Total number and ratio of excitatory and inhibitory synapses converging onto single interneurons of different types in the CA1 area of the rat hippocampus. *J Neurosci* 19:10082–10097.
- Gustafsson B, Wigström H, Abraham WC, Huang YY (1987) Long-term potentiation in the hippocampus using depolarizing current pulses as the conditioning stimulus to single volley synaptic potentials. *J Neurosci* 7:774–780.
- Halasy K, Buhl EH, Lörinczi Z, Tamás G, Somogyi P (1996) Synaptic target selectivity and input of GABAergic basket and bistratified interneurons in the CA1 area of the rat hippocampus. *Hippocampus* 6:306–329.
- Heifets BD, Chevalyere V, Castillo PE (2008) Interneuron activity controls endocannabinoid-mediated presynaptic plasticity through calcineurin. *Proc Natl Acad Sci U S A* 105:10250–10255.
- Isaac JT, Ashby M, McBain CJ (2007) The role of the GluR2 subunit in AMPA receptor function and synaptic plasticity. *Neuron* 54:859–871.
- Isaac JT, Buchanan KA, Muller RU, Mellor JR (2009) Hippocampal place cell firing patterns can induce long-term synaptic plasticity *in vitro*. *J Neurosci* 29:6840–6850.
- Jonas P, Racca C, Sakmann B, Seeburg PH, Monyer H (1994) Differences in Ca<sup>2+</sup> permeability of AMPA-type glutamate receptor channels in neocortical neurons caused by differential GluR-B subunit expression. *Neuron* 12:1281–1289.
- Jonas P, Bischofberger J, Fricker D, Miles R (2004) Interneuron diversity series: fast in, fast out—temporal and spatial signal processing in hippocampal interneurons. *Trends Neurosci* 27:30–40.
- Kairiss EW, Abraham WC, Bilkey DK, Goddard GV (1987) Field potential evidence for long-term potentiation of feed-forward inhibition in the rat dentate gyrus. *Brain Res* 401:87–94.
- Klausberger T, Somogyi P (2008) Neuronal diversity and temporal dynamics: the unity of hippocampal circuit operations. *Science* 321:53–57.
- Klausberger T, Magill PJ, Márton LF, Roberts JD, Cobden PM, Buzsáki G, Somogyi P (2003) Brain-state- and cell-type-specific firing of hippocampal interneurons *in vivo*. *Nature* 421:844–848.
- Klausberger T, Márton LF, Baude A, Roberts JD, Magill PJ, Somogyi P (2004) Spike timing of dendrite-targeting bistratified cells during hippocampal network oscillations *in vivo*. *Nat Neurosci* 7:41–47.
- Klausberger T, Marton LF, O'Neill J, Huck JH, Dalezios Y, Fuentealba P, Suen WY, Papp E, Kaneko T, Watanabe M, Csicsvari J, Somogyi P (2005) Complementary roles of cholecystokinin- and parvalbumin-expressing GABAergic neurons in hippocampal network oscillations. *J Neurosci* 25:9782–9793.
- Kullmann DM, Lamsa KP (2007) Long-term synaptic plasticity in hippocampal interneurons. *Nat Rev Neurosci* 8:687–699.
- Laezza F, Dingledine R (2004) Voltage-controlled plasticity at GluR2-deficient synapses onto hippocampal interneurons. *J Neurophysiol* 92:3575–3581.
- Laezza F, Doherty JJ, Dingledine R (1999) Long-term depression in hippocampal interneurons: joint requirement for pre- and postsynaptic events. *Science* 285:1411–1414.
- Lamsa K, Heeroma JH, Kullmann DM (2005) Hebbian LTP in feed-forward inhibitory interneurons and the temporal fidelity of input discrimination. *Nat Neurosci* 8:916–924.
- Lamsa KP, Heeroma JH, Somogyi P, Rusakov DA, Kullmann DM (2007) Anti-Hebbian long-term potentiation in the hippocampal feedback inhibitory circuit. *Science* 315:1262–1266.
- Lapointe V, Morin F, Ratté S, Croce A, Conquet F, Lacaille JC (2004) Synapse-specific mGluR1-dependent long-term potentiation in interneurons regulates mouse hippocampal inhibition. *J Physiol* 555:125–135.
- Lei S, McBain CJ (2004) Two loci of expression for long-term depression at hippocampal mossy fiber-interneuron synapses. *J Neurosci* 24:2112–2121.
- Losonczy A, Zhang L, Shigemoto R, Somogyi P, Nusser Z (2002) Cell type dependence and variability in the short-term plasticity of EPSCs in identified mouse hippocampal interneurons. *J Physiol* 542:193–210.
- Maccaferri G, McBain CJ (1996) Long-term potentiation in distinct subtypes of hippocampal nonpyramidal neurons. *J Neurosci* 16:5334–5343.
- Maccaferri G, Tóth K, McBain CJ (1998) Target-specific expression of presynaptic mossy fiber plasticity. *Science* 279:1368–1370.
- Maccaferri G, Roberts JD, Szucs P, Cottingham CA, Somogyi P (2000) Cell surface domain specific postsynaptic currents evoked by identified GABAergic neurons in rat hippocampus *in vitro*. *J Physiol* 524:91–116.
- Mahanty NK, Sah P (1998) Calcium-permeable AMPA receptors mediate long-term potentiation in interneurons in the amygdala. *Nature* 394:683–687.
- Mann EO, Paulsen O (2007) Role of GABAergic inhibition in hippocampal network oscillations. *Trends Neurosci* 30:343–349.

- McBain CJ (2008) Differential mechanisms of transmission and plasticity at mossy fiber synapses. *Prog Brain Res* 169:225–240.
- McMahon LL, Kauer JA (1997) Hippocampal interneurons express a novel form of synaptic plasticity. *Neuron* 18:295–305.
- Oren I, Nissen W, Kullmann DM, Somogyi P, Lamsa KP (2009) Role of ionotropic glutamate receptors in long-term potentiation in rat hippocampal CA1 oriens-lacunosum moleculare interneurons. *J Neurosci* 29:939–950.
- Pawelzik H, Hughes DI, Thomson AM (2002) Physiological and morphological diversity of immunocytochemically defined parvalbumin- and cholecystokinin-positive interneurons in CA1 of the adult rat hippocampus. *J Comp Neurol* 443:346–367.
- Pelletier JG, Lacaille JC (2008) Long-term synaptic plasticity in hippocampal feedback inhibitory networks. *Prog Brain Res* 169:241–250.
- Perez Y, Morin F, Lacaille JC (2001) A hebbian form of long-term potentiation dependent on mGluR1a in hippocampal inhibitory interneurons. *Proc Natl Acad Sci U S A* 98:9401–9406.
- Ross ST, Soltesz I (2001) Long-term plasticity in interneurons of the dentate gyrus. *Proc Natl Acad Sci U S A* 98:8874–8879.
- Santhakumar V, Soltesz I (2004) Plasticity of interneuronal species diversity and parameter variance in neurological diseases. *Trends Neurosci* 27:504–510.
- Sarihi A, Jiang B, Komaki A, Sohya K, Yanagawa Y, Tsumoto T (2008) Metabotropic glutamate receptor type 5-dependent long-term potentiation of excitatory synapses on fast-spiking GABAergic neurons in mouse visual cortex. *J Neurosci* 28:1224–1235.
- Sohal VS, Zhang F, Yizhar O, Deisseroth K (2009) Parvalbumin neurons and gamma rhythms enhance cortical circuit performance. *Nature* 459:698–702.
- Somogyi P, Freund TF, Hodgson AJ, Somogyi J, Beroukas D, Chubb IW (1985) Identified axo-axonic cells are immunoreactive for GABA in the hippocampus and visual cortex of the cat. *Brain Res* 332:143–149.
- Tóth K, McBain CJ (1998) Afferent-specific innervation of two distinct AMPA receptor subtypes on single hippocampal interneurons. *Nat Neurosci* 1:572–578.
- Tukker JJ, Fuentealba P, Hartwich K, Somogyi P, Klausberger T (2007) Cell type-specific tuning of hippocampal interneuron firing during gamma oscillations *in vivo*. *J Neurosci* 27:8184–8189.
- Varga V, Losonczy A, Zemelman BV, Borhegyi Z, Nyiri G, Domonkos A, Hangya B, Holderith N, Magee JC, Freund TF (2009) Fast synaptic subcortical control of hippocampal circuits. *Science* 326:449–453.
- Yazaki-Sugiyama Y, Kang S, Câteau H, Fukai T, Hensch TK (2009) Bidirectional plasticity in fast-spiking GABA circuits by visual experience. *Nature* 462:218–221.

# IV

# Long-term plasticity in identified hippocampal GABAergic interneurons in the CA1 area in vivo

Petrina Yau-Pok Lau<sup>1</sup> · Linda Katona<sup>2</sup> · Peter Saghy<sup>2</sup> · Kathryn Newton<sup>1,2</sup> · Peter Somogyi<sup>2</sup> · Karri P. Lamsa<sup>1,3</sup> 

Received: 26 March 2016 / Accepted: 11 September 2016 / Published online: 25 October 2016  
© The Author(s) 2016. This article is published with open access at Springerlink.com

**Abstract** Long-term plasticity is well documented in synapses between glutamatergic principal cells in the cortex both in vitro and in vivo. Long-term potentiation (LTP) and -depression (LTD) have also been reported in glutamatergic connections to hippocampal GABAergic interneurons expressing parvalbumin (PV+) or nitric oxide synthase (NOS+) in brain slices, but plasticity in these cells has not been tested in vivo. We investigated synaptically-evoked suprathreshold excitation of identified hippocampal neurons in the CA1 area of urethane-anesthetized rats. Neurons were recorded extracellularly with glass microelectrodes, and labelled with neurobiotin for anatomical analyses. Single-shock electrical stimulation of afferents from the contralateral CA1 elicited postsynaptic action potentials with monosynaptic features showing short delay ( $9.95 \pm 0.41$  ms) and small jitter in 13 neurons through the commissural pathway. Theta-burst stimulation (TBS) generated LTP of the synaptically-evoked spike probability in pyramidal cells, and in a bistratified cell and two unidentified fast-spiking interneurons. On the contrary, PV+ basket cells and NOS+ ivy cells exhibited either LTD or LTP. An identified axo-axonic cell failed to show long-term change in its response to

stimulation. Discharge of the cells did not explain whether LTP or LTD was generated. For the fast-spiking interneurons, as a group, no correlation was found between plasticity and local field potential oscillations (1–3 or 3–6 Hz components) recorded immediately prior to TBS. The results demonstrate activity-induced long-term plasticity in synaptic excitation of hippocampal PV+ and NOS+ interneurons in vivo. Physiological and pathological activity patterns in vivo may generate similar plasticity in these interneurons.

**Keywords** LTP · LTD · Parvalbumin · Ivy cell · Interneuron · Oscillation

## Introduction

Activity-induced long-term plasticity characterizes neuronal communication widely in the brain providing cellular level mechanisms for learning and memory (Morris 2013). Various long-term plasticity forms have been characterized in interactions between glutamatergic neurons in the cortex in ex vivo slice preparation and in the intact brain in vivo. These include activity-induced synaptic long-term potentiation (LTP) and -depression (LTD), and changes in postsynaptic neuron excitability (Collingridge et al. 2010; Luscher et al. 2000; Lisman and Spruston 2005; Daoudal and Debanne 2003). Studies in ex vivo slice preparation have reported long-term plasticity also in glutamatergic excitation of many cortical GABAergic interneurons (Kullmann et al. 2012; Kullmann and Lamsa 2011; Topolnik 2012; Laezza and Dingledine 2011; Bartos et al. 2011; Galvan et al. 2011; McBain 2008). Experiments in hippocampal slices have demonstrated LTP in interneurons in CA1 that requires NMDA receptors (Lamsa et al.

✉ Peter Somogyi  
peter.somogyi@pharm.ox.ac.uk

✉ Karri P. Lamsa  
klamsa@bio.u-szeged.hu

<sup>1</sup> Department of Pharmacology, University of Oxford, Oxford OX1 3QT, UK

<sup>2</sup> MRC Brain Network Dynamics Unit, Department of Pharmacology, University of Oxford, Oxford OX1 3TH, UK

<sup>3</sup> Department of Anatomy, Physiology and Neuroscience, University of Szeged, Középfásor, Szeged 6720, Hungary

dc\_1581\_1807a; Le Roux et al. 2013) as well as different forms of long-term potentiation independent of NMDARs (Perez et al. 2001; Le Duigou and Kullmann 2011; Pelkey et al. 2008; Topolnik et al. 2006; Camire and Topolnik 2014; Lamsa et al. 2007b; Galvan et al. 2008; Nicholson and Kullmann 2014; Hainmuller et al. 2014; Campanac et al. 2013). In addition, excitatory synapses in CA1 interneurons exhibit long-term depression by endocannabinoids (Peterfi et al. 2012; Edwards et al. 2012). Although only few studies have investigated long-term plasticity in interneurons in vivo, potentiation and depression akin to LTP and LTD between some CA1 interneurons and their afferent excitatory fibers have been reported after high-frequency electrical stimulation or by learning-driven hippocampal activity (Buzsaki and Eidelberg 1982b; Dupret et al. 2013). However, the hippocampal CA1 area contains a great diversity of GABAergic interneuron types with specialized activity and connectivity (Somogyi and Klausberger 2005). Whether the different types of identified interneurons show plasticity in vivo and how this plasticity is regulated by brain states are unknown. Importantly, ex vivo studies have shown that long-term plasticity in CA1 interneurons is regulated by neuromodulator mechanisms from extrahippocampal sources such as cholinergic transmission (Le Duigou et al. 2015; Griguoli et al. 2013). The activity of many of these ascending fibers is brain state dependent (Vandecasteele et al. 2014) suggesting that interneuron plasticity might also differ during different brain states.

In the present study, we have investigated activity-induced long-term plasticity in synaptically evoked firing of identified CA1 interneurons in vivo in rats under urethane anesthesia in order to improve recording stability, and compared plasticity results after TBS stimulation during different oscillatory network states recorded as local field potential.

## Methods

### Animals and surgical procedures

Experiments were carried out on adult male (weight 280–350 g) Sprague–Dawley rats (Charles River, UK) according to the Animal Scientific Procedures Act, 1986 (UK) using a heating mattress ( $37.5 \pm 0.5$  °C) with an external abdominal temperature measurement probe with feedback to the heating pad. Anesthesia was induced with isoflurane (4 % v/v in O<sub>2</sub>) and maintained by a single intraperitoneal (i.p.) injection of urethane (1.25–1.3 mg/kg in 0.9 % saline, i.p.). Ketamine (30 mg/kg i.p.) and xylazine (3 mg/kg i.p.) were given at the start of the procedure and in supplementary small doses during recording to

maintain anesthesia. Saline-based glucose solution (5 % v/v glucose) was injected subcutaneously (2 ml/2 h) to compensate for fluid loss during the experiment. A rostrocaudal incision was performed to expose the skull, and surgical windows were made above the right and left dorsal hippocampal CA1 areas with a dental drill. A wall of dental cement was built to protect the openings and saline was applied regularly to the exposed brain surface. For accurate measurement of penetration depth, saline solution was drained before inserting electrodes into the brain. The windows were covered with warm paraffin wax once the electrodes were lowered into the brain.

### Electrophysiological recording, cell labeling, data acquisition and electrical stimulation

Microelectrodes were pulled from borosilicate glass capillaries (GC120F-10, Harvard Apparatus, UK) using a vertical puller (PE-2, Narishige, Japan) and were filled with 1.5–3 % (w/v) neurobiotin (Vector Laboratories, UK) in 0.5 M NaCl. The recording electrodes were lowered into the brain at 20 μm/s, and into the hippocampus at 5 μm/s using a micro drive holder (EXFO-8200 IMMS, Canada) and a computer-controlled 0.5 μm-stepping interface. Stereotaxic co-ordinates for the recording electrodes were: 3.0 mm posterior to Bregma ( $\pm 0.3$  mm), 3.6 mm from midline ( $\pm 0.5$  mm), and depth 2.2 mm ( $\pm 0.3$  mm). The electrode resistance was 15–21 MΩ.

Following extracellular recording, the electrode was moved into juxtacellular position and the recorded cells were modulated by applying a series of +10 to +50 nA square pulses of 200 ms duration in 30 s episodes for 2–3 minutes continuously (Brown et al. 2009). We verified that the action potential properties (extracellular spike kinetics) of the modulated cell corresponded to the action potential properties recorded during plasticity experiment. This labeling procedure was followed by a period from 1 to 5 hours (Klausberger et al. 2005), which allowed for the diffusion of neurobiotin inside the modulated cells.

Signal was amplified 1000× (10×, head-stage amplifier, Axon Instruments, USA; 100×, NL-106, Digitimer™, UK) and band-pass filtered between 0.3 and 300 Hz for local field potentials (LFP) and between 300 Hz and 5 kHz for detection of single spikes. The LFP and single neuron activity were acquired at 1 and 19.841 kHz, respectively using Spike2 (version 7.0; Cambridge Electronic Design, UK).

Concentric bipolar stimulating electrodes (125 μm tip diameter, FHC Inc., USA) were stereotaxically placed in the left hippocampal CA1 area 3.0–3.2 mm posterior and 3.0–4.0 mm lateral to Bregma and at 2.1–2.5 mm depth from the cortical surface (Buzsaki and Eidelberg 1982b). Single-shock stimulation (100 μs, 150–600 μA) was

dc\_15811\_1811 every 5 s using current isolator stimulator (DS3; Digitimer, UK) to elicit spikes. The train of theta-burst stimulation (TBS) consisted of 20 bursts (at 200 ms intervals) of five stimuli at 100 Hz.

### Data analysis and statistics

Data analyses were performed using Spike2 and MATLAB (MathWorks). The spike shape, width and amplitude were carefully monitored throughout the experiment and compared between spontaneous and evoked spikes using Principal Component Analysis (PCA) in Spike2. In the LFP, periods of theta frequency (3–6 Hz) oscillation were identified off-line using custom-made script in Spike2 (Tukker et al. 2007) as at least three consecutive windows of 2 s each during which the ratio between the power in 3–6 and 2–3 Hz frequency bands was  $>4$ . The start and end point of theta cycles defined by the script were confirmed by visual inspection. Theta oscillatory cycle troughs were identified and the theta phase of the single neuron action potentials was established (Tukker et al. 2007). The spontaneous firing was considered modulated by theta oscillations when the phases of action potentials were non-uniformly distributed along theta cycles ( $P \leq 0.05$ , Rayleigh's method). Phase histograms with  $18^\circ$  bin size were used to illustrate the average phase coupling to theta cycles. The preferential mean angle of firing was calculated using normalized vector addition (Klausberger et al. 2005).

To test for any changes in the LFP caused by TBS, we have calculated the wavelet power spectrogram of the LFP in 2 s time windows before and after TBS. The LFP signal was wavelet transformed using complex Morlet function (nondimensional central frequency of 6) evenly spaced between 1.25 and 40 Hz on a log scale. From this, the power spectrogram was calculated as the wavelet amplitude squared. We have derived an LFP index by calculating the average wavelet power in the frequency bands 1–3 Hz (avgPower1\_3Hz) and 3–6 Hz (avgPower3\_6Hz), respectively, restricted to 1 s before and after TBS and using the formula,

$$\frac{\text{avgPower3\_6Hz} - \text{avgPower1\_3Hz}}{\text{avgPower3\_6Hz} + \text{avgPower1\_3Hz}},$$

where index values of 1 and  $-1$  represent spectral power components only in the frequency ranges 3–6 or 1–3 Hz, respectively; whereas 0, represents exactly the same average power in both frequency ranges. The average wavelet power across a range of frequencies (e.g. 1–3 and 3–6 Hz) was determined as the weighted sum of the wavelet power spectrum over the respective frequencies.

Stimulus-evoked fEPSP and spikes were analyzed using Spike2. fEPSP onset and time to peak values as well as initial slope (from onset to 30 %) were

determined from 3 kHz off-line low-pass filtered raw signals. Evoked spikes were detected from band-pass filtered 300 Hz–5 kHz signals. In each cell, episodes of consecutive (at least 120) “monosynaptic time windows” (up to 15 ms) following stimulation were compared with episodes of spontaneous activity in similar (15 ms) time windows immediately before the stimulation to test whether the number of spikes was different in the two periods (Chi-square test) (Buzsaki and Eidelberg 1982a, b). During baseline conditions, i.e., before TBS, the 13 of 72 cells reported here showed higher number of cases with spikes in the “monosynaptic time window” than in the equal time window preceding the stimulation (Chi-square test). None of the seventy-two cells showed significantly higher number of time windows with spikes in the late period (post-stimulation 15–50 ms) compared to periods preceding the stimulation (measured in 35–0 ms before stimulation) in at least 120 consecutive windows. However, six cells fired with lower rates during the 15–50 ms post-stimulation period (at least 120 for each cell) than in 35–0 ms before stimulation (for each cell  $P < 0.05$ , Chi-square test). Changes in evoked spike probability (as failure or spike in 3–15 ms from stimulation, at least 120 windows) before and after TBS (post-TBS) in individual cells was analyzed using Chi-square test. ANOVA and post hoc Bonferroni test for multiple comparisons or *t*-test were used to analyze changes in spike delay. Using *t*-test the evoked spike probability, spike delay, or spike delay time  $1/CV^2$  values were compared between baseline and post-TBS in groups of cells. Spikes during TBS were summed between the 1st stimulation and 50 ms after the 5th stimulation of each burst. *P*-values  $< 0.05$  indicate significant difference in the mean firing rates between post-TBS periods and baseline.

Spike probability and spike delay time values (including the  $1/CV^2$ ) were normalized using the baseline average for presentation and analyses in Fig. 6 to show a relative change.

Spontaneous firing levels were calculated during 1 s episodes immediately preceding the stimulations throughout the experiment. For presentation in figures and for statistical analyses, values of spontaneous firing level (number of spikes in 1 s windows) data were pooled giving average number of spikes in 12 consecutive episodes of 1 s, every 5 s resulting in 1 min bin. Statistical comparison of spontaneous firing level during baseline and post-TBS periods was performed using ANOVA and Bonferroni test for multiple comparisons and comprised at least ten consecutive 1 min bins for each condition.

Normal distributions of data were tested with Kolmogorov–Smirnov test. Data are shown as mean ( $\pm$ SEM) unless otherwise stated. For testing correlation and significance in scatter plots of data in Fig. 6 data have been fitted

dc\_1581e18 efficient of determination ( $r^2$ ) and tested with the Pearson's test.

### Visualization of recorded neurons, immunohistochemistry and electron microscopy

Animals were perfused with 0.1 M phosphate buffered saline solution (PBS, pH 7.4, at 22–24 °C) followed by ice-cold fixative solution; 4 % w/v paraformaldehyde (PFA) with 15 % v/v saturated picric acid solution in 0.1 M phosphate buffer (PB) with freshly added glutaraldehyde to a final content of 0.05 % w/v. Brains were kept in fixative (4 % PFA in 0.1 M PB) at 4 °C for 24 hours, then stored in 0.1 M PB with 0.05 % sodium azide preservative at 4 °C. Vibratome (VT1000S Leica Microsystems, UK) was used for cutting coronal brain sections (60–70 µm thickness). Sections were washed in PB three times for 10 minutes at 24.0 °C, then incubated overnight in streptavidin-conjugated AlexaFluor488 in 0.1 M Tris-buffered saline (TBS, pH 7.4) with 0.3 % TritonX-100 (Sigma-Aldrich Inc., USA) on a shaker at 4 °C. Sections were mounted using Vectashield (Vector Laboratories Inc, USA) under cover slips and were examined using epifluorescence microscopy (AxioImager Z1, Carl Zeiss, UK). Some sections used for electron microscopy were cryoprotected in 20 % sucrose dissolved in PB and permeabilized using a 'freeze-thaw' procedure instead of Triton-X treatment.

For immunohistological reactions, free-floating sections were washed three times in TBS (15 minutes) at 24 °C, and then incubated in 20 % horse or goat serum in TBS for blocking non-specific antibody attachment. The sections were incubated in primary antibodies diluted in 1 % horse or goat serum in TBS over two nights at 4 °C. After washes, the same sections were incubated in relevant fluorochrome-conjugated secondary antibodies in 1 % of blocking serum in TBS for overnight at 4 °C, or 2–4 hours at 24.0 °C. Sections were washed in TBS (20 minutes) three times, and mounted on glass slides. The characterizations of antibodies (host, dilution, source) to cannabinoid receptor CB1 (goat, 1:1000, Frontier Institute Co. Ltd., Hokkaido, Japan, <http://www.frontier-institute.com>), neuronal nitric oxide synthase (mouse, 1:2000, Sigma, USA), neuropeptide Y (NPY, rabbit, 1:5000, ImmunoStar, Inc., USA, <http://www.immunostar.com>), parvalbumin (rabbit, 1:1000, Swant, Switzerland, <http://www.swant.com>), pro-CCK (rabbit, 1:500, Frontier Institute Co. Ltd., Japan), special AT-rich sequence-binding protein-1 (SATB1, goat, 1:1000, Santa Cruz Biotechnology Inc., USA, <http://www.scbt.com>.) have been reported earlier (Viney et al. 2013; Unal et al. 2015). Fluorophore-labeled secondary antibodies are described in Unal et al. (2015). Labelling of neurons using neurobiotin and immunoreactions were evaluated using both epifluorescence (Ferraguti et al. 2005) and laser

scanning confocal microscopy (Somogyi et al., 2012). Immunoreaction was considered to be negative when fluorescence was not detected in relevant neurobiotin-labelled cell, but immunopositivity was detected in the same area in unlabeled cells.

Following fluorescence microscopic analysis, neurobiotin was revealed by horseradish peroxidase reaction, the sections were treated with osmium tetroxide for increasing contrast, dehydrated and mounted on slides in epoxy resin for light microscopic identification of the axonal and dendritic patterns (Viney et al. 2013). Some cells were partially reconstructed from serial sections using a drawing tube and a PL Apo 63×/1.4 numerical aperture (n.a.) oil immersion objective. The axon terminals of two neurons were evaluated by electron microscopy as described earlier to aid their identification by revealing some of the post-synaptic elements (Viney et al. 2013).

### Confocal microscopy

Parameters and methods used for confocal microscopic image acquisition were as reported earlier (Viney et al. 2013), except that in some cases multiple channels were captured in the same track, if they were suitably distant from each other in wavelength. Briefly, multi-channel fluorescence images were acquired using ZEN 2008 software v5.0 on a Zeiss LSM 710 laser scanning confocal microscope (Zeiss Microscopy GmbH, Germany), equipped with DIC M27 Plan-Apochromat 40×/1.3 n.a., DIC M27 Plan-Apochromat 63×/1.4 n.a. and alpha Plan-Apochromat 100×/1.46 n.a. oil immersion objectives. Channel specifications were (laser/excitation wavelength, beam splitter, emission spectral filter) for detection of Alexa405, 405–430 solid state 405 nm with attenuation filter ND04, MBS-405, 409–499 nm; for Alexa488, argon 488 nm, MBS-488, 493–542 nm; for Cy3, HeNe 543 nm, MBS-458/543, 552–639 nm; For Cy5, HeNe 633 nm, MBS 488/543/633, 637–757 nm. Pinhole sizes were chosen by selecting 1 Airy Unit for the channel of the shortest wavelength, and matching the resulting optical section height across the other channels. For illustrations, all manipulations to brightness and contrast, and median filtering (if applied), were carried out on whole images, not selectively.

## Results

### Short delay synaptic excitation in CA1 area from the contralateral hippocampus

Electrical stimulation was applied from the contralateral (left) hippocampal CA1 area aiming to antidromically

dc\_15811\_18 CA3 pyramidal cells and their Schaffer collaterals in the right hemisphere and antidromically stimulate left hippocampal CA3 pyramidal cells and their commissural fibers to the right hippocampal CA1 (Buzsaki and Eidelberg 1982a, b). We first confirmed that single-shock stimulation was able to elicit field EPSP (fEPSP) in the right hippocampal CA1 with a short phase-locked delay ( $6.23 \pm 0.43$  ms to the fEPSP onset,  $n = 13$ ) and short time to peak (from onset  $2.52 \pm 0.63$  ms,  $n = 13$ ) (Buzsaki and Eidelberg 1982b; Bliss and Lomo 1973) (Fig. 1a).

Action potentials of individual CA1 area neurons were measured extracellularly (Fig. 1a). In 13 out of 72 spontaneously active cells recorded in the CA1 area, phase-

locked action potential to single-shock stimulation (interval 5 s) was elicited with a short delay ( $9.95 \pm 0.41$  ms,  $n = 13$ , see methods for criteria) that corresponds to monosynaptic excitatory pathway (Buzsaki and Eidelberg 1982a, b). The probability of the phase-locked spike was modulated by stimulation strength with minor alterations in spike latency (Fig. 1b). Stimulus intensity was then adjusted to elicit the spike with an approximate half-maximal probability. In 59 out of the 72 cells, single-shock stimulation failed to elicit spikes (see “Methods”). Antidromic action potentials due to stimulation were not observed in the cells reported here (Buzsaki and Eidelberg 1982b).

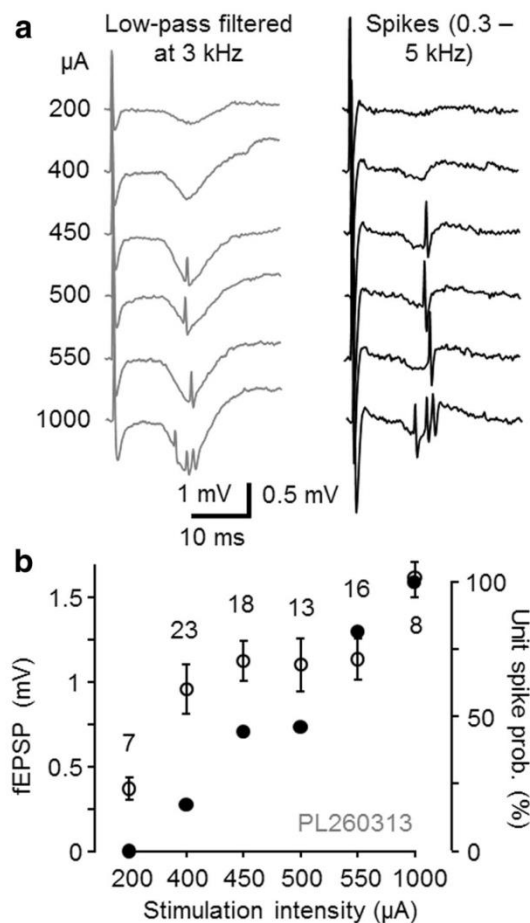


**Fig. 1** Electrical stimulation from contralateral hippocampus elicits fEPSP and postsynaptic action potential with phase-locked short delay in CA1. **a** Extracellularly recorded traces from one experiment with fEPSP and postsynaptic cell spikes evoked by different stimulus intensities from contralateral CA1 area. Increasing the stimulation intensity (left  $\mu\text{A}$ ) augmented fEPSP amplitude (signals low-pass filtered at 3 kHz) and action potential (spikes, band-pass filtered between 0.3 and 5 kHz) probability without a significant effect on the spike delay indicating monosynaptic transmission. **b** Amplitude of fEPSPs (open symbols mean  $\pm$  SD) and spike probability (solid symbols) of a pyramidal cell (PL260313) evoked with different stimulus intensities. Intensity was finally set to elicit spikes with approximate half-maximal probability

### Long-term potentiation of synaptic excitation in identified CA1 pyramidal cells

Three postsynaptic pyramidal cells were identified by their spontaneous electrical activity and spike waveform, and two of them were confirmed by visualization (Pyapali et al. 1998). The pyramidal cells fired spontaneously at low rate with the highest probability close to the LFP theta cycle trough. They showed characteristic slow spike kinetics (Table 1) and two of three cells showed occasional complex spikes (Fig. 2a–c) (Harris et al. 2001).

Pyramidal cells generated spikes to afferent stimulation with  $11.44 \pm 0.71$  ms delay ( $n = 3$ ) at approximate half-maximal spike probability, which in two experiments was associated with fEPSPs. After recording baseline (at least 10 min), high-frequency theta burst stimulation (TBS, 5 pulses at 100 Hz, repeated 20 times at 200 ms interval) was delivered in the left CA1, whereupon the single-pulse stimulation was resumed (Fig. 2d). The TBS increased the stimulus-evoked spike probability for at least 45 min in all three pyramidal cells ( $n = 3$ , for each cell  $P < 0.005$ , Chi-square test) while the average spike delay to the stimulation remained unchanged ( $n = 3$ ,  $t$  test) making it unlikely that the potentiation was conveyed polysynaptically via a recurrent circuit (Buzsaki and Eidelberg 1982b; Maccaferri and McBain 1996). While the spike probability potentiated from  $0.38 \pm 0.07$  during baseline to  $0.93 \pm 0.04$  in 15–45 min during post-TBS ( $n = 3$ ,  $P < 0.005$ ,  $t$  test) the mean spike delay time remained unchanged ( $t$  test) in the three cells (post-TBS  $11.29 \pm 0.79$  ms). The coefficient of variance (CV) of the delay time decreased in two of the three cells, but  $1/\text{CV}^2$  of the three cells was not significantly changed after LTP (15–45 min) ( $n = 3$ ,  $t$  test). Baseline-normalized  $1/\text{CV}^2$  for the three cells after LTP (15–45 min) was  $2.41 \pm 1.18$ . In the two experiments with fEPSP, the spike probability increase was accompanied by LTP in fEPSP initial slope to 127 and 124 % from baseline, respectively (at 15–45 min post-TBS, for each recording  $P < 0.01$ ,  $t$  test). Spontaneous firing level remained unchanged between the baseline and the period

dc\_1581\_18 Summary of spontaneous firing properties and spike kinetics of pyramidal cells

Spontaneous spiking properties				
Cell code	Firing rate during LFP theta (Hz)	Mean angle phase ( $\pm$ cSD) to LFP theta cycle ( $^{\circ}$ )	Depth of modulation ( $r$ ) during the theta and $n$ of cycles	Spike durations (ms) (mean $\pm$ SEM)
PL120811	2.94	84 $\pm$ 64	0.38, $n = 34$	1.98 $\pm$ 0.04
PL240113	3.29	34 $\pm$ 49	0.64, $n = 852$	1.90 $\pm$ 0.04
PL260313	2.96	358 $\pm$ 40	0.76, $n = 833$	1.41 $\pm$ 0.04

The three pyramidal cells showed low spontaneous firing rate during theta oscillations in the LFP. The cells fired with highest probability close to LFP theta cycle troughs ( $180^{\circ}$  peak of cycle, cSD means circular standard deviation). Extracellularly recorded action potential showed slow kinetics (close to 1.5 ms or longer)

following TBS in two cells and was reduced after TBS in one pyramidal cell ( $P < 0.01$ ,  $t$  test) (Fig. 2e, f; Table 2). In two out of three experiments 1–3 Hz oscillations occurred in the local field potential (LFP) at the time of TBS application (measured over 1 s prior to TBS), whereas in one experiment the LFP was dominated by 3–6 Hz oscillatory activity (see Table 7 for summary of all 13 cells in this study). Data on the stimulus-evoked spikes and level of spontaneous firing in the plasticity experiments are summarized in Table 2.

### Plasticity of synaptic excitation in fast-spiking PV+ interneuron types

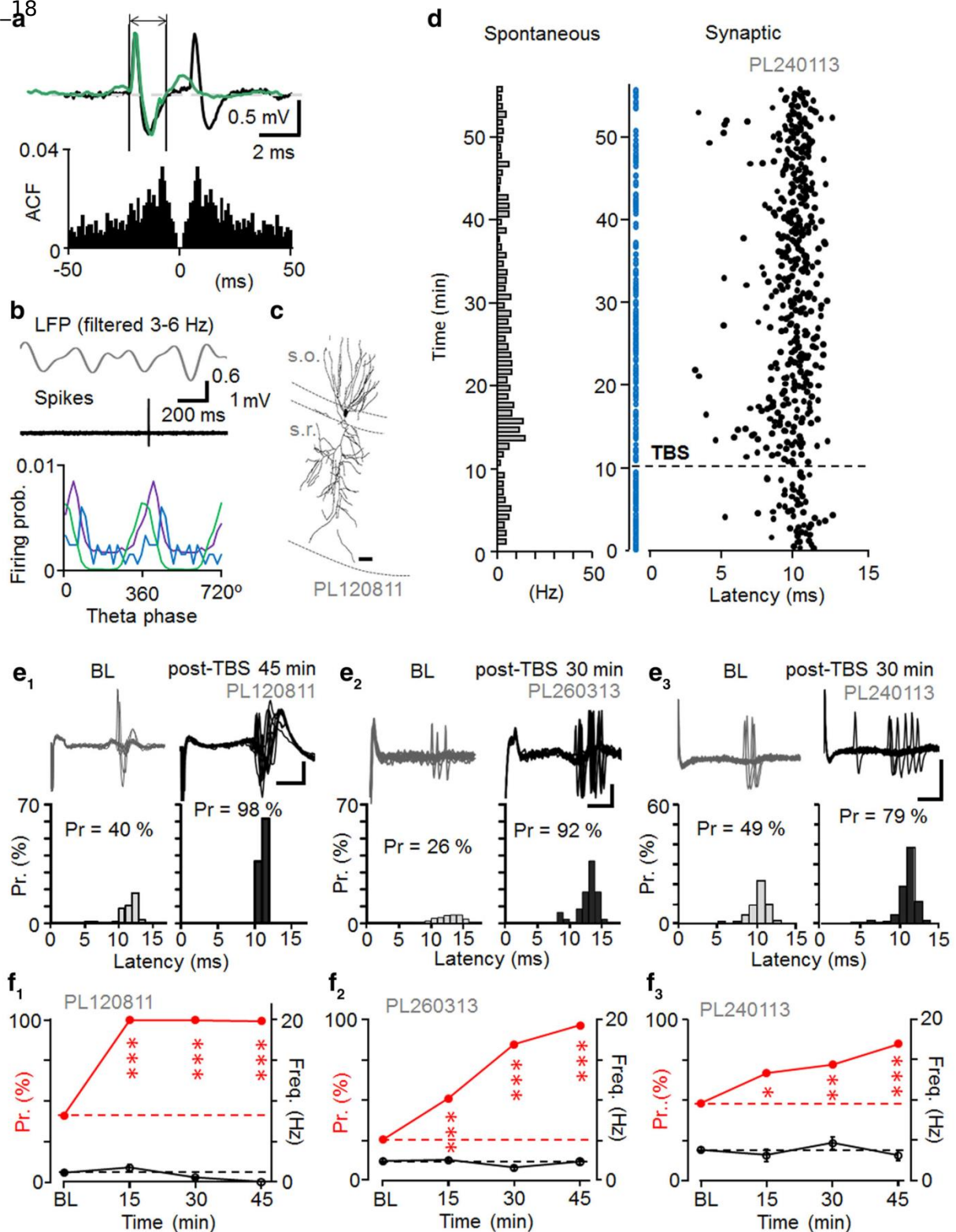
Fast-spiking interneurons defined by spike duration ( $1.02 \pm 0.05$  ms,  $n = 7$  cells) (Fig. 3a). On average exhibited higher spontaneous discharge levels than pyramidal cells (Table 3) (Klausberger et al. 2003). Autocorrelogram of spontaneous firing exhibited no peaks at intervals up to 50 ms indicating a lack of complex spikes in the cells. Anatomical analysis revealed three of the fast-spiking cells as basket cells (Fig. 3), one axo-axonic cell (AAC) and one bistratified cell (Fig. 4) (Klausberger et al. 2003; Klausberger and Somogyi 2008). All five recovered cells were immunopositive for PV. In line with previous findings, the AAC was immunonegative for the transcription factor SATB1 (Viney et al. 2013) (Table 3). The axon of the AAC was weakly labelled by neurobiotin and appeared in both the pyramidal cell layer and in *stratum oriens*. We tested some boutons by electron microscopy and they were aligned with axonal initial segments (Fig. 4). The preferred firing phase of one basket cell (Table 3) was on the early descending slope of the LFP theta cycle close to where axo-axonic cells may also fire (Klausberger et al. 2003). Therefore, we tested some of the axon terminals for postsynaptic targets by electron microscopy and found that they innervated cell bodies and dendrites (not shown) consistent with this neuron being a basket cell. The bistratified cell showed characteristic axon distribution in *strata radiatum*, *pyramidale* and *oriens* (Halasy et al. 1996). Its dendrites did not extend into *stratum lacunosum-*

**Fig. 2** Long-term potentiation of synaptic excitation in identified CA1 pyramidal cells. **a** Occasional complex spikes characterized spontaneous CA1 pyramidal cell firing. *Top* spontaneous single spike (green) and complex spike (black) superimposed from the same cell. *Vertical lines* define onset and the end of single spike showing slow ( $>1.5$  ms) spike duration. *Bottom* autocorrelogram of spontaneous spiking. A peak at approximately 10 ms reflects the spike interval of complex spikes. **b** Pyramidal cells fired spontaneously with highest probability around the trough of LFP theta cycles. *Top* band-pass filtered LFP (3–6 Hz) and a spontaneous pyramidal cell spike (band-pass filtered at 0.3–5 kHz) during theta oscillations. *Bottom* spike timing histogram showing firing preference of the pyramidal cells around the theta cycle trough ( $n = 3$ , cells shown in different colors). **c** Recorded pyramidal cell partially visualized from one  $60 \mu\text{m}$  thick section. *Scale*  $20 \mu\text{m}$ . **d** Synaptically evoked spike probability and delay (latency) to single-shock stimulation in one pyramidal cell during baseline and after theta-burst stimulation of the contralateral hippocampus (TBS, *horizontal dotted line*). Stimuli failing to evoke spike are shown with *blue dots* (abscissa). Spontaneous firing of the cell is shown in Hz as bar histogram on the left (1 min bin). **e, f** Long-term potentiation (LTP) in the synaptically-evoked spike probability in three identified pyramidal cells after the TBS. **e1–e3** *Top* superimposed traces showing synaptically-evoked spikes with occasional failures in the three cells during baseline (BL) and after the TBS (post-TBS). *Scales* 1, 0.2, and 0.5 mV, respectively; 5 ms. *Bottom* histograms show increased spike probability (Pr) (Chi square test), but unaltered spike latency post-TBS ( $t$  test). The potentiation is significant in each cell ( $P < 0.005$ ). **f1–f3** Spike probability in the three cells at different time points (*red symbols* scaling left, significance compared to baseline, Chi square test). *Black symbols* show spontaneous firing (scaling right). Spontaneous firing level was significantly reduced long-term from baseline only in **f1** at the last two time points (ANOVA with Bonferroni test)

*moleculare*. The cell was immunopositive for NPY (Klausberger et al. 2004). Two fast-spiking cells were not recovered following the labeling attempt, but both cells had preferred spontaneous firing close to the LFP theta cycle trough indicating possible dendrite-targeting PV+ cells (Klausberger et al. 2003, 2004). Spiking features of the cells including their spontaneous firing during LFP theta periods in baseline are detailed in Table 3.

In baseline conditions, afferent stimulation with estimated half-maximal intensity elicited spikes with  $0.59 \pm 0.14$  probability and  $9.71 \pm 0.62$  ms latency ( $n = 7$ ) (Table 4). Unlike in the pyramidal cell recordings,

dc\_1581\_18



detectable fEPSP was generated in only one of the seven recordings with the stimulus intensity criteria used (Buzsáki and Eidelberg 1982b). Following TBS, at >15 min,

two basket cells exhibited long-lasting depression of the evoked spike probability from 0.52 to 0.35 ( $P < 0.005$ ) and from 0.32 to 0.19 ( $P < 0.01$ ). One basket cell showed LTP-

dc\_1581e\_18 Summary of pyramidal cell firing

Synaptically evoked spike properties and spontaneous firing rate during plasticity experiment									
Cell code	Probability to the afferent stimulation			Latency to the afferent stimulation (ms) (mean $\pm$ SEM)			Overall spontaneous firing of the cell during the experiment (Hz)		
	Baseline	Post-TBS (0–15 min)	Post-TBS (15–45 min)	Baseline	Post-TBS (0–15 min)	Post-TBS (15–45 min)	Baseline	Post-TBS (0–15 min)	Post-TBS (15–45 min)
PL120811	0.41	1.00***	0.99***	11.79 $\pm$ 0.11	10.17 $\pm$ 0.06	11.06 $\pm$ 0.03	1.11	1.78	0.32**
PL240113	0.48	0.64*	0.85***	10.01 $\pm$ 0.16	9.64 $\pm$ 0.26	10.05 $\pm$ 0.23	3.78	3.15	3.12
PL260313	0.26	0.51***	0.96***	12.35 $\pm$ 0.48	13.51 $\pm$ 0.29	12.78 $\pm$ 0.23	2.43	2.12	2.36

Average probability (Chi square test) and latency of synaptically evoked postsynaptic spikes (ANOVA with Bonferroni test) in the experiments during baseline and at two different periods following TBS (post-TBS). The overall spontaneous firing frequency in the baseline and at early (0–15 min) and late (15–45 min) post-TBS time windows are shown at right

\*  $P < 0.05$ , \*\*  $P < 0.01$ , \*\*\*  $P < 0.005$

**Table 3** Summary of spontaneous firing properties and spike kinetics of fast-spiking interneurons

Spontaneous spiking properties					Immunohistochemistry
Cell code, cell type	Firing rate during LFP theta (Hz)	Mean angle phase ( $\pm$ cSD) to LFP theta cycle ( $^{\circ}$ )	Depth of modulation ( $r$ ) during the theta and $n$ of cycles	Spike duration (ms) (mean $\pm$ SEM)	
PL210213, BC	21.6	239 $\pm$ 71	0.24, $n = 1804$	1.07 $\pm$ 0.01	PV+
PL230313, BC	14.9	305 $\pm$ 75	0.14, $n = 4947$	0.88 $\pm$ 0.03	PV+, CB1R–
PL190912, BC	20.1	303 $\pm$ 64	0.38, $n = 1842$	1.11 $\pm$ 0.02	PV+
PL311012, AAC	35.4	213 $\pm$ 65	0.36, $n = 825$	0.96 $\pm$ 0.02	PV+, SATB1–
PL200711, Bistratified	2.25	358 $\pm$ 48	0.64, $n = 243$	1.08 $\pm$ 0.03	PV+, NPY+
PL020213, Unidentified	14.0	311 $\pm$ 67	0.31, $n = 7114$	0.83 $\pm$ 0.06	N/A
PL030412, Unidentified	13.2	337 $\pm$ 75	0.13, $n = 18579$	1.17 $\pm$ 0.03	N/A

Spontaneous firing rates of the recorded fast-spiking interneurons during LFP theta oscillations and their average firing phase during LFP theta cycles (cSD indicates circular standard deviation). The axo-axonic cell showed firing preference close to the peak of theta cycles followed by basket cells firing along the descending slope. A bistratified cell and the two unrecovered fast-spiking cells fired close to the trough. All cells showed fast spike kinetics (spike duration below or close to 1 ms). Immunohistochemical reactions

+, positive; –, negative; N/A, not applicable

like potentiation ( $P < 0.05$ ) (Chi square test) (Fig. 3c–e) (Peterfi et al. 2012). In the case of the basket cell with LTP, during the one second prior to TBS, the LFP was dominated by slow oscillations (1–3 Hz) in contrast to the two basket cell recordings with LTD, which were dominated by 3–6 Hz oscillations in the LFP. The axo-axonic cell did not show significant long-lasting change in the probability or delay of evoked spikes (Chi square test) although its spontaneous firing level was reduced long term (>15 min post-TBS, see Table 4) (Nissen et al. 2010) and the LFP during the one second immediately prior to TBS was dominated by 3–6 Hz oscillations. In contrast, the identified bistratified cell and the two unidentified fast-spiking cells showed LTP of the stimulus-evoked spike probability after TBS (Fig. 4c–h; Table 4). In the cells with LTP, spontaneous firing level changed long term (post-TBS >15 min) only in one unidentified cell (PL020213) showing a moderate decrease (see Table 4). The TBS was

applied at a time dominated by 3–6 Hz oscillations in the LFP for one unidentified fast-spiking cell with LTP (PL020213), and by slow oscillations (1–3 Hz) in the other two experiments resulting in LTP (PL030412, PL200711). LFP oscillation analysis results for all cells in this study are summarized in Table 7.

The changes in spike probability in the fast-spiking cells were not associated with significant long-term alterations in the average spike delay or the spike delay variance. In the four cells with significant LTP (see Table 4) average spike probability increased from  $0.66 \pm 0.03$  to  $0.85 \pm 0.03$  (15–45 min post-TBS,  $n = 4$ ,  $P < 0.01$ , Chi square test) with no change in the average spike delay ( $9.93 \pm 0.51$  vs.  $9.49 \pm 0.30$  ms,  $t$  test). In parallel coefficient of variance (CV) of the delay time decreased from baseline in three of the four cells (from 0.13 to 0.08; from 0.08 to 0.05; from 0.28 to 0.16), but remained unaltered in one neuron (0.20 vs. 0.21). However,  $1/CV^2$  of the four

dc\_1581\_18 not significantly changed after LTP (15–45 min) from baseline ( $n = 4$ ,  $t$  test). Baseline-normalized  $1/CV^2$  of the cells was  $2.29 \pm 0.47$  ( $n = 4$ ). Likewise, the spike average delay for the two basket cells with LTD was unaltered between the baseline and the depression (see Table 4). Spontaneous firing level during the recording, and the results of immunohistochemical reactions are shown in Table 3. Details on the evoked spike probability and delay are seen in Table 4.

### Plasticity of synaptic excitation in NOS+ ivy cells

Identified ivy cells (Fuentelba et al. 2008) showed slow spike kinetics ( $1.60 \pm 0.09$  ms,  $n = 3$ ) close to that found in pyramidal cells (Fig. 5a). Anatomical analysis of the recorded cells uncovered characteristic dense axons in *stratum radiatum* and immunopositivity for neuronal nitric oxide synthase (NOS) (Fuentelba et al. 2008; Szabo et al. 2012; Somogyi et al. 2012; Armstrong et al. 2012) (Fig. 5b). The cell bodies were at different laminar locations: PL170412 was in *stratum radiatum* (Fig. 5b), PL310812 in *stratum radiatum* one third from the border with *stratum lacunosum-moleculare* (Fig. 5f), and PL160413 was located in *s. pyramidale*. The dendritic trees were also variable. The ivy cells fired with highest probability after or close to the LFP theta cycle trough (Table 5). Their average spontaneous firing rate during theta frequency (3–6 Hz) oscillations was similar to that of pyramidal cells (Table 5).

During baseline conditions, single shock stimulation evoked a spike with  $0.39 \pm 0.07$  probability and  $9.63 \pm 0.91$  ms delay to the stimulation ( $n = 3$ ) without detectable fEPSP in any of the recordings. Two ivy cells showed long-lasting depression of spike probability at >15 min following TBS (for each cell  $P < 0.005$ , Chi square test). One ivy cell exhibited long-lasting potentiation of spike probability from 0.24 during baseline to 0.52 post-TBS ( $P < 0.005$ , Chi square test) (Fig. 5c–e). None of the three cells showed significant change in average spike delay ( $t$  test) (see Table 6). Interestingly, both ivy cells with LTD also showed increase in spike delay time coefficient of variance (CV) from baseline after TBS (>15 min) (from 0.11 to 0.29 and 0.10 to 0.21), whereas the cell with potentiation showed no alteration (0.23 vs. 0.25).

The spontaneous firing level of all three cells increased long-term (>15 min post-TBS) from baseline ( $P < 0.05$  and  $P < 0.005$ , ANOVA with Bonferroni test) (Table 6). All three recordings from ivy cells showed theta-like (3–6 Hz) activity in the LFP during the period one second prior to TBS (see Table 7). Moreover, the LFP power spectrogram for the ivy cell PL170412 also showed an additional clear peak in the slow frequency range (1–3 Hz) (data not shown). In this neuron TBS led to LTP in contrast

to the other two cells. Moreover, there was a quarter of oscillatory cycle difference in the preferential theta phase of firing of this neuron compared to the other two cells (see Table 5).

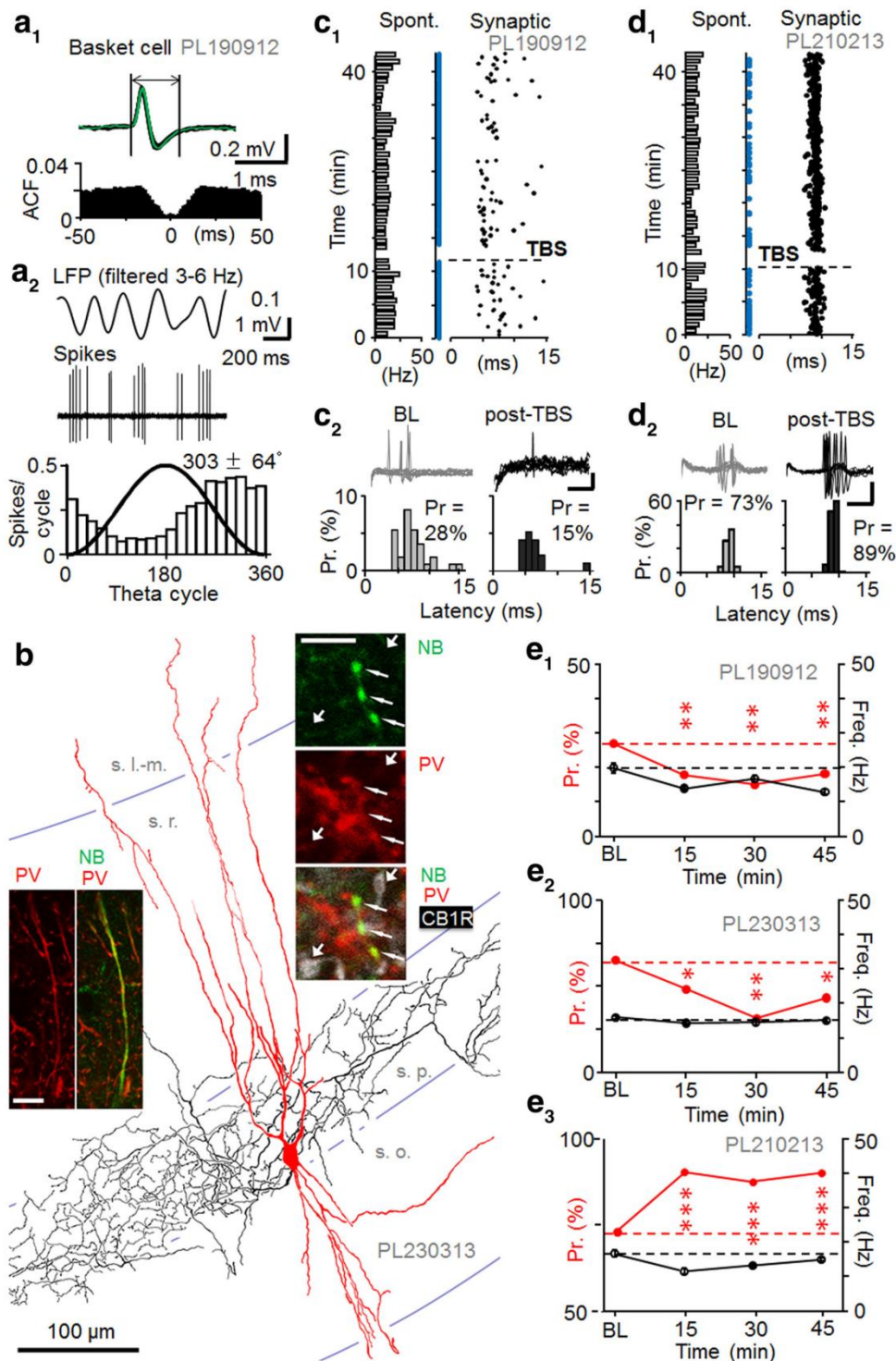
### Analysis of spike delay time in all cells with LTP or LTD

In each identified cell population, the pyramidal cells, the fast-spiking interneurons and the ivy cells, individual neurons showing LTP or LTD comprise a small sample making statistical analyses of the spike delay properties unreliable or untestable. Therefore, we analyzed the spike probability and delay properties pooling all cells showing either LTP or LTD. In the cells showing LTP, spike probability was potentiated from  $0.50 \pm 0.06$  to  $0.84 \pm 0.05$  at 15–45 min post-TBS ( $n = 8$ ,  $P < 0.01$ ,  $t$  test). Although the average spike delay, measured in the same time windows remained unchanged ( $10.64 \pm 0.43$  vs.  $10.24 \pm 0.41$  ms), the spike delay time coefficient of variance showed a significant reduction from baseline (compared as  $1/CV^2$ ,  $n = 8$ ,  $P < 0.05$ ,  $t$  test) with baseline-normalized  $1/CV^2$  of  $1.96 \pm 0.35$  ( $n = 8$ ). In cells showing LTD, spike probability decreased from  $0.44 \pm 0.04$  in baseline to  $0.21 \pm 0.06$  at 15–45 min post-TBS,  $n = 4$ ,  $P < 0.05$ ,  $t$  test), but no significant change was detected in either the average delay ( $8.43 \pm 0.54$  vs.  $8.70 \pm 0.86$  ms,  $n = 4$ ,  $t$  test) or the  $1/CV^2$  (baseline-normalized  $0.65 \pm 0.28$ ) ( $n = 4$ ,  $t$  test).

### Comparison of postsynaptic cell firing and network oscillation activity with the plasticity in fast-spiking cells

We studied whether differences in firing rates of the fast-spiking interneurons, or any potential change in underlying LFP activity due to TBS could explain differences observed in the plasticity results. For the analyses, synaptically-evoked spike probability following TBS (post-TBS >15 min) was normalized by baseline in each cell. We found that although the correlation coefficient might indicate a linear relationship between the spontaneous firing level of fast-spiking interneurons and the baseline-normalized plasticity of spike probability ( $r^2 = 0.36$ ,  $n = 7$ , Pearson's test), correlation of the variables was not significant ( $P = 0.15$ ) and cells showing either LTD or LTP had similar spontaneous firing rates (Fig. 6a). In addition, the firing level of fast-spiking cells during the TBS did not correlate with the plasticity generated ( $r^2 = 0.05$ ,  $n = 7$ , Pearson's test). However, mean firing >200 Hz during TBS in one PV+ basket cell was accompanied by LTP, contrary to LTD induction in the other two PV+ basket cells with firing rates <100 Hz during TBS (Fig. 6b). Yet,

dc\_1581\_18



similar firing levels of <100 Hz during TBS observed for the other fast-spiking cells elicited LTP (Fig. 6b). Interestingly, when we compared baseline-normalized plasticity with LFP power ratio of two spectral components (1–3 and 3–6 Hz) measured in 1 s immediately prior to the TBS (see

“Methods”), we found that LTD in the two basket cells and in the two ivy cells was evoked from a predominant 3–6 Hz LFP oscillatory network state without clear 1–3 Hz component (Table 7). On the contrary, LTP was evoked in the basket cell when 1–3 Hz oscillatory component

dc\_15813\_18ng-term plasticity of synaptic excitation in PV+ basket cells. **a** Spontaneous firing and spike properties of a PV+ basket cell. **a1** Top sample traces showing fast-kinetic action potentials of a basket cell (PL190912). The *vertical lines* define spike duration. *Bottom* autocorrelation of spontaneous firing lacks a clear peak. **a2** Spontaneous firing during theta frequency (3–6 Hz) oscillations. *Top* traces show LFP theta oscillations (band-pass filtered 3–6 Hz) and basket cell spikes (band-pass filtered at 0.3–5 kHz). *Bottom* histogram shows firing preference (18° bins) along the descending slope (mean  $\pm$  cSD) of the LFP theta cycle (*black line* sine wave). **b** Partial reconstruction of the dendrites (*red* from four 70  $\mu$ m-thick sections) and axon (*black* from two sections) of a recorded basket cell. Confocal microscopic images show parvalbumin immunopositivity (*red*) in neurobiotin-labeled (NB, *green*) dendrite (*left*, scale 10  $\mu$ m) and boutons (*right*, *thin arrows*, scale 5  $\mu$ m). The boutons were immunonegative for CB1 receptor (*white*, CB1R) evident from neurobiotin-free boutons nearby (*thick arrows*). **c** LTD in an identified basket cell. **c1** Raster plot shows synaptically-evoked spikes (*black dots*) and stimuli with spike failures (*blue dots*). Spontaneous firing shown on *left* (1 min bins). **c2** Synaptically-evoked spikes during baseline and 15–30 min after TBS. *Top* superimposed traces showing spikes at baseline and post-TBS (*scales* 0.2 mV, 5 ms). *Bottom* histograms of spike probability (Pr, %) and delay (latency). Spike probability decreased after TBS ( $P < 0.01$ , Chi square test). **d** Corresponding data from another basket cell showing long-term potentiation of Pr after TBS ( $P < 0.005$ , Chi square test). *Scales* 0.2 mV, 5 ms. **e** Synaptic spike probability in three identified basket cells. **e1–e3** Tested for plasticity and showing either LTD-like decreased Pr or LTP-like increased Pr. Post-TBS time points are compared to baseline (Chi square test). Spontaneous firing level was significantly reduced long-term ( $>15$  min post-TBS) from baseline in cell PL190912 (ANOVA with Bonferroni test)

dominated the LFP 1 s before TBS, and the hippocampus showed both 1–3 and 3–6 Hz LFP oscillatory activity in the 1 s before TBS for the ivy cell (PL170412) with LTP. However, in the two unidentified fast-spiking cells LTP was observed with either 1–3 or 3–6 Hz predominant LFP component, and TBS to the axo-axonic cell that showed no lasting plasticity had predominant 3–6 Hz LFP oscillation before the TBS. Therefore, as a group, the fast-spiking cells did not show correlation between plasticity and LFP oscillatory patterns ( $r^2 = 0.11$ ,  $n = 7$ , Pearson's test) immediately before the TBS (Fig. 6c). Due to the small number of identified cells of the same type, we cannot exclude that the different outcome in individual basket and ivy cells were a result of the difference in oscillatory network states, as reflected in the LFP, at the time of initiating the TBS.

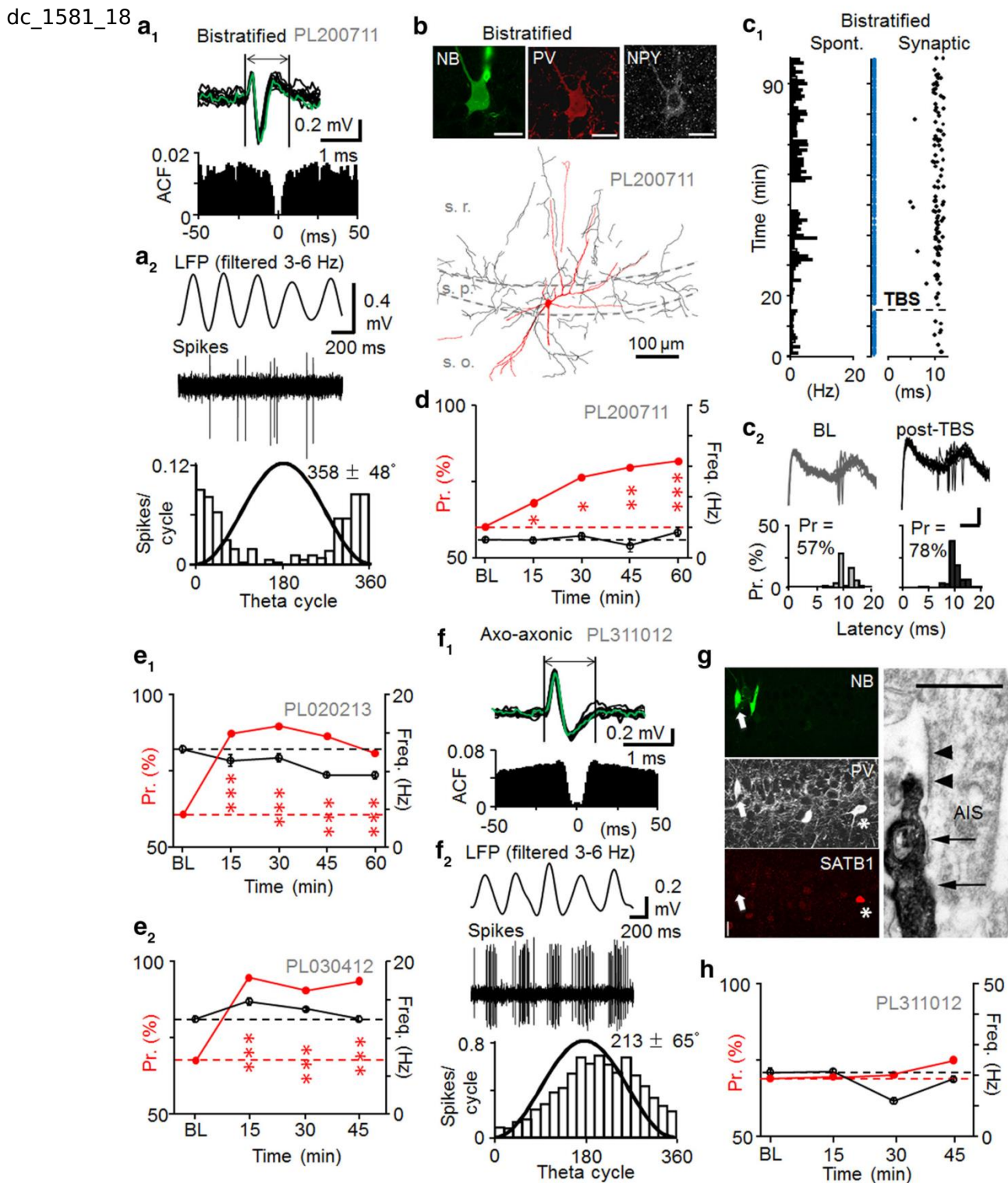
With the exception of the PV+ basket cell recording PL230313, TBS only slightly changed the LFP power ratio of the two spectral components (1–3 and 3–6 Hz) in 1 s following TBS as compared to 1 s prior TBS (Table 7). The results suggest that, on average, the firing levels of the interneurons or the potential change in network excitability evoked by TBS in the experiments were unlikely causes of the potentiation or the depression generated by TBS.

## Discussion

Our experiments demonstrate that extracellular recording with juxtacellular labeling for neuron identification allows a stable and non-invasive approach for measurements of changes in synaptic excitation in hippocampal neurons in vivo. We have shown activity-induced long-term plasticity of evoked spike probability in identified hippocampal interneuron types in the CA1 area. In line with previous reports from ex vivo slice preparations we demonstrated that PV+ basket cells can generate either LTP or LTD following high frequency afferent stimulation (Nissen et al. 2010; Peterfi et al. 2012; Le Roux et al. 2013; Campanac et al. 2013; Camire and Topolnik 2014). However, we found that NOS+ ivy cells in the CA1 area can show either potentiation akin to LTP or LTD-like depression in vivo, which differs from an earlier report using slices, in which only LTP has been reported (Szabo et al. 2012). Interestingly, a dendrite-targeting bistratified cell and one putative but unidentified dendrite-targeting fast-spiking cell showed LTP in vivo. Both LTP and LTD have been reported in dendrite-targeting CA1 PV+ interneurons (Nissen et al. 2010; Oren et al. 2009; Perez et al. 2001). The occasional failure of some PV+ cells to show long-term synaptic plasticity, as seen here in one AAC, has been reported in slices (Nissen et al. 2010). All the three pyramidal cells showed robust LTP as has been demonstrated both in vitro and in vivo. Our results show that distinct CA1 interneuron types exhibit long-term plasticity in vivo and PV+ basket and NOS+ ivy cells can show either LTP or LTD.

A possible explanation to the variable plasticity results in basket cells and ivy cells may be a different activation of receptors and molecular pathways by electrical stimulation. Although CA1 interneurons mostly show NMDAR-independent potentiation and depression of synaptic excitation (Nissen et al. 2010; Campanac et al. 2013; Szabo et al. 2012; Peterfi et al. 2012), PV+ basket cells also exhibit NMDAR-dependent LTP in some of their excitatory afferents (Le Roux et al. 2013). Ketamine, which was used here as a supplementary anesthetic inhibits NMDARs (Harrison and Simmonds 1985), and may have differentially inhibited NMDAR-mediated plasticity in some of the experiments. Hence, different contribution of NMDAR-mediated LTP (Le Roux et al. 2013) might explain some of the variability in the plasticity results observed in the PV+ basket cells in our study.

A second possible explanation of variability is differences in neuromodulator release in the experiments and their effect on interneuron plasticity. Endocannabinoids are powerful modulators of long-term plasticity in glutamatergic synapses onto PV+ neurons in the CA1 area. Experiments in slices have demonstrated that LTD rather



than LTP is induced in these cells when endocannabinoids are released by high-frequency stimulation (Peterfi et al. 2012; Le Roux et al. 2013; Nissen et al. 2010; Campanac et al. 2013). Importantly, activation of endocannabinoid system results in LTD not only in PV+ interneurons, but

also in many non-fast spiking GABAergic neurons (Edwards et al. 2012). It is possible that whether LTP or LTD is generated in NOS+ ivy cells also depends on concomitant endocannabinoid release or is due to the effects of other neuromodulators. This could also explain some

dc\_15814\_18 long-term plasticity in fast-spiking interneurons. A bistratified cell and two unidentified fast-spiking interneurons. **a** Spontaneous firing of a bistratified cell (PL200711). **a1** *Top* fast-kinetic action potentials of the cell. *Bottom* autocorrelation lacks a distinct peak within 50 ms. **a2** Spontaneous firing of the cell during theta frequency (3–6 Hz) oscillations. *Top* band-pass filtered LFP (3–6 Hz) and bistratified cell spikes (band-pass filtered at 0.3–5 kHz). *Bottom* spike occurrence histogram shows firing preference (mean  $\pm$  cSD) at the trough of LFP theta cycle (18° bins; *black line* sine wave). **b** The bistratified cell soma and proximal dendrites are immunopositive for PV (Cy3) and NPY (Cy5) as shown by confocal microscopy (*top*). *Scale* 20  $\mu$ m. *Bottom* reconstructed soma and dendrites (*red*), and axon (*black*) of the cell in one 70  $\mu$ m-thick section. Note distribution of the axon in *strata radiatum* (s.r.) and *oriens* (s.o.). **c** Synaptically evoked spike probability in the bistratified cell showed persistent potentiation after TBS. **c1** Raster plot of synaptically-evoked spikes (*black dots*) before and following TBS (*dotted horizontal line*) in the cell. Spike failures to stimuli are shown in *blue*. Spontaneous firing of the cell shown on the *left* (1 min bins). **c2** Superimposed LFP traces with spikes and histograms show probability (Pr) and delay (latency) in baseline and 45–60 min after the TBS. *Scales* 0.2 mV, 5 ms. **d** Average synaptically-evoked spike probability in the cell at different time points (Chi square test). Spontaneous firing level was altered from baseline at 45 min and 60 min post-TBS time ( $P < 0.05$ , ANOVA with Bonferroni test). **e** Two fast-spiking unidentified interneurons show persistent potentiation of Pr after TBS (Chi square test). **e1** LTP in PL020213 was associated with decreased spontaneous spiking at late post-TBS times (45–60 min,  $P < 0.05$ , ANOVA with Bonferroni test). **e2** The LTP in PL030412 was associated with transiently increased spontaneous firing level at 15 min post-TBS time ( $P < 0.05$ , ANOVA, with Bonferroni test). **f–h** Lack of lasting plasticity of synaptically-evoked spike probability in an identified axo-axonic cell. **f** Spontaneous firing and spike properties of the axo-axonic cell. **f1** *Top* traces show fast-kinetics of the action potential. *Bottom* autocorrelation of spontaneous firing lacks a distinct peak within 50 ms. **f2** Spontaneous firing shows phase preference close to LFP theta cycle peak. *Top* band-pass filtered LFP (3–6 Hz) and axo-axonic cell spikes (band-pass filtered at 0.3–5 kHz). *Bottom* histogram shows the firing phase preference (mean  $\pm$  cSD) during LFP theta (18° bins, *black line* sine wave). **g** Molecular analysis and synaptic targets identify the axo-axonic cell. *Left* the neurobiotin-filled soma (NB, Alexa488, *white arrow*) is immunopositive for PV (Cy3) and immunonegative for the transcription factor SATB1 (Cy3; *asterisk*, nucleus of another PV+ cell). *Scale* 20  $\mu$ m. *Right* electron micrograph of an axon initial segment (AIS) recognized by the membrane undercoating (*arrowheads*). It is innervated (*arrows*) by a neurobiotin-labelled bouton (*left*) of the axo-axonic cell visualized by electron opaque peroxidase reaction end-product. *Scale* 0.5  $\mu$ m. **h** Synaptically-evoked average Pr of the axo-axonic cell in baseline and after TBS (*red*). Spontaneous firing (*black*) transiently suppressed from baseline only at 30 min post-TBS period ( $P < 0.005$ , ANOVA with Bonferroni test)

discrepancies reported in long-term plasticity between *ex vivo* and *in vivo* conditions in these interneuron types; intact brain circuits *in vivo* might provide stronger endocannabinoid release and cannabinoid receptor activation than the conditions in brain slices. Likewise, antidromic activation of fibers innervating hippocampus from extrahippocampal loci could contribute to the plasticity. Activation of acetylcholine receptors has been demonstrated to promote NMDAR-independent LTP in CA1 area interneurons through both nicotinic and muscarinic

receptors (Le Duigou et al. 2015; Griguoli et al. 2013). However, the impact of many other neuromodulatory signaling pathways on interneuron long-term plasticity is unknown. Activation of serotonergic, noradrenergic or dopaminergic fibers antidromically in the hippocampus either by electrical stimulation or occurring naturally in behaving animal have strong acute effects on GABAergic interneuron function (Bohm et al. 2015; Rosen et al. 2015; Maccaferri 2011). Dopaminergic fiber activity facilitates LTP in CA1 pyramidal cells and promotes hippocampal spatial memory persistence (Li et al. 2003; McNamara et al. 2014), but any impact on hippocampal interneuron plasticity remains to be tested.

Thirdly, we also analyzed the potential influence of rhythmic network states at the time of TBS application on plasticity in the interneurons. In general, the presence or absence of 1–3 and 3–6 Hz frequency oscillatory components in the LFP, did not explain whether LTP or LTD was generated in fast-spiking interneurons as a group. However, because of low number of cells the results on LFP oscillatory patterns and the direction of plasticity needs further investigation. We also observed that, on average neither the spontaneous firing rate of the neurons, nor their discharge during TBS correlated with LTP or LTD. We cannot exclude the possibility that in some cases altered excitability during the course of the experiment had an impact on the synaptically-evoked spike probability. For instance, ivy cell PL170412 with LTP showed a prominent increase in spontaneous firing after the TBS which might reflect changes in its excitability. However, in most cells the spontaneous firing level changes were small or moderate and in many cells were of opposite direction than the evoked spike probability.

Finally, it is important to consider if the stimulus-evoked spikes and their plasticity were mediated via a monosynaptic excitatory pathway to the recorded neurons or possibly by polysynaptic activity triggered in the antidromically stimulated CA3 area. We confirmed that stimulation from the contralateral left CA1 area elicited a phase-locked short-delay field EPSP in the CA1 of the right hemisphere (Bliss and Lomo 1973; Buzsaki and Eidelberg 1982b) in all experiments included in this study. In addition, the phase-locked action potentials in the recorded cells to the contralateral stimulation were generated with short delay and small jitter that correspond to signaling through a monosynaptic excitatory pathway (Buzsaki and Eidelberg 1982a, b). Neither the LTP-like spike probability potentiation nor the depression were associated with significant changes in the average spike delay in the reported cells (Maccaferri and McBain 1996; Buzsaki and Eidelberg 1982b), but in cells with LTP, the synaptically evoked spike delay variance decreased in parallel with the increased spike probability (Pouille and Scanziani 2001;

## dc\_1551e\_18 Summary of firing of PV+ interneurons

## Synaptically evoked spike properties and spontaneous firing rate during plasticity experiments

Cell code and type	Probability to the afferent stimulation			Latency to the afferent stimulation (ms) (mean $\pm$ SEM)			Overall spontaneous firing of the cell during the experiment (Hz)		
	Base-line	Post-TBS (0–15 min)	Post-TBS (>15 min)	Baseline	Post-TBS (0–15 min)	Post-TBS (>15 min)	Base-line	Post-TBS (0–15 min)	Post-TBS (>15 min)
PL210213, BC	0.73	0.90***	0.86*	9.05 $\pm$ 0.07	9.22 $\pm$ 0.05	8.79 $\pm$ 0.09	18.0	11.5**	15.2
PL230313, BC	0.52	0.39*	0.35***	9.11 $\pm$ 0.46	9.34 $\pm$ 0.33	8.14 $\pm$ 0.38	15.9	14.3	15.1
PL190912, BC	0.32	0.19**	0.19**	7.04 $\pm$ 0.82	7.00 $\pm$ 0.70	7.36 $\pm$ 0.58	19.8	13.9**	12.9**
PL311012, AAC	0.69	0.70	0.75	12.04 $\pm$ 0.28	11.12 $\pm$ 0.29	11.78 $\pm$ 0.35	21.1	21.2	14.7**
PL200711, Bistr.	0.61	0.69*	0.80***	11.40 $\pm$ 0.16	10.49 $\pm$ 0.12	10.08 $\pm$ 0.15	0.6	0.6	0.5
PL020213, Unid	0.60	0.87***	0.81***	9.38 $\pm$ 0.24	9.45 $\pm$ 0.25	9.19 $\pm$ 0.25	12.8	11.3	9.4*
PL030412, Unid	0.69	0.93***	0.93***	9.94 $\pm$ 0.46	9.95 $\pm$ 0.35	9.89 $\pm$ 0.12	12.7	14.7*	12.7

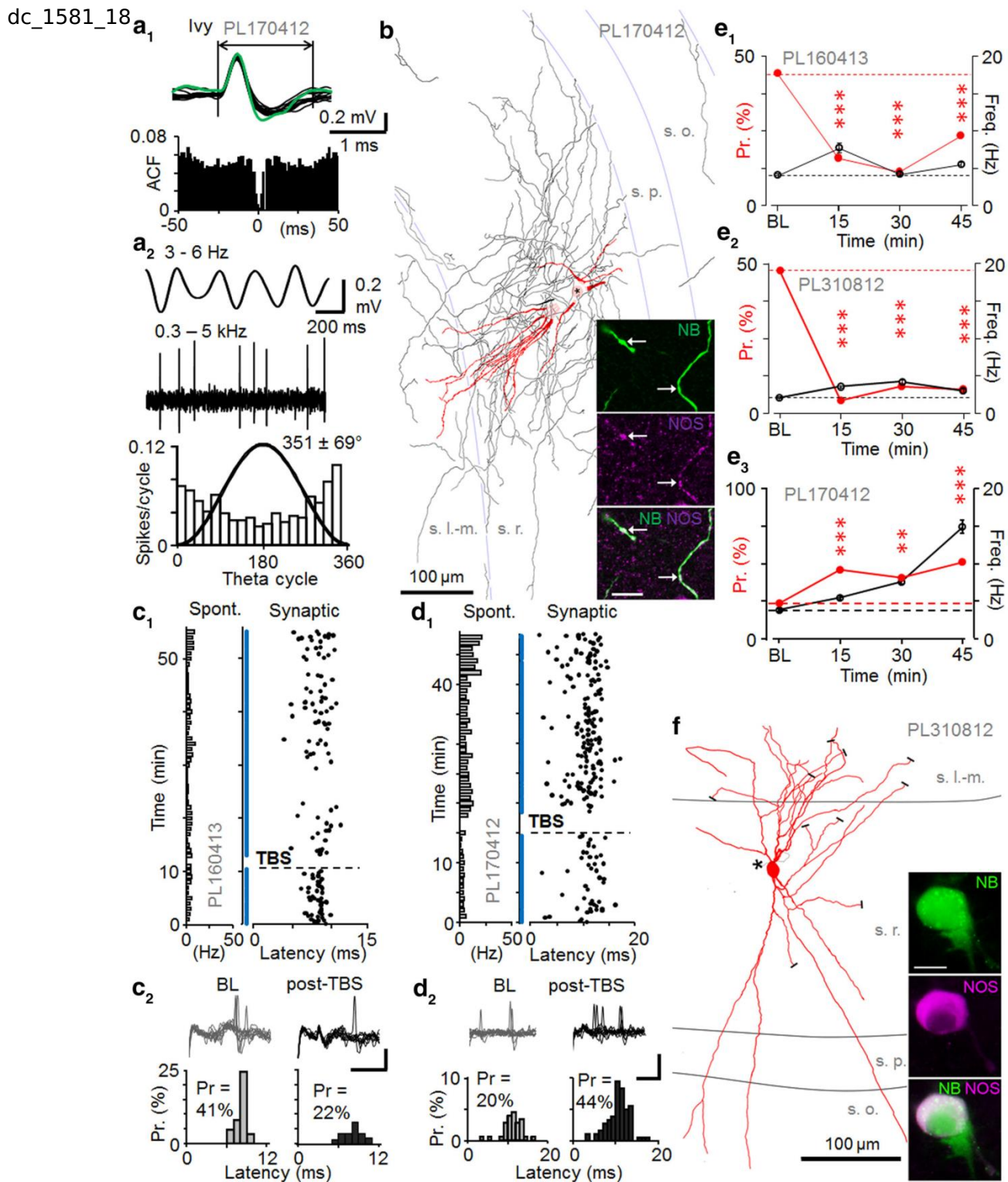
Average probability (Chi square test) and latency (ANOVA with Bonferroni test) of the synaptically evoked spikes are compared during baseline and following TBS (post-TBS). Columns at right show the overall spontaneous firing frequency in the baseline and at early (0–15 min) and late (from 15 min until the end of recording) post-TBS time windows including theta and non-theta periods

\*  $P < 0.05$ , \*\*  $P < 0.01$ , \*\*\*  $P < 0.005$

Lamsa et al. 2005). Although we were unable to directly demonstrate monosynaptic generation of the spikes, which would have required intracellular recordings, the above lines of evidence indicate stimulus-evoked monosynaptic spike generation in these cells.

Although synaptic long-term plasticity provides a valid explanation to the potentiation and depression of the evoked spike probability reported here, other mechanisms may also be involved. High-frequency local stimulation can increase intrinsic excitability of some interneurons (Ross and Soltesz 2001; Campanac et al. 2013). In parallel with synaptic LTP, postsynaptic cell input resistance can increase through decreased K<sup>+</sup> channel-mediated conductance in PV<sup>+</sup> cells (Campanac et al. 2013). Similar increase in input resistance has been reported in dentate gyrus interneurons following local high-frequency stimulation (Ross and Soltesz 2001). Hence, potentiation of the synaptic excitation could be explained at least partly by changes in the postsynaptic cell intrinsic excitability and EPSP-spike coupling. In addition, compensation of synaptic LTD by increased intrinsic excitability may explain the lack of plasticity in the axo-axonic cell observed here. However, it is noteworthy that in hippocampal slice experiments the electrical stimulation is usually applied close to the recording site, and it is unclear to what extent stimulation in the close proximity contributes to the non-synaptic plasticity mechanisms. In our in vivo experiments the stimulation was applied far from the postsynaptic recording site in the contralateral hippocampus. However, we cannot exclude that in addition to synaptic plasticity non-synaptic mechanisms (Campanac et al. 2013) contributed to the spike probability changes reported here.

**Fig. 5** Persistent potentiation or depression of synaptic excitation in NOS<sup>+</sup> ivy cells. **a** Spontaneous firing of an ivy cell (PL170412). **a1** Top superimposed spontaneous (black) and synaptically-evoked (green) spikes in the cell (spike waveform >1.5 ms). Bottom autocorrelogram of spontaneous firing. **a2** Spiking during LFP theta frequency (3–6 Hz) oscillations. Top band-pass filtered LFP (3–6 Hz) and ivy cell spikes (band-pass filtered at 0.3–5 kHz). Bottom spike histogram (18° bins) shows slight firing preference at the LFP trough (black line sine wave). **b** Partial reconstruction of the dendrites (red) and axon (black both from four 70  $\mu$ m-thick sections) of the ivy cell with cell body in stratum radiatum (s.r.). White matter is to the right. Damage to the soma by the labelling resulted in a spillage of neurobiotin, but all the dendrites converged to one site (circle, star). The axon was most dense in s.r. but collaterals were present in all layers. Confocal microscopic images show NOS immunopositive (purple) neurobiotin-labeled (NB, green) dendrites. Scale 10  $\mu$ m. **c–d** Ivy cells with LTD-like depression or LTP-like potentiation of action potential probability. **c** Persistent depression of spike probability by TBS (horizontal line) with no significant change in spike latency. **c1** Stimulation cycles with failures to evoke spike are shown by blue dots. Horizontal bars on left indicate spontaneous firing of the cell (1 min bins). **c2** Synaptically-evoked spikes in baseline and following TBS (30 min). Scales 0.2 mV, 3 ms. Top superimposed traces. Bottom histograms of spike probability (Pr) and delay (latency). Pr decreased from baseline ( $P < 0.005$ , Chi square test). **d** Another ivy cell showing persistent potentiation. **d1** Synaptically-evoked spike probability and delay (black) with failures (blue), and spontaneous firing on the left. **d2** Top traces in baseline and post-TBS. Scales 0.5 mV, 10 ms. Bottom histograms of the evoked spike occurrence. Probability (Pr) increased after TBS ( $P < 0.01$ , Chi square test). **e** Synaptic spike probability (red) at different times in three recorded and identified NOS<sup>+</sup> ivy cells (**e1–e3**). Average spontaneous firing in parallel shown in black. Changes in Pr are compared to baseline (Chi square test). Spontaneous firing level was significantly changed long term from baseline in PL170412 (at 30 and 45 min  $P < 0.005$ , ANOVA with Bonferroni test). **f** Reconstruction of the ivy cell PL310812 with soma in stratum radiatum that showed LTD of spike probability (see **e2**). Dendrites (red) are shown from three 70  $\mu$ m thick sections, cut dendrites indicated with black bars, and asterisk shows the origin of the axon (black). Inset the neurobiotin (NB, green) labelled soma is immunopositive for NOS (purple); a microglial cell attached at lower right took up neurobiotin. Scale 10  $\mu$ m



Spatial learning and memory storage in the hippocampus are associated with dynamic and persistent changes in communication between excitatory pyramidal place cells and their postsynaptic inhibitory interneurons in the CA1 area (Dupret et al. 2013). In a novel environment the

establishment of new place cells is associated with long-lasting changes in their activation of fast-spiking CA1 interneurons. As a consequence, place cells can either increase or decrease their spike coupling to as yet unknown types of interneurons (Dupret et al. 2013). One interpretation

**Table 18** Spontaneous firing properties and spike kinetics of ivy cells

Spontaneous spiking properties					Immunohistochemistry
Cell code, cell type	Firing rate during LFP theta (Hz)	Mean angle phase ( $\pm$ cSD) to LFP theta cycle ( $^{\circ}$ )	Depth of modulation ( $r$ ) during the theta and $n$ of cycles	Spike duration (ms) (mean $\pm$ SEM)	
PL170412, Ivy	4.0	352 $\pm$ 69	0.28, $n = 388$	1.49 $\pm$ 0.02	NOS+
PL310812, Ivy	1.5	34 $\pm$ 66	0.33, $n = 346$	1.88 $\pm$ 0.02	NOS+, proCCK–
PL160413, Ivy	4.5	99 $\pm$ 58	0.48, $n = 2332$	1.54 $\pm$ 0.04	NOS+, PV–, proCCK–

Firing phase preference during LFP theta cycles was calculated from spontaneous activity during theta epochs (cSD means circular standard deviation). All three cells had low spontaneous firing rates. The mean firing phase of two ivy cells was on the early ascending slope of theta cycles and the third ivy cell coupled its spikes to the theta cycle troughs. Action potentials showed slow kinetics ( $\geq 1.5$  ms duration). Immunohistochemical reactions; + positive, – negative

**Table 6** Summary of firing of ivy cells

Synaptically evoked spike properties and spontaneous firing rate during plasticity experiments

Cell code and type	Probability to the afferent stimulation			Latency to the afferent stimulation (ms) (mean $\pm$ SEM)			Overall spontaneous firing of the cell during the experiment (Hz)		
	Base-line	Post-TBS (0–15 min)	Post-TBS (>15 min)	Baseline	Post-TBS (0–15 min)	Post-TBS (>15 min)	Base-line	Post-TBS (0–15 min)	Post-TBS (>15 min)
PL170412, Ivy	0.24	0.47***	0.52***	11.30 $\pm$ 0.47	11.29 $\pm$ 0.28	10.12 $\pm$ 0.47	3.8	5.5	15.0***
PL310812, Ivy	0.48	0.03***	0.06***	9.43 $\pm$ 0.22	9.84 $\pm$ 1.63	11.23 $\pm$ 1.50*	2.2	3.3	3.6*
PL160413, Ivy	0.44	0.16***	0.23***	8.16 $\pm$ 0.13	8.77 $\pm$ 0.53	8.05 $\pm$ 0.31	4.1	7.7	5.5*

Table shows comparisons of the average probability (Chi square test) and latency (ANOVA with Bonferroni test) of the synaptically evoked postsynaptic spikes during baseline and following high-frequency theta-burst stimulation (post-TBS). Columns at right show the overall spontaneous firing frequency in the baseline and at early (0–15 min) and late (from 15 min until the end of recording) post-TBS time

\*  $P < 0.05$ , \*\*\*  $P < 0.005$

**Table 7** Summary of LFP index pre-TBS (1 s) and post-TBS (1 s) and long-term plasticity changes of the recorded neurons

Cell ID	Cell type	Cell code	Pre-TBS	Post-TBS	Outcome
PL120811	PC	PL120811	–0.1	–0.5	LTP
PL240113	PC	PL240113	0.1	–0.3	LTP
PL260313	PC	PL260313	–0.5	–0.7	LTP
PL210213	BC	PL210213	–0.2	–0.5	LTP
PL230313	BC	PL230313	0.2	–0.1	LTD
PL190912	BC	PL190912	0.3	0.3	LTD
PL311012	AAC	PL311012	0.4	0.2	No change
PL200711	Bistratified	PL200711	–0.9	–0.6	LTP
PL020213	Unidentified	PL020213	0.8	0.8	LTP
PL030412	Unidentified	PL030412	–0.6	–0.8	LTP
PL170412	Ivy	PL170412	0.4	0.5	LTP
PL310812	Ivy	PL310812	0.4	0.4	LTD
PL160413	Ivy	PL160413	0.7	0.3	LTD

Wavelet power spectrogram of the LFP was calculated in time windows before and after TBS. Index values of 1 and –1 would represent spectral power components only in the frequency ranges of 3–6 or 1–3 Hz, respectively; 0, represents exactly same average power in both frequency ranges. The average wavelet power across a range of frequencies was determined as the weighted sum of the wavelet power spectrum over the respective frequencies. In the group of fast-spiking cells, TBS only changed the LFP power ratio in one cell (PV+ basket cell recording PL230313)

dc\_1581\_18

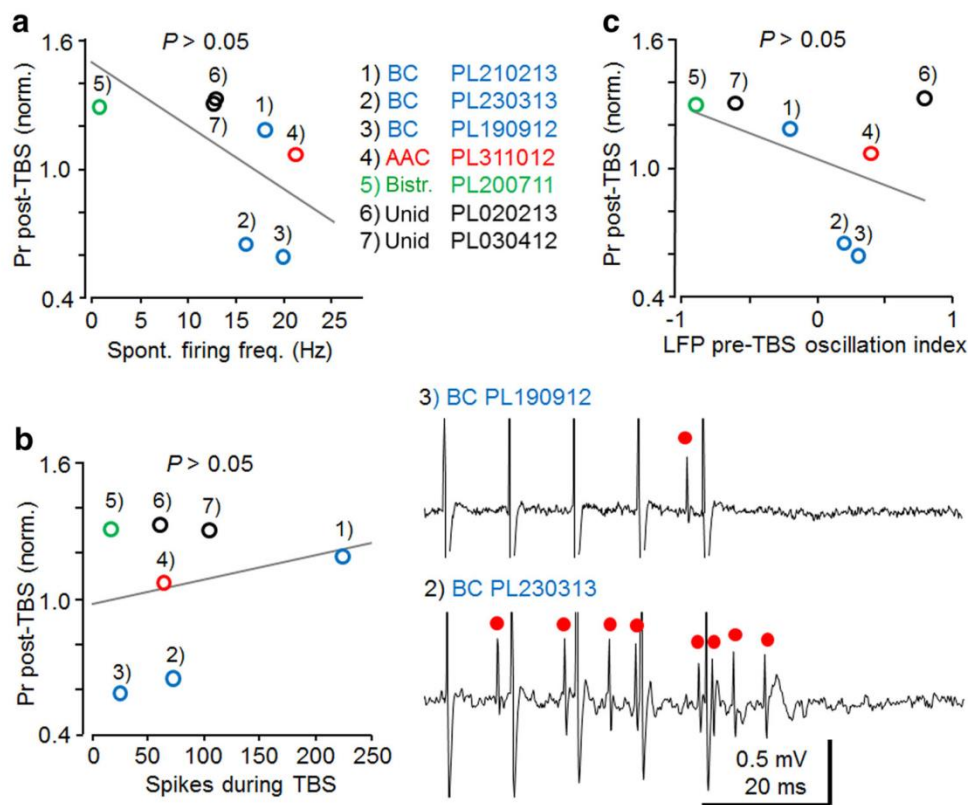


**Fig. 6** The effect of postsynaptic cell firing and hippocampal network oscillatory states on plasticity in fast-spiking interneurons. Individual cells are annotated and cell types shown in different colors as indicated. **a** Spontaneous firing level of the recorded fast-spiking interneurons and baseline-normalized plasticity (>15 min post-TBS) failed to show significant correlation ( $n = 7$ , Pearson's test). The correlation coefficient suggests linear relationship between the variables ( $r^2 = 0.36$ ,  $n = 7$ , Pearson's test), but correlation is not significant ( $P > 0.05$ ). **b** The firing level of the cells during afferent TBS, on average, did not explain whether LTP or LTD was generated in the fast-spiking interneurons. However, note differences in the direction of plasticity for PV+ basket cells with mean rate >200 Hz vs. mean rate <100 Hz. *Left* the plot shows averaged baseline-normalized spike probability (Pr) post-TBS and the number of spikes

generated during TBS ( $r^2 = 0.05$ ). No correlation was found between the factors ( $n = 7$ , Pearson's test). *Right* sample traces (one theta burst of 5 pulses at 100 Hz) in the two LTD-exhibiting PV+ basket cells with very different TBS-associated firing. *Red dots* mark evoked action potentials. **c** Relationship of the LFP index for pre-TBS, based on wavelet power spectrogram (1 s before TBS), and long-term plasticity of evoked spike probability (Pr) in the fast-spiking interneurons. Index values of 1 and -1 represent spectral power components only in the frequency ranges of 3–6 or 1–3 Hz, respectively; 0, represents equal average power in both frequency ranges. As a group, the fast-spiking cells did not show correlation between pre-TBS LFP oscillatory components and the direction of plasticity ( $n = 7$ , Pearson's test) ( $r^2 = 0.19$ )

for these results is that learning-associated neuronal activity generates long-term plasticity between the excitatory place cells and their postsynaptic interneurons in the CA1 area, as demonstrated here *in vivo*. If so, use-dependent LTP and LTD could contribute to learning processes in the hippocampus (Kullmann and Lamsa 2007), and might also be driven by synchronous high-frequency discharges in pathological conditions (Jefferys 2014). In line with results obtained *in vitro* (Kullmann and Lamsa 2011), the form of plasticity may depend on the identity of the interneurons and their synaptic properties. Both PV+ basket cells and NOS+ ivy cells were able to generate potentiation and depression, whereas other cells showed LTP in these conditions (Kullmann and Lamsa 2011).

**Acknowledgments** This study was funded by The Wellcome Trust (K.L.) and Medical Research Council UK (K.L., K.N., P.L., L.K., P. Saghy, P. Somogyi). We acknowledge Norbert Hajos for comments on an earlier version of the manuscript and Peter Magill for help and advice with juxtacellular labeling. We thank Jozsef Somogyi and Ben Micklem for help with confocal microscopy and Mrs Kristina Wagner for help in histological processing, Andrea Papp for the reconstruction of PL230313 (Fig. 3) and Ben Micklem for PL310812 (Fig. 5).

**Open Access** This article is distributed under the terms of the Creative Commons Attribution 4.0 International License (<http://creativecommons.org/licenses/by/4.0/>), which permits unrestricted use, distribution, and reproduction in any medium, provided you give appropriate credit to the original author(s) and the source, provide a link to the Creative Commons license, and indicate if changes were made.

## dc\_1References

- Armstrong C, Krook-Magnuson E, Soltesz I (2012) Neurogliaform and Ivy cells: a major family of nNOS expressing GABAergic neurons. *Front Neural Circ* 6:23
- Bartos M, Alle H, Vida I (2011) Role of microcircuit structure and input integration in hippocampal interneuron recruitment and plasticity. *Neuropharmacology* 60(5):730–739
- Bliss TV, Lomo T (1973) Long-lasting potentiation of synaptic transmission in the dentate area of the anaesthetized rabbit following stimulation of the perforant path. *J Physiol* 232(2):331–356
- Bohm C, Pangalos M, Schmitz D, Winterer J (2015) Serotonin attenuates feedback excitation onto O-LM interneurons. *Cereb Cortex* 25(11):4572–4583
- Brown MT, Henny P, Bolam JP, Magill PJ (2009) Activity of neurochemically heterogeneous dopaminergic neurons in the substantia nigra during spontaneous and driven changes in brain state. *J Neurosci* 29(9):2915–2925
- Buzsaki G, Eidelberg E (1982a) Convergence of associational and commissural pathways on CA1 pyramidal cells of the rat hippocampus. *Brain Res* 237(2):283–295
- Buzsaki G, Eidelberg E (1982b) Direct afferent excitation and long-term potentiation of hippocampal interneurons. *J Neurophysiol* 48(3):597–607
- Camire O, Topolnik L (2014) Dendritic calcium nonlinearities switch the direction of synaptic plasticity in fast-spiking interneurons. *J Neurosci* 34(11):3864–3877
- Campanac E, Gasselín C, Baude A, Rama S, Ankri N, Debanne D (2013) Enhanced intrinsic excitability in basket cells maintains excitatory-inhibitory balance in hippocampal circuits. *Neuron* 77(4):712–722
- Collingridge GL, Peineau S, Howland JG, Wang YT (2010) Long-term depression in the CNS. *Nat Rev Neurosci* 11(7):459–473
- Daoudal G, Debanne D (2003) Long-term plasticity of intrinsic excitability: learning rules and mechanisms. *Learn Mem* 10(6):456–465
- Dupret D, O'Neill J, Csicsvari J (2013) Dynamic reconfiguration of hippocampal interneuron circuits during spatial learning. *Neuron* 78(1):166–180
- Edwards JG, Gibson HE, Jensen T, Nugent F, Walther C, Blickenstaff J, Kauer JA (2012) A novel non-CB1/TRPV1 endocannabinoid-mediated mechanism depresses excitatory synapses on hippocampal CA1 interneurons. *Hippocampus* 22(2):209–221
- Ferraguti F, Klausberger T, Cobden P, Baude A, Roberts JD, Szucs P, Kinoshita A, Shigemoto R, Somogyi P, Dalezios Y (2005) Metabotropic glutamate receptor 8-expressing nerve terminals target subsets of GABAergic neurons in the hippocampus. *J Neurosci* 25(45):10520–10536
- Fuentealba P, Begum R, Capogna M, Jinno S, Marton LF, Csicsvari J, Thomson A, Somogyi P, Klausberger T (2008) Ivy cells: a population of nitric-oxide-producing, slow-spiking GABAergic neurons and their involvement in hippocampal network activity. *Neuron* 57(6):917–929
- Galvan EJ, Calixto E, Barrionuevo G (2008) Bidirectional Hebbian plasticity at hippocampal mossy fiber synapses on CA3 interneurons. *J Neurosci* 28(52):14042–14055
- Galvan EJ, Cosgrove KE, Barrionuevo G (2011) Multiple forms of long-term synaptic plasticity at hippocampal mossy fiber synapses on interneurons. *Neuropharmacology* 60(5):740–747
- Griguoli M, Cellot G, Cherubini E (2013) In hippocampal oriens interneurons anti-Hebbian long-term potentiation requires cholinergic signaling via alpha7 nicotinic acetylcholine receptors. *J Neurosci* 33(3):1044–1049
- Hainmuller T, Kriegstein K, Kulik A, Bartos M (2014) Joint CP-AMPA and group I mGlu receptor activation is required for synaptic plasticity in dentate gyrus fast-spiking interneurons. *Proc Natl Acad Sci USA* 111(36):13211–13216
- Halasy K, Buhl EH, Lorinczi Z, Tamas G, Somogyi P (1996) Synaptic target selectivity and input of GABAergic basket and bistratified interneurons in the CA1 area of the rat hippocampus. *Hippocampus* 6(3):306–329
- Harris KD, Hirase H, Leinekugel X, Henze DA, Buzsaki G (2001) Temporal interaction between single spikes and complex spike bursts in hippocampal pyramidal cells. *Neuron* 32(1):141–149
- Harrison NL, Simmonds MA (1985) Quantitative studies on some antagonists of N-methyl D-aspartate in slices of rat cerebral cortex. *Br J Pharmacol* 84(2):381–391
- Jefferys JG (2014) Are changes in synaptic function that underlie hyperexcitability responsible for seizure activity? *Adv Exp Med Biol* 813:185–194
- Klausberger T, Somogyi P (2008) Neuronal diversity and temporal dynamics: the unity of hippocampal circuit operations. *Science* 321(5885):53–57
- Klausberger T, Magill PJ, Marton LF, Roberts JD, Cobden PM, Buzsaki G, Somogyi P (2003) Brain-state- and cell-type-specific firing of hippocampal interneurons in vivo. *Nature* 421(6925):844–848
- Klausberger T, Marton LF, Baude A, Roberts JD, Magill PJ, Somogyi P (2004) Spike timing of dendrite-targeting bistratified cells during hippocampal network oscillations in vivo. *Nat Neurosci* 7(1):41–47
- Klausberger T, Marton LF, O'Neill J, Huck JH, Dalezios Y, Fuentealba P, Suen WY, Papp E, Kaneko T, Watanabe M, Csicsvari J, Somogyi P (2005) Complementary roles of cholecystokinin- and parvalbumin-expressing GABAergic neurons in hippocampal network oscillations. *J Neurosci* 25(42):9782–9793
- Kullmann DM, Lamsa KP (2007) Long-term synaptic plasticity in hippocampal interneurons. *Nat Rev Neurosci* 8(9):687–699
- Kullmann DM, Lamsa KP (2011) LTP and LTD in cortical GABAergic interneurons: emerging rules and roles. *Neuropharmacology* 60(5):712–719
- Kullmann DM, Moreau AW, Bakiri Y, Nicholson E (2012) Plasticity of inhibition. *Neuron* 75(6):951–962
- Laezza F, Dingledine R (2011) Induction and expression rules of synaptic plasticity in hippocampal interneurons. *Neuropharmacology* 60(5):720–729
- Lamsa K, Heeroma JH, Kullmann DM (2005) Hebbian LTP in feed-forward inhibitory interneurons and the temporal fidelity of input discrimination. *Nat Neurosci* 8(7):916–924
- Lamsa K, Irvine EE, Giese KP, Kullmann DM (2007a) NMDA receptor-dependent long-term potentiation in mouse hippocampal interneurons shows a unique dependence on Ca(2+)/calmodulin-dependent kinases. *J Physiol* 584(Pt 3):885–894
- Lamsa KP, Heeroma JH, Somogyi P, Rusakov DA, Kullmann DM (2007b) Anti-Hebbian long-term potentiation in the hippocampal feedback inhibitory circuit. *Science* 315(5816):1262–1266
- Le Duigou C, Kullmann DM (2011) Group I mGluR agonist-evoked long-term potentiation in hippocampal oriens interneurons. *J Neurosci* 31(15):5777–5781
- Le Duigou C, Savary E, Kullmann DM, Miles R (2015) Induction of anti-Hebbian LTP in CA1 stratum oriens interneurons: interactions between group I metabotropic glutamate receptors and M1 muscarinic receptors. *J Neurosci* 35(40):13542–13554
- Le Roux N, Cabezas C, Bohm UL, Poncer JC (2013) Input-specific learning rules at excitatory synapses onto hippocampal parvalbumin-expressing interneurons. *J Physiol* 591(Pt 7):1809–1822
- Li S, Cullen WK, Anwyl R, Rowan MJ (2003) Dopamine-dependent facilitation of LTP induction in hippocampal CA1 by exposure to spatial novelty. *Nat Neurosci* 6(5):526–531

- dc\_158118 Spruston N (2005) Postsynaptic depolarization requirements for LTP and LTD: a critique of spike timing-dependent plasticity. *Nat Neurosci* 8(7):839–841
- Luscher C, Nicoll RA, Malenka RC, Muller D (2000) Synaptic plasticity and dynamic modulation of the postsynaptic membrane. *Nat Neurosci* 3(6):545–550
- Maccaferri G (2011) Modulation of hippocampal stratum lacunosum-moleculare microcircuits. *J Physiol* 589(Pt 8):1885–1891
- Maccaferri G, McBain CJ (1996) Long-term potentiation in distinct subtypes of hippocampal nonpyramidal neurons. *The Journal of Neuroscience* 16(17):5334–5343
- McBain CJ (2008) Differential mechanisms of transmission and plasticity at mossy fiber synapses. *Prog Brain Res* 169:225–240
- McNamara CG, Tejero-Cantero A, Trouche S, Campo-Urriza N, Dupret D (2014) Dopaminergic neurons promote hippocampal reactivation and spatial memory persistence. *Nat Neurosci* 17(12):1658–1660
- Morris RG (2013) NMDA receptors and memory encoding. *Neuropharmacology* 74:32–40
- Nicholson E, Kullmann DM (2014) Long-term potentiation in hippocampal oriens interneurons: postsynaptic induction, presynaptic expression and evaluation of candidate retrograde factors. *Philos Trans R Soc Lond B Biol Sci* 369(1633):20130133
- Nissen W, Szabo A, Somogyi J, Somogyi P, Lamsa KP (2010) Cell type-specific long-term plasticity at glutamatergic synapses onto hippocampal interneurons expressing either parvalbumin or CB1 cannabinoid receptor. *J Neurosci* 30(4):1337–1347
- Oren I, Nissen W, Kullmann DM, Somogyi P, Lamsa KP (2009) Role of ionotropic glutamate receptors in long-term potentiation in rat hippocampal CA1 oriens-lacunosum moleculare interneurons. *J Neurosci* 29(4):939–950
- Pelkey KA, Topolnik L, Yuan XQ, Lacaille JC, McBain CJ (2008) State-dependent cAMP sensitivity of presynaptic function underlies metaplasticity in a hippocampal feedforward inhibitory circuit. *Neuron* 60(6):980–987
- Perez Y, Morin F, Lacaille JC (2001) A hebbian form of long-term potentiation dependent on mGluR1a in hippocampal inhibitory interneurons. *Proc Natl Acad Sci USA* 98(16):9401–9406
- Peterfi Z, Urban GM, Papp OI, Nemeth B, Monyer H, Szabo G, Erdelyi F, Mackie K, Freund TF, Hajos N, Katona I (2012) Endocannabinoid-mediated long-term depression of afferent excitatory synapses in hippocampal pyramidal cells and GABAergic interneurons. *J Neurosci* 32(41):14448–14463
- Pouille F, Scanziani M (2001) Enforcement of temporal fidelity in pyramidal cells by somatic feed-forward inhibition. *Science* 293(5532):1159–1163
- Pyapali GK, Sik A, Penttonen M, Buzsaki G, Turner DA (1998) Dendritic properties of hippocampal CA1 pyramidal neurons in the rat: intracellular staining in vivo and in vitro. *J Comp Neurol* 391(3):335–352
- Rosen ZB, Cheung S, Siegelbaum SA (2015) Midbrain dopamine neurons bidirectionally regulate CA3-CA1 synaptic drive. *Nat Neurosci* 18(12):1763–1771
- Ross ST, Soltesz I (2001) Long-term plasticity in interneurons of the dentate gyrus. *Proc Natl Acad Sci USA* 98(15):8874–8879
- Somogyi P, Klausberger T (2005) Defined types of cortical interneurone structure space and spike timing in the hippocampus. *J Physiol* 562(Pt 1):9–26
- Somogyi J, Szabo A, Somogyi P, Lamsa K (2012) Molecular analysis of ivy cells of the hippocampal CA1 stratum radiatum using spectral identification of immunofluorophores. *Front Neural Circ* 6:35
- Szabo A, Somogyi J, Cauli B, Lambollez B, Somogyi P, Lamsa KP (2012) Calcium-permeable AMPA receptors provide a common mechanism for LTP in glutamatergic synapses of distinct hippocampal interneuron types. *J Neurosci* 32(19):6511–6516
- Topolnik L (2012) Dendritic calcium mechanisms and long-term potentiation in cortical inhibitory interneurons. *The European journal of neuroscience* 35(4):496–506
- Topolnik L, Azzi M, Morin F, Kougioumoutzakis A, Lacaille JC (2006) mGluR1/5 subtype-specific calcium signalling and induction of long-term potentiation in rat hippocampal oriens/alveus interneurons. *J Physiol* 575(Pt 1):115–131
- Tukker JJ, Fuentealba P, Hartwich K, Somogyi P, Klausberger T (2007) Cell type-specific tuning of hippocampal interneuron firing during gamma oscillations in vivo. *J Neurosci* 27(31):8184–8189
- Unal G, Joshi A, Viney TJ, Kis V, Somogyi P (2015) Synaptic targets of medial septal projections in the hippocampus and extrahippocampal cortices of the mouse. *J Neurosci* 35(48):15812–15826
- Vandecasteele M, Varga V, Berenyi A, Papp E, Bartho P, Venance L, Freund TF, Buzsaki G (2014) Optogenetic activation of septal cholinergic neurons suppresses sharp wave ripples and enhances theta oscillations in the hippocampus. *Proc Natl Acad Sci USA* 111(37):13535–13540
- Viney TJ, Lasztozci B, Katona L, Crump MG, Tukker JJ, Klausberger T, Somogyi P (2013) Network state-dependent inhibition of identified hippocampal CA3 axo-axonic cells in vivo. *Nat Neurosci* 16(12):1802–1811

**V**

## RESEARCH ARTICLE

# Plasticity in Single Axon Glutamatergic Connection to GABAergic Interneurons Regulates Complex Events in the Human Neocortex

Viktor Szegedi<sup>1</sup>, Melinda Paizs<sup>1</sup>, Eszter Csakvari<sup>1</sup>, Gabor Molnar<sup>2</sup>, Pal Barzo<sup>3</sup>, Gabor Tamas<sup>2</sup>, Karri Lamsa<sup>1,4\*</sup>

**1** MTA-NAP Research Group for Inhibitory Interneurons and Plasticity, Department of Physiology, Anatomy and Neuroscience, University of Szeged, Szeged, Hungary, **2** MTA-SZTE Research Group for Cortical Microcircuits, Department of Physiology, Anatomy and Neuroscience, University of Szeged, Szeged, Hungary, **3** Department of Neurosurgery, University of Szeged, Szeged, Hungary, **4** Department of Pharmacology, Oxford University, Oxford, United Kingdom

\* [klamsa@bio.u-szeged.hu](mailto:klamsa@bio.u-szeged.hu)



## OPEN ACCESS

**Citation:** Szegedi V, Paizs M, Csakvari E, Molnar G, Barzo P, Tamas G, et al. (2016) Plasticity in Single Axon Glutamatergic Connection to GABAergic Interneurons Regulates Complex Events in the Human Neocortex. *PLoS Biol* 14(11): e2000237. doi:10.1371/journal.pbio.2000237

**Academic Editor:** Alberto Bacci, ICM - Institut du Cerveau et de la Moelle épinière, France

**Received:** June 17, 2016

**Accepted:** October 12, 2016

**Published:** November 9, 2016

**Copyright:** © 2016 Szegedi et al. This is an open access article distributed under the terms of the [Creative Commons Attribution License](https://creativecommons.org/licenses/by/4.0/), which permits unrestricted use, distribution, and reproduction in any medium, provided the original author and source are credited.

**Data Availability Statement:** All relevant data are within the paper and its Supporting Information files.

**Funding:** Medical Research council UK. Received by KL (MRC Anatomical Neuropharmacology Unit Senior Scientist). The funder had no role in study design, data collection and analysis, decision to publish, or preparation of the manuscript. ERC INTERIMPACT project (ERC-2010-AdG). Received by GT. The funder had no role in study design, data collection and analysis, decision to publish, or preparation of the manuscript. National Brain Research (Nemzeti Agykutatási) program agykutatás.

## Abstract

In the human neocortex, single excitatory pyramidal cells can elicit very large glutamatergic EPSPs (VLEs) in inhibitory GABAergic interneurons capable of triggering their firing with short (3–5 ms) delay. Similar strong excitatory connections between two individual neurons have not been found in nonhuman cortices, suggesting that these synapses are specific to human interneurons. The VLEs are crucial for generating neocortical complex events, observed as single pyramidal cell spike-evoked discharge of cell assemblies in the frontal and temporal cortices. However, long-term plasticity of the VLE connections and how the plasticity modulates neocortical complex events has not been studied. Using triple and dual whole-cell recordings from synaptically connected human neocortical layers 2–3 neurons, we show that VLEs in fast-spiking GABAergic interneurons exhibit robust activity-induced long-term depression (LTD). The LTD by single pyramidal cell 40 Hz spike bursts is specific to connections with VLEs, requires group I metabotropic glutamate receptors, and has a presynaptic mechanism. The LTD of VLE connections alters suprathreshold activation of interneurons in the complex events suppressing the discharge of fast-spiking GABAergic cells. The VLEs triggering the complex events may contribute to cognitive processes in the human neocortex, and their long-term plasticity can alter the discharging cortical cell assemblies by learning.

## Author Summary

Many microscale features in the human neocortex—a part of the brain involved in higher functions such as sensory perception, generation of motor commands, spatial reasoning, and language—are closely similar to those reported in experimental animals commonly

dc\_1581\_18

com. Received by KL (KTIA\_NAP\_13-2-2015-0005), GM (KTIA\_13\_NAP-A-I/16) and GT. The funder had no role in study design, data collection and analysis, decision to publish, or preparation of the manuscript. Hungarian Academy of Sciences, the Hungarian National Office for Research and Technology (GINOP-2.3.2-15-2016-00018), the National Research Development and Innovation Office of Hungary (VKSZ-14-1-2015-0155). Received by GT. The funder had no role in study design, data collection and analysis, decision to publish, or preparation of the manuscript.

**Competing Interests:** The authors have declared that no competing interests exist.

**Abbreviations:** AP, action potential; CV, coefficient of variation; dIPSC, disynaptic GABA<sub>A</sub>R-mediated inhibitory current; DL-APV, DL-2-Amino-5-phosphonopentanoic acid; EPSC, excitatory postsynaptic current; EPSP, excitatory postsynaptic potential; FSIN, fast-spiking GABAergic interneuron; LTD, long-term depression; mGluR, metabotropic glutamate receptor; monIPSC, monosynaptic GABA<sub>A</sub>R-mediated inhibitory current; MPEP, 2-Methyl-6-(phenylethynyl)pyridine hydrochloride; NMDAR, *N*-methyl-D-aspartate receptor; non-FSIN, non-fast-spiking GABAergic interneuron; IPSC, inhibitory postsynaptic current; PC, pyramidal cell; PPR, paired-pulse ratio; pv, parvalbumin; SD, standard deviation; s.e.m., standard error of the mean; sst, somatostatin; SW, spike inward current width; vgat, vesicular GABA transporter; VLE, very large glutamatergic EPSP.

used in neuroscience, like mice. However, the human neocortical neurons also exhibit specializations only reported in our species. One such feature is the capacity of excitatory principal cells to elicit firing in local inhibitory interneurons with a single action potential via very strong excitatory synapses. It has been suggested that this feature has specifically evolved to enhance coordinated firing of neuronal ensembles in higher brain functions. However, it is unknown how these circuits are modified by learning. Therefore, we investigated how these very strong excitatory synapses are changed, and if their impact on the firing of local inhibitory neurons is altered by repetitive action potentials mimicking learning-related activity. By recording in human neocortical slices, we report that the strong excitatory synapses on interneurons exhibit robust activity-dependent long-term plasticity. The plasticity also regulates the discharge of local interneurons driven by these synapses. Although these specialized synapses have only been reported in the human neocortex, their plasticity mechanism is evolutionarily conserved. We suggest that the strong synapses with robust plasticity have evolved to enhance complex brain functions and learning.

## Introduction

Evolution has shaped the human neocortex producing microcircuit features that are specific to our species [1]. Neuronal density, ultrastructural features, and functional properties of neurons [2–4] reflect specific adaptations in the human neocortex to perform complex and fast signal processing [5–13]. A remarkable feature in the human neocortex is that single pyramidal cell (PC) action potentials (APs) are able to generate di- and polysynaptic GABAergic interneuron discharge known as complex events [10,11]. The events emerge from the activity of a small subset of excitatory connections forming very large glutamatergic excitatory postsynaptic potentials (VLEs), specifically to GABAergic interneurons in supragranular layers of the frontal, the temporal, and the prefrontal cortices [10,11]. Similar strong excitatory connections between individual neocortical neurons have not been found in nonhuman brains. Therefore, it has been proposed that the VLEs and the complex events participate in cortical information encoding in high order cognitive processes [10]. However, this would predict that these events are dynamically modulated by learning [14,15]. Yet, it is unknown whether the VLEs show use-dependent long-term plasticity, and if their specific modulation indeed affects the complex events. We hypothesize that the immense strength of VLEs is generated and regulated by common activity-driven synaptic long-term plasticity processes, and that they may occur in various different inhibitory interneuron types [16,17]. Alternatively, these connections could be hard-wired selectively in a specific, yet unknown, subset of postsynaptic GABAergic interneurons without prominent lasting plasticity in the adult neocortex [18,19].

We asked whether VLEs show activity-induced long-term plasticity, and if their selective modulation had impact on the local complex events. By performing triple and dual whole-cell recordings of synaptically connected identified neurons, we found that VLEs exhibit metabotropic glutamate receptor (mGluR)-dependent long-term depression (LTD) that converts them to common weak excitatory postsynaptic potential (EPSP) connections. In addition, this alters the neocortical complex events suppressing the cell assemblies activated by the PC. Thus, the VLEs occur in various interneuron types, and their occurrence is regulated by the synapse's activity history. To the best of our knowledge, this is the first study reporting synaptic plasticity in human neocortical interneurons.

## Results

### VLEs Occur in GABAergic Interneurons

By performing triple and dual whole-cell recordings from identified L2–3 human neocortical neurons, we found that some fast-spiking GABAergic interneurons (FSINs) receive glutamatergic input from individual afferent PCs showing VLEs (Fig 1A and 1B). Simultaneous recording from three neurons demonstrated that a fast-spiking GABAergic cell can receive VLEs (average amplitude  $9.60 \pm 0.20$  mV, showing no failures) from one L2–3 PC and small amplitude glutamatergic EPSPs (average  $3.29 \pm 0.12$  mV, showing no failures) similar to EPSPs between PCs from another PC [10]. Recordings from 21 synaptically connected PC–FSIN pairs revealed vast differences in the single AP-evoked EPSP amplitudes between the pairs (Fig 1B, S1 Table, S1 Data). In FSINs, the EPSP averages showed a range from 0.62 mV to 16.49 mV,

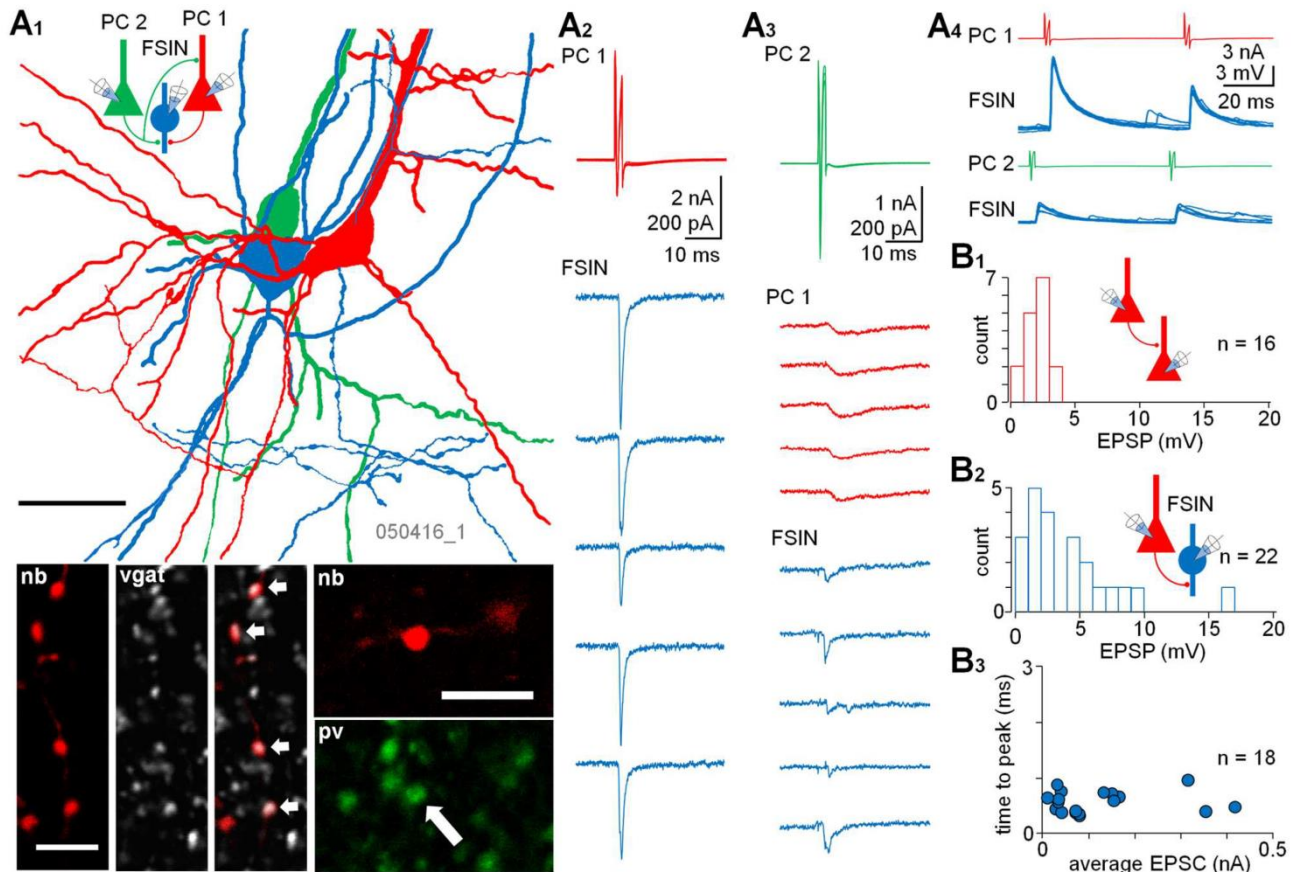


**Fig 1. A subset of human neocortical PCs innervate FSINs with VLEs.** (A) Triple whole-cell recording demonstrating the rich glutamatergic connectivity in the human neocortex layers 2–3 (L2–3). Two PCs (PC1 red and PC2 green) in L2–3 synaptically excite the same FSIN (blue). (A1) Partial reconstruction of the cells with color-coding presented in the schematic inset. Scale 25  $\mu$ m. Confocal images illustrate positive immunoreactions of the neurobiotin (nb, Cy3)-filled interneuron axon boutons for vgat (Cy5, arrows in merged image) and pv (Alexa488, arrow). Scales 5  $\mu$ m. (A2–3) Sample traces show presynaptic spikes (superimposed) and postsynaptic currents in the synaptic connections (cells voltage clamped at  $-60$  mV). PC1 generates large monosynaptic EPSC in the interneuron (A2), whereas PC2 evokes small EPSC in the same cell (A3). In addition, PC2 is synaptically connected to PC1. The EPSCs from the PCs show fast kinetics in the interneuron, whereas EPSC in the PC–PC connection is slow. (A4) The two glutamatergic inputs to the FSIN show very different amplitude EPSPs and distinct paired-pulse ratios in current clamp (at  $E_m - 69$  mV). (B) Histograms show the distribution of average EPSP amplitude (1 mV bin, failures excluded) in 16 identified L2–3 PC–PC pairs (B1) and in 22 PC–FSIN pairs (B2). (B3) The very large and the small amplitude EPSCs from PCs to FSINs show similarly fast time-to-peak time. Values are average EPSCs (of at least five) from individual pairs. The underlying data are shown in S1 Data.

doi:10.1371/journal.pbio.2000237.g001

with nonparametric distribution (failures excluded, evoked with 10 s interval at  $E_m -68.5 \pm 1.4$  mV,  $n = 21$ , Shapiro-Wilk test). Despite the amplitude difference, the excitatory postsynaptic currents (EPSCs) in FSINs similarly exhibited fast time-to-peak kinetics ( $0.59 \pm 0.04$  ms,  $n = 18$ ) (Fig 1B, S1 Data), indicating that the amplitude variability is unlikely to derive from different electrotonic filtering of the glutamatergic synaptic inputs. Likewise, distribution of the average EPSP amplitudes in PCs to non-fast-spiking interneuron (non-FSIN) pairs showed nonparametric distribution with a range from 0.7 mV to 6.9 mV (failures excluded, at  $E_m -70.3 \pm 1.5$  mV,  $n = 9$ , Shapiro-Wilk test) (S1 Table). Thus, VLEs are not occurring solely in FSINs, but are exhibited in various types of GABAergic neurons including fast- and non-fast-spiking cells. On the contrary, PC-PC connections showed parametric distribution of average EPSPs with small amplitude ( $2.01 \pm 0.02$  mV at  $E_m -69.4 \pm 1.8$  mV, failures excluded, Shapiro-Wilk test,  $n = 16$ ) (Fig 1B, S1 Table, S1 Data). The interneuron EPSPs were defined as VLEs when their average (failures excluded) was larger than mean + 2 x standard deviation (SD) of the EPSPs in PC-PC connections (4.21 mV, failures excluded) in baseline conditions (mean  $\pm$  SD =  $2.01 \pm 1.10$  mV,  $n = 480$  in 16 cells). The postsynaptic interneurons in the triple and paired recordings were immunohistochemically confirmed positive for vesicular GABA transporter (vgat+) ( $n = 31$ ). Cells that in addition were immunopositive for parvalbumin (pv+) showed rapid axon currents (spike inward current width [SW] of  $0.43 \pm 0.02$  ms,  $n = 11$ ) characteristic of the FSINs [10,11]. The pv+ cells, together with vgat+ interneurons showing similar fast spike kinetics (SW  $0.49 \pm 0.02$  ms,  $n = 11$ ), but with nonconclusive or untested pv reaction, were considered FSINs ( $n = 22$ ). Ten FSINs were further identified as putative basket cells by their axon morphology [10]. The non-fast-spiking vgat+ interneurons and the PCs had significantly longer spike kinetics with SW of  $0.96 \pm 0.04$  ms ( $n = 9$ ) and  $1.18 \pm 0.06$  ms ( $n = 16$ ), respectively ( $p < 0.01$  between all groups, ANOVA with Tukey's posthoc test) [13]. The non-FSINs with intact soma were immunohistochemically tested for somatostatin (sst) for further identification of the cells [20]. Detailed results on the EPSPs excluding and including failures, the EPSCs, and the immunohistochemical reaction analyses with cell type identification are shown in S1 Table. In all potential connections tested between neurons ( $n = 1,056$ ), we found (including connections lost during baseline) a monosynaptic response in 11.0% of cases. Success rate for identified PC-FSIN pairs was 4.0%, PC-non-FSINs connections: 1.9%, PC-PC pairs: 1.1%, and FSIN-PC connections: 3.8%, showing similar or slightly lower connectivity rates than reported in the rodent neocortex L2-3 [21-23].

## VLEs in FSINs Are Subject to Group I mGluR-Dependent LTD

We asked whether glutamatergic connections to interneurons showed long-term plasticity akin to that reported in the rodent cortex [24,25]. To test this, we performed experiments applying high frequency bursts of APs (5 APs at 40 Hz, x 40 with 0.5 s interval) in the presynaptic PC after a baseline of EPSPs (at least 5 min, but less than 10 min, analyzed including failures) [26,27]. Postsynaptic FSINs (SW  $0.40 \pm 0.02$  ms) were held in resting membrane potential in current clamp ( $-67.6 \pm 2.2$  mV,  $n = 9$ ) (Fig 2). First, we tested VLEs (average in baseline  $5.85 \pm 0.59$  mV, did not show failures,  $n = 5$ ) in control conditions and found that the afferent PC bursts firing generated an LTD of the EPSPs (amplitude to  $0.52 \pm 0.02$  of baseline at 20-25 min after 40 Hz bursts,  $n = 5$  cells,  $p < 0.01$ , Wilcoxon test) (Fig 2A, S1 Fig, S2 Data, S7 Data). The LTD was associated with a reduced paired-pulse EPSP ratio (1<sup>st</sup>/2<sup>nd</sup> EPSP amplitude with 50 ms interval) to  $0.74 \pm 0.06$  of baseline ( $p < 0.05$ , Mann-Whitney test, baseline mean  $1.41 \pm 0.22$ ) and a decrease in the EPSP amplitude  $CV^{-2}$  (1/squared coefficient of variation) value (to  $0.44 \pm 0.12\%$  from baseline,  $p < 0.05$ , Mann-Whitney test) (S3 Data), indicating presynaptic site of depression [28]. The results on the paired-pulse ratio (PPR) and altered EPSP

dc\_1581\_18

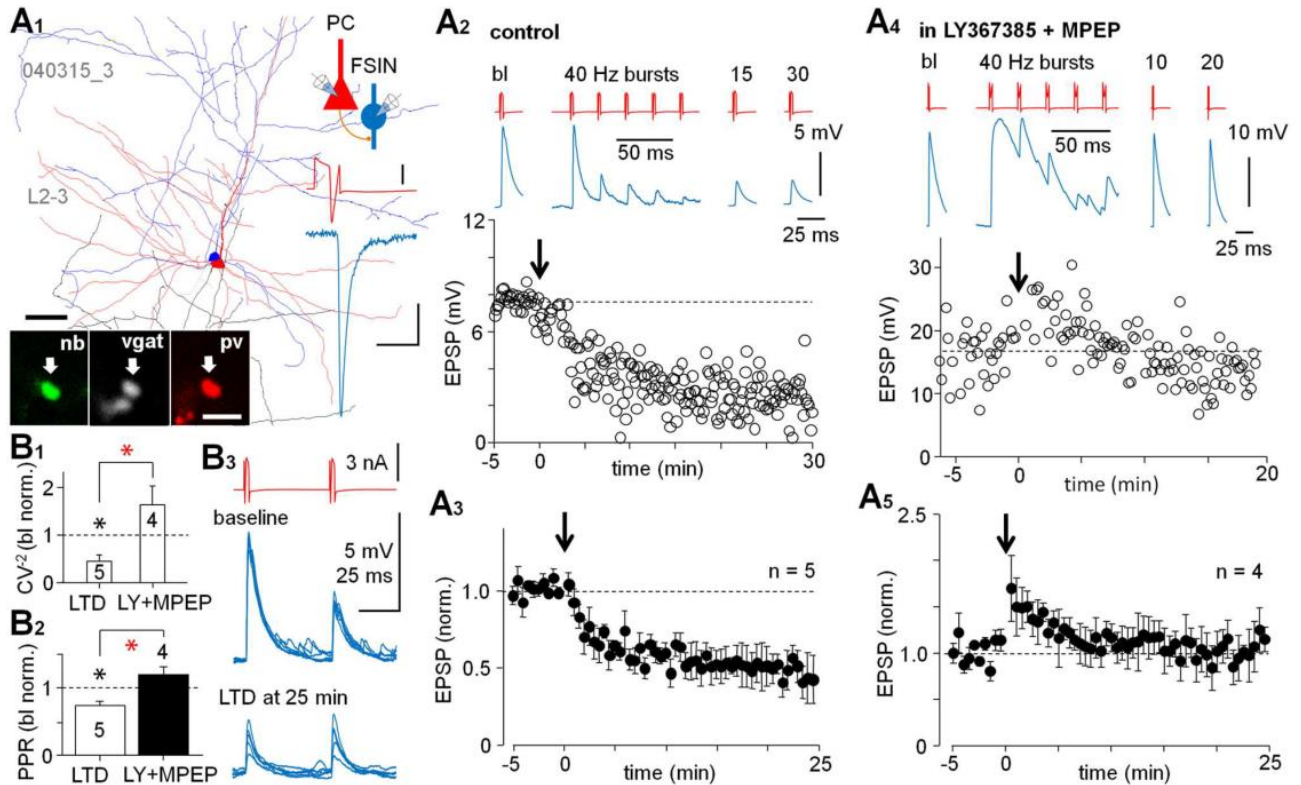


**Fig 2. Single fiber connections to FSINs with large EPSP show group I mGluR-dependent LTD.** (A) Paired recordings from synaptically connected layer 2–3 PCs and FSINs with large amplitude EPSCs/EPSPs show LTD. The LTD is generated by the presynaptic PC firing 40 Hz bursts (5 pulses, 40 times), while the postsynaptic cell is at Em. (A1) Partial reconstruction of one recorded PC (red, axon orange)–FSIN (blue, axon light blue) pair with large EPSCs/EPSPs. Scale 50  $\mu$ m. L2–3 indicates layer 2–3. Schematic shows experimental design and color-coding for the cells and traces. Confocal micrographs illustrate vgat+ and pv+ axon bouton of the FSIN filled with neurobiotin (nb, scale 2  $\mu$ m). A PC spike and averaged EPSC (5 at  $-60$  mV) in the cell pair below. Scales 1 nA and 100 pA/5 ms. (A2) Single AP-evoked EPSP amplitude (interval 10 s) in the same experiment at baseline and following the PC 40 Hz burst firing (arrow at 0 time point). The afferent single fiber burst firing induced LTD (at 20–25 min  $p < 0.001$ , paired  $t$ -test). The EPSPs (blue, average of 5 at Em  $-62$  mV) and presynaptic cell spikes (red) at different time points and one 40 Hz burst illustrated on top. The FSIN is at Em during the recording. (A3) Mean  $\pm$  standard error of the mean (s.e.m.) in five PC–FSIN pairs with large EPSP ( $5.85 \pm 0.59$  mV at baseline, showing no failures) show prominent LTD (30 s bin, baseline-normalized,  $n = 5$  pairs,  $p < 0.01$ , Wilcoxon test). (A4) The LTD requires group I mGluRs. A PC–FSIN pair with large EPSP in the presence of group I mGluR blockers LY367385 (100  $\mu$ M) and 2-Methyl-6-(phenylethynyl)pyridine hydrochloride (MPEP, 25  $\mu$ M) (applied 5 min before the bursts indicated by arrow). The EPSPs (blue, at Em  $-67$  mV) and presynaptic cell spikes (red) shown on top. The FSIN is at Em during recording. (A5) Mean  $\pm$  s.e.m. of similar PC–FSIN pairs with large EPSPs ( $8.42 \pm 2.83$  mV in baseline, showing no failures) in four experiments (30 s bin, baseline-normalized). The underlying data are shown in [S2 Data](#). (B) EPSP analyses indicate presynaptic LTD. (B1) LTD ( $n = 5$ ) is associated with an increased ratio of the EPSP amplitude SD/mean illustrated here as decreased baseline-normalized  $CV^{-2}$  (mean  $\pm$  s.e.m. black asterisk,  $p < 0.05$ , Mann-Whitney test). Red asterisk compared with the non-LTD experiments ( $n = 4$ ) ( $p < 0.05$ , Mann-Whitney test). (B2) Likewise, the EPSP amplitude PPR (1<sup>st</sup> versus 2<sup>nd</sup> EPSP) is reduced in the LTD experiments (black asterisk,  $p < 0.05$ , Mann-Whitney test), but not in the presence of group I mGluR blockers. Red asterisk indicates significance between the groups ( $p < 0.05$ , Mann-Whitney test). Baseline-normalized time window is 20–25 min after afferent bursts. The data are available in [S3 Data](#). (B3) Sample traces from one experiment above showing the PC firing (paired-pulse 50 ms)-evoked EPSPs in the FSIN during baseline and in LTD.

doi:10.1371/journal.pbio.2000237.g002

amplitude variation by LTD are summarized in histograms in [Fig 2B](#). Likewise, corresponding experiments in occasional PC–non-FSIN pairs with VLEs ( $n = 2$ , averages in the baseline including failures 5.81 mV and 6.89 mV, failure rates 0% and 13%, respectively) showed that single fiber burst firing can also generate LTD in some non-FSINs ([S2 Fig](#)).

We next tested whether LTD in VLEs requires group I mGluRs as various forms of long-term plasticity in glutamatergic synapses to FSINs depend on these receptors in the rodent cortex [[24,29–32](#)]. We studied four PC–FSIN pairs with VLEs (average in baseline  $8.42 \pm 2.83$  mV

at  $E_m -69.5 \pm 2.1$  mV, did not show failures,  $n = 4$ ) as above, but in the presence of LY367385 (100  $\mu$ M) and 2-Methyl-6-(phenylethynyl)pyridine hydrochloride (MPEP, 25  $\mu$ M). Thus, LTD was blocked in the VLE connections (Fig 2A) with no significant change in the amplitude ( $1.03 \pm 0.04$  of baseline at 20–25 min,  $n = 4$  cells, Wilcoxon test), PPR ( $1.21 \pm 0.11$  of baseline, baseline mean  $1.07 \pm 0.17$ ) or  $1/CV^2$  ( $1.63 \pm 0.39$  of baseline) (Mann-Whitney test) (Fig 2B, S2 and S3 Data). To conclude, PC–FSIN connections with large EPSPs show activity-driven LTD, which requires group I mGluRs.

### LTD by Single PC Bursting Is Specific to VLEs

In contrast to VLEs, the PC–FSIN pairs with small EPSPs (average in baseline with failures  $1.89 \pm 0.43$  mV at  $E_m -69.2 \pm 3.5$  mV, failure rate  $11.2 \pm 9.5\%$ , SW  $0.48 \pm 0.04$  ms,  $n = 5$ ) failed to show lasting plasticity following the 40 Hz bursts (amplitude  $1.07 \pm 0.06$  of baseline at 20–25 min) (Fig 3A, S1 Fig, S4 Data). Likewise, no lasting plasticity was seen in any (paired  $t$ -test) of the three vgat+ non-FSINs (SW  $0.91 \pm 0.07$ ,  $n = 3$ ) with small amplitude EPSP ( $2.08 \pm 0.58$  mV,  $n = 3$ ) in similar experiments. Given that LTD in the VLEs was accompanied by stronger postsynaptic depolarization during the presynaptic spike bursts, we studied whether small amplitude EPSP connections would show plasticity if the postsynaptic FSIN was depolarized during the PC bursts. We reproduced experiments above with a separate set of PC–FSIN (SW  $0.47 \pm 0.03$  ms,  $n = 5$ ) pairs with small amplitude EPSP (average with failures  $1.44 \pm 0.22$  mV, failure rate  $11.0 \pm 3.3\%$ ,  $n = 5$ ), and paired presynaptic PC spike bursts with postsynaptic cell depolarization (20–30 mV, 250 ms steps from  $E_m$ , see Methods for details) beyond the firing threshold (Fig 3A). This protocol also failed to generate long-lasting change in EPSPs in the PC–FSIN pairs ( $0.94 \pm 0.04$  of baseline at 20–25 min,  $n = 5$ , Wilcoxon test) (Fig 3A, S4 Data). Interestingly, a small but significant LTD was observed with this configuration in two ( $0.71 \pm 0.10$  and  $0.83 \pm 0.05$  at 20–25 min compared to baseline,  $p < 0.05$  for both cells, paired  $t$ -test) of three individual PC–non-FSIN (vgat+) pairs tested. Finally, we studied the synaptic connections between L2–3 PCs applying presynaptic 40 Hz bursts while the postsynaptic cell was at resting membrane potential. The PC–PC pairs were connected with small amplitude EPSPs (average with failures  $1.40 \pm 0.30$  mV at  $E_m -65.9 \pm 5.4$  mV, failure rate  $4.2 \pm 3.2\%$ ,  $n = 4$ ), and the 40 Hz bursts failed to generate lasting plasticity in the EPSP ( $1.01 \pm 0.05$  of baseline at 20–25 min,  $n = 4$  cells, Wilcoxon test) (Fig 3B, S4 Data), possibly because LTP and LTD in human PCs require strong postsynaptic depolarization for either activation of glutamate NMDA receptors or L-type voltage-gated calcium channels [7]. Input resistance in the plasticity recordings showed small increase to  $1.09 \pm 0.01$  (baseline-normalized) at 20–25 min from baseline ( $n = 26$ ,  $p < 0.01$ ,  $t$ -test) [33]. The results show that following just a single PC burst firing, LTD specifically occurs in large EPSPs between PCs and interneurons, and not in other investigated synaptic connections.

### Co-activation of Many Weak Glutamatergic Synapses Evokes mGluR-Dependent LTD in Fast-Spiking Interneurons

Because studies in rodents have reported LTD in glutamatergic synapses to cortical interneurons either by chemical or strong synaptic activation of group I mGluRs, we studied whether FSINs with weak excitatory inputs showed the LTD when multiple glutamatergic fibers were simultaneously activated (Fig 3C) [27,29,34]. Evoking compound EPSCs from many small glutamatergic inputs with extracellular electrical stimulation (see Methods), we applied 40 Hz bursts to the glutamatergic pathway as above after baseline (at least 5 min, but less than 10 min). Focusing the EPSC analysis in the FSINs on the monosynaptic component of the current (see Fig 3C) [35,36] we found that the 40 Hz burst stimulation resulted in LTD (EPSC

dc\_1581\_18

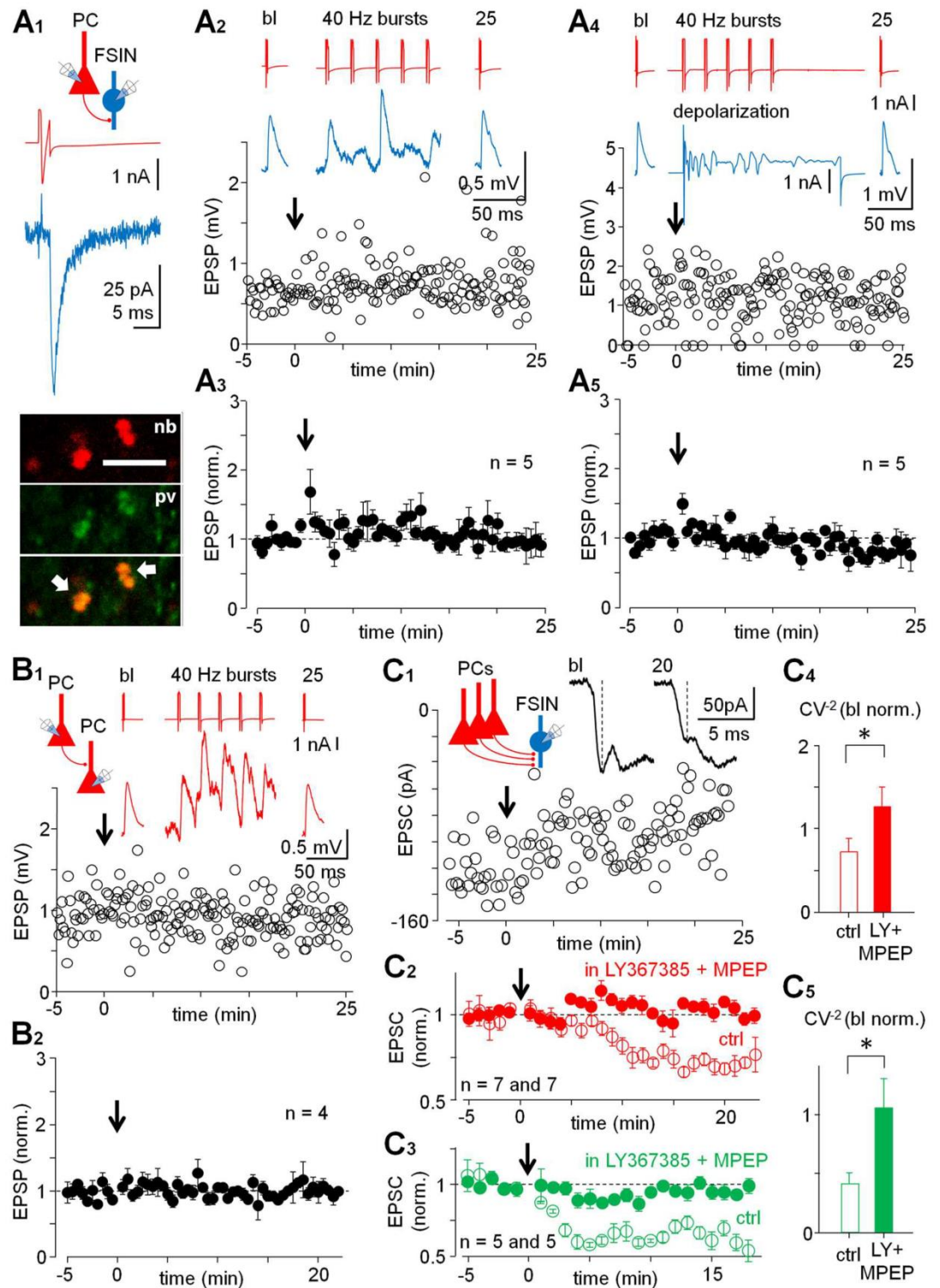


**Fig 3. LTD fails in weak single-fiber PC-FSIN connections, but is generated by coactivity of multiple glutamatergic fibers.** (A) LTD fails in PC-FSIN pairs with small EPSP. (A1) Schematic shows experimental design. A presynaptic PC spike (red) with postsynaptic EPSCs (blue, average of 5 at -60 mV) in one recording and confocal micrographs of the FSIN axon (nb, neurobiotin) with pv+ boutons (scale 5  $\mu$ m, arrows point colabeling in merged image). (A2) One PC-FSIN pair with the EPSPs in baseline and after the afferent cell 40 Hz bursts (arrow). Averaged EPSPs (5) at Em -72 mV on top at different time points and a 40 Hz burst. Postsynaptic cell is at Em (current clamp)

dc\_1581\_18

during the recording and the bursts. (A3) Mean  $\pm$  s.e.m. (30 s bin, baseline-normalized) of similar experiment in five PC–FSIN pairs with small amplitude EPSPs ( $1.89 \pm 0.43$  mV in baseline with failures). (A4) Failure of the LTD in weak PC–FSIN connections is not due to insufficient postsynaptic depolarization. Plot shows EPSP in one PC–FSIN pair before and following the presynaptic bursts, now paired with FSIN depolarization beyond the firing threshold (see [Methods](#)). Averages of EPSPs (5 at  $E_m -66$  mV) and a 40 Hz burst with simultaneous depolarization (30 mV, 250 ms) in voltage clamp shown on top. (A5) Mean  $\pm$  s.e.m. of five similar experiments with small EPSP ( $1.44 \pm 0.22$  mV in baseline with failures) PC–FSIN pairs (baseline-normalized, 30 s bin). The underlying data are shown in [S4 Data](#). (B) Connections between PCs exhibit small amplitude EPSPs with no long-term plasticity when PC1 bursts, while PC2 is at resting membrane potential. (B1) EPSP amplitude in one experiment before and after the 40 Hz presynaptic cell bursts (arrow, postsynaptic cell at  $E_m -78$  mV). Averaged EPSPs (five at  $E_m$ ) shown on top with a 40 Hz burst, and a schematic showing the experimental design. (B2) Mean  $\pm$  s.e.m. of baseline-normalized EPSPs ( $1.40 \pm 0.30$  mV in baseline with failures) in four PC–PC pairs as in *B1* (30 s bin) ([S4 Data](#)). (C) Activation of multiple afferent pathways to FSINs using extracellular stimulation reveals group I mGluR-dependent LTD in weak PC–FSIN synapses ([S5 Data](#)). (C1) One experiment with monosynaptic EPSC in FSIN (voltage clamped at  $-60$  mV) at baseline and following the 40 Hz bursts applied to the stimulation pathway (arrow at 0 time point). Inset traces (averages of 5) show evoked EPSCs in baseline and in LTD. The monosynaptic component is indicated by dotted vertical line. Schematic shows experimental design. (C2) Mean  $\pm$  s.e.m. of seven baseline-normalized experiments as in *C1* showing the LTD in control conditions (open symbols,  $p < 0.001$ , paired *t*-test) and blockade of the LTD in experiments with LY367385 (100  $\mu$ M) and MPEP (25  $\mu$ M) (solid symbols,  $n = 7$ , paired *t*-test). (C3) Generation of group I mGluR-dependent LTD by 40 Hz stimulation is conserved in mammalian neocortex occurring also in rat FSINs. Multiple fiber extracellular stimulation with LTD in rat L2–3 somatosensory cortex FSINs. Open symbols show experiments in control conditions ( $n = 5$ ,  $p < 0.01$ ) and solid symbols in the presence of LY367385 (100  $\mu$ M) and MPEP (25  $\mu$ M) ( $n = 5$ ) (Wilcoxon test). Blockers for glutamate *N*-methyl-D-aspartate receptors (NMDARs) (DL-2-Amino-5-phosphonopentanoic acid; DL-APV, 100  $\mu$ M) and GABA<sub>A</sub>Rs (PiTX, 100  $\mu$ M) were present in *C1*–*C3*. (C4–C5) Likewise, LTD of the EPSCs in both species is associated with an increased amplitude SD versus the mean. Data shows decreased  $CV^{-2}$  (baseline-normalized at 20 min after 40 Hz) in LTD in control conditions, but not when LTD is blocked in the presence of group I mGluR blockers ( $p < 0.05$  between groups, Mann-Whitney test).

doi:10.1371/journal.pbio.2000237.g003

$0.72 \pm 0.02$  from baseline at 20 min,  $n = 7$  cells,  $p < 0.001$ , *t*-test). Blockers for glutamate *N*-methyl-D-aspartate receptor (NMDARs) (DL-2-Amino-5-phosphonopentanoic acid [DL-APV], 100  $\mu$ M) and GABA<sub>A</sub>Rs (PiTX, 100  $\mu$ M) were present in the experiments. The EPSC amplitude LTD was accompanied by decreased  $CV^{-2}$  (baseline-normalized to  $0.72 \pm 0.16\%$ ,  $n = 7$ , *t*-test). This LTD was blocked in experiments with group I mGluR antagonists LY367385 (100  $\mu$ M) and MPEP (25  $\mu$ M) ( $n = 7$ ,  $p < 0.05$ , *t*-test) ([Fig 3C](#), [S5 Data](#)). The FSINs in these extracellular stimulation experiments showed narrow SW  $0.62 \pm 0.04$  ms,  $n = 14$ . Accordingly, we reproduced these experiments with rat glutamatergic fibers to FSINs in L2–3 (SW  $0.64 \pm 0.06$  ms,  $n = 10$ ) and confirmed LTD (EPSC  $0.64 \pm 0.04$  from baseline at  $>15$  min,  $n = 5$ ,  $p < 0.01$ , Wilcoxon test) and its blockade with the group I mGluR antagonists (EPSC from baseline  $0.95 \pm 0.5$ ,  $n = 5$ , Wilcoxon test) ([Fig 3C](#), [S5 Data](#)). The EPSC amplitude in LTD showed reduced  $CV^{-2}$  (baseline-normalized to  $0.41 \pm 0.09\%$ ,  $n = 5$ , Mann-Whitney test), but not when LTD was blocked with the mGluR antagonists ( $1.04 \pm 0.24\%$  of baseline at  $>15$  min) ( $p < 0.05$  between the groups at  $>15$  min, Mann-Whitney test) ([Fig 3C](#), [S5 Data](#)). We tested three of the recorded rat FSINs for pv immunoreaction and found them all positive. Thus, in both human and rat cortex, weak glutamatergic connections to L2–3 FSINs exhibit group I mGluR-dependent LTD if multiple glutamatergic inputs are activated simultaneously.

## LTD of VLEs Is Sufficient to Modify Network Activity

Given that interneuron–PC connections with VLEs have been proposed to be essential in generation of the neocortical complex events, we studied whether the LTD in these connections would selectively modify network activity. First, we confirmed that single PC AP-evoked VLEs in the FSIN as well as in the non-FSIN elicited firing of these interneurons from the resting membrane potential [[11](#)]. We found that VLE-evoked postsynaptic spikes in a FSIN ( $E_m -69$  mV) typically followed with a short 3–5 ms delay ([Fig 4A](#)) [[10](#)], whereas in a non-FSIN, ( $E_m -69$  mV) the spikes showed long delay with large jitter ([S2 Fig](#)). Similarly, whole-cell

dc\_1581\_18

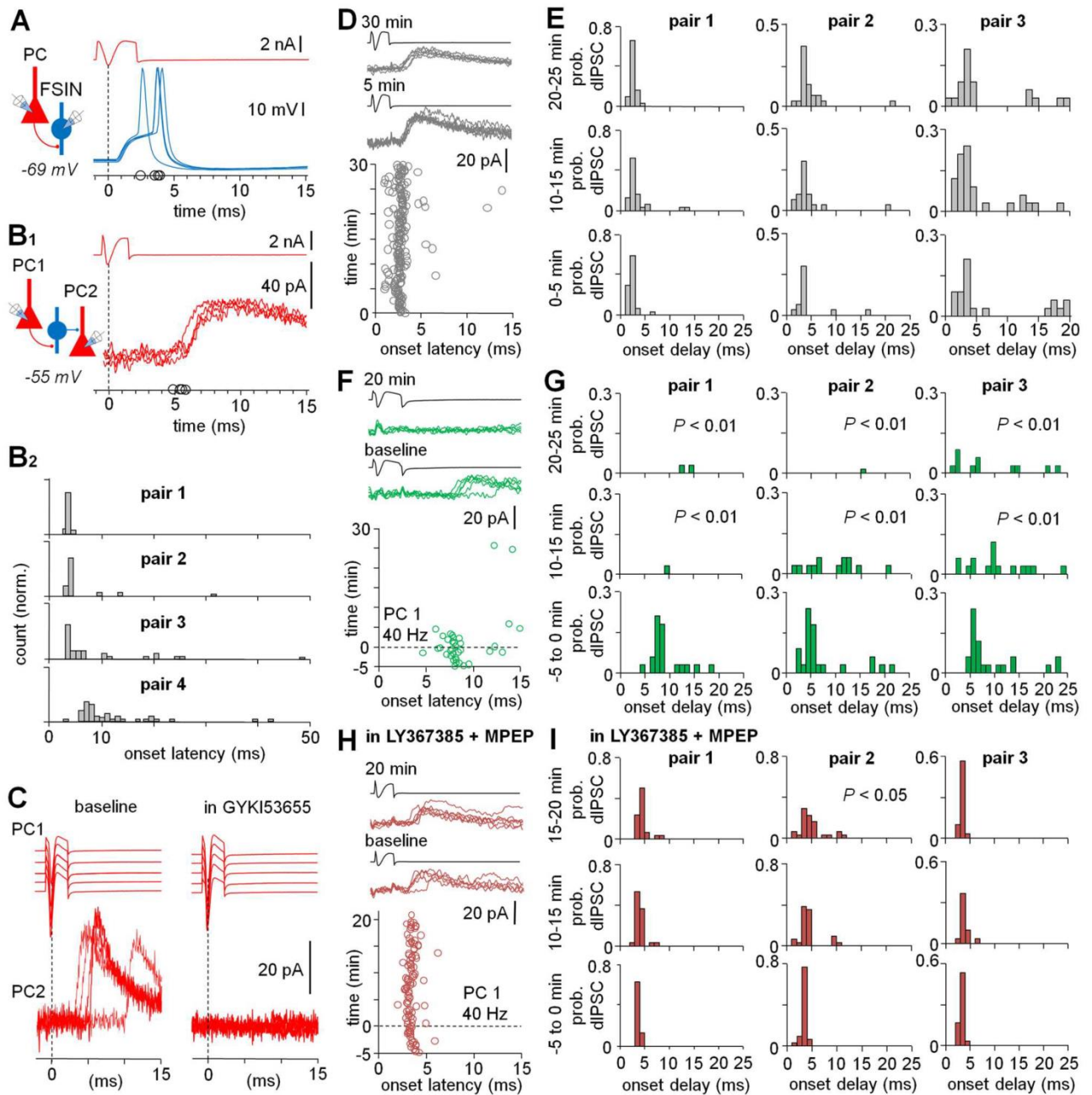


**Fig 4. The LTD depresses discharge of FSINs in complex events.** (A) Large EPSPs and APs in FSIN (blue) with short 3 to 5 ms delay elicited by single PC spike (red, peak indicated by vertical line). The figure shows four consecutive cycles with 10 s interval in one *vgat+* and *pv+* FSIN at *Em* (−69 mV) (note short AP duration, the positive peaks are indicated in the abscissa). Schematic shows experimental setting. (B) Single PC spike triggers disynaptic GABAergic currents in the layers 2–3. Dual whole-cell PC recordings (voltage-clamp) show that single PC1 APs trigger dIPSCs in PC2 with high probability and short delay. Schematic shows experimental design. (B1) Traces show consecutive events (4) in one experiment. The dIPSC onsets are marked in abscissa. (B2) Histograms (ordinates normalized and show from 0 to 1) illustrate delay distribution of the first dIPSC onset in four experiments (each 6–9 min, indicated as pairs 1–4) in control conditions. Most evoked dIPSCs are phase-locked to the presynaptic PC spike with <10 ms delay with obvious moderate variability of the mode of delay between experiments (S6 Data). (C) The dIPSCs are generated by glutamatergic excitation. Sample traces show five consecutive dIPSCs between PC1 and PC2 in baseline conditions and the blockade with AMPAR blocker GYKI53655 (25 μM) (see S4 Fig). (D–E) The single AP-evoked dIPSCs between PCs are stable over a long period (S6 Data). (D) Raster plot illustrates timing of dIPSC onset (in PC2) evoked by an AP in the presynaptic PC (PC1) in one 30 min experiment. Consecutive (6) presynaptic spikes and dIPSCs at different time points shown on top. (E) Three experiments (pairs 1, 2, and 3) as in D (pair 1), illustrated with histograms showing the dIPSC onset delay in different time windows (0–5 min, 10–15 min, and 20–25 min). The dIPSC probability and delay are stable for at least 30 min

dc\_1581\_18

(Chi-square test). (F–G) dIPSCs show LTD after presynaptic PC 40 Hz burst firing (S6 Data). (F) 40 Hz spike bursts in the presynaptic PC (similar to the LTD experiments in Fig 2) induce LTD of the dIPSCs. Raster plot shows dIPSCs in one paired PC recording. After baseline, the 40 Hz spike bursts in PC1 (at 0 time point, dotted horizontal line) induce permanent depression of the dIPSC occurrence. Traces illustrate the presynaptic cell spike and the dIPSCs (6) at baseline and the absence of dIPSCs after 20 min. (G) Three similar experiments (pairs 1, 2, and 3) as in F (pair 1), showing the LTD of dIPSCs after the 40 Hz presynaptic bursts (BL –5 to 0 min) ( $p < 0.01$ , Chi-square test). (H–I) The LTD of dIPSCs is blocked with group I mGluR antagonists (S6 Data). (H) Similar experiment as in F, but in the presence of LY367385 (100  $\mu$ M) and MPEP (25  $\mu$ M). Traces on top show the pre- and disynaptic currents at baseline and 20 min after the 40 Hz bursts. (I) Three experiments as in H (pair 1) illustrated with dIPSC onset delay histograms at the baseline (–5 to 0 min) and at two time windows after the 40 Hz presynaptic bursts.

doi:10.1371/journal.pbio.2000237.g004

recordings between identified PCs revealed disynaptic GABA<sub>A</sub>R-mediated inhibitory currents (dIPSCs) in complex events elicited by a single AP (interval 10 s) (Fig 4B) [10,11]. The dIPSCs occurred with short delay ( $6.23 \pm 0.72$  ms,  $n = 16$  pairs) and high probability ( $0.70 \pm 0.05$ ,  $n = 16$  pairs in baseline conditions) (S6 Data). The dIPSCs showed longer and more variable delay to the presynaptic spike than monosynaptic GABA<sub>A</sub>R-mediated inhibitory currents (monIPSCs) from FSINs ( $0.96 \pm 0.10$  ms,  $n = 9$ ,  $p < 0.001$ ,  $t$ -test) (SW  $0.48 \pm 0.03$  ms,  $n = 9$ ) (S3 Fig, S9 Data). In addition, dIPSCs were blocked by the glutamate AMPAR blocker GYKI53655 (25  $\mu$ M) ( $n = 3$ ,  $p < 0.001$ , Chi-square test) (Fig 4C, S4 Fig, S6 Data). The evoked dIPSC amplitudes (averages excluding failures in all plasticity recordings  $32.1 \pm 3.7$  pA,  $n = 12$ ) were similar to monIPSCs ( $35.2 \pm 5.6$  pA,  $n = 9$ ,  $t$ -test) (S5 Fig, S10 Data), indicating that these early complex event inhibitory currents (IPSCs) were generated by a single FSIN. The dIPSCs and the monIPSCs were recorded at –55 mV. The dIPSCs were detected in 3.0% of all potential connections tested ( $n = 1,056$ ).

To determine whether plasticity modified this network, we performed long recordings from PC pairs showing that the probability and delay of the dIPSCs were stable for at least 30 min ( $n = 3$ ) in normal conditions (Fig 4D, 4E and S6 Data). However, if the 40 Hz burst firing was delivered in the presynaptic PC (similar to the VLE LTD experiments in Fig 2), the dIPSC occurrence (total in 25 ms from PC spike) rapidly and permanently attenuated after a baseline showing strong LTD (from  $0.71 \pm 0.04$  in baseline to  $0.14 \pm 0.09$  at 15–20 min,  $n = 3$ ,  $p < 0.05$ , Chi-square test) (Fig 4F, 4G and S6 Data). Interleaved experiments in the presence of group I mGluR antagonists LY367385 (100  $\mu$ M) and MPEP (25  $\mu$ M) showed that LTD of dIPSCs was blocked in the presence of the group I mGluR antagonists ( $0.81 \pm 0.10$  in baseline and  $0.88 \pm 0.12$  at 15–20 min,  $n = 3$ , Chi-square test) (Fig 4H, 4I and S6 Data). In conclusion, the results demonstrate that a single PC burst firing at 40 Hz elicits robust LTD in VLE connections to FSINs and causes suppression of phase-locked early dIPSCs between PCs. These two LTDs both require group I mGluRs. Thus, the results show that plasticity of VLEs in FSINs changes the activation pattern of the neurons discharging in supragranular layers during complex events.

## Discussion

Almost a decade ago, Molnar et al. [10] first reported that a subset of excitatory PC synapses in the human neocortex form VLEs in local GABAergic interneurons in supragranular layers. These strong connections specifically from PCs to inhibitory interneurons have since been reported in the frontal, prefrontal, parietal, and temporal cortices, where the VLEs often are suprathreshold, driving assemblies of inhibitory interneurons to fire after a single PC spike [11,37]. Similar strong connections between two individual neocortical neurons have not been found in nonhuman species [37–39]. Analyses of large datasets from rodent visual and somatosensory cortices have revealed that neurons in local networks are not randomly connected, but specific local connectivity patterns exist between neuron types, and the strongest excitatory

dc\_1581\_18

synapses control local network activity [40–42]. This suggests that there is a skeleton of strong connections in the network that dominates the activity [40]. Therefore, it has been proposed that the VLE connections in the human might be important in generating neocortical cell assemblies and be involved in higher cognitive functions [11]. However, until now it had remained unknown how neuronal plasticity regulates these connections and whether their selective modulation indeed alters discharge of neuronal assemblies in the human neocortical network activity.

Our result that the VLEs occur specifically in human interneurons, and not in between PCs, is consistent with previous studies [10,11]. In addition, we demonstrate that VLEs are generated in different interneuron subpopulations, including fast-spiking (such as basket cells) and non-fast-spiking supragranular vgat+ neurons. Furthermore, single GABAergic interneurons receive both VLEs and more common small EPSP connections from layer 2–3 PCs. Indeed, anatomically identified L2–3 basket cells show huge variability in strength of PC inputs. It is likely, although we do not directly demonstrate it here, that a single presynaptic L2–3 PC cell evokes VLEs and small EPSPs in different L2–3 postsynaptic interneurons showing synapse specificity. A comprehensive recent study in rodent demonstrated that certain connectivity patterns between neurons are repeated in the neocortex across different regions [39]. The strong VLE connection, occurring between PCs and L2–3 inhibitory interneurons in various neocortical regions is one such feature, and probably specific to the human neocortical microcircuits.

We show that strength of VLE connections is controlled by their activity history. A common form of mGluR-dependent LTD characterized in the extracellular stimulation experiments of glutamatergic synapses in the rodent cortex [24] converts the VLEs to small amplitude EPSPs. This LTD suppresses VLE synapses through a presynaptic mechanism most likely controlling the vesicular transmitter release as indicated by the changes in the EPSP amplitude PPR and the coefficient of variation in the depressed synapses [37]. The LTD of VLEs in FSINs, many of which are also pv+, involves the group I mGluRs. In the rodent cortex, group I mGluRs have been shown to play a central role in long-term plasticity processes including presynaptic LTD and LTP [24,29–31,34,43–46]. Our results from the group I mGluR-dependent LTD in FSINs in the human and the rodent neocortex indicate that this is an evolutionarily conserved plasticity mechanism for controlling the fast-spiking interneuron activity in the mammalian brain.

Interestingly, we report that in a non-fast-spiking cell, LTD was not blocked by the group I mGluR antagonists (see S2 Fig). In addition, we found significant LTD in two of three PC–non-FSIN connections with small EPSP when the postsynaptic cell was depolarized during PC bursts. These suggest that there may be various LTD forms in human cortical interneuron synapses [24,25], and that non-FSINs may exhibit different LTD mechanism than the FSINs, possibly depending on postsynaptic depolarization. Indeed, many synapse-specific properties including long-term plasticity have been reported in glutamatergic fibers in the rodent cortex [21,32,47–50]. Correspondingly, synapses originating from the same PC in the human neocortex may exhibit distinct long-term plasticity, depending upon the postsynaptic target cell; and different activity patterns may be required for plasticity in the synapses [24,50]. In this study, we have used elevated extracellular calcium (3 mM) to increase the stability of disynaptic IPSCs in baseline conditions. However, compared to recordings with 2 mM extracellular calcium, this modification is unlikely to strongly affect the high-frequency firing-evoked synaptic release and the long-term plasticity in FSIN synapses: the probability of synaptic release in VLEs in FSINs is already very high at 2 mM  $\text{Ca}^{2+}$ , and only slightly modulated by further increase of calcium [37]. Yet, as demonstrated in the recent study by Molnar et al. [37], the VLE release probability can markedly decrease when extracellular calcium is reduced from 3 mM to 1.5 mM, which is considered lower range of the cerebrospinal fluid total calcium level

in physiological conditions [51]. Therefore, it is also possible that in calcium concentrations close to 1.5 mM, the PC firing pattern used in this study may not be sufficient for such a robust LTD as reported here in the FSINs. Importantly, some non-FSINs show VLEs with low presynaptic release probability even in 3 mM calcium, as indicated by the large EPSP amplitude coefficient of variation. In these synapses, extracellular calcium modulations may have even stronger effects on the short- and long-term plasticities than in the FSINs.

Strikingly, in the human neocortex, the activity of a single PC is sufficient to trigger mGluR-dependent LTD in the VLE connections, but not in weak glutamatergic pathways. The level of the postsynaptic depolarization does not explain the failure of LTD in small EPSP connections to fast-spiking cells, and a potential explanation is that there is insufficient activation of the postsynaptic group I mGluRs [34,43]. The connections with VLEs are likely to release more glutamate and activate the critical mGluRs [52–54]. The hypothesis on strong glutamate release is supported by our finding that the small EPSP connections were unable to generate LTD by single fiber activity, but they showed the mGluR-dependent plasticity when multiple fibers were activated simultaneously with local extracellular stimulation [55]. Indeed, a recent study revealed that human neocortical PC–FSIN synapses with VLEs have more transmitter vesicle release sites, although the glutamate release quantal size is similar compared to synapses in rat neocortex [37]. This indicates multivesicular release in synapses with VLEs, and it is interesting to speculate that the conversion to common small EPSPs via the presynaptic LTD might reflect their transformation from a multivesicular release site to a single vesicle-releasing synapse.

Although a link between very large excitatory synapses and human cortical complex events has been suggested earlier [10,11], a relation between their selective modulation and complex events had not been directly demonstrated until this study. The LTD triggered by a single PC firing in the current conditions is specific to connections with VLEs and therefore provides a useful tool to test the relation between VLEs and neocortical network activity. Results here show that the VLE connections indeed trigger the complex events, and the LTD changes their temporal structure. The activation of individual fast-spiking interneurons was commonly observed in dual PC recording as disynaptic GABAergic currents with timing corresponding to the APs in fast spiking interneurons [11]. LTD of the VLE in FSINs and the suppression of dIPSCs in complex events were both induced by single PC burst firing, and they both required group I mGluRs. Some non-FSINs also exhibit VLEs and can show LTD, although these cells were unlikely to contribute to the GABAergic disynaptic currents investigated here: the dIPSCs occurred with short delay and high precision, whereas the non-FSINs show long and variable delay in their response to fire APs (see S2 Fig). However, the results of non-FSINs are based on small sample sizes, and should therefore be interpreted with caution.

In conclusion, the human neocortex is unique in many aspects, since its microcircuits show differences at the molecular, ultrastructural, and physiological levels compared to other mammalian species [1,3,56]. The capacity of the human neocortex to perform extraordinary and highly complex tasks may at least partly result from these microcircuit level specializations. We propose that VLEs with robust activity-induced plasticity and their contribution to neocortical cell assemblies may be crucial for higher cognitive functions and abstract mental abilities of the human brain. In addition, evidence in animal models suggests the involvement of group I mGluR-mediated plasticity in neocortical learning processes, and perturbation of the mGluR-dependent plasticity has been reported with mental decline [43]. Therefore, the human-specific microcircuit features may also be substrates for pathological processes resulting in cognitive decline and other neurological and neuropsychiatric dysfunctions that we as a species are vulnerable to [57–61].

## Materials and Methods

### Ethics Statement

All procedures were performed according to the Declaration of Helsinki with the approval of the University of Szeged Ethical Committee and Regional Human Investigation Review Board (ref. 75/2014).

### Electrophysiology and Analysis

Human neocortical slices were derived from material that had to be removed to gain access to the surgical treatment of deep-brain tumors from the left and right frontal, temporal, and parietal regions with written informed consent of the patients prior to surgery. The patients were 10–85 y of age (mean  $\pm$  SD =  $50 \pm 4$  y), including 17 males and 14 females. The tissue obtained from underage patients was provided with agreement from a parent or guardian. The resected samples were cut from the frontal and temporal lobes of left or right hemisphere. Anesthesia was induced with intravenous midazolam and fentanyl (0.03 mg/kg, 1–2  $\mu$ g/kg, respectively). A bolus dose of propofol (1–2 mg/kg) was administered intravenously. The patients received 0.5 mg/kg rocuronium to facilitate endotracheal intubation. After 2 min, the trachea was intubated and the patient was ventilated with O<sub>2</sub>/N<sub>2</sub>O mixture (a ratio of 1:2). Anesthesia was maintained with sevoflurane at monitored anesthesia care volume of 1.2–1.5. After surgical removal, the resected tissue blocks were immediately immersed in ice-cold standard solution containing (in mM): 130 NaCl, 3.5 KCl, 1 NaH<sub>2</sub>PO<sub>4</sub>, 24 NaHCO<sub>3</sub>, 1 CaCl<sub>2</sub>, 3 MgSO<sub>4</sub>, 10 D(+)-glucose, and saturated with 95% O<sub>2</sub> and 5% CO<sub>2</sub>. Slices were cut perpendicular to cortical layers at a thickness of 350  $\mu$ m with a microtome (Microm HM 650 V) and were incubated at room temperature (20–24°C) for 1 h in the same solution. Rat neocortical slices were prepared as described before [62]. Male Wistar rats were anaesthetized using halothane, and following decapitation (320  $\mu$ m thick), coronal slices were prepared from the somatosensory cortex. The solution used during electrophysiology experiments was identical to the slicing solution, except it contained 3 mM CaCl<sub>2</sub> and 1.5 mM MgSO<sub>4</sub>. Recordings were performed in a submerged chamber (perfused 8 ml/min) at approximately 36–37°C. Cells were patched using water-immersion 20 $\times$  objective with additional zoom (up to 4 $\times$ ) and infrared differential interference contrast video microscopy. Micropipettes (5–8 M $\Omega$ ) were filled with intracellular solution for whole-cell patch-clamp recording (in mM): 126 K-gluconate, 8 KCl, 4 ATP-Mg, 0.3 Na<sub>2</sub>-GTP, 10 HEPES, 10 phosphocreatine (pH 7.20; 300 mOsm) with 0.3% (w/v) biocytin. Current and voltage clamp recordings were performed with Mutliclamp 2B amplifier (Axon Instruments), low-pass filtered at 6 kHz (Bessel filter). Series resistance (R<sub>s</sub>) and pipette capacitance were compensated in current clamp mode and pipette capacitance in voltage clamp mode. Cell capacitance compensation was not applied. R<sub>s</sub> was monitored and recorded continuously during the experiments. The recording in voltage clamp mode was discarded if the R<sub>s</sub> was higher than 25  $\Omega$ M or changed more than 20%.

In paired cell recordings, APs were generated in the presynaptic cell with brief (2–3 ms) suprathreshold depolarizing (60–70 mV) paired pulses (50 ms interval) in voltage clamp delivered every 10 s from –60 mV. Postsynaptic cells were at resting membrane potential in current clamp mode. In some cells with VLEs, the postsynaptic cell was hyperpolarized (up to –10 mV) with constant current to prevent the VLE from triggering an AP. The 40 Hz firing protocol was similarly applied in voltage clamp mode with series of 2–3 ms depolarizing pulses (5 pulses at 40 Hz, delivered every 0.5 sec 40 times), while the postsynaptic cell was held in current clamp resting membrane potential. In some experiments (Fig 3A, 4–5), the postsynaptic cell was depolarized in voltage clamp during presynaptic 40 Hz firing with a continuous step

dc\_1581\_18

(20–30 mV, 250 ms). This elicited on average 2.2 postsynaptic spikes for 1<sup>st</sup> presynaptic spike (in following 25 ms,  $n = 200$  in 5 cells) of the 40 Hz train, and on average 0.80 postsynaptic spike probability for the 2<sup>nd</sup>–5<sup>th</sup> PC AP.

Extracellular stimulation was applied with a concentric bipolar electrode (125  $\mu\text{m}$  tip diameter, FHC Inc., US) positioned on L2–3. Paired pulse stimuli (50  $\mu\text{s}$ , with 50 ms interval, intensity range from 20 to 300  $\mu\text{A}$ ) were delivered every 15 s with current isolator stimulator (Model DS3, Digitimer, UK). Compound EPSCs in Fig 3 were confirmed by observing less than 100 pA increases in the evoked EPSC amplitude when gradually increasing stimulation intensity.

## Data Analysis and Statistics

Data were acquired with Clampex software (Axon Instruments, US) at 20 kHz. EPSC/P, IPSC, action current duration, and the cell input resistance were analyzed off-line with p-Clamp software (Axon Instruments, US) and Spike2 (version 7.0, Cambridge Electronic Design, UK). Liquid junction potential was not corrected. EPSC amplitude and kinetics analysis in voltage clamp mode (time-to-peak from onset) was omitted when access resistance was higher than 25 M $\Omega$ . SW was calculated from the onset of inward action current till recovery to baseline holding level. Data for SWs were collected in the beginning of experiments when synaptic connections from all cells were briefly tested in voltage clamp mode. All data are presented as mean  $\pm$  s.e.m. and when showing baseline-normalized EPSPs of many cells, the values were calculated from binned (30 s bin) data. In rare cases when cell-spiked and accurate EPSP amplitude data was not available, bin includes two instead of three data points. For statistical analysis, ANOVA with posthoc Tukey's test and  $t$ -test were used for data with normal distribution (Shapiro-Wilk test) and sample sizes larger than  $n = 6$ . Chi-square test was used for categorical variables (occurrence of dIPSC in 25 ms time window from PC spike). Otherwise, Mann-Whitney U-test (unpaired) and Wilcoxon Signed Rank Test (paired) were used. EPSP amplitude in individual plasticity experiments was tested with paired  $t$ -test comparing data points in 5 min baseline and an equal time window at 20–25 min following the presynaptic bursts, unless stated otherwise (in some shorter experiments in the last 5 min of the recording). Correlation was determined with Pearson's  $r$ -test. Differences were accepted as significant if  $p < 0.05$ . Failures were included in the EPSP mean values (in binned data) in plasticity analysis.

## Drugs

DL-APV, GYKI53655, LY367385, MPEP, and picrotoxin (PiTX) were applied via bath and purchased from Sigma Aldrich (Hungary).

## Cell Visualization and Image Reconstruction

After electrophysiological recording, slices were immediately fixed in a fixative containing 4% paraformaldehyde and 15% picric acid in 0.1 M phosphate buffer (PB; pH = 7.4) at 4°C for at least 12 h, then stored in 0.1 M PB with 0.05% sodium azide as a preservative at 4°C. Slices were embedded in 10% gelatin and further sectioned into slices of 50  $\mu\text{m}$  thickness in cold PB using a vibratome VT1000S (Leica Microsystems, UK). After sectioning, the slices were rinsed in 0.1 M PB (3 x 10 min) and cryoprotected: first step in 10% (30 min), and later in 20% sucrose (1 h) dissolved in PB and then permeabilized using a freeze and thaw procedure. Finally, they were incubated in fluorophore (Cy3)-conjugated streptavidin (1:400, Jackson ImmunoResearch Lab. Inc. US) in 0.1 M Tris-buffered saline (TBS, pH 7.4) for 2.5 h (at 22–24°C). After washing with 0.1 M PB (3 x 10 min), the sections were covered in Vectashield mounting medium (Vector Laboratories Inc, US), put under cover slips, and examined under

epifluorescence microscope (Leica DM 5000 B, UK). Sections selected for immunohistochemistry and cell reconstruction were dismantled and processed as explained below.

Some sections for cell structure illustrations were further incubated in a solution of conjugated avidin-biotin horseradish peroxidase (ABC; 1:300; Vector Labs, UK) in Tris-buffered saline (TBS, pH = 7.4) at 4°C overnight. The enzyme reaction was revealed by the glucose oxidase-DAB-nickel method using 3,3'-diaminobenzidine tetrahydrochloride (0.05%) as chromogen and 0.01% H<sub>2</sub>O<sub>2</sub> as oxidant. Sections were postfixed with 1% OsO<sub>4</sub> in 0.1M PB. After several washes in distilled water, sections were stained in 1% uranyl acetate and dehydrated in ascending series of ethanol. Sections were infiltrated with epoxy resin (Durcupan) overnight and embedded on glass slices. Three-dimensional light microscopic reconstructions from sections were carried out using the NeuroLucida system with 100 x objective (Olympus BX51, Olympus UPlanFI, Hungary). Images were collapsed in z-axis for illustration. Cells in Fig 1 were reconstructed from confocal microscope z-stack images of streptavidin fluorophore signal using Image-J software as described previously [32]. Vgat immunoreaction analysis was used in parallel to confirm the interneuron axon.

## Immunohistochemistry

For immunohistological reactions, free-floating sections were washed 3 times in TBS-TX 0.3% (15 min) at 22–24°C, then moved in 20% blocking solution with horse serum in TBS-TX 0.3%. The sections were incubated in primary antibodies diluted in 1% serum in TBS-TX 0.3% over three nights at 4°C, then put in relevant fluorochrome-conjugated secondary antibodies in 1% of blocking serum in TBS-TX 0.3% overnight at 4°C. Sections were washed at first step in TBS-TX 0.3% (3 x 20 min) and later in 0.1 M PB (3 x 20 min) and mounted on glass slides with Vectashield mounting medium (Vector Lab.Inc., UK). The characterizations of antibodies: pv (goat anti-pv, 1:500, Swant, Switzerland, [www.swant.com](http://www.swant.com)), sst (rat anti-sst, 1:50, Merck Millipore, Germany, [www.merckmillipore.com](http://www.merckmillipore.com)) and vgat (rabbit anti-vgat, 1:500, Synaptic Systems, Germany, [www.ssysy.com](http://www.ssysy.com)). Fluorophore-labelled secondary antibodies were: DyLight 488 (Donkey anti goat, 1:400, Jackson ImmunoResearch Lab. Inc., [www.jacksonimmuno.com](http://www.jacksonimmuno.com), US), Alexa488 (Donkey anti rat, 1:400, Jackson ImmunoResearch Lab. Inc.) and Cy5 (Donkey anti rabbit, 1:500, Jackson ImmunoResearch Lab. Inc.). Labelling of neurons by neurobiotin and immunoreactions were evaluated using first epifluorescence (Leica DM 5000 B, UK) and then laser scanning confocal microscopy (Olympus FV1000, Hungary). Immunoreaction was considered to be negative when fluorescence was not detected in relevant neurobiotin-labelled cell, but immunopositivity was detected in the same area in unlabelled cells. Immunoreactions were studied in axon boutons (vgat and pv) and soma and dendrites (pv, sst).

## Supporting Information

**S1 Fig. LTD is generated in PC-FSIN pairs with VLEs.** The data include all FSINs stimulated with 40 Hz in control conditions at resting membrane potential of the postsynaptic cell (n = 10). The LTD fails in pairs with small EPSP. Plot shows the average baseline EPSP amplitude (failures excluded) versus the baseline-normalized EPSP amplitude (failures included) after (20–25 min) the 40 Hz presynaptic bursts (ordinate). Cells with significant LTD (studied with paired *t*-test in each experiment) are illustrated with open symbols (n = 5). Cells not showing LTD are shown with solid symbols (n = 5). Linear regression demonstrates a relation ( $r^2 = 0.75$ ) and Pearson's test shows strong correlation ( $P < 0.001$ ) between the baseline EPSP amplitude and the level of LTD. The amplitudes of the LTD cells and the non-LTD cells are significantly different in baseline ( $P < 0.01$ , Mann-Whitney test) (S7 Data). (TIF)

dc\_1581\_18

**S2 Fig. Single fiber connections from pyramidal cells to non-fast-spiking vgat+ interneurons (nonFSIN) with large amplitude EPSP can show LTD.** (A) (A1) Partial reconstruction of a synaptically connected pyramidal cell (soma and dendrites red, axon orange)–non-fast spiking interneuron (blue, axon light blue) pair visualized with streptavidin-DAB and reconstructed from one 60  $\mu\text{m}$ -thick section. Schematic shows experimental design. L1 = layer 1, L2-3 = layers 2–3, separated by grey line. Scale 50  $\mu\text{m}$ . (A2) Single EPSPs from the PC trigger action potentials in the postsynaptic interneuron in resting membrane potential ( $E_m$  -69 mV). Compared to the fast-spiking cell, the interneuron fires with long and variable delay to the PC spike (see Fig 4A). The action potential positive peaks are marked in the abscissa. Note also the slow spike waveform. (A3) PC spike (red) and large amplitude EPSC (blue, average of 5) in the same connection in voltage-clamp (at -60 mV). Scales 1 nA and 200 pA / 5 ms. (A4) Confocal micrographs show neurobiotin (nb, top) -filled axon of the postsynaptic cell with positive immunoreaction for vgat in boutons (middle). Arrows in merged images (bottom) show co-labelled boutons (scale 5  $\mu\text{m}$ ). (B) (B1) EPSP amplitude in the same synaptic pair (110615\_1) before and after pyramidal cell 40 Hz bursts (arrow at 0-time point). EPSP amplitude depression at 20–25 min ( $P < 0.001$ , paired  $t$ -test) is preceded by a transient enhancement of the EPSP. Postsynaptic EPSPs (blue, average of 5 at  $E_m$  -68 mV) and presynaptic spikes (red) shown on top at time points indicated. One presynaptic 40 Hz burst illustrated. (B2) Similar experiment with another postsynaptic non-fast spiking interneuron with large EPSP, but now in the presence of mGluR blockers LY367385 (100  $\mu\text{M}$ ) and MPEP (25  $\mu\text{M}$ ). Unlike in FSINs (see Fig 2A and 2B), the EPSP amplitude shows significant depression (at 20–25 min,  $P < 0.001$ , paired  $t$ -test) in the presence of the drugs (S8 Data). (TIF)

**S3 Fig. Monosynaptic IPSCs from FSIN to PC have submillisecond delay to the presynaptic spike.** Onsets of the monosynaptic IPSCs from FSINs to pyramidal cells exhibit submillisecond (average  $0.96 \pm 0.10$  ms,  $n = 9$ , mean  $\pm$  s.e.m) delay to the presynaptic cell spike. This is significantly shorter than the onset delay of dIPSCs ( $6.23 \pm 0.72$  ms,  $n = 16$  pairs,  $P < 0.001$ ,  $t$ -test). Schematic on top illustrates experimental design. Traces on top are from one cell pair (blue, FSIN spike) showing 5 superimposed consecutive monosynaptic IPSCs (red) in the postsynaptic pyramidal cell. Plot below shows mean  $\pm$  s.e.m. of the monosynaptic IPSC ( $n = 20$  in each cell) onset delay in the FSIN–PC cell pairs (experiment codes indicated in the ordinate) (S9 Data). (TIF)

**S4 Fig. The dIPSCs evoked by single PC spike are blocked with ionotropic glutamate AMPA receptor antagonist GYKI53655.** (A) Raster plot of single PC spike -evoked dIPSC onset delay in one experiment. AMPAR blocker GYKI53655 (25  $\mu\text{M}$ ) was applied at 0 -time point (dotted horizontal line). Traces above show consecutive dIPSCs (blue) in the postsynaptic pyramidal cell during the baseline and in the presence of GYKI (5 min). Schematic inset shows experimental design with pre- (PC1) and postsynaptic pyramidal cell (PC2) for the dIPSCs. (B) dIPSC onset delay histograms in three experiments (shown as pairs 1, 2 and 3) showing probability and delay of the first dIPSC evoked by PC spike. After baseline, the dIPSCs are blocked by GYKI. The pair 1 is the same experiment as shown in the raster plot (S6 Data). (TIF)

**S5 Fig. Amplitude of the dIPSCs is similar to the amplitude of monosynaptic IPSCs from FSINs to PCs ( $t$ -test).** The plot shows in left the average amplitudes of monosynaptic IPSCs (monIPSCs) elicited in 9 FSIN–PC pairs (failures excluded) as reported in the results. Average amplitudes of the disynaptic IPSCs (dIPSCs, failures excluded) shown in right. This suggests

dc\_1581\_18

the earliest complex event IPSCs with  $6.23 \pm 0.72$  ms delay are generated by single fast-spiking interneurons. Plot shows mean  $\pm$  s.e.m. of the amplitudes in baseline conditions ([S10 Data](#)). (TIF)

**S1 Table. Results on EPSP/EPSC analyses and immunohistochemical reactions of the three postsynaptic cell populations: fast-spiking interneurons (FSINs), non-fast-spiking interneurons (nonFSINs) and pyramidal cells (PCs).** The table comprises EPSP data in baseline conditions for 31 postsynaptic vgat+ cells studied for long-term plasticity and 16 PCs in the triple- and paired recordings. Experiment code identifies the postsynaptic cell recorded. Ten fast-spiking putative basket cells were anatomically identified. EPSP average amplitude is shown without synaptic failures and including the failures. Experiments are listed in a descending order starting from cells with the largest average EPSPs. EPSP failure rate is a percentage of failures of the EPSP to the presynaptic spike. EPSP rise time (from 20% to 80% of maximum) was measured from averaged EPSPs. Paired-pulse ratio (PPR) is defined as 1<sup>st</sup> EPSP / 2<sup>nd</sup> EPSP amplitude. EPSCs represent an average of 5 responses recorded in first 2 minute period in the voltage-clamp after break-in to the whole cell mode from the giga-seal. Because the EPSCs were recorded immediately after break-in (when whole-cell properties are typically not yet stabilized), the measured values may represent underestimate of the current. Note that in 3 FSINs and in one PC, EPSCs were not measured. Immunohistochemical reactions for vesicular GABA transporter (vgat), parvalbumin (pv) and somatostatin (sst) are indicated by (+) for positive and (-) for negative. The vgat was analyzed in axon terminals, pv in axon terminals, soma or dendrites, and sst in soma and dendrites. Putative basket cells in the FSINs were identified by their axon forming collaterals around L2-3 neuron somata. No axo-axonic cell types were identified. Pyramidal cells showed characteristic densely spiny dendrites with filopodial, stubby and mushroom-shaped spines, and main axon projecting towards infragranular layers. In the PCs table “a” and “b” indicate distinct postsynaptic cells in a mutually connected PC couple. (DOCX)

**S1 Data. Data for [Fig 1B1–1B3](#).**  
(XLSX)

**S2 Data. Data for [Fig 2A2–2A5](#).**  
(XLSX)

**S3 Data. Data for [Fig 2B1 and 2B2](#).**  
(XLSX)

**S4 Data. Data for [Fig 3A2–3A5, 3B1 and 3B2](#).**  
(XLSX)

**S5 Data. Data for [Fig 3C2–3C5](#).**  
(XLSX)

**S6 Data. Data for [Fig 4B2, 4D–4I and S4 Fig](#).**  
(XLSX)

**S7 Data. Data for [S1 Fig](#).**  
(XLSX)

**S8 Data. Data for [S2B1 and S2B2 Fig](#).**  
(XLSX)

dc\_1581\_18

**S9 Data. Data for S3 Fig.**

(XLSX)

**S10 Data. Data for S5 Fig.**

(XLSX)

## Acknowledgments

We thank Drs. Norbert Hajos and Stephanie Schorge for critical reading of the manuscript and Ms. Nelli Toth for help with cell reconstructions.

## Author Contributions

**Conceptualization:** Karri Lamsa.**Data curation:** Karri Lamsa.**Formal analysis:** Eszter Csakvari, Karri Lamsa, Melinda Paizs, Viktor Szegedi.**Funding acquisition:** Gabor Tamas, Karri Lamsa.**Investigation:** Eszter Csakvari, Karri Lamsa, Melinda Paizs, Viktor Szegedi.**Methodology:** Karri Lamsa, Melinda Paizs, Viktor Szegedi.**Project administration:** Karri Lamsa, Melinda Paizs.**Resources:** Gabor Molnar, Gabor Tamas, Pal Barzo.**Supervision:** Karri Lamsa.**Validation:** Karri Lamsa.**Visualization:** Eszter Csakvari, Karri Lamsa, Melinda Paizs, Viktor Szegedi.**Writing – original draft:** Karri Lamsa.**Writing – review & editing:** Gabor Molnar, Gabor Tamas, Karri Lamsa.

## References

1. Roth G, Dicke U. Evolution of the brain and intelligence. *Trends Cogn Sci.* 2005; 9(5):250–7. doi: [10.1016/j.tics.2005.03.005](https://doi.org/10.1016/j.tics.2005.03.005) PMID: [15866152](https://pubmed.ncbi.nlm.nih.gov/15866152/).
2. Hof PR, Glezer II, Nimchinsky EA, Erwin JM. Neurochemical and cellular specializations in the mammalian neocortex reflect phylogenetic relationships: evidence from primates, cetaceans, and artiodactyls. *Brain Behav Evol.* 2000; 55(6):300–10. 6665. PMID: [10971015](https://pubmed.ncbi.nlm.nih.gov/10971015/).
3. Defelipe J. The evolution of the brain, the human nature of cortical circuits, and intellectual creativity. *Frontiers in neuroanatomy.* 2011; 5:29. doi: [10.3389/fnana.2011.00029](https://doi.org/10.3389/fnana.2011.00029) PMID: [21647212](https://pubmed.ncbi.nlm.nih.gov/21647212/).
4. Rockel AJ, Hiorns RW, Powell TP. The basic uniformity in structure of the neocortex. *Brain.* 1980; 103(2):221–44. PMID: [6772266](https://pubmed.ncbi.nlm.nih.gov/6772266/).
5. Tian C, Wang K, Ke W, Guo H, Shu Y. Molecular identity of axonal sodium channels in human cortical pyramidal cells. *Front Cell Neurosci.* 2014; 8:297. doi: [10.3389/fncel.2014.00297](https://doi.org/10.3389/fncel.2014.00297) pmcid: PMC4172021. PMID: [25294986](https://pubmed.ncbi.nlm.nih.gov/25294986/)
6. Elston GN, Benavides-Piccione R, DeFelipe J. The pyramidal cell in cognition: a comparative study in human and monkey. *The Journal of Neuroscience.* 2001; 21(17):RC163. PMID: [11511694](https://pubmed.ncbi.nlm.nih.gov/11511694/).
7. Verhoog MB, Goriounova NA, Obermayer J, Stroeder J, Hjorth JJ, Testa-Silva G, et al. Mechanisms underlying the rules for associative plasticity at adult human neocortical synapses. *The Journal of Neuroscience.* 2013; 33(43):17197–208. PMID: [24155324](https://pubmed.ncbi.nlm.nih.gov/24155324/).
8. Testa-Silva G, Verhoog MB, Linaro D, de Kock CP, Baayen JC, Meredith RM, et al. High bandwidth synaptic communication and frequency tracking in human neocortex. *PLoS Biol.* 2014; 12(11): e1002007. Epub 2014/11/26. doi: [10.1371/journal.pbio.1002007](https://doi.org/10.1371/journal.pbio.1002007) PMID: [25422947](https://pubmed.ncbi.nlm.nih.gov/25422947/).

dc\_1581\_18

9. Mohan H, Verhoog MB, Doreswamy KK, Eyal G, Aardse R, Lodder BN, et al. Dendritic and Axonal Architecture of Individual Pyramidal Neurons across Layers of Adult Human Neocortex. *Cereb Cortex*. 2015; 25(12):4839–53. doi: [10.1093/cercor/bhv188](https://doi.org/10.1093/cercor/bhv188) PMID: [26318661](https://pubmed.ncbi.nlm.nih.gov/26318661/).
10. Molnar G, Olah S, Komlosi G, Fule M, Szabadics J, Varga C, et al. Complex events initiated by individual spikes in the human cerebral cortex. *PLoS Biol*. 2008; 6(9):e222. Epub 2008/09/05. doi: [10.1371/journal.pbio.0060222](https://doi.org/10.1371/journal.pbio.0060222) PMID: [18767905](https://pubmed.ncbi.nlm.nih.gov/18767905/).
11. Komlosi G, Molnar G, Rozsa M, Olah S, Barzo P, Tamas G. Fluoxetine (prozac) and serotonin act on excitatory synaptic transmission to suppress single layer 2/3 pyramidal neuron-triggered cell assemblies in the human prefrontal cortex. *The Journal of Neuroscience*. 2012; 32(46):16369–78. PMID: [23152619](https://pubmed.ncbi.nlm.nih.gov/23152619/).
12. Wang B, Yin L, Zou X, Ye M, Liu Y, He T, et al. A Subtype of Inhibitory Interneuron with Intrinsic Persistent Activity in Human and Monkey Neocortex. *Cell Rep*. 2015. Epub 2015/03/11. doi: [10.1016/j.celrep.2015.02.018](https://doi.org/10.1016/j.celrep.2015.02.018) PMID: [25753411](https://pubmed.ncbi.nlm.nih.gov/25753411/).
13. Varga C, Tamas G, Barzo P, Olah S, Somogyi P. Molecular and Electrophysiological Characterization of GABAergic Interneurons Expressing the Transcription Factor COUP-TFII in the Adult Human Temporal Cortex. *Cereb Cortex*. 2015; 25(11):4430–49. Epub 2015/03/20. doi: [10.1093/cercor/bhv045](https://doi.org/10.1093/cercor/bhv045) PMID: [25787832](https://pubmed.ncbi.nlm.nih.gov/25787832/).
14. Ramaswami M. Network plasticity in adaptive filtering and behavioral habituation. *Neuron*. 2014; 82(6):1216–29. Epub 2014/06/20. doi: [10.1016/j.neuron.2014.04.035](https://doi.org/10.1016/j.neuron.2014.04.035) PMID: [24945768](https://pubmed.ncbi.nlm.nih.gov/24945768/).
15. Maffei A. The many forms and functions of long term plasticity at GABAergic synapses. *Neural Plast*. 2011; 2011:254724. Epub 2011/07/27. doi: [10.1155/2011/254724](https://doi.org/10.1155/2011/254724) PMID: [21789285](https://pubmed.ncbi.nlm.nih.gov/21789285/).
16. Kullmann DM, Moreau AW, Bakiri Y, Nicholson E. Plasticity of inhibition. *Neuron*. 2012; 75(6):951–62. Epub 2012/09/25. doi: [10.1016/j.neuron.2012.07.030](https://doi.org/10.1016/j.neuron.2012.07.030) PMID: [22998865](https://pubmed.ncbi.nlm.nih.gov/22998865/).
17. Barnes SJ, Finnerty GT. Sensory experience and cortical rewiring. *Neuroscientist*. 2010; 16(2):186–98. Epub 2009/10/06. doi: [10.1177/1073858409343961](https://doi.org/10.1177/1073858409343961) PMID: [19801372](https://pubmed.ncbi.nlm.nih.gov/19801372/).
18. Chen JL, Nedivi E. Highly specific structural plasticity of inhibitory circuits in the adult neocortex. *Neuroscientist*. 2013; 19(4):384–93. Epub 2013/03/12. doi: [10.1177/1073858413479824](https://doi.org/10.1177/1073858413479824) PMID: [23474602](https://pubmed.ncbi.nlm.nih.gov/23474602/).
19. McBain CJ, Freund TF, Mody I. Glutamatergic synapses onto hippocampal interneurons: precision timing without lasting plasticity. *Trends Neurosci*. 1999; 22(5):228–35. Epub 1999/05/14. PMID: [10322496](https://pubmed.ncbi.nlm.nih.gov/10322496/).
20. Hornung JP, De Tribolet N, Tork I. Morphology and distribution of neuropeptide-containing neurons in human cerebral cortex. *Neuroscience*. 1992; 51(2):363–75. Epub 1992/11/01. PMID: [1281528](https://pubmed.ncbi.nlm.nih.gov/1281528/).
21. Banerjee A, Gonzalez-Rueda A, Sampaio-Baptista C, Paulsen O, Rodriguez-Moreno A. Distinct mechanisms of spike timing-dependent LTD at vertical and horizontal inputs onto L2/3 pyramidal neurons in mouse barrel cortex. *Physiological reports*. 2014; 2(3):e00271. Epub 2014/04/25. doi: [10.1002/phy2.271](https://doi.org/10.1002/phy2.271) PMID: [24760524](https://pubmed.ncbi.nlm.nih.gov/24760524/).
22. Thomson AM, West DC, Wang Y, Bannister AP. Synaptic connections and small circuits involving excitatory and inhibitory neurons in layers 2–5 of adult rat and cat neocortex: triple intracellular recordings and biocytin labelling in vitro. *Cereb Cortex*. 2002; 12(9):936–53. Epub 2002/08/17. PMID: [12183393](https://pubmed.ncbi.nlm.nih.gov/12183393/).
23. Feldmeyer D. Excitatory neuronal connectivity in the barrel cortex. *Frontiers in neuroanatomy*. 2012; 6:24. Epub 2012/07/17. doi: [10.3389/fnana.2012.00024](https://doi.org/10.3389/fnana.2012.00024) PMID: [22798946](https://pubmed.ncbi.nlm.nih.gov/22798946/).
24. Kullmann DM, Lamsa KP. LTP and LTD in cortical GABAergic interneurons: emerging rules and roles. *Neuropharmacology*. 2011; 60(5):712–9. Epub 2010/12/28. doi: [10.1016/j.neuropharm.2010.12.020](https://doi.org/10.1016/j.neuropharm.2010.12.020) PMID: [21185319](https://pubmed.ncbi.nlm.nih.gov/21185319/).
25. McBain CJ, Kauer JA. Presynaptic plasticity: targeted control of inhibitory networks. *Curr Opin Neurobiol*. 2009; 19(3):254–62. Epub 2009/07/08. doi: [10.1016/j.conb.2009.05.008](https://doi.org/10.1016/j.conb.2009.05.008) PMID: [19581079](https://pubmed.ncbi.nlm.nih.gov/19581079/).
26. Alle H, Jonas P, Geiger JR. PTP and LTP at a hippocampal mossy fiber-interneuron synapse. *Proc Natl Acad Sci USA*. 2001; 98(25):14708–13. Epub 2001/12/06. doi: [10.1073/pnas.251610898](https://doi.org/10.1073/pnas.251610898) PMID: [11734656](https://pubmed.ncbi.nlm.nih.gov/11734656/).
27. Peterfi Z, Urban GM, Papp OI, Nemeth B, Monyer H, Szabo G, et al. Endocannabinoid-mediated long-term depression of afferent excitatory synapses in hippocampal pyramidal cells and GABAergic interneurons. *The Journal of Neuroscience*. 2012; 32(41):14448–63. Epub 2012/10/12. PMID: [23055515](https://pubmed.ncbi.nlm.nih.gov/23055515/).
28. Min MY, Asztely F, Kokaia M, Kullmann DM. Long-term potentiation and dual-component quantal signaling in the dentate gyrus. *Proc Natl Acad Sci USA*. 1998; 95(8):4702–7. Epub 1998/05/16. PMID: [9539802](https://pubmed.ncbi.nlm.nih.gov/9539802/).
29. Le Duigou C, Holden T, Kullmann DM. Short- and long-term depression at glutamatergic synapses on hippocampal interneurons by group I mGluR activation. *Neuropharmacology*. 2011; 60(5):748–56. Epub 2010/12/28. doi: [10.1016/j.neuropharm.2010.12.015](https://doi.org/10.1016/j.neuropharm.2010.12.015) PMID: [21185314](https://pubmed.ncbi.nlm.nih.gov/21185314/).

dc\_1581\_18

30. Galvan EJ, Calixto E, Barrionuevo G. Bidirectional Hebbian plasticity at hippocampal mossy fiber synapses on CA3 interneurons. *The Journal of Neuroscience*. 2008; 28(52):14042–55. Epub 2008/12/26. PMID: [19109487](#).
31. Sarihi A, Jiang B, Komaki A, Sohya K, Yanagawa Y, Tsumoto T. Metabotropic glutamate receptor type 5-dependent long-term potentiation of excitatory synapses on fast-spiking GABAergic neurons in mouse visual cortex. *The Journal of Neuroscience*. 2008; 28(5):1224–35. Epub 2008/02/01. PMID: [18234900](#).
32. Nissen W, Szabo A, Somogyi J, Somogyi P, Lamsa KP. Cell type-specific long-term plasticity at glutamatergic synapses onto hippocampal interneurons expressing either parvalbumin or CB1 cannabinoid receptor. *The Journal of Neuroscience*. 2010; 30(4):1337–47. Epub 2010/01/29. PMID: [20107060](#).
33. Campanac E, Gasselien C, Baude A, Rama S, Ankri N, Debanne D. Enhanced intrinsic excitability in basket cells maintains excitatory-inhibitory balance in hippocampal circuits. *Neuron*. 2013; 77(4):712–22. Epub 2013/02/27. doi: [10.1016/j.neuron.2012.12.020](#) PMID: [23439123](#).
34. Camire O, Lacaille JC, Topolnik L. Dendritic Signaling in Inhibitory Interneurons: Local Tuning via Group I Metabotropic Glutamate Receptors. *Front Physiol*. 2012; 3:259. Epub 2012/08/31. doi: [10.3389/fphys.2012.00259](#) PMID: [22934015](#).
35. Oren I, Nissen W, Kullmann DM, Somogyi P, Lamsa KP. Role of ionotropic glutamate receptors in long-term potentiation in rat hippocampal CA1 oriens-lacunosum moleculare interneurons. *The Journal of Neuroscience*. 2009; 29(4):939–50. Epub 2009/01/30. PMID: [19176803](#).
36. Maccaferri G, McBain CJ. Long-term potentiation in distinct subtypes of hippocampal nonpyramidal neurons. *The Journal of Neuroscience*. 1996; 16(17):5334–43. Epub 1996/09/01. PMID: [8757246](#).
37. Molnar G, Rozsa M, Baka J, Holderith N, Barzo P, Nusser Z, et al. Human pyramidal to interneuron synapses are mediated by multi-vesicular release and multiple docked vesicles. *eLife*. 2016; 5. Epub 2016/08/19. doi: [10.7554/eLife.18167](#) PMID: [27536876](#).
38. Miles R, Wong RK. Excitatory synaptic interactions between CA3 neurones in the guinea-pig hippocampus. *J Physiol. (Lond)*. 1986; 373:397–418. Epub 1986/04/01. PMID: [3018233](#).
39. Jiang X, Shen S, Cadwell CR, Berens P, Sinz F, Ecker AS, et al. Principles of connectivity among morphologically defined cell types in adult neocortex. *Science*. 2015; 350(6264):aac9462. Epub 2015/11/28. doi: [10.1126/science.aac9462](#) PMID: [26612957](#).
40. Song S, Sjöström PJ, Reigl M, Nelson S, Chklovskii DB. Highly nonrandom features of synaptic connectivity in local cortical circuits. *PLoS Biol*. 2005; 3(3):e68. Epub 2005/03/02. doi: [10.1371/journal.pbio.0030068](#) PMID: [15737062](#).
41. Lefort S, Tómm C, Floyd Sarria JC, Petersen CC. The excitatory neuronal network of the C2 barrel column in mouse primary somatosensory cortex. *Neuron*. 2009; 61(2):301–16. Epub 2009/02/03. doi: [10.1016/j.neuron.2008.12.020](#) PMID: [19186171](#).
42. Lu J, Tucciarone J, Lin Y, Huang ZJ. Input-specific maturation of synaptic dynamics of parvalbumin interneurons in primary visual cortex. *Proc Natl Acad Sci USA*. 2014; 111(47):16895–900. Epub 2014/11/12. doi: [10.1073/pnas.1400694111](#) PMID: [25385583](#).
43. Luscher C, Huber KM. Group 1 mGluR-dependent synaptic long-term depression: mechanisms and implications for circuitry and disease. *Neuron*. 2010; 65(4):445–59. Epub 2010/03/02. doi: [10.1016/j.neuron.2010.01.016](#) PMID: [20188650](#).
44. Lu JT, Li CY, Zhao JP, Poo MM, Zhang XH. Spike-timing-dependent plasticity of neocortical excitatory synapses on inhibitory interneurons depends on target cell type. *The Journal of Neuroscience*. 2007; 27(36):9711–20. Epub 2007/09/07. PMID: [17804631](#).
45. Lamsa KP, Heeroma JH, Somogyi P, Rusakov DA, Kullmann DM. Anti-Hebbian long-term potentiation in the hippocampal feedback inhibitory circuit. *Science*. 2007; 315(5816):1262–6. Epub 2007/03/03. doi: [10.1126/science.1137450](#) PMID: [17332410](#).
46. Perez Y, Morin F, Lacaille JC. A hebbian form of long-term potentiation dependent on mGluR1a in hippocampal inhibitory interneurons. *Proc Natl Acad Sci USA*. 2001; 98(16):9401–6. Epub 2001/07/12. doi: [10.1073/pnas.161493498](#) PMID: [11447296](#).
47. Lei S, McBain CJ. Two Loci of expression for long-term depression at hippocampal mossy fiber-interneuron synapses. *The Journal of Neuroscience*. 2004; 24(9):2112–21. Epub 2004/03/06. PMID: [14999062](#).
48. Lei S, McBain CJ. Distinct NMDA receptors provide differential modes of transmission at mossy fiber-interneuron synapses. *Neuron*. 2002; 33(6):921–33. Epub 2002/03/22. PMID: [11906698](#).
49. Szabo A, Somogyi J, Cauli B, Lambolez B, Somogyi P, Lamsa KP. Calcium-permeable AMPA receptors provide a common mechanism for LTP in glutamatergic synapses of distinct hippocampal interneuron types. *The Journal of Neuroscience*. 2012; 32(19):6511–6. Epub 2012/05/11. PMID: [22573673](#).

dc\_1581\_18

50. Larsen RS, Sjöström PJ. Synapse-type-specific plasticity in local circuits. *Curr Opin Neurobiol.* 2015; 35:127–35. Epub 2015/08/28. doi: [10.1016/j.conb.2015.08.001](https://doi.org/10.1016/j.conb.2015.08.001) PMID: [26310110](https://pubmed.ncbi.nlm.nih.gov/26310110/).
51. Jones HC, Keep RF. Brain fluid calcium concentration and response to acute hypercalcaemia during development in the rat. *J Physiol. (Lond).* 1988, 402: 579–593. PMID: [3236250](https://pubmed.ncbi.nlm.nih.gov/3236250/).
52. Mitchell SJ, Silver RA. Glutamate spillover suppresses inhibition by activating presynaptic mGluRs. *Nature.* 2000; 404(6777):498–502. Epub 2000/04/13. doi: [10.1038/35006649](https://doi.org/10.1038/35006649) PMID: [10761918](https://pubmed.ncbi.nlm.nih.gov/10761918/).
53. Mitchell SJ, Silver RA. GABA spillover from single inhibitory axons suppresses low-frequency excitatory transmission at the cerebellar glomerulus. *The Journal of Neuroscience.* 2000; 20(23):8651–8. Epub 2000/01/11. PMID: [11102470](https://pubmed.ncbi.nlm.nih.gov/11102470/).
54. Coddington LT, Rudolph S, Vande Lune P, Overstreet-Wadiche L, Wadiche JI. Spillover-mediated feedforward inhibition functionally segregates interneuron activity. *Neuron.* 2013; 78(6):1050–62. Epub 2013/05/28. doi: [10.1016/j.neuron.2013.04.019](https://doi.org/10.1016/j.neuron.2013.04.019) PMID: [23707614](https://pubmed.ncbi.nlm.nih.gov/23707614/).
55. Govindaiah G, Wang T, Gillette MU, Cox CL. Activity-dependent regulation of retinogeniculate signaling by metabotropic glutamate receptors. *The Journal of Neuroscience.* 2012; 32(37):12820–31. Epub 2012/09/14. PMID: [22973005](https://pubmed.ncbi.nlm.nih.gov/22973005/).
56. Clark DA, Mitra PP, Wang SS. Scalable architecture in mammalian brains. *Nature.* 2001; 411(6834):189–93. Epub 2001/05/11. doi: [10.1038/35075564](https://doi.org/10.1038/35075564) PMID: [11346794](https://pubmed.ncbi.nlm.nih.gov/11346794/).
57. Alvarado-Rojas C, Huberfeld G, Baulac M, Clemenceau S, Charpier S, Miles R, et al. Different mechanisms of ripple-like oscillations in the human epileptic subiculum. *Ann Neurol.* 2015; 77(2):281–90. Epub 2014/12/03. doi: [10.1002/ana.24324](https://doi.org/10.1002/ana.24324) PMID: [25448920](https://pubmed.ncbi.nlm.nih.gov/25448920/).
58. Cohen I, Navarro V, Clemenceau S, Baulac M, Miles R. On the origin of interictal activity in human temporal lobe epilepsy in vitro. *Science.* 2002; 298(5597):1418–21. Epub 2002/11/16. doi: [10.1126/science.1076510](https://doi.org/10.1126/science.1076510) PMID: [12434059](https://pubmed.ncbi.nlm.nih.gov/12434059/).
59. Scimemi A, Andersson A, Heeroma JH, Strandberg J, Rydenhag B, McEvoy AW, et al. Tonic GABA(A) receptor-mediated currents in human brain. *Eur J Neurosci.* 2006; 24(4):1157–60. Epub 2006/08/26. doi: [10.1111/j.1460-9568.2006.04989.x](https://doi.org/10.1111/j.1460-9568.2006.04989.x) PMID: [16930441](https://pubmed.ncbi.nlm.nih.gov/16930441/).
60. Whittaker RG, Devine HE, Gorman GS, Schaefer AM, Horvath R, Ng Y, et al. Epilepsy in adults with mitochondrial disease: A cohort study. *Ann Neurol.* 2015; 78(6):949–57. Epub 2015/09/19. doi: [10.1002/ana.24525](https://doi.org/10.1002/ana.24525) PMID: [26381753](https://pubmed.ncbi.nlm.nih.gov/26381753/).
61. Cowie CJ, Cunningham MO. Peritumoral epilepsy: relating form and function for surgical success. *Epilepsy Behav.* 2014; 38:53–61. Epub 2014/06/05. doi: [10.1016/j.yebeh.2014.05.009](https://doi.org/10.1016/j.yebeh.2014.05.009) PMID: [24894847](https://pubmed.ncbi.nlm.nih.gov/24894847/).
62. Molnar G, Farago N, Kocsis AK, Rozsa M, Lovas S, Boldog E, et al. GABAergic neurogliaform cells represent local sources of insulin in the cerebral cortex. *The Journal of Neuroscience.* 2014; 34(4):1133–7. Epub 2014/01/24. PMID: [24453306](https://pubmed.ncbi.nlm.nih.gov/24453306/).